Seismic Fragility Assessment and Resilience of Reinforced Masonry Shear Wall Systems

Shadman Hosseinzadeh

A Thesis

In the Department

of

Building, Civil and Environmental Engineering

Presented in Partial Fulfillment of the Requirements

for the Degree of

Doctor of Philosophy (Civil Engineering) at

Concordia University

Montréal, Québec, Canada

September 2020

CONCORDIA UNIVERSITY

School of Graduate Studies

This is to certify that the thesis prepared

By: Shadman Hosseinzadeh

Entitled: Seismic Fragility Assessment and Resilience of Reinforced Masonry Shear Wall Systems

and submitted in partial fulfillment of the requirements for the degree of

Doctor of Philosophy (Civil Engineering)

complies with the regulations of the university and meets the accepted standards with respect to originality and quality.

Signed by the final examining committee:

_____ Chair
Dr. Ahmed Kishk

_____ External Examiner
Dr. Tony Yang

_____ External to Program
Dr. Ramin Sedaghati

_____ Examiner
Dr. Lucia Tirca

_____ Examiner
Dr. Ashutosh Bagchi

_____ Thesis supervisor
Dr. Khaled Galal

Approved by _____
Dr. Michelle Nokken, Graduate Program Director

_____

Tuesday 2020-10-27   Dr. Mourad Debbabi, Dean
                            Gina Cody School of Engineering and Computer Science

ABSTRACT

Seismic Fragility Assessment and Resilience of Reinforced Masonry Shear Wall Systems

Shadman Hosseinzadeh, Ph.D.

Concordia University, 2020

Reinforced Masonry Shear Walls (RMSWs) are commonly used in low- to high-rise buildings as the lateral load resisting system. There have been several experimental and analytical studies that evaluated the seismic response of RMSW either as a single element (i.e., planar rectangular walls) or as a building consisting of planar walls. However, research on Reinforced Masonry Shear Walls (RMSWs) with end-confined Boundary Elements and flanged shear walls are scarce, especially considering the effects of design parameters on the system's seismic inelastic response. The end confined RMSWs proved to have a higher level of ductility since they can postpone the reinforcement buckling in compression while increasing the compressive strength of the shear walls' component at the same time.

The objectives of the current study are to: (i) assess the seismic performance and collapse capacity of the RMSW with end confined Boundary Elements and Flanged shear walls at both structural element, and entire building level, (ii) evaluate the seismic resilience and functionality of the RMSW system when subjected to severe earthquake events, (iii) to quantify and assess the resilience index versus the uncertainty of the studied parameters.

To achieve the first goal, at the structural element level, the RM shear walls were designed with different heights to investigate the effect of the wall's height on its seismic performance. The impact of utilizing flanged walls was assessed and characterized through new seismic performance standards and assessment approaches. In this respect, a modified macro-modelling approach has been proposed to numerically model and capture the inelastic behaviour of the RM shear walls. The proposed model can capture both flexural and shear deformations. The nonlinear model was

first validated against experimental data of RM rectangular and flanged shear walls and walls with masonry boundary elements (MBEs); afterwards, the model has been utilized in simulating RM flanged wall archetypes. Collapse risk evaluation has been conducted by subjecting the wall's numerical model to various ground motions scaled at different intensity levels. Nonlinear static pushover analysis and incremental dynamic analysis (IDA) has been conducted on numerical models. Quantification of the seismic parameters of the flanged wall system, including period-based ductility, overstrength, and collapse margin ratios, has been conducted to help better understanding the seismic response and collapse capacity of the component. Lastly, the seismic resilience of the archetypes against the expected collapse risk was evaluated, before and after adding flanges and boundary elements to the walls, in terms of functionality curves. Damage levels were considered as performance level functions correlated to the earthquake intensity and were used to estimate total loss and recovery time of the archetypes.

To reach the second objective, the study is extended to investigate the impact of using end-confined masonry boundary elements at the building level by the adoption of such elements for multi-storey RMSW buildings. In this respect, the developed macro-model was updated to take the impact of out-of-plane walls' shear flexibility into account, after adding an out-of-plane shear spring. The outcome of the test results of a one-third scale two-storey building was used to validate the modelling approach at the system level. Subsequently, the archetype buildings were subjected to multiple ground motion records using Incremental Dynamic Analysis to identify the collapse initiation and derive fragility curves. The results indicate a significant enhancement of the resilience index by using end-confined Masonry Boundary Elements (MBEs).

To accomplish the third objective, a probabilistic approach was utilized to quantify the seismic resilience index of the RMSW building with MBEs located in a high seismic zone of Canada. The uncertainties associated with the losses and expected recovery time and sensitivity of each parameter were studied and depicted using the resilience index threshold and the Monte Carlo simulation method. The storey shear contribution of in-plane and out-of-plane walls were also quantified for all archetype buildings. The results indicate sufficient seismic resilience of ductile RMSW buildings with MBEs when subjected to the Maximum Credible Earthquake (MCE). The findings of this part are crucial for earthquake mitigation practice and disaster risk reduction plans.

Acknowledgements

First and foremost, I would like to thank my supervisor, Professor Khaled Galal, for his support, help, and guidance throughout this research study. His continuous encouragement has provided me with the confidence to learn and progress all the time. His dynamism, vision, sincerity and motivation have deeply inspired me. He taught me the way to carry out the research and to present the research works as clearly as possible. It was a great privilege and honour to work and study under his guidance.

I am extending my heartfelt thanks to my family for their love, caring and sacrifices for educating and preparing me for my future. I express my special thanks to my sisters and to my one and only brother for their support and valuable devotions. My father, who always cared about me, supported me and tolerated me while I was impatient. My lovely mother, who always sent me endless love and encouragement from miles away!

I would like to say thanks to my friends and research colleagues, Hamid Arabzadeh, Armin Farahbakhshtooli, Nader Aly, Ahmed Ashour, Farzad Ghodoosipour, Farzad Rouhani, Pejman Aghababaee, Layane Hamzeh, Mohammed Al Butainy, and Omar Yagoub for their genuine support and valuable hints throughout this research work. There are so many others whom I may inadvertently leave out, and I sincerely thank all of them for their help.

Finally, my thanks go to all the people who have supported me to complete the research work directly or indirectly.

Dedication

To my beloved parents;

To my Brother,

& To my Sisters

Co-Authorship

This thesis has been prepared in accordance with the regulations for a sandwich (manuscript-based) thesis format. The research presented herein includes numerical and analytical studies carried out solely by Shadman Hosseinzadeh. Advice and guidance were provided for the whole thesis by the academic supervisor Professor Khaled Galal. This thesis consists of the following chapters, which are based on published and submitted papers in peer-reviewed journals:

Chapter 3

Hosseinzadeh, S., Ashour, A., Aly, N., and Galal, K. (2017) "Seismic collapse evaluation of reinforced masonry core wall systems." 13th Canadian Masonry Symposium, Halifax, Canada.

Hosseinzadeh S., and Galal K. (2019). "Enhancing the Seismic Resilience of Reinforced Masonry Shear Wall Building using Boundary Elements." 12th Canadian Conference on Earthquake Engineering, Quebec City, Canada.

Chapter 4

Hosseinzadeh, S, and Galal, K. (2020). "Seismic Fragility Assessment and Resilience of Reinforced Masonry Flanged Wall Systems." ASCE Journal of Performance of Constructed Facilities. 34(1).

Chapter 5

Hosseinzadeh, S., and Galal, K. (2020). "System-level Seismic Resilience Assessment of Reinforced Masonry Shear Wall Buildings with Masonry Boundary Elements." Structures Journal, Elsevier, 26, 686-702.

Chapter 6

Hosseinzadeh, S., and Galal, K. (2020). "Probabilistic Seismic Resilience Quantification of Reinforced Masonry Shear Wall System with Boundary Elements under Bidirectional Horizontal Excitations." Engineering Structures, Elsevier, Under Review.

Table of Contents

List of Figures

List of Tables

Chapter 1

Introduction

1.1 Background and Problem Definition

Utilizing reinforcement into the conventional masonry structures started in the eighteenth century by testing reinforced masonry lintels (Ashour et al. 2017). The idea led to introducing the Reinforced Masonry (RM) structures into the engineering platform. Concrete masonry blocks were commercially available by the end of the nineteenth century to make the feasibility of the Concrete-Block Masonry Structural Walls possible. During the past few decades, there have been many research studies addressing the seismic response of the Reinforced Masonry Shear Wall (RMSW) components made up of Concrete-Blocks Masonry. However, all studies addressed rectangular shear wall systems, and scarce studies investigated walls incorporating Flanges and/or Masonry Boundary Elements (MBEs) (e.g., Shedid et al. 2009, Ahmadi et al. 2015, and Aly and Galal 2020). These RMSWs can be utilized as fully or partially grouted, end-confined, or non-confined walls depending on the level of seismicity, providing the designers with the versatility needed to integrate an efficient Seismic Force Resisting System (SFRS) into mid and high-rise buildings.

During the last few decades, there has been a significant advancement in the definition of resilience-based engineering as an updated alternative to performance-based design engineering. Natural hazards such as earthquakes have a tremendous social and economic impact on individuals and societies. Natural disasters are unpredictable and inevitable, while almost being impossible to predict and determine the possible vulnerabilities that may cause. That said, the preparation and mitigation actions can be considered as a part of the resilience technique against these disastrous events, which can reduce their unfavourable consequences. There is a need for a resilience approach to address necessary actions to mitigate the losses and casualties, primarily before the event occurs. It has been known that a resilience perspective can help with preparation, response, recovery action, and mitigation efforts against probable risks.

1.2 Research Significance and Motivation

Analytical and Numerical modelling is more recently considered and used by many

researchers since they are less expensive and more effective in estimating the structural response without the limitations of experimental tests such as the high cost, scaling method, etc. The numerical modelling approach is shown to be capable of capturing experimental response with a great level of accuracy. In contrast, these approaches provide the user with more control over the failure modes, loading protocols, and collapse criteria assessment (Stavridis et al. 2010, Ezzeldin et al. 2016). The literature indicates a lack of relatively simplified macro-models in predicting the inelastic behaviour of the RM Shear walls. As will be discussed later in the thesis, these macro-models are key, not only to facilitate evaluating the overall response of the entire building but also to help better understand the performance data following new seismic performance standards and assessment approaches. [e.g., ASCE 41-13 (ASCE 2014), FEMA P-695 (FEMA 2009), and FEMA P-58 (FEMA 2012)].

The current capacity design methodology that was initially introduced by Park and Paulay (1975) for the seismic design of buildings provides an efficient design and detailing of structural elements to avoid non-ductile sudden failures of the whole structure during seismic events. Therefore, the Reinforced Masonry (RM) shear walls should possess sufficient ductility to undergo seismic events while being able to sustain large reversible cycles of inelastic deformations without significant degradation in strength. This goal can be achieved by adopting a confined zone at the outermost ends of rectangular RM shear walls. Incorporating end zone confinement results in attaining a higher level of displacement and curvature ductility and enhances the overall performance of the wall during the seismic events compared to that of RM rectangular walls. (Banting and El-Dakhakhni, 2012, 2014; Ezzeldin et al., 2017; Ezzeldin et al., 2016; Shedid et al., 2010b). This can be done by utilizing different end zone shapes such as flanges and rectangular boundary zones.

In addition, when the resilience engineering approach is adopted, there is a challenge for identifying the effective system that would have better post-disaster performance, especially when there are limited resources for fast recovery. It is important to try to use a more competent lateral load resisting system to reduce the losses from earthquakes to have a more resilient structure. Also, the quantification of the seismic resilience of the utilized seismic force resisting system is vital and needs to be studied to evaluate the effectiveness of the system.

2

1.3 Objectives and Scope of Work

The main objective of this research is to investigate the effectiveness of different end configurations, including flanges and confined masonry boundary elements on the seismic performance and resilience of reinforced masonry shear wall system buildings at both structural elements and building level.

The following sub-objectives are also considered for the present research:

- Developing and validating a robust numerical modelling approach capable of predicting the nonlinear response of RM shear walls with various end configuration
- Examination of the impact of end-shape configuration on collapse capacity and seismic performance of the RMSW flanged walls and walls with rectangular masonry boundary elements
- Performing incremental dynamic analysis and seismic assessment of RMSW system using the proposed methodology by FEMA P695 (2009)
- Evaluating the impact of utilizing various end configurations on seismic resilience and structural and non-structural losses of the RMSW buildings due to the earthquake.
- Quantification of seismic resilience and its sensitivity against loss ratio and recovery time variables
- Quantification of the out-of-plane response of RMSW building using full 3D numerical simulation

1.4 The Thesis Layout

The thesis will be comprised of seven chapters, as follows:

- Chapter 1 consists of an introduction, research significance and motivation; objectives and scope of work; and a brief literature review and the layout of the thesis.
- Chapter 2 comprises a review on the background of the study, including the effect of using boundary elements and/or different end configuration on the response of RMSW system, and the numerical micro and macro-model studies proposed for the simulation of the seismic behaviour of RMSWs. A general background of the reinforced masonry rectangular shear walls, non-planar walls, Flanged walls, walls with Boundary Elements, and their nonlinear structural response is also presented in this chapter.

- Chapter 3 focuses on the development of a numerical model using available commercial software and its limitation. Also, the initiative taken to develop a modified wide column model is discussed in this chapter addressing the advantages of using an open-source program. This chapter comprised of two subchapters, including the seismic performance of the core wall system, as well as studying the behaviour of a five-storey building at building level as a benchmark for further reference.

- Chapter 4 focuses on the "Seismic Fragility Assessment and Resilience of Reinforced Masonry Flanged Wall Systems." Also, the developed numerical macro-modelling approach of the RMSW components under Incremental Dynamic Analysis will be described in this chapter.

- Chapter 5 consists of "System-Level Seismic Resilience Assessment of the Reinforced Masonry Shear Wall Buildings with Masonry Boundary Elements" which focuses on the response of the RMSW building after incorporating Masonry Boundary Elements at the system level and assess the seismic resilience and structural and non-structural losses after the adoption of end-confined zones.

- Chapter 6 includes "Probabilistic Seismic Resilience Quantification of End-Confined Reinforced Masonry Shear Wall Buildings Under Bidirectional Horizontal Excitations" quantifies the seismic resilience of RMSW having MBEs and assess the sensitivity of resilience index against loss ratio and expected recovery time through developed fragility surfaces. Also, the quantification of the out-of-plane storey shear contribution of RMSW buildings is elaborated in this chapter.

- Chapter 7 consists of the summary of the research project, the main contributions and conclusions, limitations associated with the study and the recommendations for future work.

Chapter 2

General Background

2.1   Literature Review

Masonry structures are among the oldest type of construction and are well-known by their durability and construction pace. Conventional masonry was able to resist a high level of compressive forces and was quite durable against gravity forces. However, the tensile strength of such elements was quite low, causing them not to act properly when subjected to cyclic load arising from wind and earthquake. Meanwhile, a series of earthquakes during the 20th century, such as San Fernando (1906), Long Beach (1933), San Fernando (1971), and Northridge (1994) caused massive deterioration on the unreinforced masonry structures resulting in the innovation of Reinforced Masonry (RM) structures. The use of RM structures has been developed in the latest 20th century and has reached up to building 28 storey buildings using RM Shear Walls (Wang et al., 2016).

As the lateral load resisting system of the building, RM Shear walls are responsible for transferring the lateral load from the horizontal diaphragm to the foundation of the structure besides carrying the gravity loads due to dead and live loads. Reinforced masonry shear walls have been widely used as the main Seismic Force Resisting System (SFRS) in low- to high-rise buildings since they inherently possess large lateral stiffness and large lateral load resistance. The above-mentioned characteristics of such walls ensure sufficient drift control capability of the well-designed structural shear walls.

There have been many research studies conducted to date addressing the in-plane behaviour of the masonry shear walls under different load conditions in terms of axial load and lateral shear forces. Observations from post-earthquake investigations such as in Chile 1985 (Wyllie et al., 1986) showed major damage due to extensive use of non-ductile shear walls. RM Shear walls have the capability to withstand severe earthquakes with less damage to structural and non-structural elements. However, some research studies proved that RM walls governed by shear failure performed poorly against lateral load and exerted low ductility in comparison to well-detailed

shear walls governed by flexural failure (Paulay et al., 1988; Priestley et al., 1992). Figure 2.1 shows sample failures of RM shear walls in the flexure and shear governed mode.
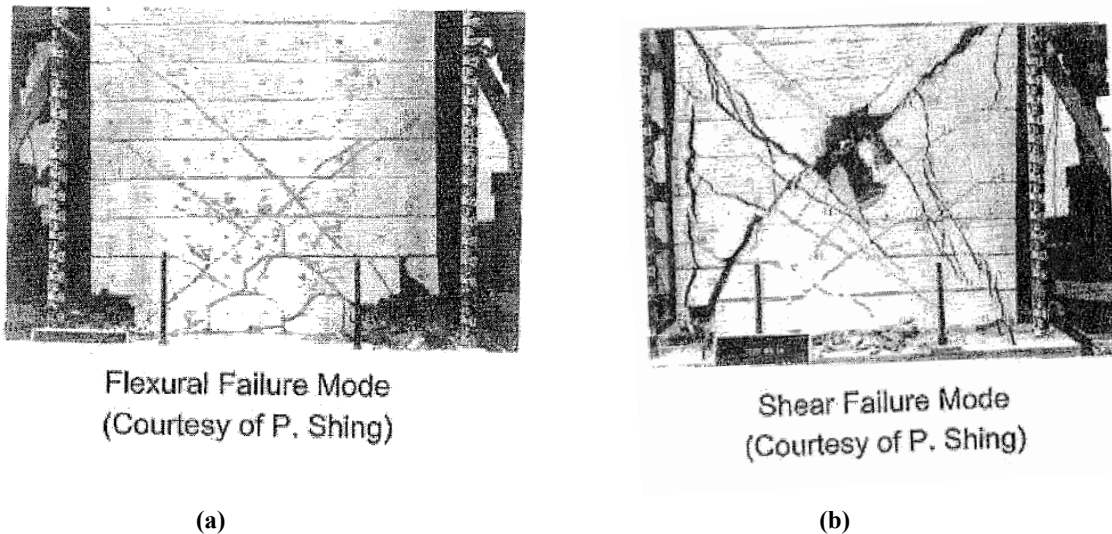
Figure 2.1. Failure of RM shear walls in (a) Shear Wall with ductile flexural failure mode (b) Shear wall with brittle shear failure mode (Shing, 1989)

The seismic response of the RM shear walls is a function of many factors in an earthquake event, including the mass, natural frequency or period of the structure, and its inherent damping ratio. The typical design standards procedures, such as equivalent static methods, consider the impact of lateral loads arising from wind or earthquake as an equivalent force acting at the center of the mass of the structure and the shear walls will resist against lateral loads by providing sufficient rigidity at the center of the rigidity of the structure. Shear walls will transfer the loads from the diaphragm to the foundation. As a result, yielding of longitudinal reinforcement and a high level of plastic deformation is expected at the RM shear wall bottom end, as well as the tip of the wall depending on the support condition. This phenomenon often referred to as plastic hinging regions in the shear wall segments. These portion of the RM shear walls plays an important role in controlling the behaviour of the wall against lateral loads as it can alter the type of failure if the wall is not appropriately designed. As a result of this mechanism, proper detailing of the plastic hinging regions is important to provide the required ductility in the wall elements. Adequate detailing of the plastic hinge zone should ensure a desirable ductile behaviour of the shear wall providing the component with flexural yielding. To reach this goal, transverse reinforcements are

6

utilized to help to postpone the longitudinal reinforcement buckling and increasing the level of ductility at these critical regions of the wall. Because of some geometrical limitations, incorporating closed-typed hoops at the wall's extreme side was not possible via regular rectangular shape RM shear walls. In the meantime, the presence of these hoops would provide the shear walls with more resistance and stability against out-of-plane buckling. A significant increase in the compressive strength of the confined zones was also observed after having closed hoops in the walls' ends (Cyrier, 2012). Different methods of confinement have been studied for application on RM shear walls, including providing steel plates and seismic combs in the bed joints, and steel rings and spirals around vertical reinforcing bars within the block cells (Priestley and Elder, 1983; Hart et al., 1988; Snook, 2005; Hervillard, 2005). The scope of all these studies was to provide sufficient confinement to the RM shear wall to increase the compressive strain capacity, hence the overall ductility of the wall segment. Ductility is an essential property of structures subjected to reversed cyclic loads. This includes the ability of the structure to sustain large inelastic deformations and dissipate the input energy by its hysteretic behaviour (Priestly et al., 2007).

Canadian design of masonry structures code, CSA S304 (2014), states that reinforced masonry shear walls shall be designed to adopt capacity design principles, including the occurrence of inelastic deformation in energy-dissipating components (i.e., RM Shear Walls), which are designed and detailed accordingly. However, all other load-bearing components are designed and detailed to exert enough strength to ensure that the shear walls can perform and fail in ductile mode. This can be done by ensuring that the failure mode at the ultimate limit state is dominated by flexure failure; due to yielding of the flexural steel reinforcement before shear failure. This structure is expected to undergo cyclic inelastic deformations without significant loss of strength and is detailed to develop the appropriate level of ductility while remaining stable.

2.2   Common Failure Modes of RM Shear Walls

Four common types of major responses were known for RM shear walls subjected to cyclic in-plane loading. The response type is important because it can characterize the shear wall's performance under seismic loading. Various design parameters can affect a wall's response, including the applied axial load, shear walls' height to length aspect ratio, longitudinal and

horizontal reinforcement ratios, and anchorage detailing. Paulay and Priestley (1992) found that four common response modes for masonry shear walls are associated with flexure, rocking, shear, and sliding deformations. These deformations are depicted in Figure 2.2. In general, the in-plane behaviour of reinforced masonry shear walls is identified to be flexural and shear types of failure. Enough anchorage of the shear wall to the foundation will allow the shear and/or flexure modes to dominate the wall's response. A ductile failure typically results from a flexural response, while a brittle failure often results from a shear response. Ductile failures are preferred because the structure possesses the ability to deform inelasticity without abrupt collapse.

Flexural failure is accompanied by tensile yielding of the vertical reinforcement, the formation of plastic hinge zone, and gradual crushing of the masonry at the wall extremes. This type of failure will provide the structure with high energy dissipation and ductile behaviour. Whereas shear failure is mostly characterized by diagonal tension cracking and shear slipping at the bed joints of the RM shear walls. This type of failure exhibits more brittle behaviour and rapid strength degradation after reaching maximum strength. Shear deformations can be observed mostly on the walls with low aspect ratio, whereas, for a relatively high aspect ratio, the response is most likely governed by flexural deformation.

Flexure	Rocking	Shear	Sliding
(a)	(b)	(c)	(d)
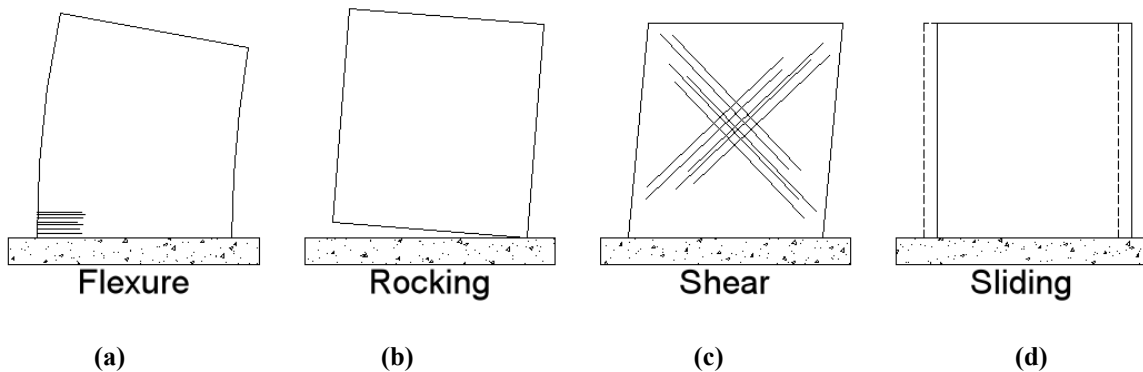
Figure 2.2. Masonry Shear Walls Failure Modes (adapted from Eikanas, 2003)

2.3   Seismic Response Assessment of RM Shear Walls

To facilitate the study of the seismic behaviour of RM shear walls and their failure modes, a review of the effect of key parameters on the performance of these components is necessary. In general, the seismic performance of the RM shear wall structures can be characterized through

performing quasi-static cyclic analysis, in terms of hysteretic lateral force-deformation curves. This can be done numerically and/or experimentally; however, numerical models are more economically beneficial compared to experimental studies. There have been many experimental studies during the past decades trying to investigate the lateral capacity and behaviour of RM shear walls (see Figure 2.3.), whereas there are some limitations accompanied with this approach such as scaling of the specimens, fabrication issues, and financial matters, that highlights the importance of numerical approaches alongside experimental studies.

(a)   (b)
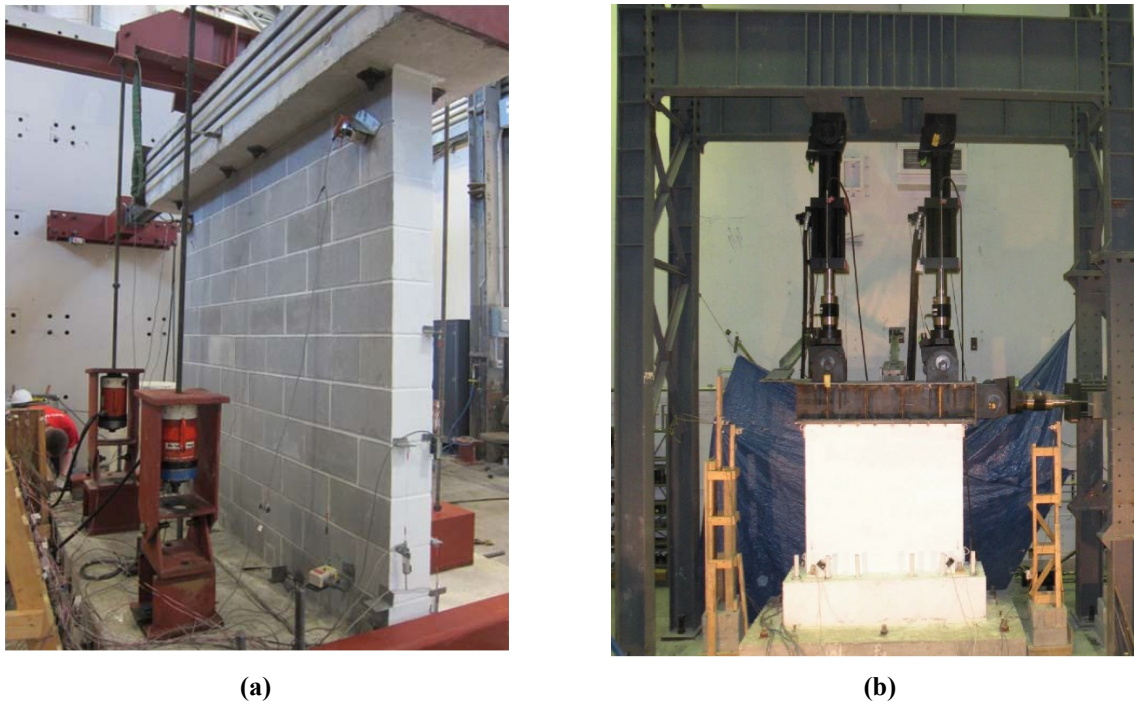
Figure 2.3. Experimental studies on the lateral performance of RM shear walls: (a) Ahmadi and Klingner (2012), (b) Seif-Eldin and Galal. (2016)

A robust numerical simulation should be able to investigate the inelastic response of RM shear wall systems by using a reliable modelling approach that can determine important characteristics and response parameters such as nonlinear shear-flexural behaviour, confinement effects, axial deformations, and sliding of cracked surfaces. A variety of numerical approaches are available in the literature; however, not all of them are suitable to capture the overall behaviour of a building and not just the shear wall component. Among different numerical modelling technique, the macro-modelling approach is the one which can capture the characteristics of the entire

building and not only the structural shear wall components. A variety of software tools are available that employ non-linear finite element methods for the analysis of reinforced masonry.

The Finite Elements (FE) modelling approach is available in most of the software tools such as ABAQUS and DIANA while they utilize built-in constitutive material strain-stress relationship to resemble the behaviour of shear walls' components including the rupture of the rebars, cracking and/or crushing of the masonry elements and bond-slip in addition to the global force-deformation responses. Different material properties need to be defined in this type of programs, and the property of the materials should be calibrated using the available constitutive material model of the software (i.e., smeared vs discrete steel reinforcement, masonry confinement) to ensure the robustness and precision of the approach to deliver a reliable outcome. This approach also conveys considering some additional parameters to drive the nonlinear solution algorithms to convergence.

FE approaches can often be used to calibrate the nonlinear load-deformation behaviour of structures using the fibre-based technique. Software tools such as OpenSees (OS), SeismoStruct, and Perform-3D are the example of the packages that can utilize Fibre-based Element (FibE) technique to capture the nonlinear strength and stiffness degradation of fibre elements of complete building structures with significantly less computational effort. It is worth noting that, the predictions of both FE and FibE models need to be validated against available experimental data to verify their performance for both ductile (flexural) and brittle (shear) failure mechanisms.

There are not many research studies conducted on developing an efficient numerical approach for modelling RM shear wall systems. However, there are many experimental tests available in the literature addressing the inelastic response of Reinforced Masonry elements. The main objective of these numerical studies is to develop and validate micro/macro models for reinforced masonry walls subjected to cyclic loads. Some also developed simplified models that can be adopted by engineering practitioners. The adopted modelling approach is elaborated in the subsequent chapter of the thesis addressing the required elements and corresponding material constitutive models in detail. The process for calibration of parameters is highlighted in some cases. An overview of the common macro-models for numerical simulation of RM shear walls is presented in Figure 2.4.

Comparison of the results from the analysis of the walls subjected to both monotonic and reversed cyclic loading protocols with the corresponding test data showed the efficiency of some of the proposed modelling approach as well as their drawbacks. Results showed that some models could consider both stiffness and strength degradations. Moreover, the proposed models are often able to capture the strain histories of the concrete and steel reinforcement with an acceptable level of accuracy.
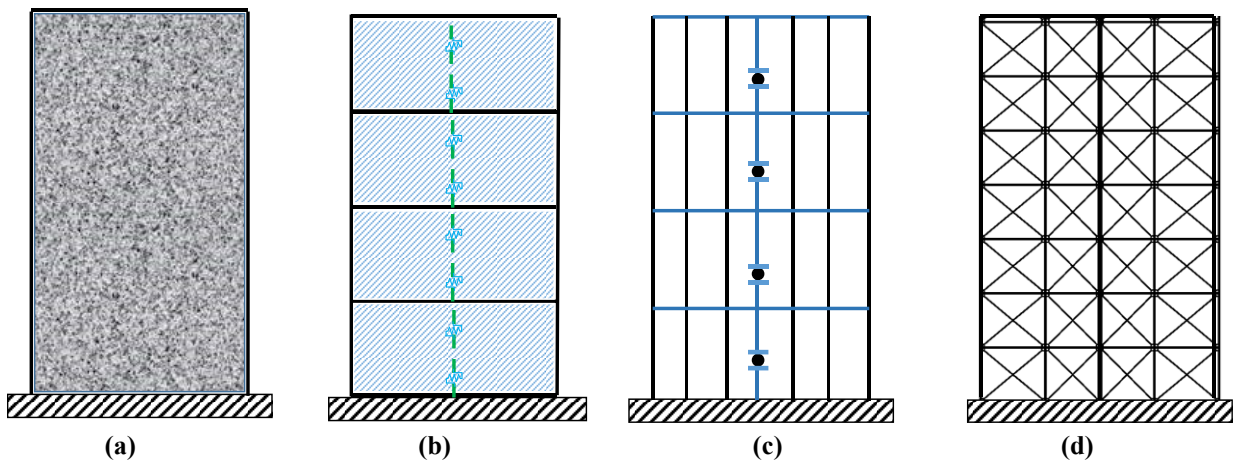
Figure 2.4. Overview of available macro modelling approaches: (a) A typical RM shear wall, (b) Wide column model (Millard, 1993), (c) Multiple vertical line element model (Vulcano et al., 1988), (d) Truss model (Panagiotou and Restrepo, 2011)

2.4   Behaviour of End-Confined RM Shear Walls

There has been a broad application of the RM shear walls with various end configuration in the recent decades (Shedid et al., 2010b, Aly and Galal, 2020); however, their cyclic response is not well known and discussed by both practice codes and research which highlight the importance of studying the behaviour of such elements more meticulously. It is worth noting that shear walls with flanges are naturally formed because of having perpendicular lateral load resisting walls. However, most of the practicing engineers typically, and conservatively, neglect the effect of the flanges, assuming two separate walls in the design without any influence on their counterpart's lateral resistance and stiffness.

In ductile masonry structural walls governed by flexural failure, a plastic hinge mechanism will form whereby inelastic rotations are concentrated at the base of the wall. The plastic hinge

zone represents the part in which the inelastic rotation of the shear wall is happening and needs more attention in terms of design and detailing since it is a critical section of the shear wall. Estimation of the plastic hinge region for RM structural wall design has been derived from the analysis of RC shear walls. The results of RC beams were used to propose a plastic hinge length (Mattock, 1967) in terms of wall parameters, which was modified by Paulay and Uzumeri (1975), who recommended two specific equations for application with RC walls, based on the height (h_w) and length (L_w) of the wall. Later, Paulay and Priestley (1992) suggest a range of values based on reinforcement and proposed equations for RM walls to relate the plastic hinge with the wall dimensions and reinforcing bar properties such as its diameter (d_b), yield strength (f_y) and ultimate strength (f_u). Lastly, Bohl and Adebar (2011) proposed a lower bound estimation for the isolated shear walls correlating it to the axial stress imposed on the wall element $(P/f_c'A_g)$.

$$(0.2l_w + 0.05h_w)(1.0 - 1.5P/f_c'A_g) \leq 0.8l_w \qquad \text{Bohl and Adebar (2011)} \qquad (2.1)$$

To develop significant displacement ductility, damping and overall energy dissipation required to resist strong ground motions in RM shear wall buildings, the plastic hinge zone must be capable of withstanding relatively high inelastic curvatures. The plasticization of RM shear walls is generally characterized by the cracking of masonry components and the yielding of vertical reinforcement. Whenever all vertical tension reinforcement within the wall cross-section develops its yield strength, it can be shown that the nominal flexural capacity (M_n) of the wall remains nearly constant. As strains in the reinforcement are increased, wall curvature will also increase, which can be determined from strain compatibility assuming plane section analysis. Subsequently, as the moment is increased to the maximum capacity of the wall, the neutral axis will shift and based on force equilibrium, much higher strains in the reinforcement will be achieved, resulting in an increased curvature. Beyond this point, there will be minor changes to the nominal flexural capacity (M_n), as well as depth of neutral axis, but the curvature keeps increasing until an ultimate strain in the reinforcement (ε_{su}) or masonry (ε_{mu}) is reached. As yield strains begin to form in the vertical reinforcement, it will gradually spread over the plastic hinge region of the walls, as shown in Figure 2.5.

|(RM shear wall's elevation)|(Curvature profile of RM shear wall)|
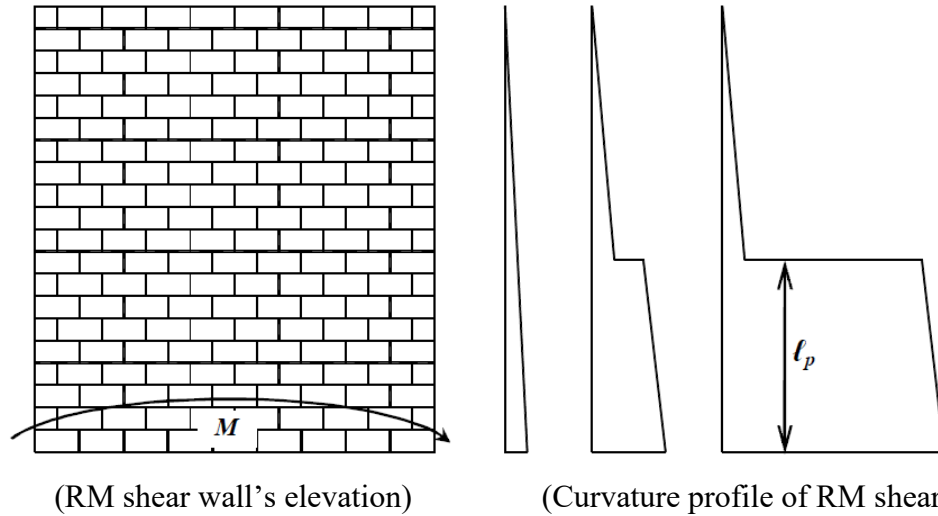
Figure 2.5. Inelastic curvature spreading over shear wall plastic hinge length (Banting, 2013)

The wall curvature capacity strongly influences the displacement capacity and displacement ductility. Curvature may be limited in an RM shear wall by tensile strains in the reinforcement associated with fracturing failure of the reinforcement. However, it is more likely to be governed by the compressive strain capacity of masonry, ε_{mu}. This phenomenon will stress the fact that by using confinement in the masonry shear walls, the curvature capacity and thus the overall capacity and ductility level can be enhanced. Priestley and Elder (1982) tested three scaled slender RMSW with an aspect ratio of 2.5. The test by Priestley and Elder (1982) studied the impact of axial stress and confinement plate at the mortar bed joints. High levels of strength and stiffness degradation were reported as a result of increasing the axial stress. The wall ductility significantly enhanced by using the steel confinement plates. More recently, Ahmadi (2012) tested 21 shear wall specimens as both cantilever and fixed-fixed elements along with two full-scale masonry buildings on a shake-table. A wide range of various aspect ratios was considered along with a different level of axial load levels. Ultimate drift levels were reported to fluctuate from 1.31% to 4.47%, with average displacement ductilities from both directions of loading that were found to range from 4.66 to 17.04. The research program concluded the fact that displacement-based design for use on masonry structures yields more reliable results in terms of ultimate and serviceability limit states and suggested that was a better approach towards the design of irregular structures when force-based procedures could not be applied.

To address the limited compressive strain of the masonry, Priestley (1976) and Priestley and Elder (1982) introduced steel confinement plates in the bed joints of the compression toes in RM structural walls. There has been a couple of efforts in the literature to address the impact of confining masonry elements to enhance the performance of the RM shear walls, which some of them are highlighted in the following.

As one of the first efforts, Bresler and Gilbert (1961) found that lateral stirrups around vertical reinforcement in RC columns can inhibit and delay the tendency for vertical reinforcement to buckle under compressive stress. The potential for inelastic buckling of reinforcement in the plastic hinge zone of RC columns has been extensively studied by Pantazopoulou (1998), Moyer and Kowalsky (2003) and Berry and Eberhard (2005) leading to detailed prescriptive requirements for RC columns as well as structural walls. The proposed detailing requires the end of the shear walls to incorporate confined zones containing a minimum of two layers of reinforcement with lateral confinement stirrups. One of the earliest means to confine masonry shear walls were stainless steel plates placed on the mortar bed on the face shell and web of the units. Tests on structural walls detailed with confinement plates were first conducted by Priestley and Bridgeman (1974) in brick walls and later by Priestley (1976) and Mayes et al. (1976) in concrete block walls and piers, respectively. In these early tests, it was observed that the confinement plates acted as a mechanism to delay the vertical splitting tension failure of the compression toes, thus increasing the effective compressive strain of the masonry. Tests on a series of walls and prisms reported by Priestley and Elder (1982) and Priestley and Elder (1983) were used to evaluate the design characteristics necessary to predict confined wall behaviour. It was suggested that a modified Kent-Park stress-strain relationship, adopted from concrete behaviour, could be used to estimate the confining effects on the masonry.

To investigate the behaviour of RM structural walls possessing different end configurations, Shedid et al. (2010a) tested seven fully grouted RM structural walls constructed of half-scale block units. This test program was aimed at comparing the seismic behaviour of walls with three different end configurations: a conventional rectangular wall cross-section, a flanged wall and a wall with confined boundary elements at its ends. The three walls detailed with a confined boundary element at the ends allow for four vertical reinforcement bars placed in two layers and confined with steel reinforcement stirrups placed in every course. Tests of boundary element prisms reported by

14

Shedid et al. (2010b) indicated an increase in the compressive strain by 51% over unreinforced and unconfined boundary elements. Shedid et al. (2010a) reported that an increase in ductility of at least 39% and 106% was achieved in walls with the addition of flanges and confined boundary elements, respectively. Additionally, the measured drift for rectangular, flanged and boundary element wall configurations at a drop of 20% from peak load was observed to be at least 1.0%, 1.5% and 2.0% drift, respectively.

2.5   Design Provisions for RM Shear Walls

A research done by Shibata and Sozen (1974) proposed that structures that contain multiple degrees-of-freedom under dynamic excitation could be represented by an SDOF substitute structure possessing similar stiffness, strength, and displacement capacity properties to the more complex structure. Moreover, since only the stiffest elements within a structure are expected to resist seismic loads, the structure can be represented solely by its seismic force resisting system (SFRS), which for masonry structures is the structural wall system. Hence, proper detailing must be provided in the structural walls to permit the required ductility-based reduction factor of seismic force. Ensuring a flexural failure mechanism governs structural wall behaviour rather than a more brittle shear failure is one means of providing the necessary ductility and is the foundation of the capacity design philosophy proposed by Park and Paulay (1975). NBCC (2015) recommended about 30 recognized seismic force resisting systems (SFRS), which can ensure energy dissipation within sufficient ductile response. The NBCC assigns two seismic force "R" modification factors by which the elastic seismic force can be reduced by the factor, which is related to the ductility of the SFRS, R_d, and the second factor is based on the ratio of the anticipated overstrength of the SFRS, R_o. The detailing requirements of each SFRS should be consistent with the associated code of design set by the relevant materials' design standard, which is, for example, the CSA S304.14 for masonry structures (CSA 2014). A higher value of R_d typically requires more stringent detailing and more complex design provisions to corroborate a safe design with enough ductility and safeguard against the abrupt failure of the structure. The elastic force-based method exercising the equal displacement assumption is employed in the Canadian code of practice as well as the American Society of Civil Engineers (ASCE) building code ASCE 7-16 (2016). On the other hand, a masonry SFRS is made of several structural walls acting together. Therefore, it is necessary for each component to comply with the design code criteria to ensure enough ductility and/or drift

capacity for the overall system. The recent RM structural wall construction in seismically active areas of Canada generally requires concrete block units, fully grouted and detailed with horizontal and vertical steel reinforcement. This is very similar to RC structural wall construction with regards to material behaviour and analysis of strength and displacement whereby RC structures are provided with three levels of ductility (i.e., limited, moderate, and ductile shear walls).

However, NBCC recently added a new level of ductility (ductile RM shear wall with R_d=3.0 and R_0=1.5) for RM shear wall buildings in the latest edition. It is worth noting that CSA S304 has limited regulation regarding the design of RM shear walls with end-confined zones and flanged walls. There is also a lack of research to evaluate the value of R_d and R_0 for this type of SFRS. Comparing the force modification factors of RM shear walls with RC shear walls, the value of R_d=3.5 and R_0=1.6 are assigned for the ductile RC shear wall structures (NBCC 2015). Furthermore, in a recent study by the National Institute of Standards and Technology (NIST) GRC 10-91-8 (2010), it was noted that both special RC and RM wall categories equally satisfied collapse prevention criteria following nonlinear dynamic analysis. In conclusion, the level of inelastic deformation capacity of masonry structures is recognized in the U.S.A. as being capable of an equal performance with RC, when similar restrictive prescriptive requirements are applied. Therefore, it is inferred that RM and RC structural wall systems could each be assigned somehow the same levels of $R_d R_o$ proposed by the NBCC, following the fact that a sufficiently conservative and thorough set of prescriptive requirements that include, for example, confinement of the masonry is fully met.

2.6   Performance-Based Seismic Design and Resilience of RM shear walls

By the advent of the Structural Engineers Association of California (SEAOC) Vision 2000 document (SEAOC 1995), a growing emphasis is being placed on the building level, rather than materially based or structural element level performance. Eventually, this will lead to a shift away from using the current qualitatively assessed force-based response modification factors towards performance-driven designs based on several factors that may include more relevant critical aspects such as life safety, the extent of damage, and rehabilitation costs.

It has been suggested that the current elastic force-based design methodology employing the equal displacement assumption and using fixed material-based seismic force modification factors

will produce widely variable results between otherwise identical SFRS when aspects such as repair costs and drift-based damage are considered (Nassar and Krawinkler 1991, Priestley 2000). Priestley et al. (2007) also describes several inconsistencies associated with using an elastic approach to design, such as period elongation from reduced wall stiffness with increased top drifts, increased damping shown by walls which have cracked or reinforcement that has yielded and system-level effects on component behaviour, which tend to be overly simplified or completely neglected. Quantifying the level of damage sustained by a structure can be related to peak displacement (drift) demands. For instance, Park and Ang (1985) expressed the damage of RC elements based on historical observations in terms of a damage index. It was observed that the extent of damage sustained in RC elements after seismic events could be related to both the level of peak drift as well as absorbed hysteretic energy by the system. It has been observed in studies by Li and Weigel (2006) and Murcio-Delco and Shing (2011) that experimentally tested RM walls sharing the same failure mechanisms could be related by their damage performance via peak lateral drift sustained during loading cycles. Therefore, drift and damage, rather than force, would be a better measure of earthquake resistance and performance.

There have been many advancements in understanding the inelastic response of RM Shear Walls (RMSW) in recent decades. This understanding is a pledge for the performance-based seismic design of the structures. The performance-based seismic design incorporates a specific performance level corresponding to the level of damage that occurred in the structure (FEMA 445, 2006). The methodology correlates the damage state to a specific functionality level and losses of the whole system when the structure is prone to seismic events. These definitions form the framework of the seismic resilience of a structure, which declares the level of functionality of a structure in the aftermath of the unwanted seismic event. The concept of resilience also shows the capability of a system to resist and maintain its functionality during and after an unwanted event (i.e., flood, earthquake, fire, etc.) (Bruneau et al., 2010). To assess the resilience of a structure against seismic events, fragility functions need to be precisely derived after performing collapse assessment (FEMA P-58). Fragility functions have been used in the past for different applications (ATC-13), where they correlate an engineering demand parameter (EDP) to the probability of collapse at a specified damage level (Hwang and Jaw, 1990). These functions are necessary for predicting the level of damages and losses to evaluate seismic resilience. Deriving fragility

functions is possible through performing collapse assessment, which can be done by following the available guidelines in the literature (FEMA P695, P-58, and ATC-13).

The risk of economic losses due to natural disasters (e.g., earthquakes, flood, etc.) is correlated with the state of building performance. Both system vulnerability and hazard are conditioning parameters. In an extended approach, other causes of disaster risk are demographic and sociopolitical. In general, vulnerability originates in physical fragility systems designed and built prior to modern codes (Bankoff et al., 2004). These are also characterized by a lack of resilience which is defined by the ability of the system "to reduce the chances of a shock, to absorb such a shock if it occurs and to recover quickly after the shock" (Bruneau et al., 2003). Seismic resilience describes the loss and loss recovery required to maintain the functionality of the system with minimum interruption (Cimellaro et al. 2006). The resilience also takes the impact of the recovery process, including the behaviour of individuals and organizations in the post-disaster phase into account. In order to quantify the seismic resiliency of structures, the alphabet of structure functionality needs to be properly defined. Loss and recovery time are estimated with respect to the fragility assessment in order to calculate the remaining functionality of the structure after an earthquake event. The resiliency function can be found as the area underneath the functionality curve, which is defined analytically as per Eq. 2.2.

$$R = \int_{T_{0E}}^{T_{0E}+T_{LC}} Q(t)/T_{LC}\,dt \qquad\qquad (2.2)$$

where the functionality, $Q(t)$, ranges from 0 to 100% meaning total loss and no reduction in the performance, respectively. If an earthquake happens at time T_{0E} it could cause enough damage to the structure and reduce its performance. Subsequently, within a period called recovery period, T_{RE}, the system will be able to recover itself to the same functionality level prior to the extreme event, which is observed over a control time period, T_{LC}.

2.7   Summary and Conclusions

RM shear walls are best known as efficient lateral resisting systems in buildings because of their high stiffness and their high flexural and shear capacities. Many studies have been carried out to investigate the structural response of RM wall systems with different geometries. However, investigation of the nonlinear response of non-planar RM walls integrating different end shape

18

condition is still necessary. Moreover, continuous advancements in seismic design codes and regulations and deterioration of existing RM structures are two major reasons for the necessity of performance-based and resilience-based design of shear wall structures. In this respect, different end configurations of the RMSW buildings have been proposed, but reliable means of estimating the behaviour of RM shear walls are required to choose the most effective approach. Therefore, numerical studies need to be conducted to assess the required design equations and the most efficient configuration of the walls.

Chapter 3

Numerical Investigation and Collapse Evaluation of Reinforced Masonry Shear Wall Systems

3.1   Seismic Collapse Evaluation of Reinforced Masonry Core Wall Systems

3.1.1   Abstract

Since the 20th century, several experimental and analytical studies have been conducted to evaluate the seismic response of RMSW element and system (i.e., building consisting of planar walls). However, research on RM core wall systems is scarce, especially considering the torsional effects on the system's seismic inelastic response. A core is a structural element with a cellular section that is typically closed on three sides and is either open or partially closed by coupling beams on the fourth side. In the current study, a five-storey building, designed according to the National Building Code of Canada (NBCC 2015) and the Canadian Standards Association (CSA) S304-14, was considered to assess the seismic performance and collapse capacity of RM core wall systems. SeismoStruct software package was used to model the building numerically. The nonlinear model is validated against experimental data of an asymmetric RM building. Collapse risk evaluation has been conducted for reliable design of RM cores within the context of FEMA P-695 by subjecting the mentioned building's numerical model to various ground motions scaled at different intensity levels. This study is proposing RM Core wall system as a reliable alternative seismic force resisting system. It also contributes to better understanding and quantification of its seismic response and collapse capacity.

3.1.2 Introduction

In the past few decades, there has been considerable advancement in understanding the RMSW response under lateral loading. Several experimental and analytical studies focused on studying the seismic performance of RMSW elements (e.g., Dhanasekar et al., 2002, Wang et al. 2016, and Beyer et al. 2008). However, previous research studies addressed rectangular shear walls, and based on the literature, no research considered the RMSW core system. More recently, RMSW was introduced in high-rise buildings, which reached up to 28 stories in China (Wang et al. 2016). The available space around the elevator service area is an optimum region to place the core wall system, similar to the common practice in reinforced concrete structures. The need for access to the lift and other services requires an open section to be applied, (i.e., a C-shaped element). This opening is partially closed by spandrel or slabs connected along each floor level.

Although reinforced concrete core walls are very popular in practice, their inelastic behaviour under seismic loading has not been examined in detail. There is a limited number of experimental studies on the cyclic response of C-shaped walls, e.g., Beyer et al. (2008). Unlike rectangular walls, which only resist lateral loads in one direction, C-shaped walls provide lateral stiffness in both loading directions and possess torsional stiffness.

In this study, a comparison was made between the seismic response of three individual rectangular RMSW connected using the rigid floor diaphragm and a C-shaped wall having similar overall dimensions. A 5-storey building is used to simulate a mid-rise building with RMSW. The rectangular walls were assembled using rigid links, with the master nodes being at the center of the wall. In addition, different torsional sensitivities have been considered as per NBCC 2015, to investigate the effect of torsion on the seismic response of the core wall system.

The nonlinear numerical model was first validated against the experimental results of the 2-storey building tested by Heerema et al. (2015). The building had rectangular and flanged shape RMSW. Furthermore, quantification of the seismic performance of RM cores has been conducted within the context of FEMA P-695 (2009). This is achieved by subjecting the reference building to various ground motions scaled at different intensity levels. Finally, the seismic collapse risk of the RM core system was assessed in terms of fragility curves considering different torsional sensitivities.

3.1.3 Building Layout

The archetype building selected in this study, shown in Figure 3.1, is a 5-storey RMSW building. The overall building height is 19.45 m, with a first-floor height of 4.85 m and a typical floor height of 3.65 m. The floor is 18 m x 18 m and is built using a 200mm thick pre-stressed hollow core concrete slab. Two C-shaped walls are located close to the building's center of mass. Each wall consists of two 3 m flanges and a 6 m web with a thickness of 250 mm. The columns are made up of reinforced masonry blocks with a dimension of 400 mm x 400 mm. The dimension, spacing, and cross-section details of the walls and columns are summarized in Table 3.1.

(a)   (b)
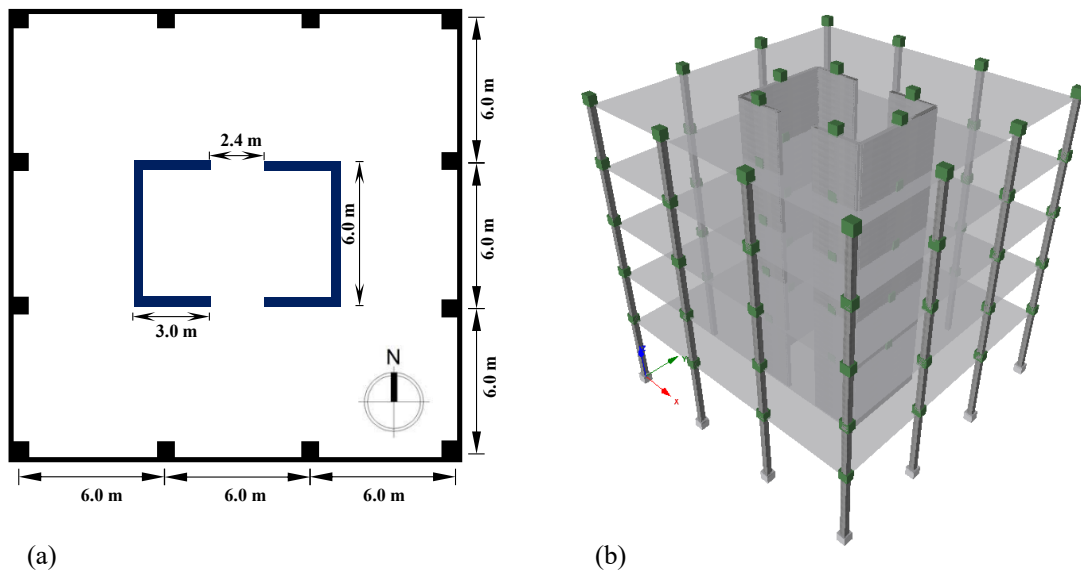
Figure 3.1. Archetype Building with C-shaped Walls: (a) Typical Floor Plan View; (b) 3-D Layout

Table 3.1. Archetype Building with C-shaped Walls: (a) Typical Floor Plan View; (b) 3-D Layout

Element type	Element ID	Type	Typical height (mm)	Web length (mm)	Flange length (mm)	Aspect ratio (shorter wall)	Vertical reinforcement φ_v (mm)	ρ_v (%)	Horizontal reinforcement φ_h (mm)	ρ_h (%)
Wall	W1,2	C-shaped	3650	6000	3000	1.22	15	0.15	15	0.4
Column	C1	RM Column	3650	400	400	-	20	1.00	10	0.063

3.1.4 Torsional Sensitivity

The structural system response to earthquake loads can include torsional forces due to the eccentricity between the Center of Mass (CM) and the Center of Rigidity (CR). In NBCC 2015, this concept is defined as inherent torsion. The uncertainties related to the position of CM and CR induce an additional seismic moment called accidental torsion. NBCC 2015 recommends a limit for classifying the torsional sensitivity of structures. The limit is based on the torsional sensitivity parameter (B), which is defined at each level, (B_x), as $\delta_{max}/\delta_{ave}$. In the equation, δ_{max} is the maximum storey displacement at the extreme point of the structure at level x induced by the equivalent static forces with accidental eccentricity, and δ_{ave} is the average displacement at the extreme points of the structure at level x produced by the above forces. According to NBCC 2015, as the value of B exceeds 1.7 and $I_E F_a S_a (0.2) > 0.35$, the building is called torsional sensitive. In this case, a 3-D dynamic analysis is mandatory for evaluating the response of the structure.

In this study, the torsional sensitivity was defined as per NBCC 2015. Three levels of torsional sensitivity (i.e., B = 1.0, 2.1 and 2.5) were considered to cover the expected range of eccentricities in buildings with core walls. This allows having a comprehensive and realistic assessment of the proposed structural system with core walls for RM buildings. The torsional sensitivity levels were achieved by shifting the CM from the CR by a certain eccentricity. The amount of eccentricity was estimated based on an iterative procedure by analyzing the structure against the design earthquake lateral forces based on NBCC 2015. The nonlinear dynamic analyses and collapse fragility assessment of the archetype building were performed at the three torsional sensitivity levels.

3.1.5 Masonry Wall Model

SeismoStruct package was used to conduct all analyses of the RMSW systems. Inelastic displacement-based beam-column fibre elements were used to model the RMSW. Different material models were assigned to the fibres to resemble the reinforcement and masonry cyclic response. Based on sensitivity analysis, it was found that the number of fibres needed in the cross-section discretization is 300 for walls and 200 for the columns. It is worth noting that increasing the number of fibres does not necessarily yield more accuracy. On the contrary, using too many fibres can negatively affect the result of analysis and increase the error if not carefully utilized.

All walls are assumed to be fixed at the base and the soil-structure interaction was neglected as per NIST (2010) recommendations.

Two uniaxial stress-strain relations were utilized to model the behaviour of the RMSW; one for the masonry and another for the reinforcing steel. The nonlinear steel model of Menegotto and Pinto (1983) is implemented with the modification of isotropic strain hardening presented by Filippou et al. (1983). A Young's modulus (E_s) of 200 GPa, a yielding strength (f_y) of 495 MPa, and a strain hardening ratio of 0.01 have been considered in modelling the reinforcement. It should be noted that these material properties are as reported by Hereema et al. (2015) and were only used in the nonlinear modelling validation. A yielding strength of 400 MPa was used in the design (i.e., as per the design code CSA S304-14 requirements) and analyses of the archetype building. The masonry behaviour was modelled based on the constitutive model proposed by Mander et al. (1988). The specified masonry compressive strength (f'_m) was assumed to be 18 MPa, and the elastic modulus (E_m) was calculated according to CSA-S304-14 (i.e., $850 f'_m$).

3.1.6   Model Validation and Calibration

Verification of the model predictions with a two-storey asymmetric RMSW building tested by Heerema et al. (2015) is presented in Figure 3.2. The same loading protocol used for the experimental program was implemented to compare the numerical and experimental hysteretic response. Figure 3.2 shows a comparison between the experimental and numerical hysteresis loops for the building. As shown in Figure 3.2, the model captures the experimental response with an acceptable accuracy with a maximum difference of 16% in the prediction of lateral force. In general, the model could capture both the elastic and inelastic response of the RM shear walls.
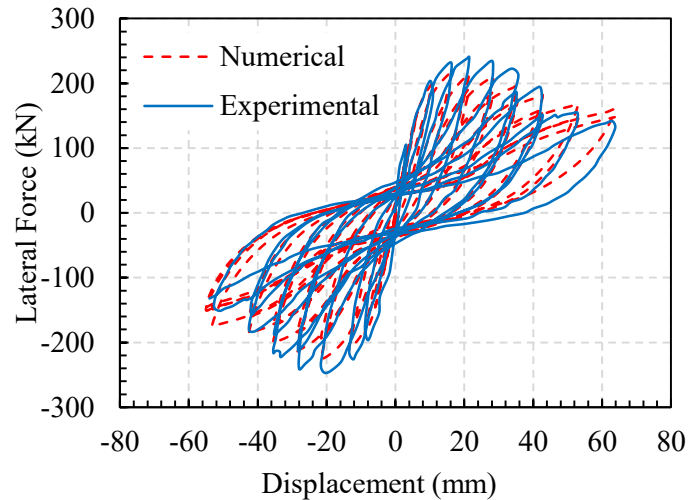
Figure 3.2. Numerical Model Validation

3.1.7 Seismic Collapse Evaluation of RM Core Walls

The seismic behaviour of the archetype building was investigated in the moderate seismic zone of eastern Canada, Montréal, Quebec (Assatourians and Atkinson 2010). The walls are founded on site class C, which represents very dense soil.

The seismic collapse evaluation methodology is based on FEMA P695 (2009), which consists of first establishing the seismic performance of the studied building using nonlinear static pushover and dynamic analyses. Afterwards, adjusting the nonlinear dynamic analyses results to explicitly consider uncertainties in ground motion, design, test data, and modelling. Finally, using the adjusted results, seismic collapse fragilities are established to assess the collapse risk of the archetype building.

3.1.7.1 Static Pushover analysis

The calibrated nonlinear model was utilized to perform pushover analysis in order to estimate the lateral force and deformation capacity of the archetype building. Pushover analysis was conducted according to FEMA P695 (2009) using a lateral load distribution proportional to the fundamental mode shape. The results were used to establish the capacity curves depicted in Figure 3.3 for the archetype building utilizing three rectangular walls and a C-shaped wall. The predicted lateral force capacity was found to be in good agreement with design capacity based on CSA S304-14.

25

Comparing the capacity curves shown in Figure 3.3, the initial stiffness values were almost identical for the C-shaped and rectangular walls. However, utilizing C-shaped walls significantly increased the lateral load capacity. In addition, the results showed an increase in the ultimate displacement and ductility capacity of the C-shaped walls compared to that of the rectangular walls.
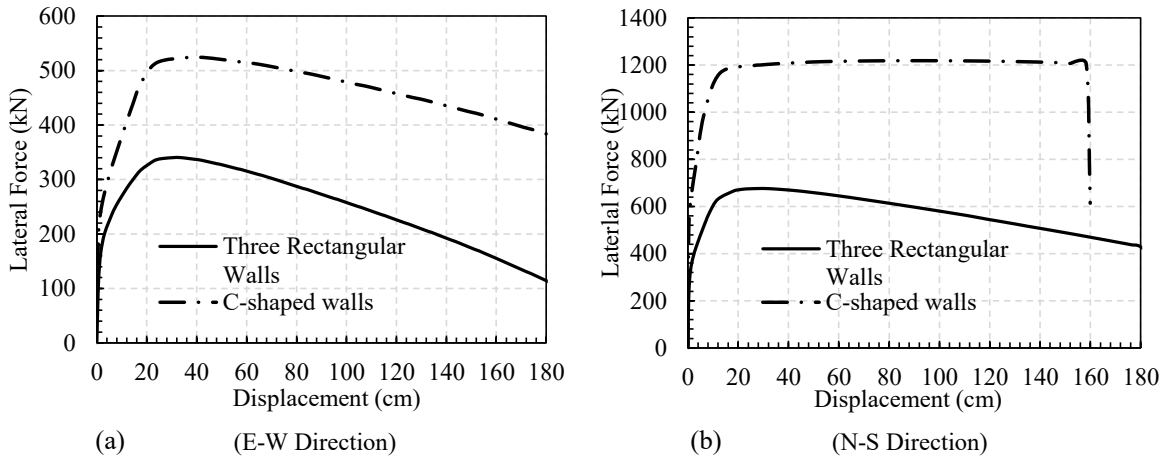
Figure 3.3. Pushover Curves: (a) E-W Direction; (b) N-S Direction

Spectral shape factors (SSF) are introduced by FEMA-P695 (2009) to adjust seismic collapse margin ratios and account for the elongation of the natural period prior to collapse. SSFs can be found in Table 7-1 of FEMA-P695, depending on the fundamental period and period-based ductility. Pushover analysis results were used to estimate the archetype building period-based ductility. The period-based ductility factor for a given structure (μ_T) is defined, as shown in Eq. (3.1), as the ratio of ultimate roof drift displacement (δ_u) to the effective yield roof drift displacement ($\delta_{y,eff}$).

$$\mu_{\mathrm{T}} = \frac{\delta_u}{\delta_{y,eff}} \tag{3.1}$$

The effective yield roof drift displacement is calculated using Eq. (3.2) according to FEMA-P695 (2009)

26

$$\delta_{y,eff} = C_0 \frac{V_{max}}{W} \left[\frac{g}{4\pi^2} \right] [\max(T,T_1)]^2 \tag{3.2}$$

Where C_0 relates fundamental-mode (single degree of freedom) displacement to roof displacement, V_{max}/W is the maximum base shear normalized by the building weight, g is the gravity constant, T is the fundamental period of the structure based on an empirical formula and T_1 is the fundamental period of the model computed using eigenvalue analysis.

The values of Period-based ductility are tabulated in Table 3.2, ($\mu_{T\,Rect.}$) for the archetype building using three individual rectangular walls, and ($\mu_{T\,C-Shaped}$) for the C-shaped configuration. It is evident that there is a clear increase in ductility as a result of using the C-shaped walls.

Table 3.2. Period based Ductility Factors

$\mu_{T\,Rect.}$	4.76
$\mu_{T\,C-Shaped}$	12.15

3.1.7.2 Incremental Dynamic Analysis

In this study, the dynamic response of the RM core wall building was determined using Incremental Dynamic Analysis (IDA). This dynamic analysis method was introduced by Vamvatsikos and Cornell (2002). In this method, the structure is subjected to a series of Nonlinear Response History Analyses (NLRHA) with increasing the intensity of the ground motions until the collapse of the structure occurs. IDA allows a complete assessment of the structure's response and properly captures the higher modes of vibration contribution to the buildings' dynamic behaviour. The intensity measure (IM) chosen in this study is the spectral acceleration (5% damping) at the fundamental period of the structure (T) specified as S_a (T, 5%). T is calculated based on the empirical formula provided in NBCC 2015. The analysis results are used to construct the IDA curves which relate the IM and the Engineering Demand Parameter (EDP). The chosen EDP in this study is the inter-storey drift ratio (IDR_{max}).

Several ground motions were selected and scaled to perform the NLRHA. A set of 22 simulated records from Assatourians and Atkinson (2010) were used to obtain Canadian design response spectrum-consistent motions for the considered region (i.e., Montréal, Quebec). The

characteristics of the selected ground motions reflected the seismicity in the region of eastern Canada, as described by Assatourians and Atkinson (2010). The selected time histories had magnitudes ranging between 6 and 7 for site class C and epicentral distance ranging between 15 and 100 km. The ground motion records are scaled based on the ratio between the design spectral acceleration $S_a(T)$ and the geometric mean spectral acceleration (S_{gm}) of each pair. The geometric mean is calculated using Eq. (3.3).

$$S_{gm}(T) = \sqrt{S_x(T)S_y(T)} \tag{3.3}$$

S_x and S_y are the orthogonal components of spectral acceleration at period T. The scale factor is calculated at T= 0.56 s, which is the average fundamental period of the orthogonal directions of the building. The scaled ground motions are then used in the IDA.

3.1.8 Seismic Collapse Risk Evaluation

To establish the collapse fragility curves, IDA results were used to determine the intensity of each ground motion, which causes the structure to collapse. The collapse probability at each IM was estimated as the number of records causing collapse divided by the total number of records. In this study, the collapse criteria of the RM core walls are defined based on the inter-storey drift limits. According to FEMA P695 the collapse of the structure occurs when a certain limit of drift is exceeded and is referred to as EDP-based rule. ASCE41 (2013) adopts the maximum inter-storey drift ratio to assess the level of damage in structural elements and SFRS. To be consistent with the ASCE41 (2013) guidelines, the collapse point is set to 2.5% inter-storey drift ratio, which corresponds to the collapse prevention performance level of NBCC 2015. The calculated collapse probabilities were then used to construct the collapse fragility curve, which is a plot that relates the probability of collapse to the ground motion intensity.

A cumulative distribution function has been recommended by the FEMA P695 to generate fragility functions based on a log-normal probability distribution. Eq. (3.4) illustrates the probability distribution function.

$$P(C \,|\, IM = x) = \phi(\frac{\ln(x/\theta)}{\beta}) \tag{3.4}$$

Where $P(C|IM = x)$ is the probability of collapse at a given intensity, ϕ is the standard normal cumulative distribution function, θ is the collapse median intensity or the intensity level with 50% probability of collapse, and β is the standard deviation (dispersion) of IM. The fragility function parameters were found using the maximum likelihood method by Baker (2015).

The collapse fragility curves for the archetype building in N-S direction utilizing three rectangular walls and C-shaped walls with the three torsional sensitivity levels is shown in Figure 3.4.
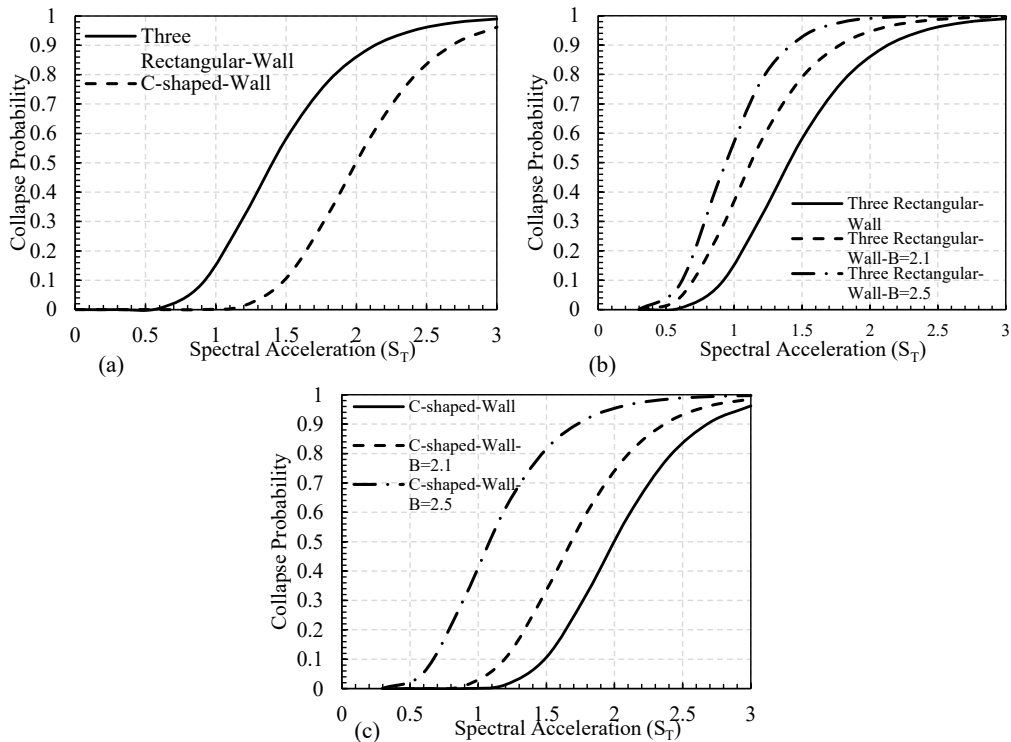
Figure 3.4. Collapse Fragility Curves: (a) C-shaped vs Three Rectangular Walls (b) Three Rectangular Walls with Different Torsional Sensitivity Levels (c) C-Shaped Walls with Different Torsional Sensitivity Levels

Figure 3.4a shows that the use of C-shaped walls resulted in a higher collapse spectral intensity ($\hat{S}_{CT}$) compared to the use of rectangular walls. The justification of this finding is because of the contribution of the effective flange width on enhancing the ultimate curvature of the walls. The larger ultimate curvature of the walls with the C-shaped configuration delayed the collapse and thus resulted in reducing the collapse risk under high seismic loads. Figure 3.4b and Figure

3.4c compares the fragility curves of different torsional sensitivity levels. As shown, the torsional sensitivity can significantly affect the collapse fragility curves. Using the collapse fragility curves, the median collapse capacity ($\hat{S}_{CT}$) is evaluated as the 5% damped spectral acceleration corresponding to a 50% probability of collapse. The median collapse intensity ($\hat{S}_{CT}$) of the RM core system decreased by approximately 20% when torsional sensitivity parameter (B) is equal to 2.1. The reduction in median collapse capacity was more than 75% when B is 2.5, in comparison with the one with no torsional sensitivity (i.e., $B = 1$).

The Collapse Margin Ratio (CMR) is calculated using Eq. (3.5) as the ratio between the median collapse intensity ($\hat{S}_{CT}$) and the Maximum Considered Earthquake (MCE) intensity (S_{MT}). CMR is a principal parameter used to characterize the collapse safety of the structure.

$$CMR = \frac{\widehat{S}_{CT}}{S_{MT}} \tag{3.5}$$

The estimated SSFs are multiplied by the calculated CMRs to account for the elongation in the natural period prior to collapse and calculate the Adjusted Collapse Margin Ratio (ACMR). The calculated ACMR values are then compared with the allowable values proposed by FEMA-P695 which are introduced in terms of the total system uncertainty (β_{TOT}). The total system collapse uncertainty is a function of record-to-record uncertainty (β_{RTR}), design requirements related uncertainty (β_{DR}), test data related uncertainty (β_{TD}) and modelling uncertainty (β_{MDL}). This value is computed using Eq. (3.6).

$$\beta_{TOT} = \sqrt{\beta_{RTR}^2 + \beta_{DR}^2 + \beta_{TD}^2 + \beta_{MDL}^2} \tag{3.6}$$

Table 7-3 of FEMA-P695 provides acceptable values of Adjusted Collapse Margin Ratio, ACMR$_{10\%}$ and ACMR$_{20\%}$, based on total system collapse uncertainty, considering values of acceptable collapse probability at MCE to be 10% and 20%, respectively. The value of β_{TOT} was calculated to be 0.725, assuming the values of the different uncertainty parameters, as shown in Table 3.3.

Table 3.3. Uncertainty Parameters

Uncertainty Parameter	Value
β_{RTR}	0.4
β_{DR}	0.35
β_{TD}	0.35
β_{MDL}	0.35
β_{TOT}	0.725

Table 3.4 summarizes the seismic collapse performance parameters of the archetype building considering the three rectangular walls or the C-shaped wall for the torsional sensitivity of $B = 1.0$. ACMR$_{10\%}$ is shown as an acceptance criterion. Ensuring calculated ACMR is higher than ACMR$_{10\%}$ reflects that the structure's probability of collapse at MCE is lower than 10%.

Table 3.4. Summary of Collapse Performance Evaluation of RM Shear Walls

Shear Wall Configuration	$\hat{S}_{CT}$	CMR	SSF	ACMR	ACMR10%
Three rectangular walls	1.3	4.44	1.36	6.04	2.53
C-shaped wall	2.0	6.83	1.36	9.29	2.53

The calculated ACMR values for both rectangular and C-shaped walls are satisfying FEMA P695 acceptance criteria. However, there is more than 50% increase in the ACMR when the C-shaped wall is utilized. This is attributable to the contribution of the effective flange wall width in improving the inelastic response of the shear walls

3.1.9 Conclusion

The current study evaluated the seismic collapse risk of a 5-storey RM core wall building. It demonstrated the significant enhancement in overall response when utilizing C-shaped walls compared to three individual rectangular walls. Nonlinear pushover analysis was conducted to evaluate the capacity and period-based ductility. The results showed that by using C-shaped walls instead of the individual walls, the ultimate curvature increased due to the contribution of the effective length of the flange. Thus, it resulted in higher values of ductility and ultimate capacity for the C-shaped walls. The lateral capacity of the structure increased by 45% in N-S direction and by 55% in the E-W direction. Furthermore, the utilization of the C-shaped wall resulted in a 190% increase in the period-based ductility of the building.

The seismic collapse fragilities demonstrated that the C-shaped walls had a greater seismic collapse capacity and a lower probability of collapse compared to rectangular walls. The results showed more than 50% increase in the Adjusted Collapse Margin Ratio when the C-shaped walls were used. This reflects a substantial improvement in the overall seismic performance when utilizing C-shaped walls. Furthermore, it was evident that torsional sensitivity can significantly affect the fragility function of C-shaped and rectangular walls. It resulted in up to 20% and 75% reduction in seismic collapse capacity for torsional sensitivity levels of B=2.1 and B=2.5, respectively. In addition, increasing the torsional sensitivity leads to steeper fragility curves reflecting higher collapse probabilities.

3.2 Enhancing the Seismic Resilience of Existing Reinforced Masonry Shear Wall Building by Incorporating Boundary Elements

3.2.1 Abstract

In this research work, a framework for the seismic collapse assessment of existing Reinforced Masonry (RM) Shear wall building was developed using a numerical modelling approach. In the current study, a five-storey RM shear wall building, located in Los Angeles and designed based on the American Masonry code which was proposed by FEMA-451, is considered to assess the seismic performance of RM shear wall systems as a benchmark. The above-mentioned building was designed using rectangular RM shear walls, while the current study investigates the impact of incorporating boundary elements at the ends of the rectangular shear walls on the seismic performance of these buildings. A macro-model numerical approach was used to simulate the dynamic response of the RM shear wall buildings. The numerical model was first validated against the available experimental results to ensure the capability of the proposed model in capturing the hysteretic response of the RM Shear Walls. Afterwards, Incremental Dynamic Analysis is conducted on the building before and after incorporation of the Boundary Elements. The fragility curves were derived subsequently and were used to evaluate the performance function of the structures. In conclusion, the results show a significant level of enhancement in the seismic performance and resilience of the buildings with boundary elements.

3.2.2 Introduction

There have been many advancements in understanding the inelastic behaviour of Reinforced Masonry Shear Walls (RMSW) in recent decades. This understanding is a pledge for the performance-based seismic design of the structures. The performance-based seismic design incorporates a specific performance level corresponding to the level of damage that occurred in the structure (FEMA 445, 2006). The methodology correlates the damage state to a specific functionality level and losses of the whole system when the structure is prone to seismic events. These definitions form the framework of the seismic resilience of a structure, which declares the level of functionality of a structure in the aftermath of the unwanted seismic event. The concept of resilience also shows the capability of a system to resist and maintain its functionality during and after an unwanted event (i.e., flood, earthquake, fire, etc.) (Cimellaro et al. 2010). To assess the resilience of a structure against seismic events, fragility functions need to be precisely derived after performing collapse assessment (FEMA P-58, 2009). Fragility functions have been used in the past for different applications (ATC-13, 1985), where they correlate an engineering demand parameter (*EDP*) to the probability of collapse at a specified damage level (Hwang and Jaw, 1990). These functions are necessary for predicting the level of damages and losses to evaluate seismic resilience. Deriving fragility functions is possible through performing collapse assessment, which can be done following the available guidelines in the literature (FEMA P695, P-58, and ATC-13). However, all these methods need Numerical and/or Experimental test matrices to predict the structural response against lateral forces. There have been a few numerical studies addressing the seismic behaviour of RMSW walls with Boundary Elements (BE), where incorporating BEs helps the RMSW to possess a greater value of displacement and curvature ductility when subjected to a high level of seismic loads (Ezzeldin and El-Dakhakhni, 2016). Among the most recent studies, Shedid et al. (2010) tested seven half-scale RM shear walls with different end configurations to assess the impact of confinement and shape configuration on the inelastic response of RMSWs. They have concluded that by using end confined BEs, the ductility level was enhanced significantly, and maximum saving of around 40% was observed in vertical longitudinal reinforcement in those types of RMSWs. More recently, Banting and El-Dakhakhni (2014) tested five half-scale fully grouted RM shear walls with confined boundary elements. They considered different seismic design parameters such as aspect ratios, reinforcement ratio, and gravity load profile to assess the effect of adding BEs on each of them. It has been concluded that by using

BEs, the buckling of the longitudinal reinforcement was postponed; therefore, the post-peak strength of the walls was enhanced relative to the walls without BEs. In terms of numerical studies, Ezzeldin and El-Dakhakhni, 2016 performed a collapse assessment analysis following FEMA P-695 (2009) methodology on the RMSWs before and after having BEs at the component level. They concluded that by using BEs, the system was able to satisfy the proposed criteria of the methodology successfully with a great safety margin.

In the current study, the impact of using BEs on seismic response of a full 3D RMSW building is studied before and after the adoption of BEs. In this regard, a macro-modelling numerical approach is used, and a numerical model is developed in *OpenSees*. The validation of the modelling approach was conducted against available experimental test results to ensure the capability of the modelling technique in the prediction of the nonlinear behaviour of the RMSW buildings. Subsequently, the above-mentioned modelling technique was utilized in modelling a five-storey RMSW building located in Los Angeles, California. The building was initially designed and proposed by FEMA 451 (2006). Afterwards, the building was redesigned to incorporate end confined BEs in the shear walls. Furthermore, Incremental Dynamic Analysis (IDA) was performed to diagnose the collapse mechanism of the building prior to and after the adoption of BEs. A suite of 44 far-field ground motion was used to perform IDA analysis in accordance with the FEMA-P695 recommendation. Fragility functions are derived for structural components based on the IDA results for different performance levels considering both analytical and EDP-based failure criteria. In addition, the inter-storey drift level and storey shear response of the building is compared before and after using BEs to assess the damage level and probable losses due to the damages.

3.2.3 Numerical modelling and analysis methodology

A new modified macro-modelling approach is utilized to capture the nonlinear response of the RM shear walls using *OpenSees*. The reason for migrating from SeismoStruct to *OpenSees* is the fact that there are limitations associated to commercial based FE software. *OpenSees* addresses most of the limitations that a commercial software has such as limitations of the cross-section shape, constitutive material model, convergence criteria, integration points, proprietary source code, and limitations of some features and output data sets. *OpenSees* owes this capability to being an open-source package which enables the user to implement various I/O and multiple features

without any notable limitation. In this light, Four Displacement-Based (DB) beam-column element with fine discretization was used to model the shear walls' segment of one-storey level along with elastic shear links to resemble the shear flexibility of the shear walls and tentative failure due to sliding shear. The fibre-based approach found to be the most suitable technique to model the inelastic response of wall components. In this regard, two different material models, namely Masonry and Steel, were assigned to the fibres to resemble the behaviour of each constituent part, which will be elaborated in the subsequent section. Five Gaussian integration points were considered in DB Beam-Column elements to precisely capture the inelastic deformation of shear wall elements. Zero-length elements were used to model the shear deformation of the walls. A linear uniaxial Force-Deformation Elastic Material model relationship, originally introduced by Beyer et al. (2011), was defined and assigned to the translational Degree of Freedom (*DOF*) respective to in-plane and out-of-plane direction of the wall and rest of the active *DOF*s were constrained to follow the previous nodal deformation using *EqualDOF* command incorporated in *OpenSees*. A fully restrained constraint was modelled, and soil-structure interaction was ignored as per a recommendation of NIST (2010). a zero-length element section was modelled at the base level of the wall to capture the effect of strain penetration of longitudinal steel reinforcement using Bond_SP01 material available in the material library of *OpenSees.* The schematic configuration of the wall segment nodes and elements are shown in Figure 3.5. Finally, *rigidDiaphragm* constraint was used to build a rigid diaphragm for the building and to assign the effective seismic masses to that center of the mass node.
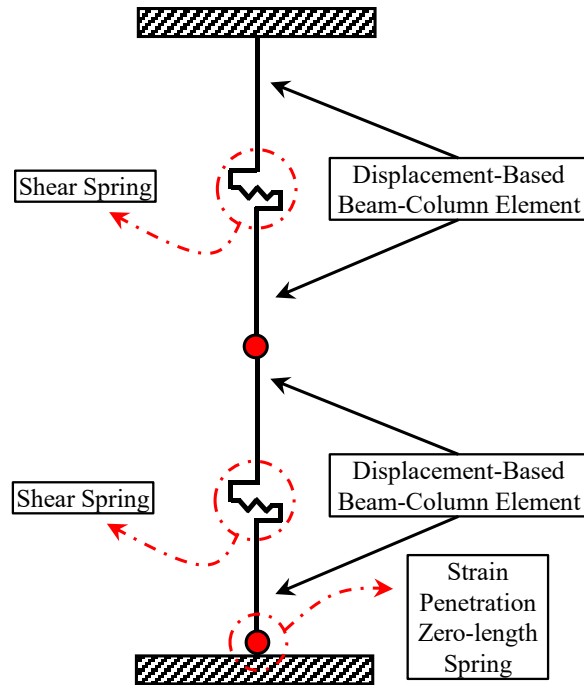
Figure 3.5. Schematic element assembly of the shear wall segment

3.2.3.1 Material properties

Fibre sections were assigned to DB Beam-Column elements to simulate the behaviour of masonry and steel reinforcement independently. Chang and Mander's (1994) uniaxial material model (*Concrete07* in *OpenSees*) was assigned to the masonry fibres and was carefully calibrated based on available experimental data, which is discussed in detail in the validation part. The benefit of using this uniaxial material model is the capability of *Concrete07* to capture the post-peak behaviour due to cracking and/or crushing of the masonry elements with a remarkable accuracy, which differentiate it from all other available constitutive material models available for concrete and masonry. The vertical reinforcement steel rebars were modelled using Menegotto-Pinto (1983) Uniaxial constitutive material model for steel (i.e., *Steel02* in *OpenSees*), which is a common material model to capture the main characteristics of steel rebars including the yield strength, initial stiffness, isotropic strain hardening, pinching and strength degradation. The value of material properties parameters is consistent with the ones reported by the authors and researchers published the work and can be found on Appendix A. The effect of buckling/rupture of the reinforcement could not be captured directly by *Steel02* Material; however, *MinMax* material model was used to mimic the aforementioned effect by restraining the ultimate strain of steel material. The value of 0.06 was considered based on the available experimental data to clarify the onset of

37

rupture/buckling of the rebars. It is worth noting that the failure criteria of the RMSW are considered in accordance with the recommendation of the original study of GCR 10-917-8 proposed by NIST (2010). The effect of confinement for the masonry material of Boundary Elements was considered following the recommendation of Chang and Mander.

3.2.3.2 Validation of the modelling approach

The model verification was performed to ensure the robustness of the proposed modelling method in predicting the hysteretic response of RMSW structures. To achieve this goal, three half-scale fully grouted RM shear walls with different end configuration originally tested by Shedid et al. (2010) was numerically modelled incorporating the above-mentioned methodology and was analyzed against reverse quasi-static cyclic loading scheme using the identical loading protocol performed in the structural lab. As can be seen in Figure 3.6, the proposed modelling approach was able to successfully capture the principal characteristics of the hysteretic response of the RMSW subjected to cyclic analysis. In general, the model was able to predict the main response characteristics of RMSW including the initial stiffness of the walls, peak strength, post-peak degradation, hysteretic shape, and pinching of the element with a great level of accuracy. A maximum difference of 7% and 13% was observed in capturing the maximum peak strength and hysteresis energy dissipation, respectively, which is considered acceptable.
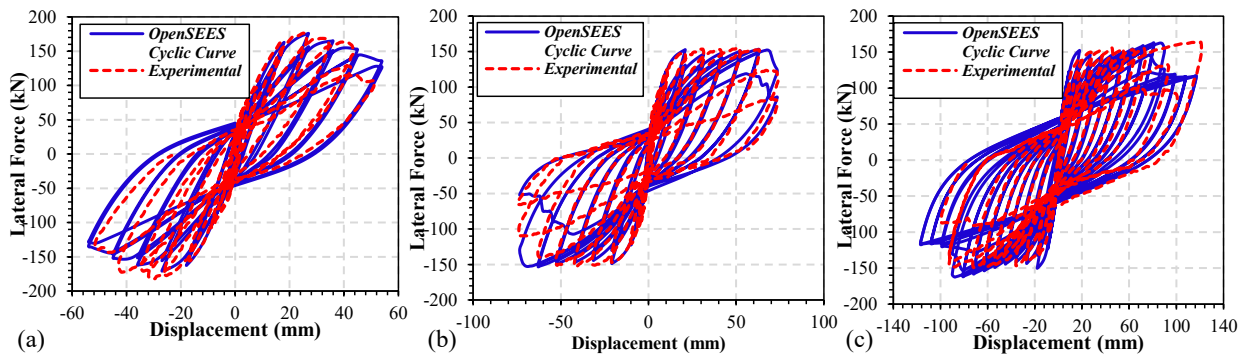
Figure 3.6. Comparison of Numerical versus Experimental Hysteretic loops: (a) W1; (b) W2; and (c) W3 (Experimental data from Shedid et al. 2010)

3.2.4 Modelling and specification of studied archetype

In this paper, a five-storey residential RMSW building designed by FEMA 451 was considered to assess the seismic performance of such buildings prior to and after adding boundary elements at the walls' ends. The building is in Los Angeles, California and has structural walls of 8-in. thick reinforced masonry units. The roof was made of 8-in. thick hollow-core precast pre-stressed concrete slabs. The building was built on site class D soil type, and the Seismic Design Category of D was considered for it. The full detail of the building besides the configuration and design procedures of the buildings is fully discussed in Appendix A of the thesis as well as FEMA 451. The building was once again designed incorporating the identical seismic design parameters (i.e., Response modification factor and deflection amplification factor) while having boundary elements at its ends to investigate the impact of using boundary elements on its response. The reinforcement detail and configuration of the RM shear walls with boundary elements are summarized in Table 3.5.

Table 3.5. Dimensions and Reinforcement Configuration of RMSW building with Boundary Elements

Wall ID	Height (mm)	Length (mm)	Vertical Reinforcement ratio (%)	Horizontal Reinforcement ratio (%)	Aspect ratio
Wall A	13818	10972.8	0.4	0.13	1.26
Wall B	13818	10363.2	0.44	0.13	1.33
Wall C	13818	9956.8	0.50	0.15	1.39
Wall D	13818	9956.8	0.50	0.15	1.39

Both RMSW buildings were analyzed against a 44 far-field ground motion proposed by FEMA P-695 to assess the seismic collapse of the structure (refer to Appendix A for more information). Based on the adopted methodology, Incremental Dynamic Analysis (*IDA*) was performed to track down the collapse initiation of the RMSW buildings. The analysis involves subjecting the structure to Nonlinear Time History Analysis by various ground motion suites and increase the intensity such that the ground motion record cause structure to fail or collapse at a certain degree in accordance with the predefined failure modes. The spectral acceleration of 5% damping was considered as intensity measure, and the maximum inter-storey drift ratio was

monitored as the demand parameter of interest. A five percent damping ratio was considered in the model analysis based on the Rayleigh damping formulation built-in command of *OpenSees,* which is a common value of damping ratio in Reinforced Masonry is building practice.

3.2.5   Selection and scaling of ground motion records

Based on the recommendation of FEMA P-695, 44 far-field ground motions proposed by the methodology were used to perform IDA analysis. It is worth noting that, using as many as possible record will help to reduce the uncertainties arising from record-to-record variability. However, the large computational effort is the main drawback of using such a large database of strong ground motions. The individual response spectrum of the unscaled records, together with the median of the spectrums and upper and lower bound of the seismic response spectrum of the specified site location, is depicted in Figure 3.7.

The scaling method was followed as per as recommendation of FEMA P-695. First, the records were normalized to their peak ground acceleration, and later the median of the spectrum was scaled such that it matches the Target response spectrum of the Maximum Credible Earthquake (MCE) level at the fundamental period of the structure, *T.*
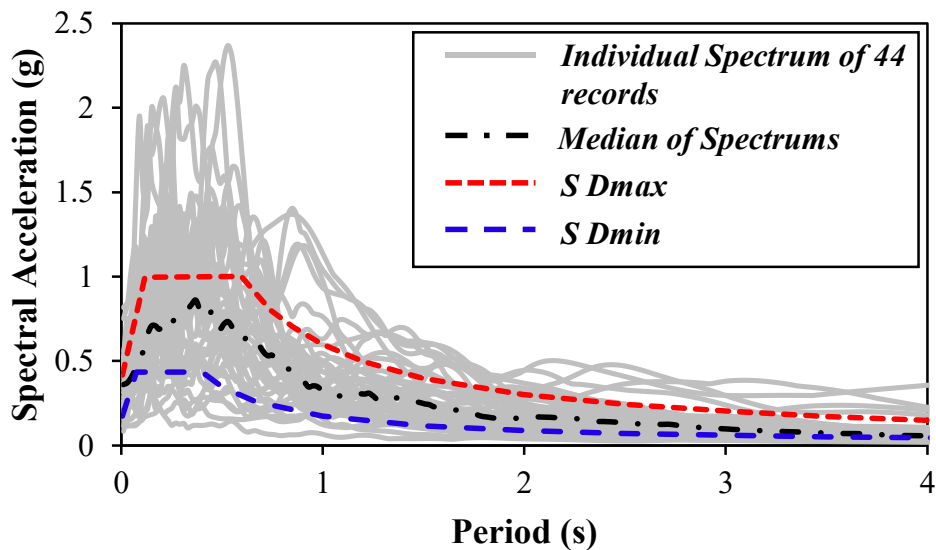
Figure 3.7. Response Spectrum of 44 unscaled Ground motions along the median spectrum; Upper bound (*S D_{max}*), and Lower bound (*S D_{min}*)

3.2.6 Seismic Assessment and performance analysis

After performing the analysis, the IDA curves were derived and are shown in Figure 3.8 for the RMSW building before and after adding boundary elements. As shown, by adding the boundary elements, the collapse capacity of the system has been increased significantly. This result can be related to the fact that the boundary elements increased the wall's curvature ductility at the ultimate stage. The IDA curves also show that the dispersion of the response data of each archetype was lowered for different ground motion frequency content in terms of inter-story drift ratio.

3.2.6.1 Quantification of performance parameters

The median collapse capacity of the structure, S_{CT}, was defined as the intensity level at which half of the records cause the structure to fail. The other term defined by the methodology is the Collapse Margin Ratio (*CMR*). This parameter is used to characterize the safety of the structure against collapse. It can be calculated as the ratio of median collapse capacity (S_{CT}) to the spectral acceleration capacity of the structure at its fundamental period (S_{MT}). The calculated *CMR* value of the building before and after adding boundary element is presented in Table 3.6. As can be seen, the *CMR* value has been increased by adding the boundary element. This is due to the fact that the boundary elements have increased the confinement at the outermost fibres of the walls and postponed the buckling of longitudinal reinforcement, hence, leading to higher curvature and overall displacement ductility.

3.2.6.2 Collapse Fragility Assessment

The probability of the collapse versus the Intensity Measure (IM) can be derived by adopting a Cumulative Distribution Function (CDF), forming Fragility functions. The IM value corresponding to initiation of collapse for each ground motion is calculated using the IDA results and a cumulative distribution function is fitted to resulting IM values. The lognormal *CDF* can be defined as follows:

$$P(C \mid IM) = \Phi\left(\frac{\ln(\frac{x}{\theta})}{\beta}\right) \tag{3.7}$$

Where $P(C|IM)$ shows the probability of collapse corresponding to specific IM; Φ is the CDF, and θ, β are the mean and standard deviation of the data, respectively. A sample curve fitting dataset is shown in Figure 3.9 using the method mentioned earlier.

Table 3.6. Summary of CMR value of the building

Building ID	Configuration	$S_{MT}[T](g)$	$S_{CT}[T](g)$	CMR
5 Storey Building Los- Angeles	Without Boundary Element	1.0	1.4	1.4
	With Boundary Element	1.0	2.1	2.1
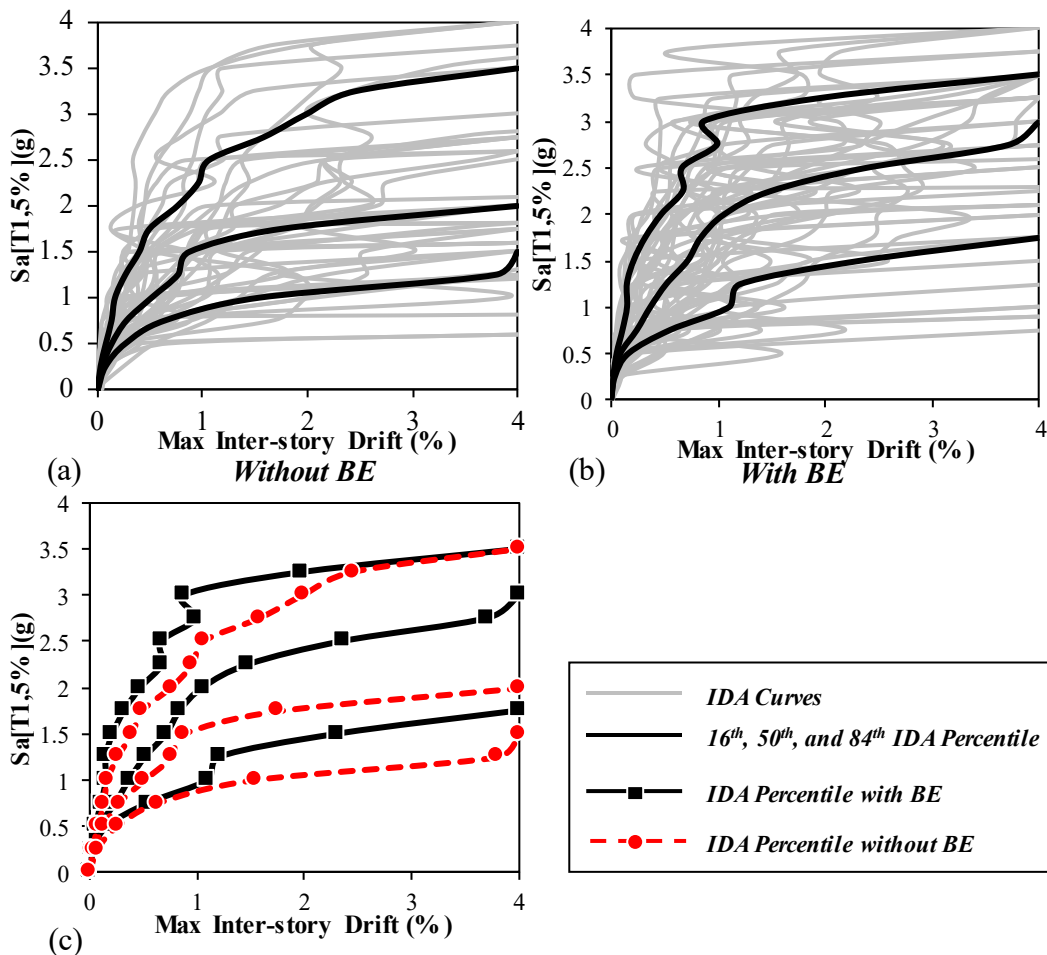
Figure 3.8. IDA Curves and 16th, 50th, and 84th percentile: (a) RMSW Building without Boundary Element; (b) RMSW Building with Boundary Element; (c) Comparison of the results
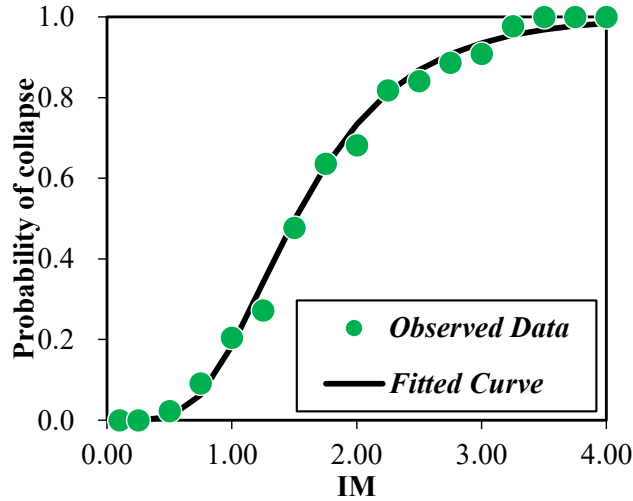
Figure 3.9. Sample Fragility Function Curve Fitting

The collapse fragility curve of the building before and after adding Boundary Elements was extracted for different performance levels proposed by ASCE 41 (2017) and presented in Figure 3.10. The results indicate that by using the boundary elements, the collapse capacity of the building was increased for all performance levels. The results highlight the impact of using boundary elements on delaying the collapse of the RMSW building at different levels of inter-story drift ratio.

3.2.6.3 Inter-storey Drift and Response Shear Variation

The variation of response storey shear and the inter-storey drift ratio of all records are shown in Figure 3.11 and Figure 3.12, respectively. The results show that by adding boundary elements, the base shear of the building has increased; however, the initial stiffness of the building was considered to be identical for the building with and without boundary elements. It can be inferred that, due to the higher level of ductility that RMSW with boundary elements have, the building could incorporate higher storey shear at the upper level of the building (i.e. the storey shear diagram shifted rightwards in the top stories). Having higher storey shear capacity within the identical initial stiffness will help to control the losses and damages caused to the overall structure and helps to increase the seismic resilience of the building.

The inter-storey drift ratio also was carefully monitored, and it can be concluded that having boundary elements helped the building to experience a lower level of inter-story drift ratio, which

in turn means a lower level of structural and non-structural damage of the components. Hence, higher seismic resilience can be estimated for such buildings.
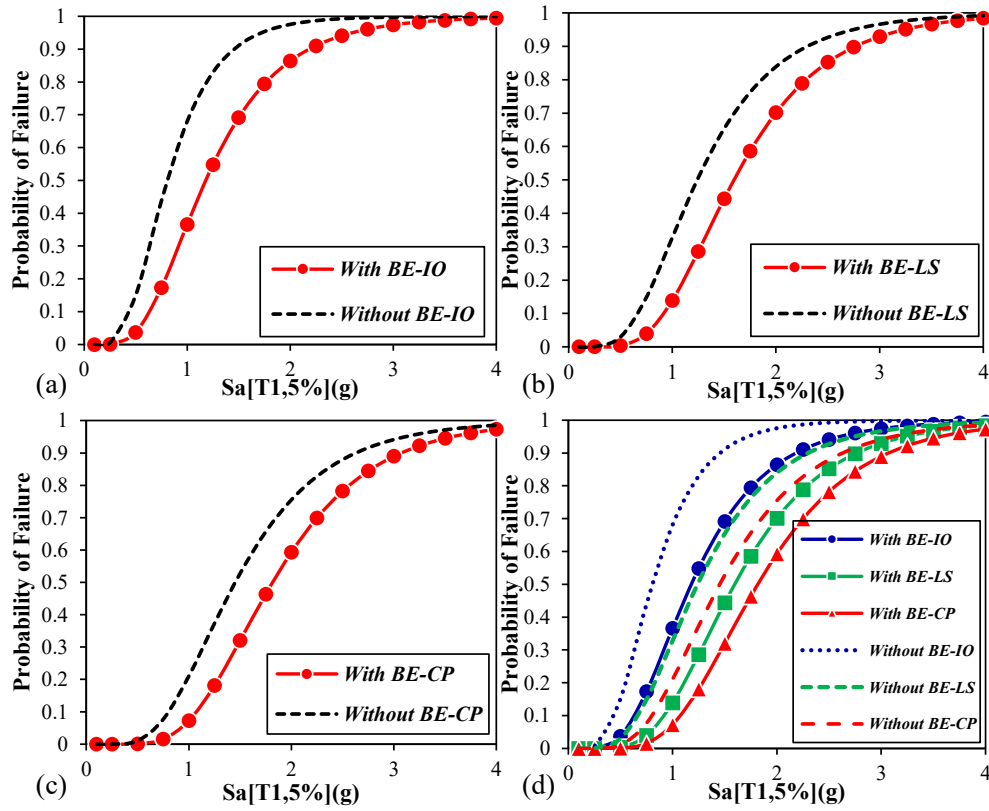
Figure 3.10. Fragility Curves of different Performance Levels: (a) IO; (b) LS;(c) CP; (d) Comparison of different performance levels
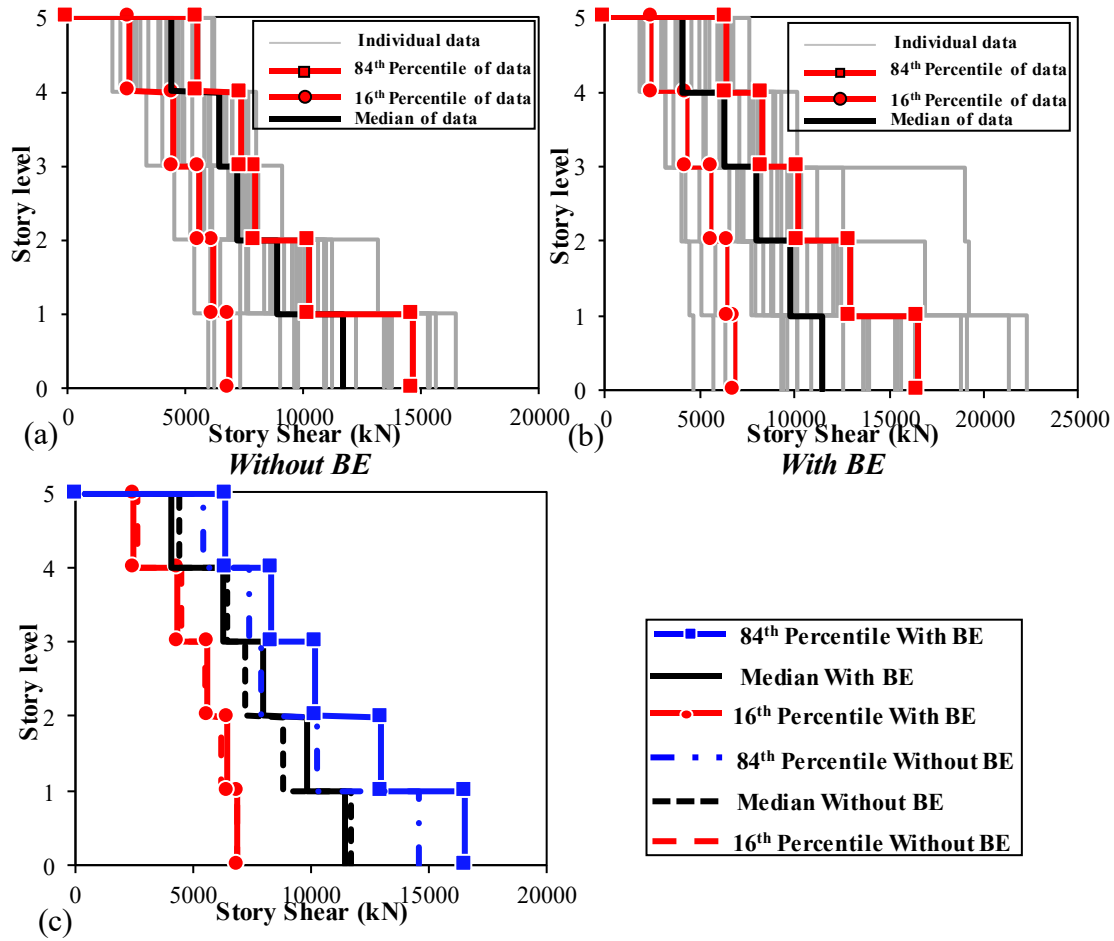
Figure 3.11. Response Storey Shear Variation before and after Boundary Elements: (a) Without Boundary Elements; (b) With Boundary Elements; (c) Comparison prior and after adding Boundary Elements.
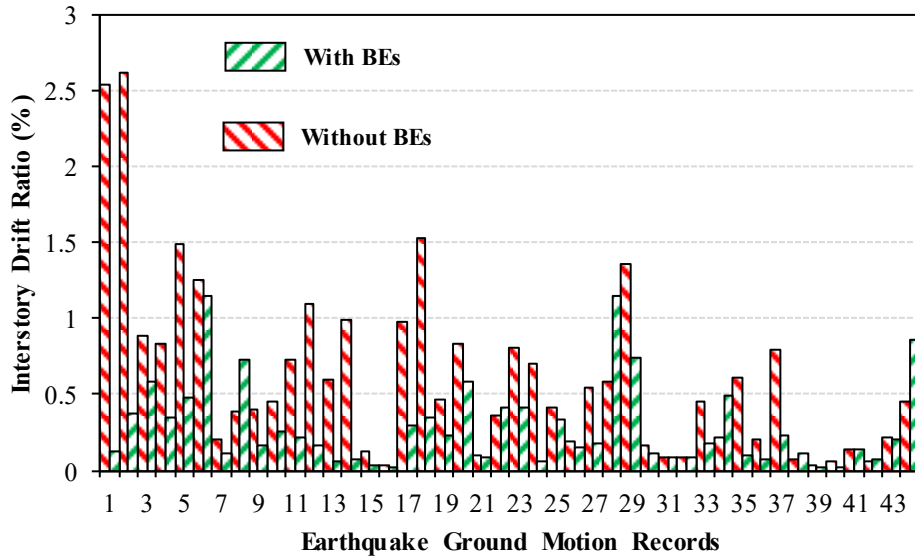
Figure 3.12. Inter-Storey Drift Variation of the RMSW Building before and after having Boundary Elements

3.2.7 Conclusions

In this study, the impact of adopting boundary elements on the seismic behaviour of a five-storey fully grouted RMSW building located in Los Angeles was investigated. A fibre-based macro-modelling approach was utilized to capture the inelastic behaviour of RMSW and was validated against the experimental data to validate the capability and robustness of the approach. Afterwards, *IDA* analysis was conducted on the numerical model, and fragility curves were derived. Also, the variation of the storey shear and inter-storey drift ratio was studied after utilizing Boundary elements. The following remarks were concluded:

- The proposed modelling approach was able to capture both elastic and inelastic characteristics of the response of RMSW with an outstanding level of accuracy. A maximum difference of 7% and 13% was observed in capturing maximum peak strength and hysteresis energy dissipation, respectively.
- The results of IDA curves show higher collapse capacity for the shear walls with Boundary elements; meanwhile, lower dispersion of data was found after utilizing Boundary Elements.
- The CMR ratio of the walls with Boundary Elements found to be higher than the rectangular walls since BEs will delay the buckling of the vertical reinforcement

46

besides confining the extreme sides of the shear walls which in turn leads to higher ductility and safeguards against collapse. A 50% increase in the *CMR* value was observed after adding Boundary Elements to the RMSW Building.

- The collapse fragility curves of the walls with BEs had up to 65% lower probability of failure for a specific intensity measure at different performance level as a result of possessing higher ductility.

- There was a maximum of 20 % increase in the response storey shear after adding BEs, and the storey shear diagram shifted rightwards in the upper stories by having BEs.

- The Inter-Storey Drift ratio of the RMSW building with BEs had decreased dramatically for most of the records. Hence, a lower level of damages is expected for structural and non-structural components of the building with Boundary Elements.

Chapter 4
Seismic Fragility Assessment and Resilience of Reinforced Masonry Flanged Wall Systems

4.1 Abstract

Several experimental and analytical studies have evaluated the seismic response of reinforced masonry (RM) shear walls either as a component (i.e., planar rectangular walls) or as a system (i.e., building consisting planar walls). In the current study, five RM flanged walls were studied in order to assess their seismic performance and collapse capacity. The impact of utilizing flanged walls was assessed and characterized through FEMA-P695 methodology. In this respect, a 2-D fibre-based modelling approach has been developed using *OpenSees* to numerically model and capture the inelastic behaviour of the walls. Collapse risk evaluation has been conducted within the context of FEMA P-695 by subjecting the wall's numerical model to various ground motions scaled at different intensity levels. Quantification of the seismic parameters of the flanged wall system, including period-based ductility, overstrength, and collapse margin ratios has been conducted to help better understanding the seismic response and collapse capacity of the component. The results indicate that the selected Reinforced Masonry Flanged walls can satisfy the acceptable criteria proposed by the methodology of the anticipated seismic collapse risk. Lastly, the seismic resilience of the archetypes against the expected collapse risk was evaluated, in terms of functionality curves before and after the adoption of the flanges to the walls. Damage levels were considered as performance level functions correlated to the earthquake intensity and were used to estimate total loss and recovery time of the archetypes. The selected RM flanged walls showed enhanced earthquake resilience and less damage compared to rectangular RM shear walls.

4.2   Introduction

Reinforced Masonry Shear Walls (RMSW) are usually used in low- to high-rise masonry structures as a part of the Seismic Force Resisting System (SFRS) providing the lateral resistance, energy dissipation and lateral stiffness required to withstand lateral loads coming from the earthquake. During the past decades, there has been a noticeable advancement in understanding the response of RMSW under seismic loading. This understanding was the result of the extensive experimental and analytical studies that addressed the seismic performance of RM shear walls as a component (e.g., Shedid et al. 2008; Ahmadi et al. 2015) or within a building (e.g. Heerema et al. 2012; Mavros et al. 2016; Stavridis et al. 2016). However, most of the literature have addressed planar RMSW systems, with a little focus on RM flanged shear walls (e.g., Heerema et al. 2015; Shedid et al. 2009; El-Dakhakhni and Ashour, 2017).

Flanged walls can be formed along the walls' intersections and enhance the overall seismic response of the building. This configuration normally exists among most of the structural plans and can be incorporated easily. One of the important characteristics of RM Flanged Shear Wall (RMFSW) system is that they resist lateral loads in both horizontal directions compared to RM planar shear walls. The following section briefs a review of the available literature with a focus on the research studies done on the non-planar walls. Thomsen and Wallace (2004) experimentally tested T-shaped reinforced concrete walls to develop a displacement-based design approach. The impact of the flange element and decreasing the hoops spacing of the transverse bars at the wall boundaries were also investigated. The results indicated that by utilizing non-planar configuration the initiation of the reinforcement buckling was delayed resulting in a substantial increase in the curvature ductility of the walls. Also, it has been proved that the variation of the yield curvature at different drift levels had a negligible impact on the ultimate curvature values. This phenomenon emphasizes the contribution of the flanged elements during severe lateral deformation. Another experimental test was conducted on the response of half-scale fully grouted RM shear walls by Shedid (2009). A quasi-static reversed cyclic loading protocol was applied to the specimens to investigate the structural response of RM shear walls with flanges or with end-confined boundary elements. A maximum saving of 40% was reported by implementing end-confined or flanged cross-sections besides significant enhancement in the level of ductility due to postponing post-yield initiation. Heerema et al. (2015) experimentally tested a one-third scale fully grouted two-

storey non-symmetrical RM building comprised of eight concrete block masonry walls. The system-level was compared against the component-level of the RM building and the seismic design parameters were quantified for the test setup by means of digital image correlation (DIC). The results indicate that the orthogonal walls contribute to the lateral force resistance of the building with respect to the induced twist. Each wall component of that study was tested individually by Siyam et al. (2015a). This test setup comprises walls with different aspect ratio, coupled or uncoupled by the slab and flanged configuration. This study characterized the effect of the slab-coupling on ductile shear walls and quantified the force-based design seismic parameter of the RM shear walls (i.e., the plastic hinge length of the walls). A recent study has been carried out by Ezzeldin et al. (2016) on the effect of using boundary elements in RM shear walls. A fibre-based modelling approach was developed by adding a uniaxial material to resemble the shear flexibility of such walls. The study reported significant enhancement on the seismic behaviour of RM walls by adding boundary elements. The boundary elements postponed the abrupt strength degradation of the walls, however, the fabrication effort using standard blocks was a drawback in this type of walls. The collapse risk evaluation of walls with boundary elements was performed through FEMA-P695 (2009) methodology on the archetype models of a recent study by NIST (2010) resulting in enhanced displacement and ductility capacity.

FEMA-P695 (FEMA 2009) methodology has been used by many researchers recently (e.g., Arabzadeh and Galal 2017; Ezzeldin et al. 2016; Purba and Bruneau 2014; Gogus and Wallace 2015; Lee and Kim 2013; Lignos et al. 2011). The procedure provides a comprehensive and reliable method of assessing the structures over a seismic event by incorporating response parameters such as response modification factor (R factor), system over-strength factor (Ω), and deflection amplification factor, (C_d) of the seismic force resisting system. Arabzadeh and Galal (2017) quantitatively evaluated the risk of collapse of coupled Reinforced Concrete Core Walls using Fibre Reinforced Polymer (FRP) laminate retrofitting method by proposing a new modified Wide Column Method (WCM) using FEMA-P695 methodology.

The objective of this study is to numerically evaluate the seismic collapse risk of RM flanged wall systems, having different heights, under seismic loading. This evaluation is performed in accordance with the FEMA-P695 methodology for RM shear wall system, and RM Flanged wall system. In this regard, an analytical macro-model was developed using *Open System for*

Earthquake Engineering Simulation software (OpenSees 2000). Subsequently, the models were calibrated against the experimental hysteresis response of RM shear walls tested by Shedid et al. (2009), and Siyam et al. (2015b) having rectangular and flanged shape cross-section. A comparison was made between the seismic responses of RM shear wall archetypes previously studied by NIST GCR 10-917-8 (2010) before and after incorporating flanges in the cross-section. The archetypes are selected to have different heights of 1, 2, 4, 8, and 12 stories. After validating the analytical model, nonlinear Incremental Dynamic Analysis (IDA) was performed, following the recommendation of FEMA-P695 methodology. A series of 22 pairs of far-field ground motions were used for IDA analyses of the RM Flanged walls. Moreover, the collapse risk of the RM flanged system was assessed in terms of fragility curves. Finally, the seismic resilience concept is defined as the perseverance of a system to remain functional after an earthquake event occurs. Lastly, the seismic resilience of the redesigned archetypes has been evaluated against the original archetypes by means of functionality curves.

4.3   Numerical Modelling for Nonlinear Analysis

In the current study, a modified wide column modelling approach has been developed using *Open System for Earthquake Engineering Simulation* (*OpenSees*) software to perform all the analysis for the RM planar and flanged shear wall systems. Inelastic displacement-based beam-column fibre elements were implemented in the model and were assigned different material models for reinforcement rebars and masonry. Among different modelling methods available in the literature the fibre-based approach was chosen because of its versatility and is easy to calibrate (Kolozvari and Wallace 2016). Constant axial strain and linear curvature distribution are considered within displacement-based beam-column element formulation without possessing any shear deformation. In addition, by using this element both the axial elongation and combined axial and bending moment interaction of the RM sections could be considered. The impact of these parameters is significant in flanged walls since the variation in axial load in segments is inevitable when subjected to loading protocols. Among different fibre-based modelling approaches that are available in the literature, the modified model has the capability of simulating the shear deformation of the walls by the implementation of a realistic shear-link possessed a multi-linear force-deformation relationship. Previous studies used beam-column elements that do not capture shear deformation caused by lateral loading (Siyam et al. 2016). A common solution was to utilize

an additional uniaxial material to represent the shear deformation characteristic of the component (Furtado et al. 2015). The aforementioned modelling approach is hard to calibrate, whereas the modified model accounts for shear deformation while being easy to model and calibrate. It is worth noting that the fibre-element-based software can also consider the damage and large displacement to the shear walls under static and dynamic loading, hence accounting for geometric and material nonlinearities. The modelling approach is elaborated in detail in the following sections.

4.3.1 Geometrical Model and Element and Section Models

The configuration of nodes and elements are schematically depicted in Figure 4.1a besides the discretization of the wall elements shown in Figure 4.1b, c. Each element was set to have ten Gauss integration points which estimate the deformation by an eleven-degree polynomial algebraic equation along its length. The wall-foundation interaction was assumed to be fully restrained at the base of the wall and no soil-structure interaction has been considered according to the studies proposed by NIST (2010). Strain penetration at the wall-foundation interface has been considered by incorporating a zero-length section element at the base of the wall model which is shown in Figure 4.1a, where the longitudinal steel reinforcement was delineated with the Bond_SP01 uniaxial material model in the *OpenSees* material library. In this material model, the total reinforcement slip is considered as a function of rebar stress that results from the strain penetration effects (Zhao and Sritharan 2007). Figure 4.2 shows the location of the zero-length section element at the base of the numerical model and Force-Deformation relationship implemented in the zero-length section element. The number of fibres for masonry and reinforcement is calibrated to create fine discretization in the section and to provide sufficient accuracy. The maximum size of 60 mm was considered for masonry fibres along the width of the RM shear walls and 100 mm along the length of the shear walls. In the flanged zones, this value was reduced to 50 mm since a higher level of strain is expected within these zones. An approximated value of 400 masonry fibres was used in total to ensure the accuracy of the results while minimizing the computational effort.

Calabrese et al. (2010) found that displacement-based beam-column elements are too sensitive to the number of elements and the length of the first element. To address this issue, a sensitivity analysis was conducted to examine the most accurate length and the number of elements per storey. The results show that using four elements per storey yields the best accuracy in terms of the peak and post-peak behaviour of the nonlinear model.

52

In order to overcome the limitation that displacement beam-column elements are not capable of capturing shear deformation, the two elements between successive nodes were connected by zero-length spring elements to consider the shear flexibility of the wall elements for each storey. Therefore, a horizontal translational degree of freedom (*DOF*) in the zero-length element was assigned to have stiffness corresponding to the shear stiffness of the two successive elements comprising the shear spring. *EqualDOF* type of constraints in *OpenSees* was also used to couple other *DOFs* of two nodes of the spring. Among different approaches for calculating the shear stiffness of zero-length element, the method proposed by Gogus and Wallace (2015) was chosen, for both flexure-dominated and shear-dominated walls, with a multilinear trend. Shear strain at the yield was set to be equal to 0.0015 based on the study by Gogus and Wallace (2015). The Force-Shear deformation relation for flexure-dominated and shear-dominated walls utilized in the definition of the shear-link elements is also shown in Figure 4.2.
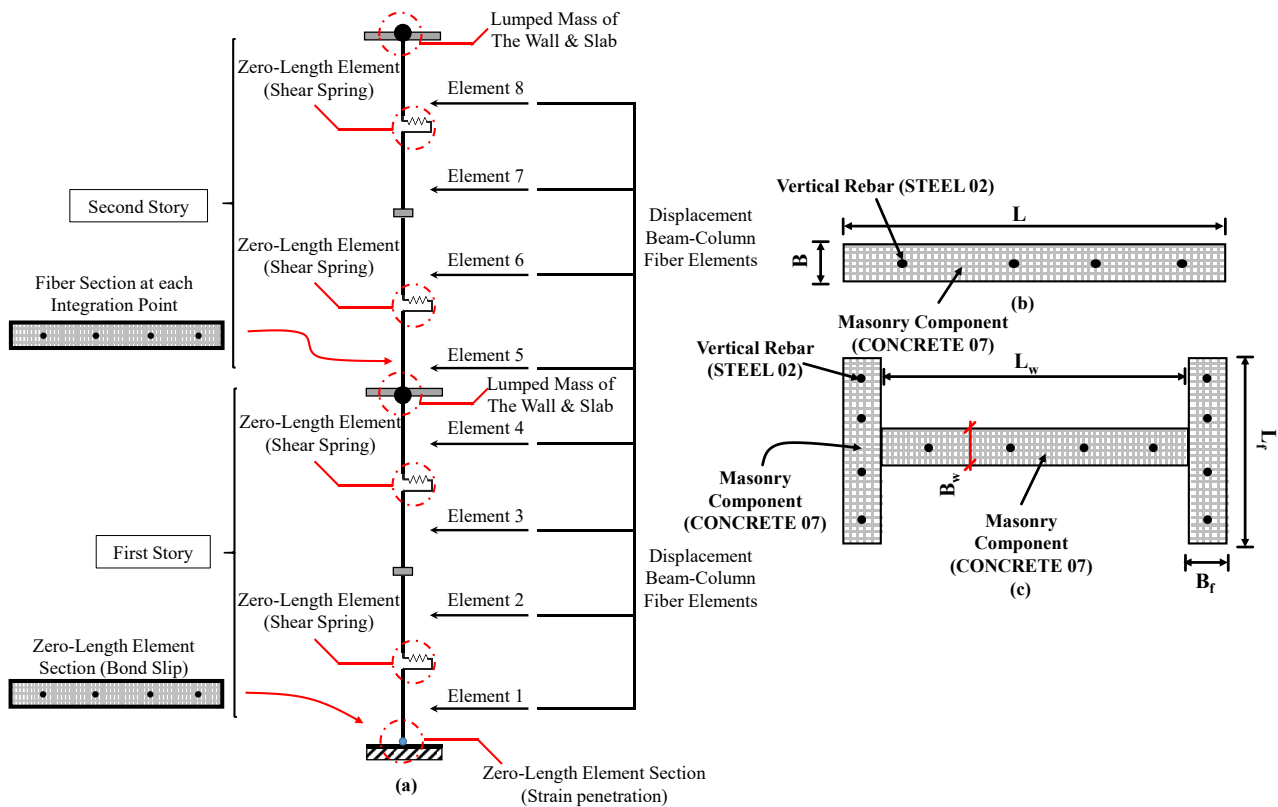
Figure 4.1. Element assembly in a typical archetype model: (a) element discretization; shear-link position; distribution of masses; and fibre sections; (b) Wall configurations and material discretization of Rectangular RM Shear wall; (c) Wall configurations and ma material discretization of RM flanged wall cross section
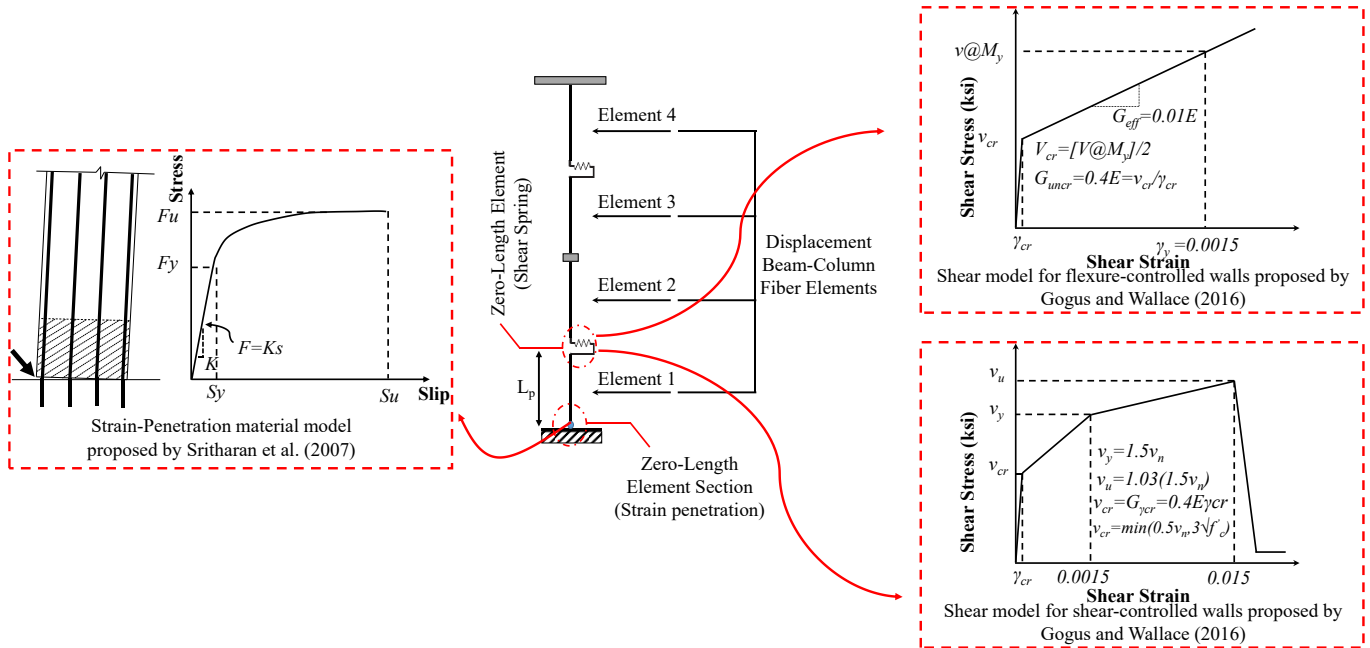
Figure 4.2. Detail of Force-Deformation relationship assigned to shear-link and strain-penetration components

4.3.2 P-Δ effects

In order to precisely capture the effect of gravity loads on the walls, the "Gravity-Leaning-Column" analogy has been implemented in the numerical model adjacent to the RM shear wall elements (Lignos et al. 2011). This modelling approach has been used by many researchers to take the effect of gravity loads into account by not modelling the whole structure which would become computationally expensive. These columns will not contribute to the lateral load resisting system, while their presence helps to capture the destabilizing *P-Δ* effects associated with the gravity loads. An Elastic Beam-Column element, provided in *OpenSees* elements package, is used to model the Gravity-Leaning Column. In this method, the gross section area of the leaning column is considered a large value (i.e., 100 times of the area of the wall) to ensure that no axial deformation occurs along the elements' length. In contrast, a relatively small value was considered as the appointed effective moment of inertia of the beam-column element (i.e., roughly 100 times smaller) to make sure that the gravity leaning column will not manipulate the lateral stiffness of the structure. This approach was utilized in order to mimic the pin-ended condition (Purba and Bruneau 2014). The leaning column elements were connected at each levels' elevation using co-rotational rigid links element. Truss elements were used to model rigid links with a cross-sectional area deliberately chosen to represent one-third of the height of the wall and the same width of the

connected adjacent wall element. All effective seismic masses were assigned on wall elements at each storey level and no mass was assigned on the corresponding leaning column element. It is worth mentioning that the leaning column frame was located at an equal distance of the typical span length of the shear wall. The tributary area was considered to estimate the gravity loads applied on the leaning column from which the tributary area of the walls is excluded. The schematic view of the leaning-column and shear wall assembly is illustrated in Figure 4.3.
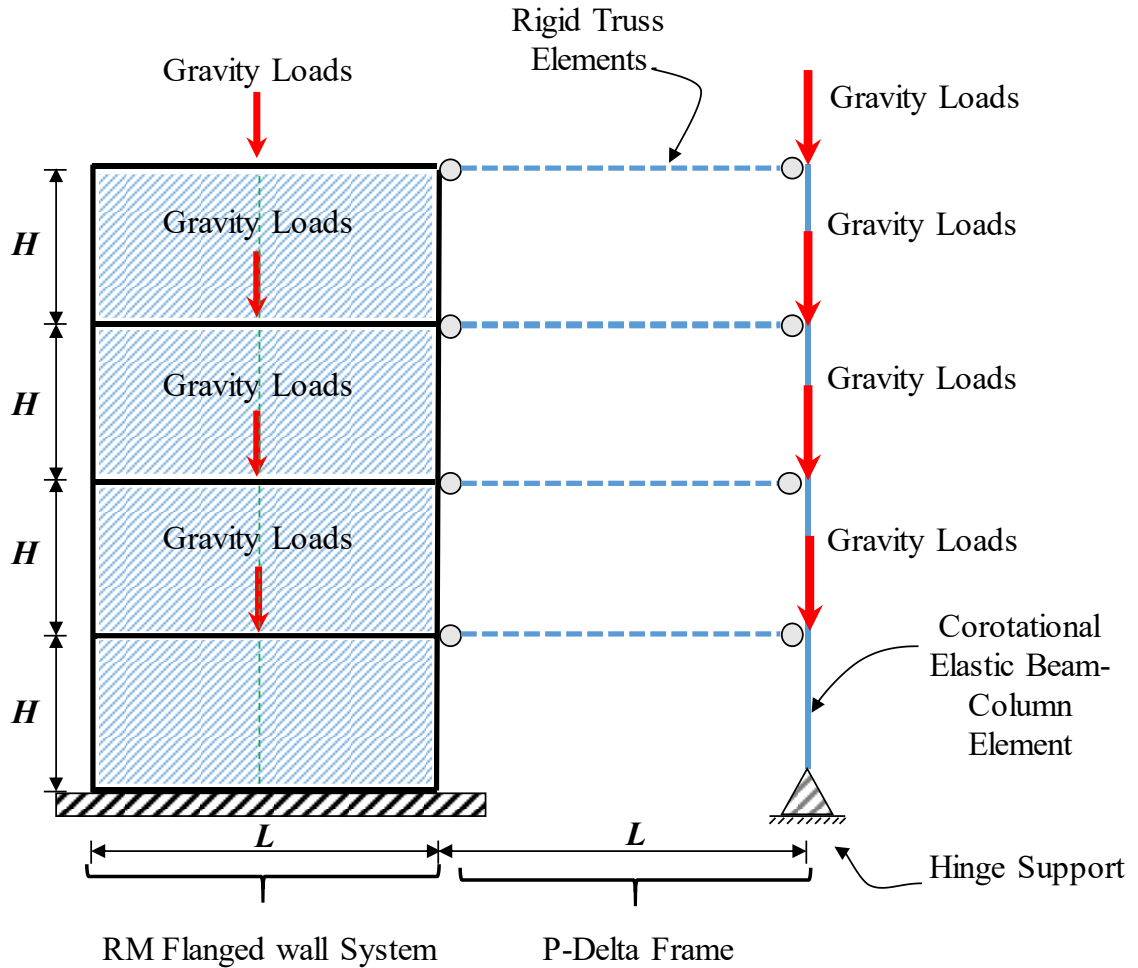
Figure 4.3. Schematic Nonlinear structural model of four-storey archetype and leaning column analogy frame

4.3.3 Definition of material properties

The properties of the materials were defined based on the reported test data or nominal strength of masonry and steel reinforcement using the available empirical equations. Figure 4.4 shows the distribution of material components over the cross-sectional area of the wall simulated

in the model. Fibre sections are defined in order to reproduce the response of RM shear walls. The cross-sectional area is discretized such that uniaxial materials are assigned to each fibre resembling the behaviour of masonry and steel reinforcements independently.

The concrete masonry material utilized in the modelling is based on Chang and Mander's model (1994) for concrete (Concrete07 in *OpenSees*). The material model relies on the compressive strength, f_m', the modulus of elasticity, E_m, the strain level corresponding to the maximum compressive strength, eps_c, and other parameters to represent stiffness and strength degradation. The most remarkable aspect of utilizing Concrete07 model is that it is capable of representing the post-peak degradation behaviour of the concrete masonry with significant accuracy. However, the other available materials (i.e., Concrete02) failed to present such accuracy, although the latter material is much easier to calibrate. It is worth mentioning that the strength parameters that were used in the validation part are different from those used in the full-scale model walls since the regular reinforcement bars possess significant strain hardening relative to the one-third scale wires. For the reinforced masonry models, the strain corresponding the maximum compressive strength, ε_m, set to be 0.0025 based on the data provided by the prism test.

The modulus of elasticity, E_m, was calculated based on MJSC 2013 code as $900 f_m'$, in which f_m' is the compressive strength of masonry material. These parameters were validated versus different experimental data as will be explained subsequently. The hysteresis stress-strain behaviour of masonry material is depicted in Figure 4.5a. As shown, the tensile strength is relatively smaller than compressive behaviour and has a minor effect on the numerical models.

As shown in Figure 4.5b, the longitudinal steel reinforcement was modelled using Menegotto-Pinto (1973) Model having Isotropic strain hardening (Steel02 in *OpenSees*). The model is capable of capturing the probable yield strength and hardening effects, nonetheless, the model is easy to calibrate. As mentioned earlier, the one-third scale reinforcements used in the verification part, possess no strain hardening while the full-scaled reinforcements have the capability of developing hardening action.

The yield strength of 495 MPa with strain hardening of 1.20% is considered to be consistent with NIST (2010) study, for the full-scale steel reinforcement. The initial elastic modulus value

set to be 200 GPa and the parameters to control the elastic to plastic transition of branches are set to be the same as the default value recommended by the developer.

In order to resemble reinforcement buckling which is highly probable to occur on the unconfined areas, the *MinMax* material model is used to determine the steel reinforcements' ultimate strain. The strain corresponding to the onset of fracture in longitudinal bars was assumed to be 0.06 in unconfined zones. This value is about 50% of the measured fracture strain estimated in the direct tension test to take the effect of low-cycle fatigue into account (Zong and Kunnath 2008; Rodriguez et al. 1999).
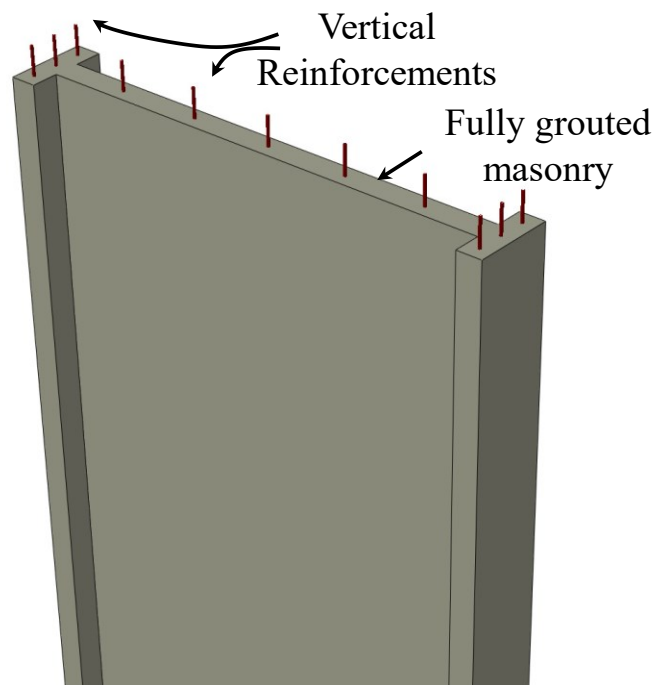
Figure 4.4. 3D Schematic View of Flanged Walls
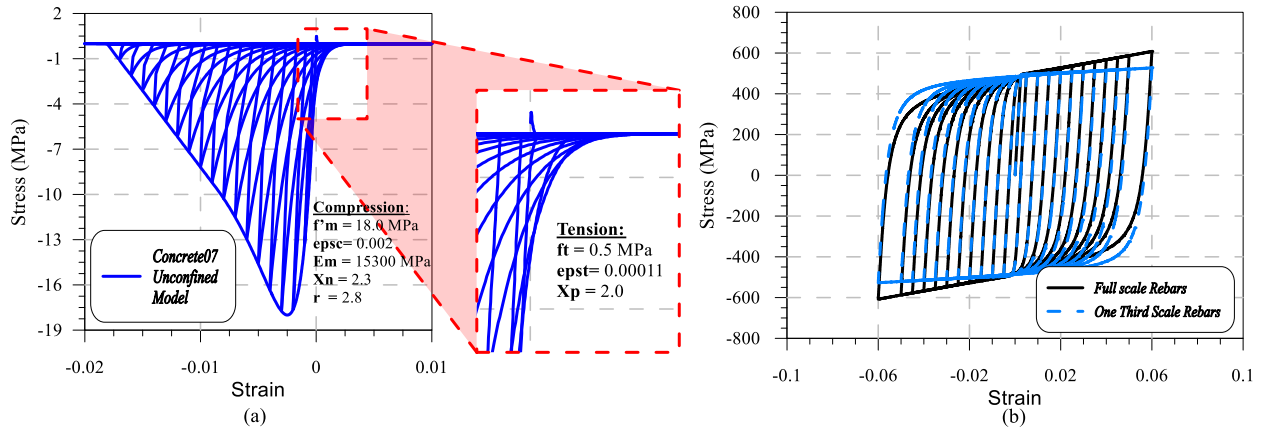
Figure 4.5. Sample stress-strain hysteretic response of material assigned in the numerical model:
(a) Masonry; (b) Reinforcement

4.3.4 Failure Criteria for Materials

Definition of the failure criteria plays an important role in diagnosing the initiation of collapse. Since there are different approaches toward identifying the failure criteria, the method proposed by NIST (2010) was utilized hereby in this study with some modifications explained subsequently.

The collapse of flexure-dominated walls is assumed to happen when the wall meets one of the following conditions:

• When 25% of the cross-section reaches the end of the softening branch of the masonry stress-strain curve (i.e., crushing strain); masonry crushing will happen. For the unconfined masonry areas, the crushing strain is considered to be 0.015, which shows the end of the descending slope.

• When 25% of the bars in the cross-section lose their tensile strength due to rupture or reach their compressive strength due to buckling. Fracture of the reinforcement happens when the bars' strain reaches 0.06 in tension (Kircher et al. 2010).

The above-mentioned criteria can be visualized through the cross-section of the wall component as shown in Figure 4.6.

(i)

$\varepsilon_s \geq \varepsilon_{failure}$

$0.25L_w$

$\varepsilon_m \geq \varepsilon_{failure}$

(ii)
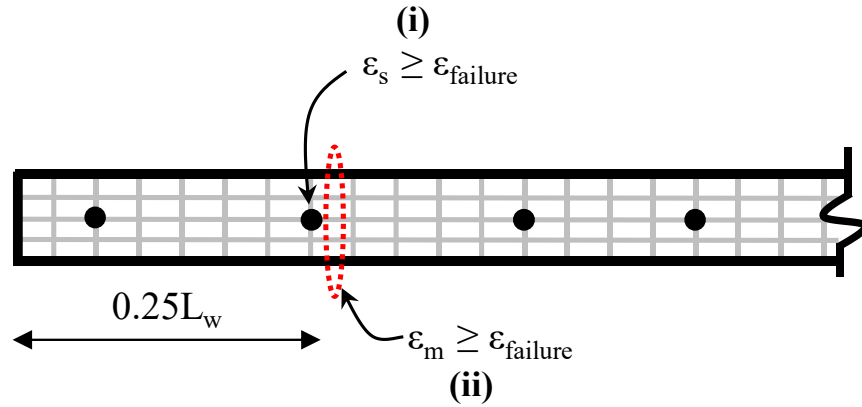
Figure 4.6. Reinforcing steel and Masonry failure criteria (i) Steel rebar rupture (ii) Masonry crushing failure

4.4   Validation of the Model

The validation of the modelling approach and presumed failure criteria were conducted against the results of Shedid et al. (2008) and Siyam et al. (2015) experimental studies. These experimental studies were considered since they are covering a wide range of reinforced masonry walls in terms of the aspect ratio, level of axial loads, and different end configurations. After applying the axial load and holding it constant, the reverse cyclic loading protocol is applied at the top of the model same as the one applied to the experimental test setup. The configuration and specification of each wall are tabulated in Table 4.1; demonstrating the aspect ratio, vertical and horizontal reinforcement ratio, level of axial load, dimensions of tested walls, masonry compressive strength, and reinforcement steel yield strength for different walls.

Figure 4.7 shows the comparison of the experimental versus the numerical cyclic response curves of the walls. As shown, the numerical model results and the experimental response are in a good agreement. The model is capable of simulating the most remarkable characteristics of the experimental cyclic hysteresis response (i.e., initial stiffness, peak- load, post-peak strength and stiffness degradation, in-cycle and cyclic deterioration, hysteretic shape, and pinching effect due to energy dissipation at different levels of inter-storey drift). Table 4.2 summarizes the results from the verification models, including the maximum lateral force capacity, V_{max}; the initial stiffness, $K_{initial}$, unloading stiffness corresponding to 1% drift, $K_{unloading}$, yield displacement, Δ_y, and shear

load corresponding to yielding, V_y. The average difference for each set of the compared results is minimal. The maximum observed divergence in the prediction of lateral load capacity and lateral stiffness was 4 and 8%, respectively. In addition to that, the maximum difference of 11% was observed in predicting the unloading stiffness of a simulated wall. The yielding displacement of the walls is also well-predicted at different levels of drift with a maximum difference of 12%. Furthermore, the results show that both the failure criteria and modelling approach used for the numerical analysis was precise and acceptable. The validated models' analogy was then used to perform a seismic collapse risk assessment on the group of walls under investigation.

Table 4.1. Wall details and specifications based on [a] Shedid et al. (2009) and [b] Siyam et al. (2015)

Wall ID number	Height (m)	Length (m)	Vertical Reinforcement ρ_v (%)	Horizontal Reinforcement ρ_h (%)	f'_m (MPa)	f_y (MPa)	Aspect Ratio
W1[a]	3.99	1.80	1.17	0.30	13.50	495	2.21
W2[a]	3.99	1.80	0.55	0.30	13.50	495	2.21
W3[a]	3.99	1.80	0.55	0.30	13.50	495	2.21
W1[b]	2.16	1.53	0.60	0.26	19.30	495	1.40
W5[b]	2.16	0.59	0.60	0.26	19.30	495	3.60
W6[b]	2.16	0.46	0.60	0.26	19.30	495	4.60

Table 4.2. Summary of verification results: Numerical results against experimental data based on [a] Shedid et al. (2009) and [b] Siyam et al. (2015)

Wall ID Number	Numerical/Experimental Ratio				
	V_{max}	$K_{initial}$	$K_{unloading}$	Δ_y	V_y
W1[a]	0.99	0.93	0.95	1.07	1.01
W2[a]	0.98	1.07	0.92	0.96	1.03
W3[a]	0.97	0.97	0.89	1.12	1.08
W1[b]	1.03	1.08	1.02	0.99	1.06
W5[b]	1.02	0.94	0.96	1.08	0.97
W6[b]	1.04	0.99	0.97	1.05	1.05
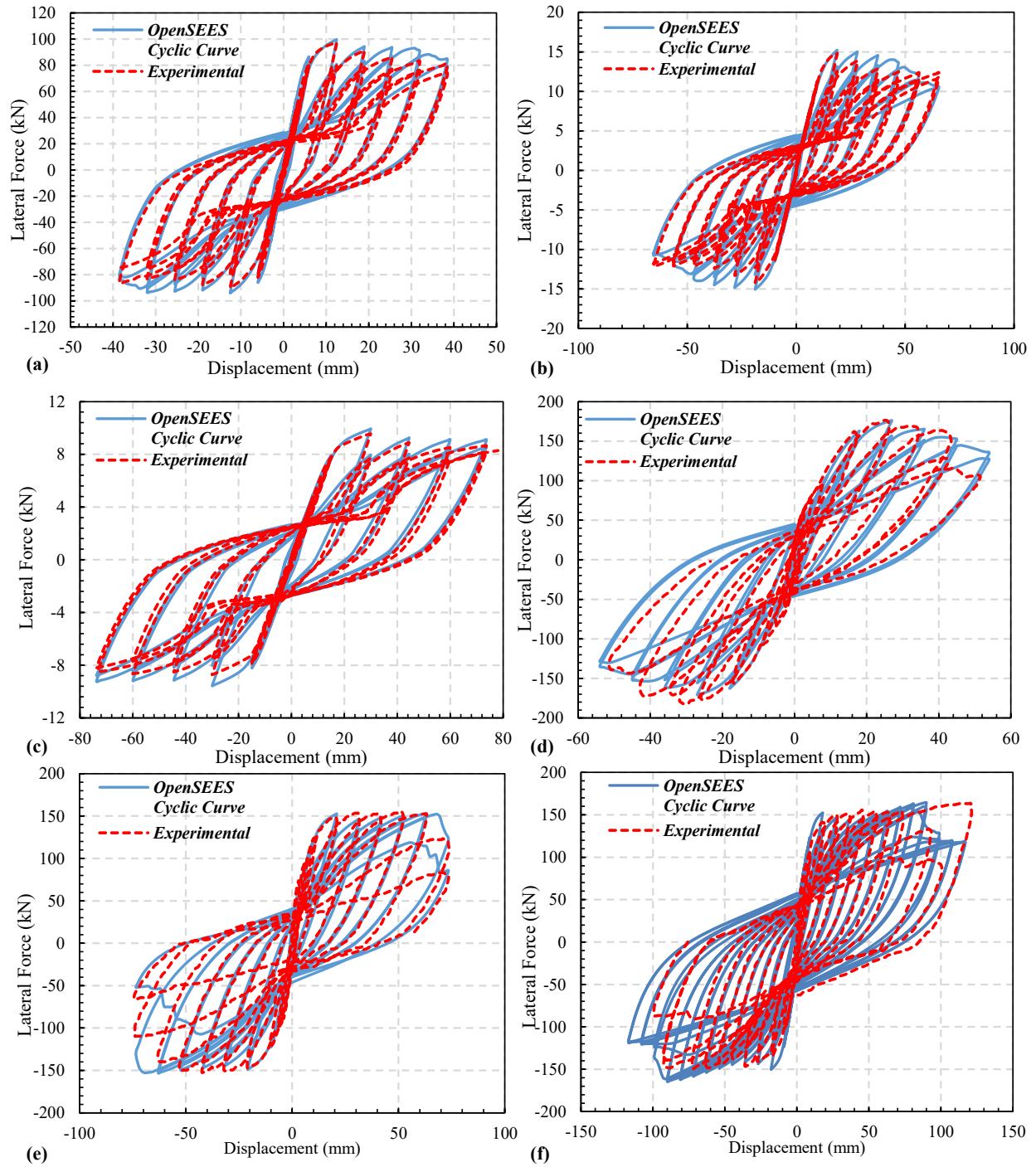
Figure 4.7. Comparison of numerical results against experimental data: (a)Wall 1 Tested by Siyam et al.; (b) Wall 5 Tested by Siyam et al.; (c) Wall 6 Tested by Siyam et al.; (d) Wall 1 Tested by Shedid et al.; (e) Wall 2 Tested by Shedid et al.; (f) Wall 3 Tested by Shedid et al.

4.5   RM Archetype and shear walls' configuration

In this paper, two critical performance group archetypes were chosen from the NIST GCR 10-917-8 (2010) RM shear wall archetypes. A total number of five archetypes were chosen namely performance groups 5 and 6 of NIST GCR 10-917-8 study. These walls incorporate various design parameters such as axial load, seismic hazard level, wall height, and different aspect ratios. These walls represent reinforced masonry buildings with different occupancies (i.e., 1-storey Commercial and 2, 4, 8, and 12-storey Residential buildings). The elaborated details of the buildings and wall design are available in Appendix A of the NIST (2010) study. For the sake of comparison, the archetype models were redesigned to incorporate a flanged cross-section while the seismic performance parameters (i.e., R, C_d, and Ω_0) remained the same as the one proposed by the original study. The index RM flanged shear walls were redesigned in accordance with design requirements of Building Code Requirements and Specification for Masonry Structures (MSJC 2013), and ASCE/SEI 7-10, Minimum Design Loads for Buildings and Other Structures (ASCE, 2010). The RM Flanged Shear Walls' dimension and the reinforcement ratio of the first floor of the walls are summarized in Table 4.3. The effective flange width was calculated in accordance with the required design criteria proposed by MSJC 2013. Horizontal ties were positioned at the same spacing as the transverse reinforcement of the walls, using the same grade. The chosen archetype possesses low gravity loads and the Seismic Design Category (SDC) of D_{max} based on the Minimum Design Loads and Associated Criteria for Buildings and Other Structures (ASCE/SEI 7-16). This data set was selected since it was found to be the most critical performance group among the rest of the proposed configurations.

Minimum base shear and storey drift limits were considered in the design process of all archetypes using the requirements of ASCE/SEI 7-16. Table 4.4 summarizes the seismic design parameters of the RM Flanged Shear Walls, including the response spectrum of Maximum Considered Earthquake (MCE) at the fundamental period of the given archetype. The code-based period is the upper-bound approximate fundamental period estimated based on the equation, $T=C_uT_a$ (ASCE/SEI 7-16). A lower bound value of 0.25 seconds is considered based on the Methodology's recommendation. The code-based period remained the same as the values of the original study since they are irrelevant to the configuration of the wall. In order to evaluate the eigenvalue periods (T_1), a linear elastic model has been developed with half of the effective

moment of inertia (I_e) of the original uncracked masonry wall cross-section considering the elasticity modulus recommended by the MSJC (2013) requirements (FEMA 2009).

Table 4.3. Configuration and reinforcement details of RM flanged shear walls

Archetype ID	Height (m)	Length (m)	Flange Length (mm)	Vertical reinforcement			Horizontal reinforcement (mm)	ρ_h(%)	Aspect Ratio
				Each Flange	Web	ρ_v(%)			
S11-F	3.65	7.31	350	4-#3	4-#4	0.07	#5@1220	0.085	0.50
S12-F	6.10	9.75	500	4-#5	6-#6	0.157	#4@800	0.082	0.63
S13-F	12.19	9.75	1000	4-#6	8-#6	0.200	#6@800	0.180	1.25
S14-F	24.38	9.75	1220	4-#8	8-#8	0.340	#4@800	0.082	2.50
S15-F	36.58	9.75	1220	4-#6	2*8-#8	0.400	2*#5@1220	0.072	3.75

Table 4.4. RM flanged shear wall archetype design characteristics

Archetype ID	No. of Stories	Gravity Loads	Key Design Parameters						S_{MT}(T) (g)
			Seismic Design Criteria						
			SDC	R	T (sec)	T_1(sec)	V/W (g)		
S11-F	1	Low	D_{max}	5	0.25	0.11	0.200		1.50
S12-F	2	Low	D_{max}	5	0.26	0.13	0.200		1.50
S13-F	4	Low	D_{max}	5	0.45	0.22	0.200		1.50
S14-F	8	Low	D_{max}	5	0.75	0.6	0.160		1.20
S15-F	12	Low	D_{max}	5	1.02	0.85	0.118		0.89

4.6   Seismic Collapse Evaluation

Based on FEMA-P695 Methodology (FEMA, 2009), quantification of building system performance and response parameters have been conducted for use in seismic design. The methodology consists of establishing seismic performance factors that comprise the development of probabilistic collapse risk assessment and detailed system design information, using nonlinear dynamic analysis and explicitly considering uncertainties associated with the test data and design, ground motion, and modelling (FEMA, 2009).

4.6.1   Nonlinear static pushover analysis

Pushover analysis was performed in order to estimate the lateral force and deformation capacity of the archetype model. The analysis was conducted according to FEMA-P695

requirements using a lateral load distribution proportional to the fundamental mode shape. The results were used to establish the capacity curves illustrated in Figure 4.8 for the archetype walls before and after incorporation of the flanged wall.

By comparing the capacity curves, the initial stiffness values were almost identical for the Flanged and Rectangular RM shear walls. However, by adding a flange, the lateral load capacity of the walls increased significantly. In addition, the results showed an increase in the ultimate displacement and ductility capacity of the flanged RM shear walls compared to their counterpart.

Over-strength of the structure, Ω, and period-based ductility, μ_T, are two parameters that can be derived directly from the pushover analysis results. The definition of the over-strength factor is shown in Eq. 4.1, as the ratio between the maximum base shear (V_{max}) to the design base shear (V) of the structure.

$$\Omega = \frac{V_{max}}{V}$$
(4.1)

The period-based ductility is, μ_T, is defined in Eq. 4.2 is the ratio of roof ultimate drift displacement, δ_u, to the roof effective yield drift displacement $\delta_{y,eff}$.

$$\mu_T = \frac{\delta_u}{\delta_{y,eff}}$$
(4.2)

The roof effective yield drift displacement is given by the following formula (Eq. 4.3) in FEMA-P695.

$$\delta_{y,eff} = C_0 \frac{V_{max}}{W} [\frac{g}{4\pi^2}][\max(T, T_1)]^2$$
(4.3)

In the above-mentioned equation, C_0 is a coefficient that relates fundamental-mode (single degree of freedom) displacement to roof displacement, V_{max}/W is the maximum normalized base shear, g is the gravity constant, T is the fundamental period of the structure based on empirical formula and T_1 is the fundamental period of the model estimated by eigenvalue analysis. The μ_T factor is later used for performance evaluation.
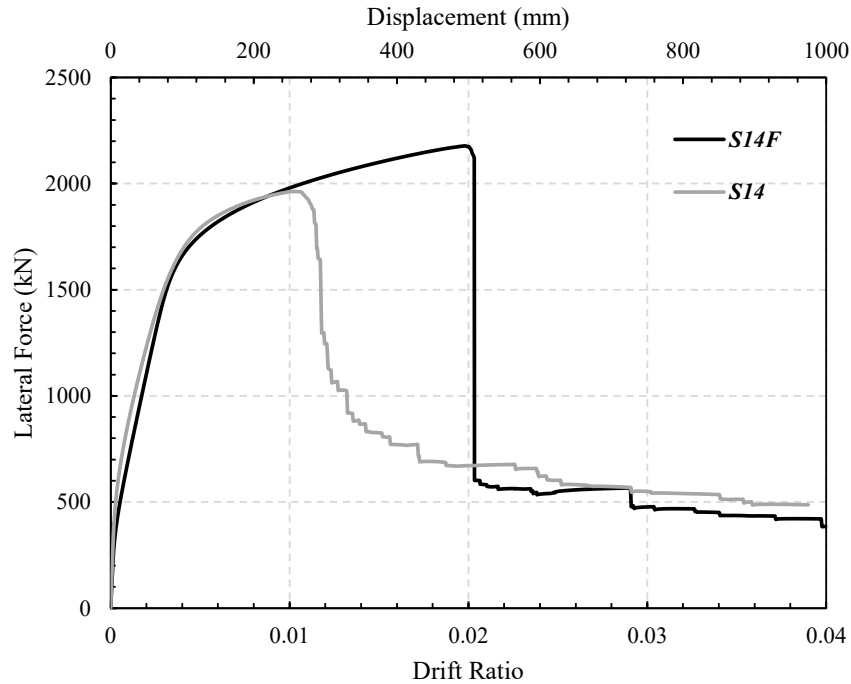
Figure 4.8. Comparison of pushover curves of Flanged against Non-Flanged archetype model S14

4.6.2 Nonlinear response history analysis

The inelastic behaviour of the RM Flanged wall system in this study was determined by means of Incremental Dynamic Analysis (IDA). The method is explained in detail by Vamvatsikos and Cornell (2002). The method involves subjecting the structure to a series of Non-linear Response History Analysis (NLRHA) increasing the intensity of the ground motion until the collapse of the structure occurs. The chosen Intensity Measure (*IM*) in this study is the 5% damping spectral acceleration estimated at the fundamental period of the structure (*T*) specified as *Sa(T,5%)*. The analysis result, IDA curves, demonstrates the relationship between Intensity Measure and the Engineering Demand Parameter (*EDP*). The chosen *EDP* in this study is the Inter-storey Drift Ratio of the structure. The structural damping was considered by means of mass and stiffness proportional Rayleigh damping method. A damping ratio of 5%, a typical value for RM structures, was assigned to the first two modes of the structure except for one storey building T_1 and $0.2T_1$ was used instead. Howbeit, the Rayleigh damping feature in *OpenSees* can estimate the damping matrix using the initial, current, and/or last committed stiffness matrix, the committed stiffness

65

matrix was used in the current work. However, the rigid truss elements that linked the frame and the leaning columns do not possess any sort of damping.

4.6.3 Selection and scaling of ground motion records

Based on FEMA-P58-1 (2012) a minimum set of 7 ground motion is required to surmount the record-to-record variability observed in a small suite of ground motions. In contrast, using more than 44 ground motion records for collapse risk assessment is recommended by FEMA-P695 to achieve more reliable results. However, the large computational effort is always a disadvantage of using a large number of strong-motion records. To be consistent with the methodology's recommendation, the applied ground motion record set is taken to be the same as the records proposed by the FEMA- P695. In this regard, 22 pairs of far-field ground motion records were selected to conduct the Time-History Analysis. The median response spectrum of all records was scaled to match the spectral acceleration of the MCE level spectrum at the fundamental period of the structure, T (Appendix A. FEMA-P695). The normalized response spectrum of the 44 ground motion records is shown in Figure 4.9.
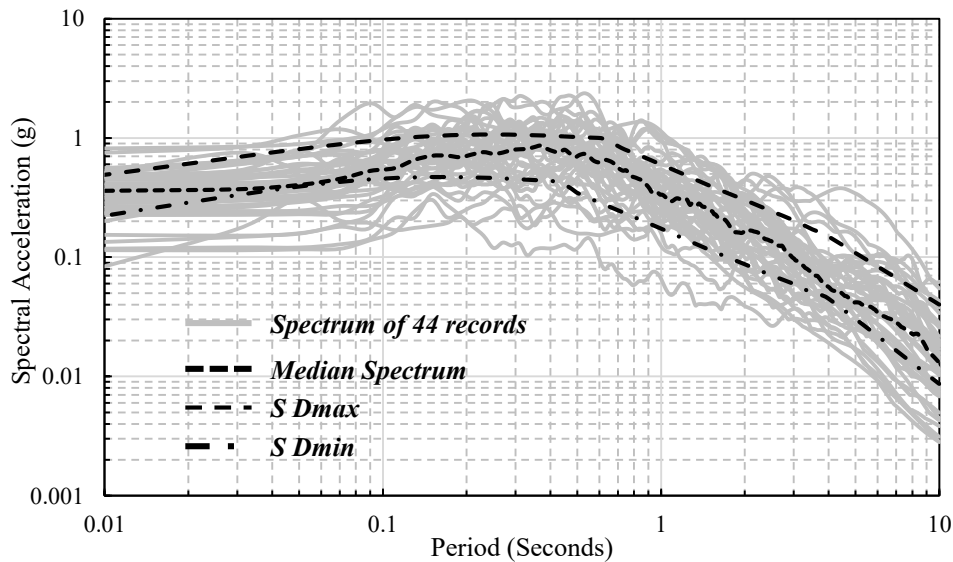
Figure 4.9. The normalized response spectrum of 44 ground motion records, median spectrum, Upper bound (S Dmax); and Lower bound (S Dmin)

4.7   Results and Discussion

4.7.1   Seismic Design Parameter and Performance Quantifications

By extracting the IDA curves and depicting the 16th, 50th, and 84th fractiles of the IDA results presented in Figure 4.10; the necessary parameters to assess collapse criteria were developed. These curves expressed the dispersion of the response of each archetype to the various ground motion frequency content in terms of inter-storey drift ratio. Figure 4.11 shows the 16th, median and 84th percentile of the RM shear walls before and after incorporating a flanged cross-section. The results indicate that by adding a flange to the archetypes the destabilizing effect of the data set ground motions are postponed and the structure shows more residual strength relative to the non-flanged models. Consequently, RM Flanged shear walls represent larger ultimate curvature that delays the collapse of these walls.

The calculation of median collapse intensity (S_{CT}) has been conducted for each model. Based on the definition, the minimal intensity at which half of the records were observed to result in collapse is the median collapse intensity, S_{CT}. In this study, the value of S_{CT} was defined based on the material strain limitation described in the previous section. The Maximum Considered Earthquake (*MCE*) spectral acceleration intensity (S_{MT}) was also calculated with respect to the fundamental period of the model. The ratio between the median collapse intensity, S_{CT}, and the MCE intensity, S_{MT}, is defined as the collapse margin ratio (*CMR*). This value is the principal parameter to characterize the collapse safety of the structure (Eq. 4.4).

$$CMR = \frac{S_{CT}}{S_{MT}} \tag{4.4}$$

The value of Ω, S_{CT}, and S_{MT} for both flanged on non-flanged walls are summarized in Table 4.5. As shown, the *CMR* values of the original archetypes are consistent with the values obtained from NIST GCR 10-917-8(2010), confirming that the approach is valid and sufficiently accurate.

Table 4.5. Summary of collapse results for RM flanged shear wall archetype

Archetype ID	Design Configuration			Pushover and IDA Results			
	No. of Stories	Gravity Loads	SDC	Static Ω	$S_{MT}[T]$ (g)	$S_{CT}[T]$ (g)	CMR
S11	1	Low	D_{max}	1.85	1.5	0.95	0.63
S11-F	1	Low	D_{max}	2.36	1.5	3.00	2.00
S12	2	Low	D_{max}	1.85	1.5	2.35	1.57
S12-F	2	Low	D_{max}	1.94	1.5	4.20	2.80
S13	4	Low	D_{max}	1.85	1.5	2.50	1.67
S13-F	4	Low	D_{max}	2.04	1.5	4.75	3.17
S14	8	Low	D_{max}	1.61	1.2	1.89	1.58
S14-F	8	Low	D_{max}	1.78	1.2	3.75	3.13
S15	12	Low	D_{max}	1.50	0.89	2.00	2.25
S15-F	12	Low	D_{max}	1.95	0.89	3.20	3.60
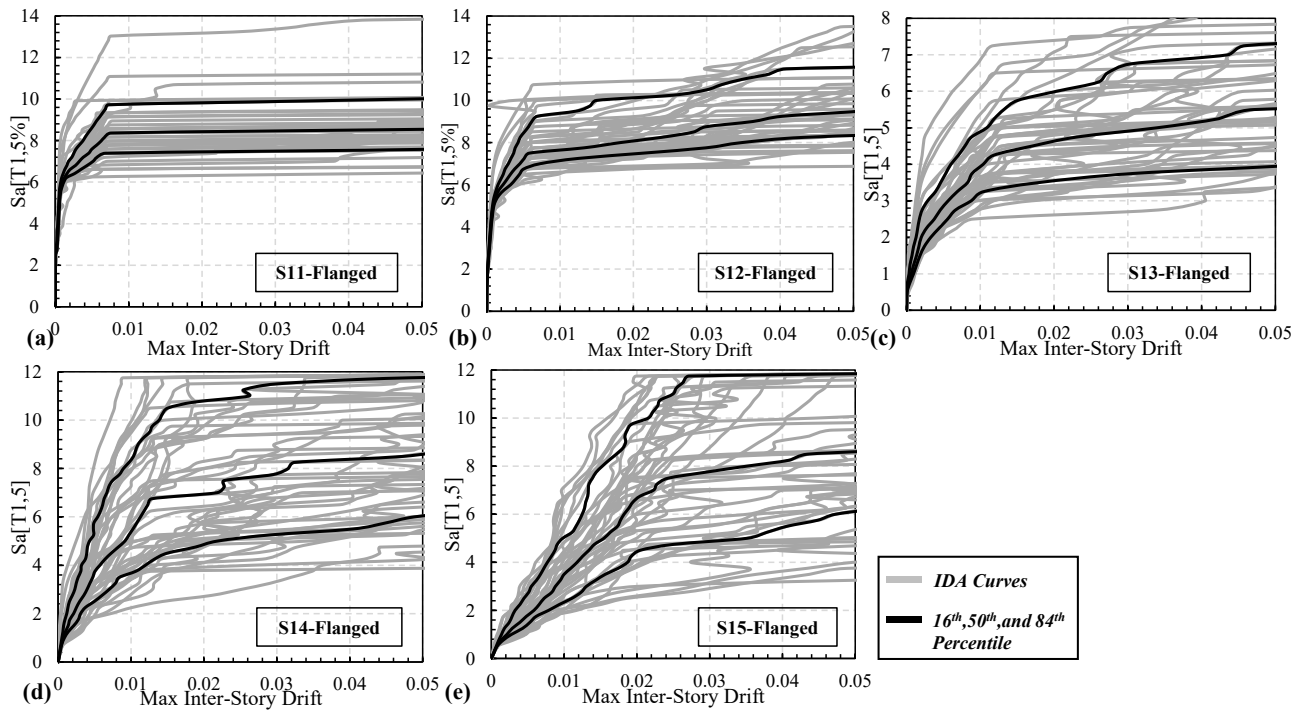
Figure 4.10. IDA response curves of each archetype and 16, 15, and 84 percentiles: (a) S11-flanged wall; (b) S12- flanged wall; (c) S13- flanged wall; (d) S14- flanged wall; (e) S15-flanged wall
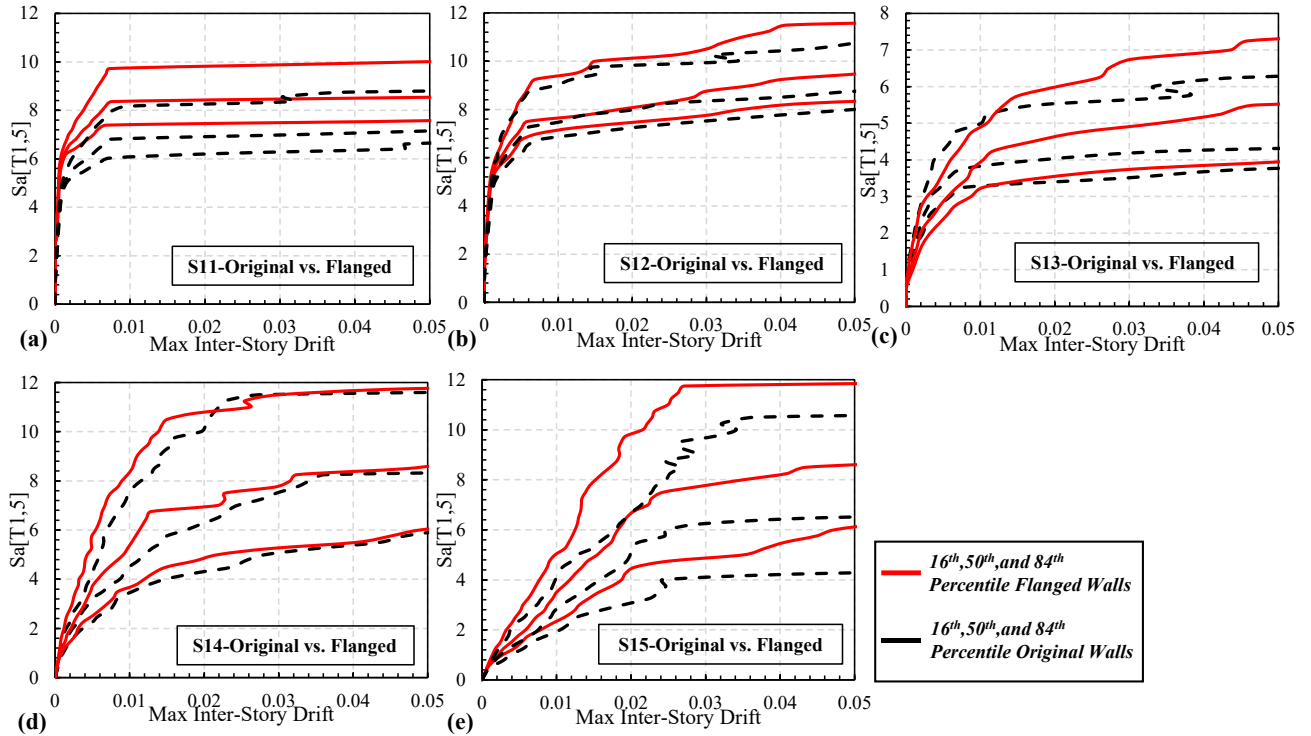
Figure 4.11. Comparison of IDA response curves of each archetype and 16, 15, and 84 percentiles with and without Flanged Cross-Section: (a) S11; (b) S12; (c) S13; (d) S14; (e) S15

4.7.2 Collapse fragility analysis

To obtain the collapse fragility curve, Incremental Dynamic Analysis was performed to determine the minimum collapse intensity of the structure. This type of analysis consists of several nonlinear time history analysis with an increasing increment such that the structure will experience dynamic instability for each record. Once a collapse occurred in the structure, additional analyses will be performed to determine the collapse intensity for a specific tolerance. Each structure was analyzed against 44 ground motion records with at least 48 different intensity factors. Therefore, 2112 time-history analysis was performed for each archetype model. This method was used by several researchers in recent years (e.g. Ezzeldin et al. 2016; Siyam et al. 2016). The collapse probability for a specified Intensity Measure (*IM*) will be estimated as the number of records causing collapse at a certain IM, divided by the total number of records as the intensity of the ground motion increases. A sample set of data used in the development of the fragility curve is summarized in Table 4.6, following the aforementioned method of calculation.

The ATC-58-1 (ATC 2009) recommends the use of cumulative distribution function to generate fragility functions based on a log-normal probability distribution. The log-normal probability distribution function is given by Eq. 4.5.

$$P(C|IM = x) = \phi\left(\frac{\ln(x/\theta)}{\beta}\right)$$

(4.5)

where $P(C|IM = x)$ is the probability of collapse at a given intensity, ϕ is the standard normal cumulative distribution function (CDF), θ is the collapse median intensity, and β is the standard deviation (dispersion) of IM. The parameters of fragility fitting function (i.e., θ and β) are estimated following the maximum likelihood method (Baker 2015). In this method, the mean and dispersion of the data are estimated in a way to maximize the likelihood of CDF function in the reproduction of the observed data points.

Although the failure criteria for the material was defined to numerically capture the instability of the structure, some failure modes are not possible to be captured during the analysis. Therefore, these failure criteria are captured after the post-processing of the obtained results. These criteria are elaborated in the subsequent section.

Table 4.6. Sample data set used in the development of the archetype's fragility curve

IM	Number of analyses	Number of collapses	Fraction causing collapse	Theoretical fragility function
0.10	44	0	0.00	0.00
0.48	44	0	0.00	0.00
0.87	44	5	0.11	0.00
1.25	44	7	0.16	0.04
1.63	44	12	0.27	0.14
2.01	44	23	0.52	0.29
2.40	44	28	0.64	0.46
2.78	44	32	0.73	0.60
3.16	44	33	0.75	0.72
3.54	44	36	0.82	0.81
3.93	44	37	0.84	0.87
4.31	44	38	0.86	0.91
4.69	44	42	0.95	0.94

| 5.08 | 44 | 43 | 0.98 | 0.96 |
| 5.46 | 44 | 44 | 1.00 | 0.97 |

4.7.3   Failure Criteria based on chosen Engineering Demand Parameter

Besides the collapse criteria that focus on the uniaxial materials, there is another type of failure criterion which is relative to the performance of the whole component or system level. The latter criteria are known as the Engineering Demand Parameter (*EDP*) based method in which the collapse occurs when a certain limit of *EDP* (i.e., inter-storey drift in this study) is exceeded. Based on the suggested requirements of FEMA-P58-1 the inter-storey drift is limited to 0.01 times the storey height in the walls classified as masonry cantilever shear wall structures. Meanwhile, the maximum allowable drift for the structures to be functional is limited to 0.025 times the height based on NBCC 2015. Currently, FEMA P58-1 designated the maximum inter-storey drift ratio to be 2.5% to evaluate the level of damage that occurred on the structural components and lateral load resisting systems, which is consistent with NBCC (2015). Another collapse assessment approach is described by Vamvatsikos and Cornell (2002), which uses the Intensity Measure to define the collapse. In this method, the last point on the IDA curve (i.e., Intensity Measure corresponding to that point) with a tangent slope equal to 20% of the elastic slope is defined as the initiation of collapse. For the sake of comparison, in the current study damage states were kept constant based on the performance levels proposed by ASCE 41-17 (2017), and fragility curves for different damage states were developed accordingly. Immediate Occupancy (IO), Life Safety (LS), and Collapse Prevention (CP) performance limits were considered for the seismic collapse assessment. The curve-fitting procedure to establish fragility curves are presented in Figure 4.12, and Figure 4.13 shows the fragility curves of the original archetypes versus the RM Flanged shear walls.

For all the archetypes shown in Figure 4.13, the walls with flanges possess larger collapse spectral capacity, S_{CT}, compared to the planar walls. As is shown, the impact of adding a flange to the walls are more significant on the walls with larger aspect ratios (i.e., taller walls), whereas for higher level of drift due to corresponding performance level (i.e., CP performance level) the walls with the flanges show less probability of collapse against imposed lateral loads. The reason is that the flanged elements decreased the curvature at the initiation of yielding of the longitudinal steel bars and increased the curvature at the ultimate state, therefore enhanced the walls' curvature.

In general, the RM flanged walls resulted in the reduction of compression zone depth, which resulted in increasing the moment arm and ultimately led to higher wall cross-section moment capacity.

4.7.4   Collapse performance evaluation

In order to evaluate the performance, the estimated *CMR* value needs to be amended to take the effect of ground motions frequency contents into account (i.e., spectral shape effect). This amendment is possible via the application of the Spectral Shape Factor (SSF) presented in Table 7-1 provided by FEMA-P695 (2009). This factor was used to adjust the pre-estimated *CMR* to obtain the *Adjusted CMR* (i.e., *ACMR* value).

ACMR value is the function of the model fundamental period (T_1) and μ_T parameter obtained from the nonlinear static analysis. Consequently, the *ACMR* values along with their corresponding *SSF* are calculated and summarized in Table 4.7 for each of the archetypes. A comparison is needed between the acceptable ACMR values and the calculated ones in order to evaluate the system's credibility in fulfilling the requirement of the methodology. The estimation of the acceptable ACMR values is possible through the evaluation of the total system uncertainty (β_{TOT}), which is presented in (Eq. 4.6). The β_{TOT} is a value that combines different uncertainty sources related to record-to-record (β_{RTR}), design requirements (β_{DR}), test data (β_{TD}), and nonlinear modelling (β_{MDL}).

$$\beta_{TOT} = \sqrt{\beta_{RTR}^2 + \beta_{DR}^2 + \beta_{TD}^2 + \beta_{MDL}^2} \tag{4.6}$$

The value of β_{RTR} was considered to be equal to 0.4 and kept constant for the selected ground motions for all of the archetypes, finding that period-based ductility, μ_T, is greater or equal to 3.

In this paper, the design procedures of the RM flanged archetypes followed the recent provisions provided by MJSC 2013. Moreover, RM Flanged walls have been utilized as the primary lateral force resisting systems in various low-rise to high-rise buildings (El-Dakhakhni and Ashour 2017). Therefore, according to the FEMA-P695 (2009) criteria, the current RM Flanged design provisions are categorized as B (good) with the uncertainty level of 0.2 (i.e., $\beta_{DR}=$ 0.2).

The data available in the literature regarding RM Flanged walls is relatively low compared to other RM rectangular walls. Moreover, the available test data are mostly focused on component behaviour rather than the global behaviour of the structure. Hence, RM Flanged walls' test data is assessed as B (good) with uncertainty corresponding to test data, (β_{TD}), of 0.2.

The developed nonlinear numerical model is determined to be B (good) with the uncertainty level for the nonlinear model (β_{MDL}) equals to 0.2. The justification of this choice is because the developed model is capable of capturing the principal factors that might collaborate into the collapse of RM Flanged walls (i.e., flexural/shear failure, sliding shear failure, and rebar buckling/rupture besides concrete crushing/cracking).

Substituting the values to Eq. 4.6, β_{TOT} is equal to 0.525. Based on a table provided in FEMA-P695 (2009), the allowable *ACMR* for 20% collapse possibility of the *MCE* ground motions records (i.e., *ACMR20%*) is 1.56. *ACMR20%* is chosen since the probability of collapse for *MCE* level should be 20% or less for each archetype of the performance group of the interest.

The comparison of the *ACMR* values with the acceptable values for each archetype model of both systems (Flanged and Non-Flanged) is summarized in Table 4.7. The first performance group of RM walls without flanges could not satisfy the required provisions proposed by the methodology. On the contrary, the selected RM Flanged walls could meet the minimum requirement demanded by FEMA-P695 methodology acquiring a higher collapse margin, despite that, these flanged walls were designed to withstand the same seismic loads as the walls without the flanges. The results show that the selected RM flanged wall system performed safely against the lateral loads by showing a lower probability of collapse due to the development of a higher level of reserved over-strength provided by the flanged segment. It can be proved that the low-rise archetypes (1 & 2 Storey archetypes) are more prone to collapse without incorporation of the flanged cross-section. Although, the response modification factor correlated to low-rise walls is large enough to suffice the performance requirement objective of the guidelines. Meanwhile, the rest of the models (4, 8, and 12 stories archetypes) can fulfill the requirement of the methodology while an adjustment is needed to R-factor for using flanged cross-section in those archetypes based on the results (i.e., R-factor can be increased since it satisfied the ACMR requirements).

Table 4.7. Summary of collapse performance evaluation of RM flanged shear wall archetype

| Archetype ID | Design Configuration | | Computed over-strength and collapse margin parameters | | | | | Acceptance check | |
	No. of Stories	End Configuration	Ω	CMR	μ_T	SSF	ACMR	Acceptable ACMR	Pass/ Fail
S11	1	Without Flange	1.85	0.63	5.22	1.26	0.80	1.56	Fail
S11-F	1	With Flange	2.36	2.00	7.57	1.33	2.66	1.56	Pass
S12	2	Without Flange	1.85	1.57	8.15	1.33	2.08	1.56	Pass
S12-F	2	With Flange	1.94	2.80	10.12	1.33	3.72	1.56	Pass
S13	4	Without Flange	1.85	1.67	11.30	1.33	2.22	1.56	Pass
S13-F	4	With Flange	2.04	3.17	16.11	1.33	4.21	1.56	Pass
Mean of Performance Group		Without Flange	1.85				1.7	1.96	Fail
		With Flange	2.11				3.53	1.96	Pass
S14	8	Without Flange	1.61	1.58	13.85	1.40	2.21	1.56	Pass
S14-F	8	With Flange	1.78	3.13	24.47	1.40	4.38	1.56	Pass
S15	12	Without Flange	1.50	2.25	42.12	1.47	3.30	1.56	Pass
S15-F	12	With Flange	1.95	3.60	47.60	1.47	5.29	1.56	Pass
Mean of Performance Group		Without Flange	1.56				2.76	1.96	Pass
		With Flange	1.87				4.84	1.96	Pass
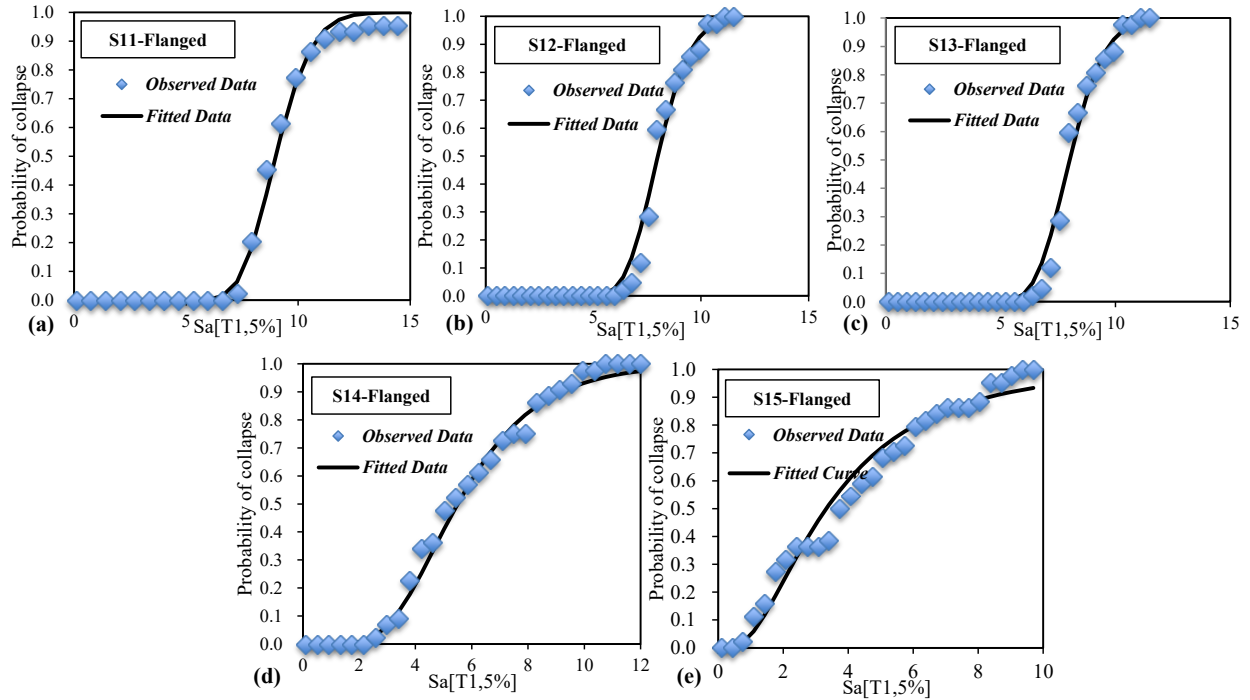
Figure 4.12. Curve fitting of fragility functions of different archetypes (a) S11-Flanged Wall; (b) S12-Flanged Wall; (c) S13-Flanged Wall; (d) S14-Flanged Wall; (e) S15-Flanged Wall
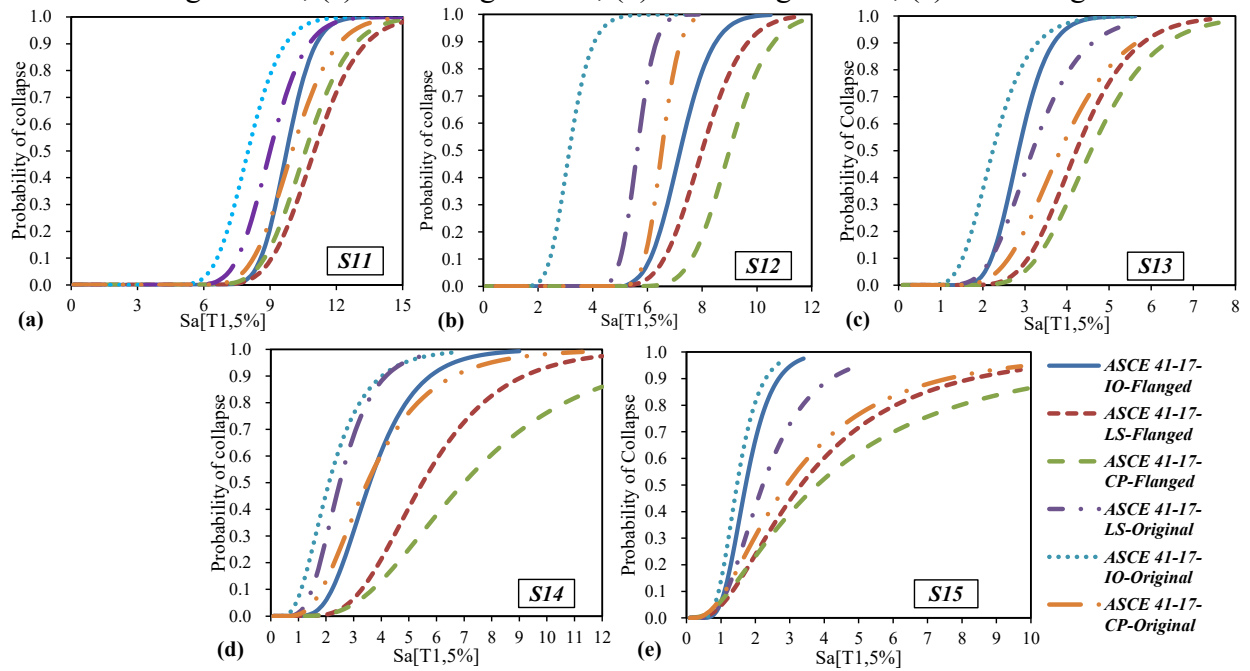
Figure 4.13. Comparison of collapse fragility curves for each archetype with and without Flanged cross-section: (a) Archetype S11; (b) Archetype S12; (c) Archetype S13; (d) Archetype S14; (e) Archetype S15

4.7.5   Inter-storey Drift variation

Inter-storey Drift variation of each archetype model is presented in the following section. Inter-storey drift is an important representative of collapse initiation in the performance-based seismic design of the structures. The variation of the drift ratio is shown in Figure 4.14 in terms of boxplots for each of the archetype walls at the design level before and after adding a flange to the cross-section. In this figure, the solid line shows the upper bound and lower bound of the drifts due to imposing 44 ground motion records on the RM walls. The beginning of the box indicates the first quartile, and the end shows the third quartile while the line in between illustrates the second quartile or the median of the observed data. As can be seen in the figure, the lower bond and upper bond for the maximum inter-storey drift ratios of the low-rise original archetypes were approximately 0.3 and 3.0%, respectively, while this value fluctuates along 0.1 and 2.5% for mid to high-rise archetypes. The median values of the drift ratios decreased dramatically by adding flanges to the archetype models. The impact of implementing flanges is more magnificent in mid to high-rise models rather than low-rise walls as a result of higher mode contribution. The results show an average decrease in the maximum drift ratio of up to 28% relative to the original structure. A significant decrease in the median inter-storey drift was observed in comparison with the original structures for all cases. The justification of this phenomenon would be the capability of the flanged walls to resist lateral loads due to possessing higher curvature ductility which can alter the behaviour of the structures to be more ductile with a higher level of energy dissipation. Therefore, it limits the inter-storey drift ratio of the flanged walls while postponing the stiffness degradation which leads to less damage to both structural and non-structural components. Meanwhile, the interquartile range was found to be smaller in the flanged walls compared to the original structures, which means a lower amount of maximum drift ratio variation to different ground motion records and more reliable and predictable behaviour of the components. However, on the high-rise model, Figure 4.14 j, the interquartile range increased on the lower stories, the median values are decreased subsequently which provides a reasonable safeguard against seismic lateral load damages. On average, all archetypes have shown more curvature ductility due to the adoption of the flanges which resulted in an overall increase of the systems' ductility while minimizing the inter-storey drift ratio and its associated damages.
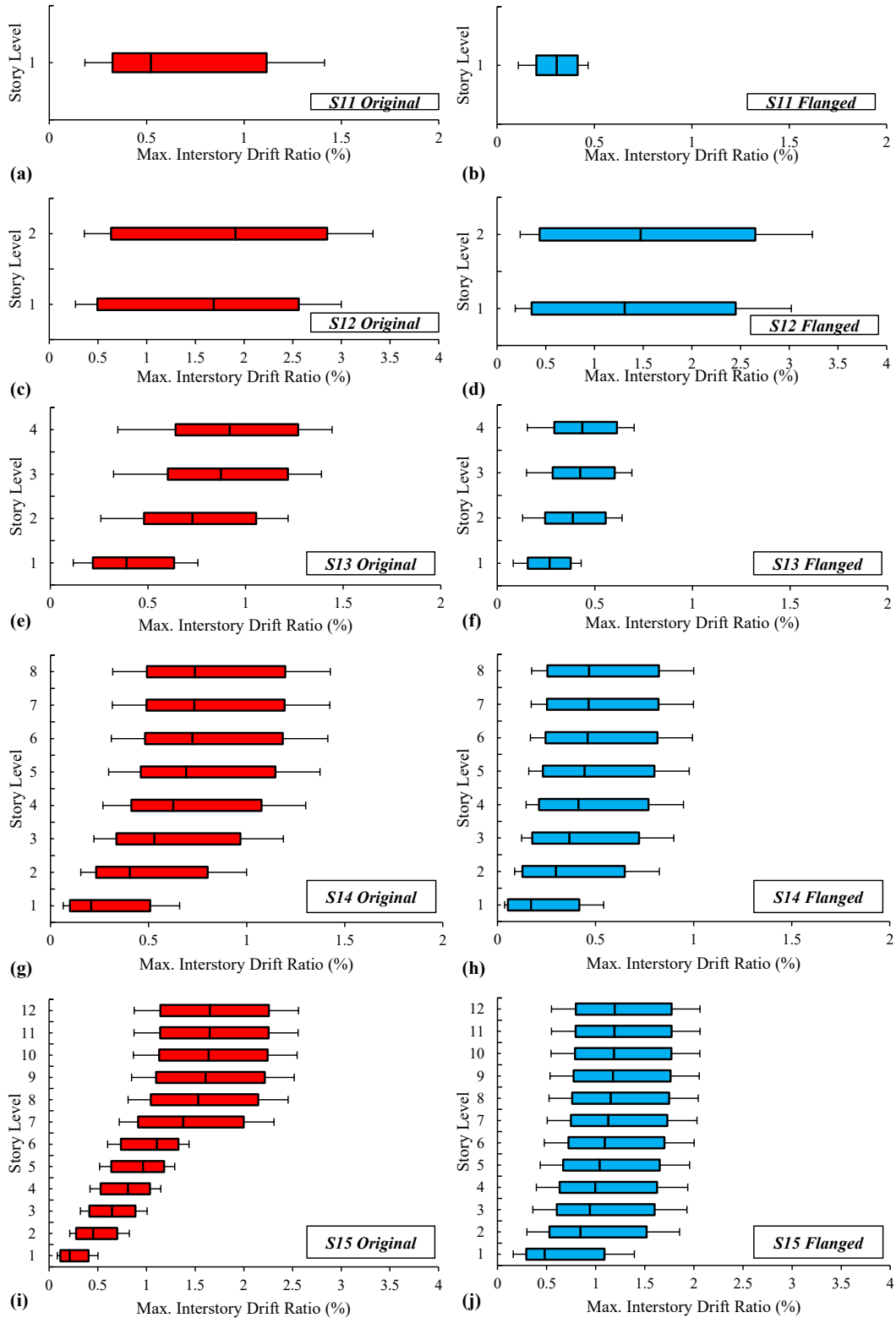
Figure 4.14. Inter-storey Drift Box-Plot variation at Design Level: (a) S11 W/O Flange; (b) S11 Flanged; (c) S12 W/O Flange; (d) S12 Flanged; (e) S13 W/O Flange; (f) S13 Flanged; (g) S14 W/O Flange; (h) S14 Flanged; (i) S15 W/O Flange; (j) S15 Flanged

77

4.8   Seismic Resilience

As a brief definition, seismic resilience describes the loss and recovery required to maintain the functionality of the system with minimum interruption (Cimellaro et al. 2006). The resilience also takes the impact of the recovery process including the behaviour of individuals and organizations in the post-disaster phase into account. In order to quantify the seismic resilience of structures, the alphabet of structure functionality needs to be defined.

Loss and recovery time are estimated with respect to the fragility assessment in order to calculate the remaining functionality of the structure after an earthquake event. The resilience function can be found as the area beneath the functionality curve which is defined analytically as per Eq. 4.7.

$$R = \int_{T_{0E}}^{T_{0E}+T_{LC}} Q(t)/T_{LC} dt \tag{4.7}$$

where the functionality, $Q(t)$, ranges from 0 to 100% meaning total loss and no reduction in the performance, respectively. Literally, if an earthquake happens at time T_{0E} it could cause sufficient damage to the structure and reduce its performance (i.e., $Q(t)$ function Figure 4.15b). Afterward, within a period called recovery period, T_{RE}, the system will be able to recover itself to the same functionality level prior to the extreme event, which is observed over a control time period, T_{LC}. There are different methods to estimate the functionality of the structure while in this study the method proposed by Cimellaro et al. (2010) is utilized to approximate the functionality over the time given in Eq. 4.8.

$$Q(t) = 1 - L(I, T_{RE})\{H(t - T_{0E}) - H[t - (T_{0E} + T_{RE})]\} \times f_{REC}(t, T_{0E}T_{RE}) \tag{4.8}$$

In this equation, I represent the intensity of the earthquake, L (I, TRE) is the loss function, f_{REC} is the recovery function and $H(t)$ is the Heaviside step function which is equal to zero for negative values and returns one when positive.

As mentioned earlier, the loss function is dependent on earthquake intensity and recovery time. The total loss, L, is comprised of structural, L_S, and non-structural loss, L_{NS}. In this study, only the structural losses are considered to determine the total loss of the archetype and the impact of the non-structural element was neglected. The damage evaluations are stated in terms of

economic cost (i.e., US Dollars) and/or the ratio of cost of repair and reinstalling the structure to the cost of full replacement of the structure (Coburn and Spencer 2002). The evaluation of the direct economic losses was conducted following Hazus MH2.1 (2016) methodology for a given damage level. Subsequently, the value of the structural losses, L_S, was determined using Eq. 4.9.

$$L_s = \sum_1^N CS_{DS} = BRC \times \sum_1^N POSTR_{DS} \times RCS_{DS}$$

(4.9)

in which CS_{DS} is the cost of the structural damage due to the given damage level (DS); $POSTR_{DS}$ equals to the probability of exceedance at a certain intensity in the damage state, RCS_{DS} shows the structural repair cost ratio associated with the damage state; and BRC is equal to the total replacement cost which is estimated based on the average cost per square feet of the wall ($/S.F) for the selective project, according to market (RS Means, 2017). The parameter N also indicates the number of damage states considered.

Different shapes of recovery functions are available in the literature namely linear, exponential, and trigonometric. In this study, the exponential method has been considered assuming a fast response of society to disaster events. Meanwhile, it is assumed that the recovery rate decreases slightly (Tirca et al. 2015). The recovery function is also a function of recovery time and the time needed for the component replacement of the structures (Eq. 4.10).

$$f_{REC}\left(t, T_{0E}, T_{RE}\right) = \exp\left[-\left(t - T_{0E}\right)\left(\ln 200 / T_{RE}\right)\right]$$

(4.10)

The Quantification of the seismic resilience of a system is possible through the definition of *robustness, rapidity, redundancy, and resourcefulness* attributes (Cimellaro et al. 2003). Robustness, *R*, is the capacity of the system to resist the earthquake's action without being affected by any probable secondary hazard that may occur and is represented by *R (%) = (1-L)*. Robustness has an impact on both economic and social aspects besides its technical dimension since damage inside a system will affect the community's economy and has a negative effect on the population. *Redundancy* is defined as the extent to that the systems' component can be replaced or their function can be satisfied by other system and/or component elements after the seismic event, such that, the system can maintain its functionality as it did initially. The latter attribute is well-tied to the social measures which are not the interest of this research study. *Resourcefulness* is the ability

to identify the appeared problems after the seismic disaster and mitigating them using the available resources in order to recover to the full functionality of the system. Finally, the *rapidity*, υ, is defined as the functionality curve slope during the recovery time, T_{RE}. In this study, only the components related to the structural components level are addressed and measures defined for the community level were excluded. The flowchart of the methodology proposed to evaluate the seismic resilience of the conventional RM shear wall is shown in Figure 4.15a. The total loss and time of recovery are calculated based on the damage level, and lastly, the seismic resilience of the studied models has been conducted following the adopted guideline. The schematic drawing of the functionality curve and recovery time function is shown in Figure 4.15b.

4.8.1 Recovery time & losses estimation

Losses are estimated due to the damages that occur to the structural components. In this research study, only the impact of direct economic losses to structural components is taken into account. To estimate the total losses (L_S) the following parameters need to be defined: (1) damage probability of structural components relative to a certain damage level, $POSTR_{DS}$; (2) corresponding repair cost ratio, RCS_{DS}, and (3) the structure replacement cost, BRC.

The damage probabilities, $POSTR_{DS}$, were determined based on the fragility curves (Table 4.10). The repair cost ratios were taken as per the values suggested by HAZUS MH2.1 (FEMA 2015). It is noted that the repair cost ratios are variables with uncertainty levels and typically are dependent on other parameters such as region, recourse capability and labour and material. The structural repair cost factor, total replacement cost, and total loss estimations are tabulated in Table 4.8 and Table 4.10 respectively. The recovery time found to be the most challenging parameter to define since it is a random parameter correlated to many uncertainties associated with the hazard level, and the quantity of the available resources. HAZUS MH2.1 recommends using roughly a year assumption as the recovery time; however, it is not applicable to all cases. In this study, the estimated recovery time is chosen to be 60 days for all archetypes assuming the fact that sufficient resources are available to meet this timeframe. This time could be less for low-rise archetype, was kept constant for the sake of comparison of both systems before and after adding flanges. The computed resilience attributes (*rapidity* and *robustness*) of the original and flanged walls are given in Table 4.9. Models with flanges proved to have a lower value of rapidity (i.e., they can recover faster). The functionality curves obtained for both Flanged and Non-flanged archetypes are

illustrated in Figure 4.16. As shown in Figure 4.16 the archetypes with flanges show larger value of seismic resilience and robustness compared with those without flanges. The stacked area cumulated between two curves indicates the percentage that the flanges contribute to seismic resilience and robustness of the selective RM walls. Consequently, the low-rise archetypes achieved lower robustness relative to mid- and high-rise buildings. This result is expected while assessing the seismic resilience of structures since taller buildings quantitatively possess more elements that are typically prone to structural and non-structural damages arising from earthquakes compared to low-rise buildings.

Table 4.8. Structural repair cost ratios (in % of structure replacement cost)

Occupancy Class	Type of component	Structural Damage State		
		Slight	Moderate	Extensive
Residential	Structural	0.2	1.4	6.8
Commercial	Structural	0.2	1.1	5.5

Table 4.9. Summary of the results from resilience analysis

ID	T_{RE} (days)	υ (%)	R (%)
S11	60	0.077	95.40
S11F	60	0.042	97.50
S12	60	0.047	97.20
S12F	60	0.033	98.00
S13	60	0.042	97.50
S13F	60	0.015	99.10
S14	60	0.058	96.50
S14F	60	0.017	99.00
S15	60	0.075	95.50
S15F	60	0.050	97.00
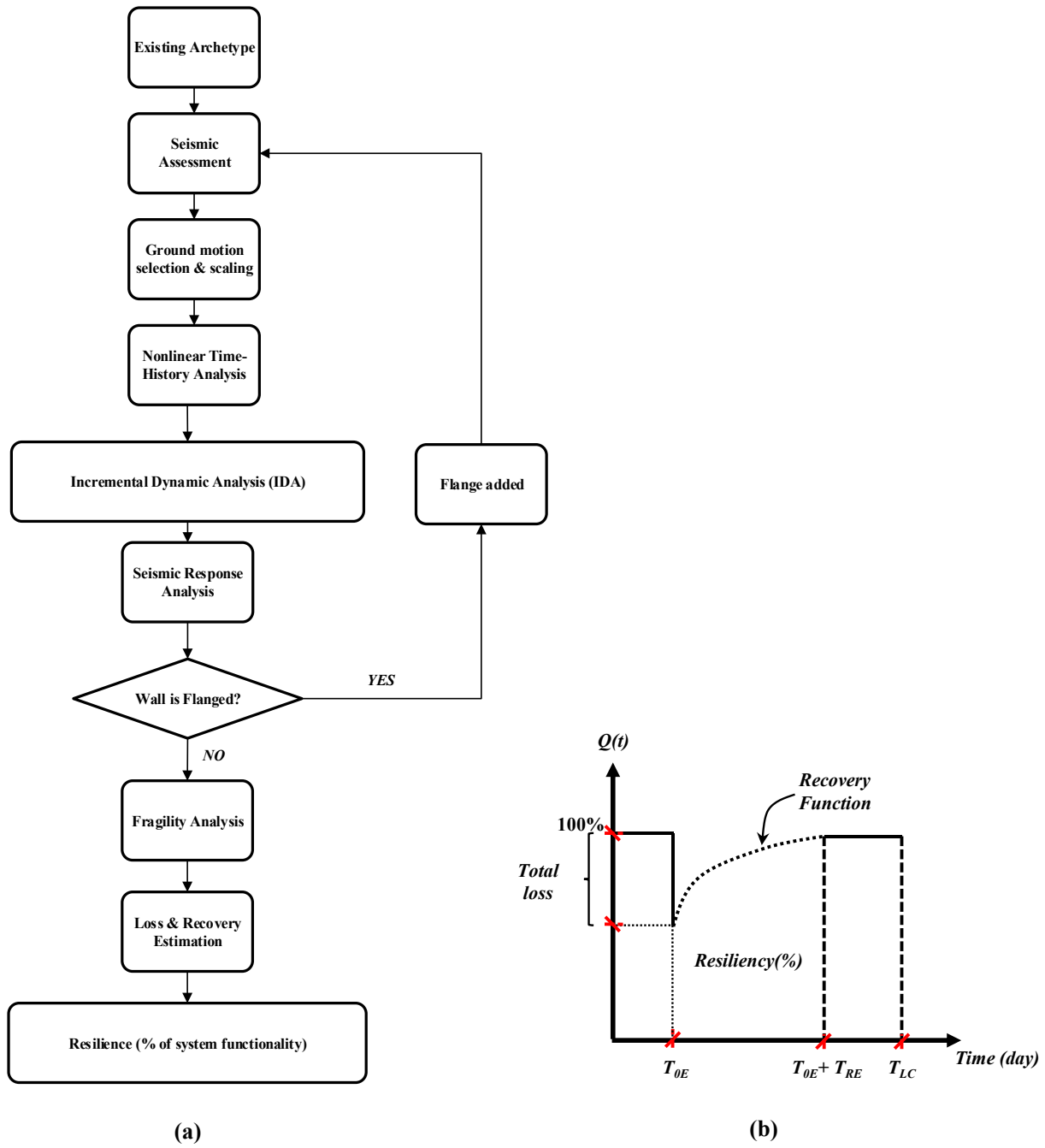
Figure 4.15. Seismic Resilience Framework (a) Resilience Functionality assessment flow chart; (b) Functionality curve and recovery time function

Table 4.10. Estimated losses of archetype structural component

Archetype ID	Replacement Cost (BRC)	Structural Losses (L$_s$)	Loss Function (%)	POSTR (From fragility Curve) %		
				Slight	Moderate	Extensive
S11	$4,423.20	$131.37	3.0	80	55	30
S11-F	$4,843.40	$45.62	0.9	33	14	10
S12	$11,795.20	$332.62	2.8	100	90	20
S12-F	$13,004.21	$283.49	2.2	60	50	20
S13	$23,590.40	$541.64	2.3	85	45	22
S13-F	$28,426.43	$184.77	0.7	78	11	5
S14	$47,180.80	$1,623.96	3.4	76	65	35
S14-F	$58,976.00	$382.16	0.6	50	10	6
S15	$70,771.20	$3,381.45	4.8	97	70	53
S15-F	$88,464.00	$2,949.39	3.3	94	45	37
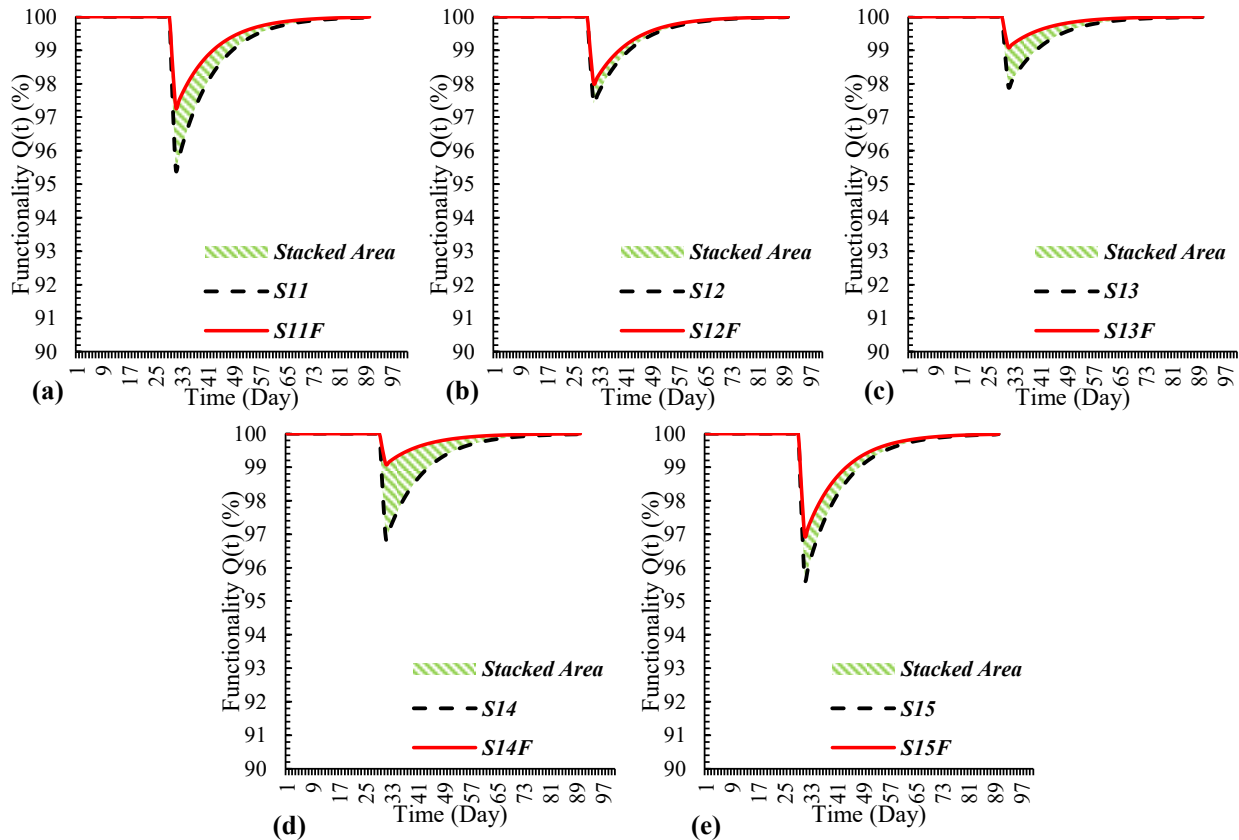
Figure 4.16. Comparison of Functionality curves of the archetypes with and without flanged cross-section (a) Archetype S11; (b) Archetype S12; (c) Archetype S13; (d) Archetype S14; (e) Archetype S15

4.9   Conclusions

In this study, the collapse risk assessment of RM flanged walls was conducted under the maximum credible earthquake using the same seismic performance factor adopted to the rectangular RM shear walls systems. The modelling approach was initially developed by other researchers for reinforced concrete structures, however, modifications were applied in the current study to consider the impact of shear flexibility and leaning column analogy on the seismic behaviour of the RM flanged shear walls. In this regard, 5 archetypes of reinforced masonry shear walls, initially proposed by NIST GCR 10-917-8 (2010), were redesigned adopting flanged cross-section. The proposed archetypes were evaluated using FEMA-P695 methodology utilizing the macro-modelling approach developed in *OpenSees*. The methodology consists of the development of the analytical model, selection and scaling of the ground motion records, conducting Nonlinear Pushover Analysis and Incremental Dynamic Analysis, generating the IDA and Fragility curves to describe the collapse probability of the structural system. The evaluation of Seismic resilience of the RM Shear wall structures before and after utilizing the flanged elements has been conducted in order to estimate total loss and recovery time due to seismic events. The concluded remarks are summarized as follows:

• The proposed modelling approach proved to be capable of simulating the behaviour of reinforced masonry shear walls (with and without flanges) under cyclic loading. The maximum difference for the prediction of lateral load capacity and lateral stiffness using the approach was 4 and 8%, respectively. Moreover, the numerical model performed well in predicting the unloading stiffness of a simulated wall with a maximum divergence of 11%;

• The pushover analysis result shows that by adding flanges to the RM shear walls, the capability of the walls to dissipate more energy caused by lateral loading can be increased significantly. The walls with the flanges proved to be more ductile and possess a higher level of lateral load resistance against applied forces relative to the rectangular walls. The overstrength factor of each archetype shows that by incorporating flanges to the cross-section, the ultimate curvature was increased and lead to increasing the displacement ductility. The results revealed an up to 70 % increase in the displacement ductility. Utilizing the RM flanged walls has reduced

compression zone depth, ended in increasing the moment arm and ultimately higher wall cross-section moment capacity;

• The study by NIST GCR (2010) proved that the RM shear walls with rectangular cross-sectional area using design factor, R-factor, of 5 did not fulfill the acceptable provisions proposed by methodology (i.e., the low-rise archetypes had a collapse margin ratio less than acceptable limits of the methodology). Based on the previous studies the response modification factor of low-rise rectangular walls can be reduced. Conversely, the results of this study suggest that adding flanges to walls enhances the low-rise walls to fulfill the methodology's criteria by obtaining greater levels of ductility, however, more numerical models with different configurations should be developed for a thorough application of FEMA P695 methodology. More importantly, the results indicate that the selected walls with two stories and taller are able to pass the methodology's requirements while the response modification factor of such walls can be increased when flanges were used;

• Incorporating flanges into the RM shear wall structure had a significant influence on the inter-storey drift ratio of the system. The results indicate that flanged walls performed well in reducing inter-storey drifts of mid and high-rise archetypes up to 28% enhanced system performance. Moreover, the fluctuation of drift ratios was lower than the corresponding values in the original structures;

• RM flanged shear walls had a slight impact on the seismic resilience and functionality of the models compared to the original archetypes. From the fragility analysis, it is concluded that RM flanged walls experience less damage and are more rapid to be functional after an earthquake event. In addition, losses calculated for the mid-rise archetypes are relatively larger than the low-rise models. The average seismic resilience of the flanged walls was 98.12% which is around 2% higher than the non-flanged walls. It can be concluded that from the structural point of view the impact of using flanges in seismic resilience of the structural elements is minor compared to the cost of fabricating the flanges. However, this research study only discussed the structural aspect of seismic resilience and direct economic losses due to structural components and did not address non-structural losses associated with the drift and acceleration level of the structures. The authors suggest additional experimental and/or numerical studies on flanged end configurations of RM shear walls.

• Some limitations in studying seismic resilience of structures can be pointed out such as the region-specific estimation of repair cost ratios, lack of more complex loss and recovery estimation functions to include the fatalities and business interruption that needs further studies to lead to a more comprehensive and inclusive understanding of economic and social impacts of resilience-based engineering.

Chapter 5

System-Level Seismic Resilience Assessment of Reinforced Masonry Shear Wall Buildings with Masonry Boundary Elements

5.1   Abstract

The concept of seismic resilience plays an important role in seismic assessment of structures as it assesses the capability of a system to withstand an unwanted event, such as earthquakes, by estimating the losses and determining the system's functionality and sustainability during and after such event. In this study, a framework was utilized to assess the seismic resilience of Reinforced Masonry Shear Wall (RMSW) buildings as well as studying the impact of incorporating Masonry Boundary Elements (MBEs) at the ends of RMSW. To achieve this goal, a ten-storey RMSW building was numerically modelled in *OpenSees* to assess the seismic performance and resilience of the system when adding confined MBEs. The selected building is located in Montreal, Canada, and initially designed to be built having rectangular walls. Subsequently, the walls were redesigned to integrate MBEs at their outermost fibre to help increase the ductility and strength of the RMSWs. A full 3D wide-column macro-modelling approach was used to simulate the dynamic response of the archetype building. Validation of the modelling approach was done against available experimental tests as an initial step to ensure the robustness of the model in predicting the inelastic response of the building. Subsequently, the models were analyzed against multiple ground motion records using Incremental Dynamic Analysis to identify the initiation of collapse alongside developing the fragility curves of the building. The system-level seismic performance of the building was assessed after incorporating MBEs. The resilience of the building was assessed using the developed fragility functions, and a comparison was made to highlight the effect of using MBEs on the response of the studied RMSW building. The results showed a significant enhancement in the seismic resilience of the building by using confined MBEs at the shear walls' extreme.

5.2   Introduction

Concrete masonry blocks were commercially available by the end of the nineteenth century to make the feasibility of the concrete-block masonry structural walls possible. During the past few decades, there has been many research addressing the seismic response of Reinforced Masonry Shear Wall (RMSW) constructed with concrete-blocks masonry. However, most of these studies addressed rectangular shear wall systems, and very rarely, they investigated walls incorporating flanges or masonry boundary elements (MBEs) (Ahmadi et al. 2015, Shedid and El-Dakhakhni 2010). These RMSWs can be utilized as fully or partially grouted, end-confined, or non-confined walls depending on the seismic hazard zone, providing the designers with the versatility needed to integrate a competent Seismic Force Resisting System (SFRS) for mid and high-rise buildings. It is worth noting that, analytical and numerical modelling are more recently considered and used by many researchers since they are less expensive and more effective in modelling different aspects of structures, hence overcoming many drawbacks caused by experimental tests such as high expenses, scaling method, etc. (Nasiri and Liu 2017, Siyam et al. 2016, Cancelliere et al. 2010, Magenes 1997). Numerical modelling proved to be capable of capturing experimental outcomes with a high level of accuracy while providing more control over the failure modes, loading protocols, and collapse assessment of the respective structure (Stavridis et al. 2010, Ezzeldin et al. 2016). However, the literature shows a lack of relatively simplified macro-models that can predict the inelastic behaviour of the RM Shear walls. As will be discussed later, these macro-models are essential, not only to facilitate evaluating the overall response of the system, but also to help better understanding the system's performance in accordance with the new seismic performance standards and assessment approaches, e.g., ASCE 41-17 (ASCE 2014), FEMA P-695 (FEMA 2009), and FEMA P-58 (FEMA 2012).

The proposed capacity design methodology introduced by Park and Paulay (1975), which emphasizes that any sudden strength loss and non-ductile failure modes (i.e., shear and brittle failure) need to be avoided, has presented appropriate detailing of structural components to ensure a stable and predictable behaviour of the whole system during a seismic event. Reinforced Masonry (RM) shear walls that are designed based on the capacity design methodology would have satisfactory ductility levels in a seismic event and be able to sustain large reversible cycles of inelastic deformations without significant degradation in strength. This level of ductility can be

achieved by integrating a confined zone at the ends of rectangular RM shear walls, which results in achieving a higher level of displacement and curvature ductility and enhances the overall performance of the component during the seismic events compared to that of RM rectangular walls (Banting and El-Dakhakhni, 2012, 2014; Ezzeldin et al., 2017; Ezzeldin et al., 2016; Shedid et al., 2010b). Priestley and Elder (1982) tested three scaled slender RMSW with an aspect ratio of 2.5. The test by Priestley and Elder (1982) studied the impact of axial stress and confinement plate at the mortar bed joints. High levels of strength and stiffness degradation were reported as a result of increasing the axial stress. The walls' ductility was significantly enhanced by using the steel confinement plates. Shedid et al. (2009, 2010) tested seven half-scale RMSW under fully reversed quasi-static cyclic loading. These walls were designed to experience ductile flexural failure and possessed different end configurations (i.e., Rectangular, Flanged, and end-confined MBE). All walls had an aspect ratio greater than 1.5 and were detailed and designed to ensure sufficient diagonal and sliding shear capacity. The effect of changing the amount and distribution of vertical reinforcement and the level of axial load on the RMSW lateral strength and ductility was evaluated, and it was concluded that the walls' lateral capacities are highly influenced by the vertical reinforcement ratio and the level of the axial stress. It was also concluded that the addition of end confinement zones increased the ductility capacity by 106% relative to the rectangular wall with similar lateral resistance. Moreover, their tested end-confined shear wall had a larger drift capacity of almost twice corresponding to the 20% strength degradation in comparison to the rectangular counterpart shear wall. A saving of 40% in the longitudinal reinforcement was also reported by the authors after using MBEs at the wall's extreme sides. Banting and El-Dakhakhni (2014) tested five half-scale RMSWs having confined scheme under reversed quasi-static cyclic loading. The specimens covered a vast range of shear walls in terms of aspect ratio, height level, and reinforcement ratios.

The results inferred that using MBEs improved the post-peak performance of the wall and postponed the shear failure of such walls almost in all cases. Also, it helped with delaying buckling of the longitudinal reinforcement and grout core crushing. Hence, preventing the walls from losing their lateral resistance abruptly because of face shell spalling of the compressive side. Overall, the performance of the walls was well-improved by showing higher curvature levels in the presence of MBEs. Siyam et al. (2016) studied the collapse probability of a Ductile Reinforced Concrete Block Wall office building having rectangular and flanged walls using the FEMA P-58

methodology through fragility curves. An analytical 2D model was developed and calibrated against the experimental data. Subsequently, an incremental dynamic analysis (IDA) was performed to determine the collapse initiation of the RMSW building under a suite of ground motions.

Most of the available numerical studies focused on simulating the nonlinear response of the individual shear wall component rather than the complete building system. Nonetheless, other parameters can be assessed through system-level studies such as the out-of-plane response of the walls as well as the impact of torsional forces due to the irregularities of the structure. An experimental study by Ashour and El-Dakhakhni (2015) highlighted the importance of slab flexural coupling at the system-level response of RM buildings. The study included the variation of the lateral load capacity, stiffness of the structure and stiffness degradation trend, and additional forces caused by torsional moments. Moreover, most of the rectangular RMSW without masonry boundary elements are reinforced with a single layer, which increases the chances of causing pre-damage when subjected to out-of-plane lateral forces, deteriorating the in-plane seismic response of the whole structure. Thus, it is crucial to assess and quantify the performance of entire RM buildings using full 3D macro models that can capture in-plane and the out-of-plane response of the whole structure in order to perform a system-level seismic resilience assessment.

In this study, a framework was utilized to assess the seismic response of the RMSW building focusing on the impact of incorporating MBEs. A full 3D 10-storey RMSW building was numerically modelled in *OpenSees* to assess the nonlinear performance and the influence of the MBEs on the overall response of the building at the system-level. The building is located in Montreal and was initially designed in accordance with the provision of the National Building Code of Canada (NBCC 2015) and CSA S304-14 using ductile RM rectangular shear wall as its SFRS. Afterward, the design was modified using identical seismic design parameters (i.e., R_d and R_o) while this time, the shear walls were designed to have the same initial stiffness with confined MBEs. An analytical macro-modelling approach, elaborated in Hosseinzadeh and Galal (2019), was chosen and updated to simulate the seismic response of RMSW building. In the current study, two perpendicular shear springs were considered to simulate in-plane and out-of-plane shear deformation of the RM walls at the system-level. To ensure the robustness of the results, the developed model was validated versus the outcome of experimental test results of a one-third scale

asymmetrical two-storey RMSW building built and tested by Heerema et al. (2015). The above-mentioned modelling method was used to perform Incremental Dynamic Analysis (IDA) on the two 3D RMSW building models, i.e., with and without MBEs. A suite of 44 far-field and 44 near-field ground motions were selected to cover a vast range of frequency content of different ground motion records in performing the IDA analysis. Different failure criteria were considered in predicting the collapse level of the building to generate seismic fragility curves for the structural elements of the studied RMSW building models. The inter-storey drift ratio of the building was monitored prior to and after adding MBEs as well as the comparison of dispersion of storey shear response forces in the entire building. The seismic resilience of the building was assessed after the adoption of MBEs to quantify their impact on the losses due to earthquakes. The outcome of such studies will promote the development of design provisions and the adoption of RMSW with masonry boundary elements in the next generation of seismic design codes in North America.

5.3   Analysis Methodology and Models' Geometry

In this research study, a fibre-based modelling approach was used to develop a numerical model in *OpenSees* software. The present study employed displacement-based beam-column elements to predict the inelastic axial and flexural deformation of the shear walls' component, whereas bilinear shear springs, were incorporated to take the effect of shear deformation into account.

The shear wall model discretization, including the nodes and elements configuration and material distribution, is shown in Figure 5.1. Four displacement-based beam-column elements were used per storey after performing sensitivity assessment targeting satisfactory accuracy in capturing the experimental results. Each element has five Gauss integration points along its length, and no soil-structure interaction was considered in the model assuming a fixed based model at the wall-foundation intersection. However, the steel reinforcement slippage in the wall-foundation intersection was modelled using a zero-length element section and stress-slip model that was proposed by Zhao and Sritharan (2007), known as strain penetration model. A uniaxial force deformation relationship was assigned to the longitudinal reinforcement using Bond SP01 material model of the *OpenSees*. The number of Masonry and Reinforcement fibres along the width of the wall was different for each model; however, they were chosen to provide fine discretization in the

cross-section while being adaptive to provide sufficient accuracy in the results. A minimum of 400 fibres was utilized to ensure the result prediction accuracy and analysis time efficiency of the model. The effect of confinement of the grout core was modelled by increasing the compressive strength and ultimate strain of masonry fibres of the confined zone using the proposed approach by Mander et al. (1988), which is accompanied by an increase in ultimate buckling/rupture strain of the reinforcement. The shear flexibility of the elements was considered using a bilinear shear spring, as shown in Figure 5.1. Zero-length spring elements were introduced at the nodes between Elements 1 & 2, and between Elements 3 & 4 to model the shear flexibility of the wall segments. The in-plane and out-of-plane shear stiffnesses of the walls were modelled by incorporating two horizontal translational degrees of freedom (*DOF*) shear links in the zero-length spring elements. The remaining *DOF*s were coupled to the adjacent node using *OpenSees equalDOF* constraints. A bilinear trend was considered to model the shear stiffness of the zero-length links based on the model proposed by Massone et al. (2006) and lately modified by Gogus and Wallace (2015). The stress-strain relation utilized in the definition of the shear-link elements is also shown in Figure 5.1.
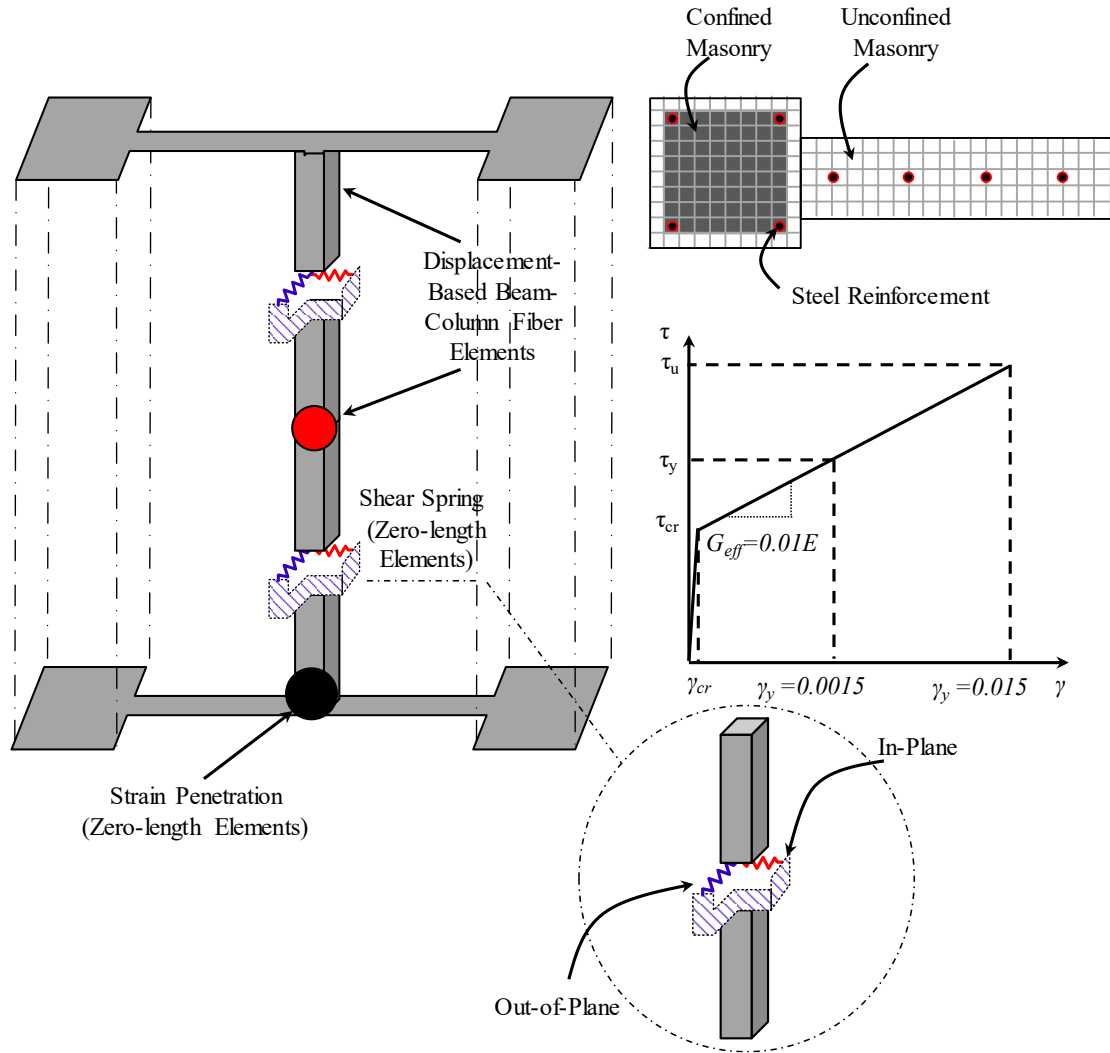
Figure 5.1. Model discretization of RM shear wall system

5.3.1 Material Characteristics and Behaviour

The material definition was considered based on the reported test data and the nominal strength of masonry and steel reinforcement. In this regard, Chang and Mander's (1994) concrete model was used to define the constitutive material laws for the masonry fibres (Concrete07 in *OpenSees*). The confined zone of the masonry was modelled using the Mander et al. (1988) stress-strain behaviour of the masonry. The maximum tensile stress of the masonry was calculated to be $f_t' = 0.623\sqrt{f_m'}$ in MPa (Yassin 1994).

The steel reinforcement was modelled by the Giuffré-Menegetto-Pinto hysteretic model (Filippou et al. 1983), also known as Steel02 in *OpenSees*. The material is capable of capturing

93

nonlinear behaviour of the steel bars with isotropic strain hardening besides being easy to calibrate. Perfectly bonded condition was assumed, and default calibration parameters were considered as recommended by *OpenSees* developers. The summary of the material properties used in the verification case and modelling the multistory building is presented in Table 5.1.

Table 5.1. Specification of the RM shear wall building used in model verification

Wall ID*	Height (mm)	Length (mm)	Aspect Ratio	Vertical Rebar ρ_v (%)	Horizontal Rebar ρ_h (%)	f_m' (MPa)	f_{yv} (MPa)	f_{yh} (MPa)
W1* W2*	2160	598	3.61	0.59	0.26-0.14	18.2	489	498
W3* W4* W6* W7*	2160	465	4.64	0.61	0.26-0.14	18.2	489	498
W5*	2160	1533	1.41	0.55	0.26-0.14	18.2	489	498
W8*	2160	1533	1.41	0.61	0.26-0.14	18.2	489	498
10-Storey Building-W1	3200	3500	0.91	0.55[a]-0.46[b]	0.42	20[c]-13.5[d]	400	400
10-Storey Building-W2	3200	6500	0.50	0.75[a]-0.66[b]	0.42	20[c]-13.5[d]	400	400

*Heerema et al. (2015), [a]RM Shear walls Without MBEs, [b]RM Shear walls With MBEs, [c]Confined Masonry zones, [d]Unconfined Masonry zones

5.3.2 Verification of the Model

The verification of the numerical models is vital to evaluate the capability of the modelling approach in predicting the experimental test results. In this regard, a one-third scale two-storey asymmetric RMSW Building tested by Heerema and El-Dakhakhni (2015) was modelled, and the result of the experimental and numerical analysis was compared. The building was made of 8 RM Shear walls, including rectangular and flanged walls. The configuration and material properties of the constituent shear walls are summarized in Table 5.1. Figure 5.2 shows the comparison of

numerical and experimental hysteresis response of Building II tested by Heerema and El-Dakhakhni (2015). The summary of the maximum difference of the experimental results versus the 3D numerical model is given in Table 5.2. The results indicate the capability of the modelling approach in predicting the most important characteristics of the RM shear wall building cyclic behaviour at different drift levels, including the peak lateral force, initial stiffness, stiffness degradation due to reinforcement buckling/rupture and masonry cracking/crushing, cyclic and in-cycle deterioration, as well as the effect of strain hardening, post-peak behaviour, and hysteretic pinching effects in the model. Based on the result presented in Table 5.2, it can be concluded that the developed model could predict the peak lateral force and the initial stiffness by a maximum difference of 7% and 9% during the whole cycles, respectively. Overall, the comparison between numerical and experimental results shows that the modelling approach is robust enough to predict the elastic and inelastic response of the RM Shear Walls. The same assumptions used in the verification were used afterward in assessing the collapse risk of the 10-storey RMSW building having various end configuration (i.e., walls without and with masonry boundary elements).

Table 5.2. Verification results summary

Specimen	Results	Initial Stiffness (kN/mm)	Error (%)	Ultimate capacity (kN)	Error (%)
Building II	Numerical	30.65	-9	221.75	-7
	Experimental (Hereema 2015)	33.41	-	238.01	-
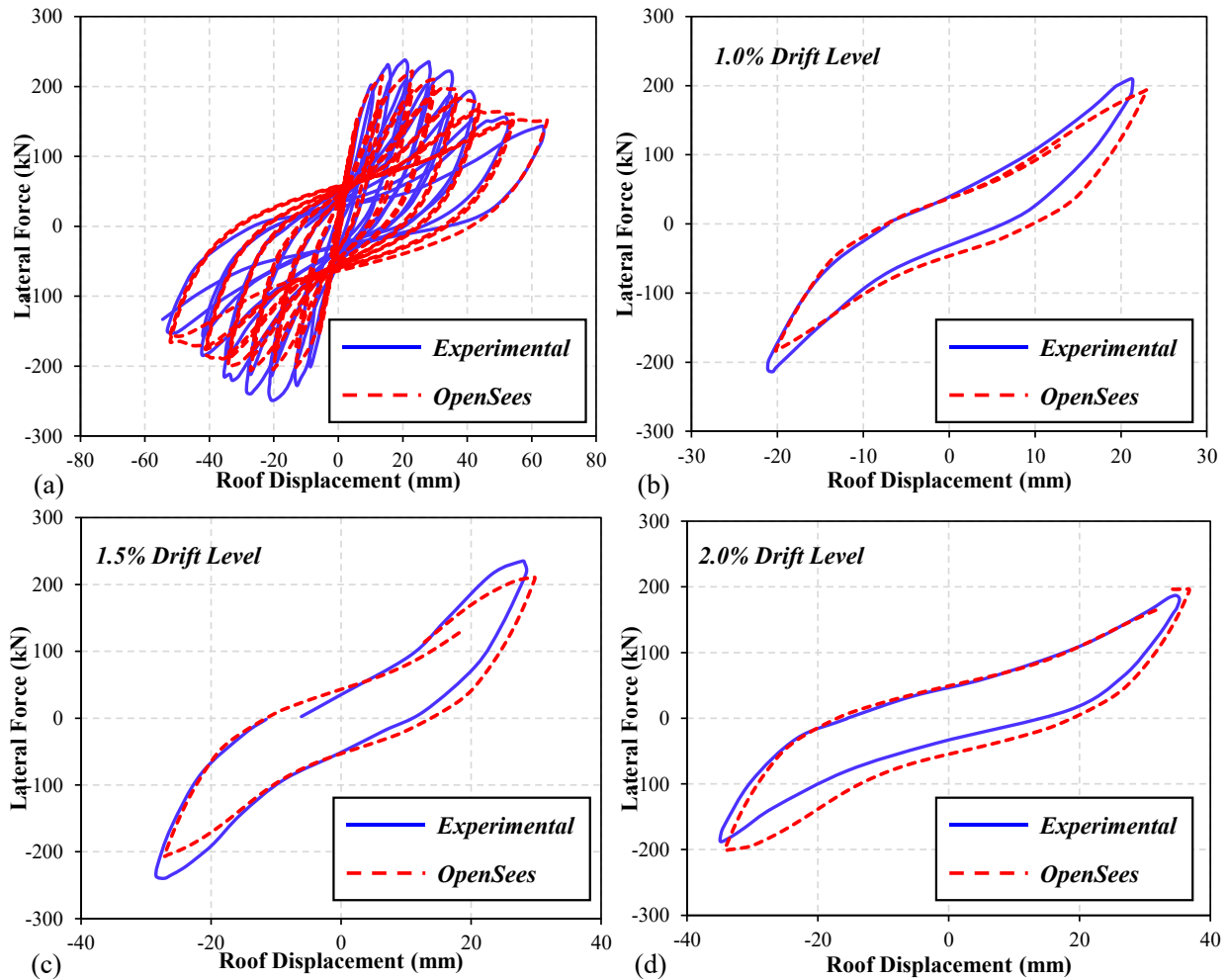
Figure 5.2. Comparison of experimental (Heerema et al. 2015) and Numerical Hysteresis loops at different drift levels

5.4 Design and Modelling of The Rectangular and Masonry Boundary Element RM Shear Wall Buildings

A 10-storey RMSW building located in Montreal, Canada, with Class-C soil subgrade, was designed based on the NBCC 2015, and the CSA S304-14. The building layout and design was originally done by Albutainy (2016, 2018) and has been used in this chapter and subsequent chapter as the case study. The floor plan is comprised of two 5.5 m end span and three 6 m interior bays in each horizontal direction, making a total plan dimension of 29 m. The typical storey height is 3.2 m for each storey, resulting in a 32 m overall height of the building. The 3D perspective, plan view, and the location of the shear walls, along the lateral loading direction of the building is

shown in Figure 5.3. The plan is comprised of 8 walls in the E-W and 8 walls in the N-S directions. The length of the walls is 6.5 meters and 3.5 meters, including the masonry boundary elements for the long and short walls, respectively. The summary of the RMSW building design and MBEs' details are shown in Figure 5.4. The ultimate compressive strength, f_m', of the confined area of the walls with masonry boundary elements was set to be 20 MPa, whereas the planar unconfined zones possess the ultimate compressive strength of 13.5 MPa. The yielding strength of steel reinforcement was also considered to be 400 MPa, which is an average value for the deformed bars as per as recommendation of CSA-G30.18-09. The building was initially designed having ductile rectangular shear walls without an end-confined zone as the main Seismic Force Resisting System (SFRS). Subsequently, the design was modified to incorporate MBEs at the extreme ends of the wall for the same lateral demand using the seismic design parameters proposed for rectangular walls by NBCC 2015 (i.e., the R_d and R_o remained identical as the rectangular walls to investigate the impact of the integration of MBEs). The design of the RMSW with MBEs and rectangular RMSWs conforms with clauses 16.9.3.2 and 16.9.3.3 of the CSA S304-14, respectively. The gravity system is made up of a 200 mm concrete slab supported by 500 mm square concrete columns. The summary of the main characteristics and the RM shear walls' details are presented in Table 5.1. A mass-stiffness Rayleigh damping method with a value of 5% was considered to model the inherent damping of the structure. The first two principal modes of vibration of the structure were considered for calculating the Rayleigh damping alongside excluding the leaning columns and rigid links from possessing any damping. A common approach of modelling a large-scale building is to consider the components that contribute to the lateral resistance of the system and entail the gravity system using a leaning column analogy to include the impact of additional second-order effects (i.e., *P-Δ* effect). In the following structural model, the lateral resistance of the building is solely provided by the RM shear walls and no lateral stiffness contribution is expected from the component other than structural elements. However, the whole building is fully modelled to include the destabilizing effect arising from the geometric nonlinearity and nonlinear *P-Δ* effect. A corotational geometric transformation built-in syntax in *OpenSees* found to be proper to transform the basic system to the global coordinate of the structure. A Rigid Diaphragm constraint was considered in each storey to restrain the rotational and translational *DOF*s of every single wall to the center of the mass of the building.
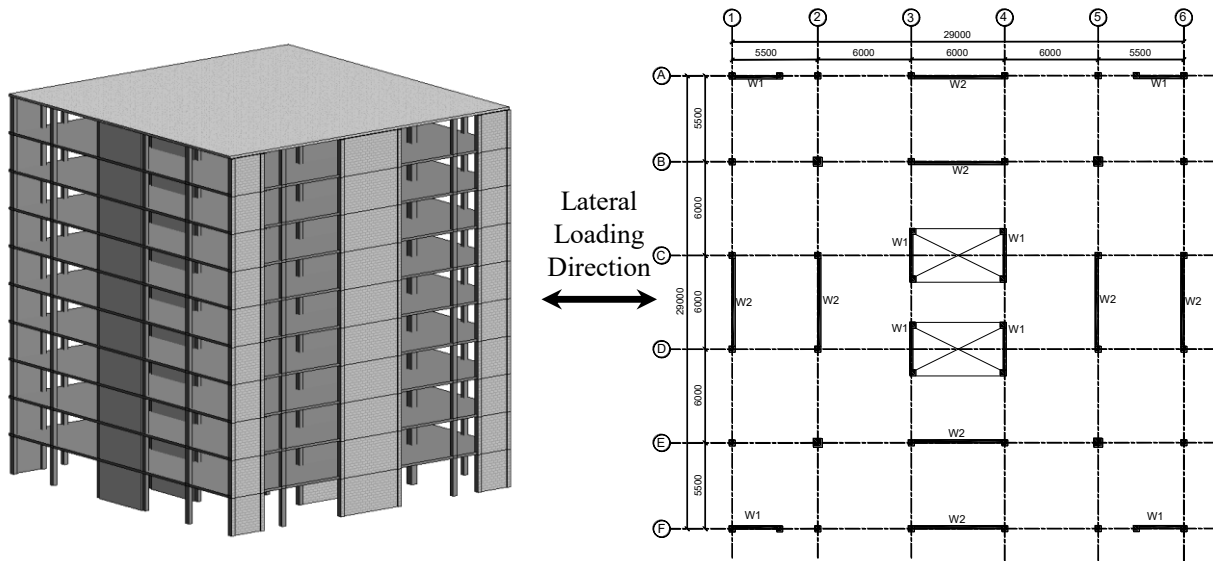
Figure 5.3. The 3D and the plan view of the studied structure

(a)

(b)
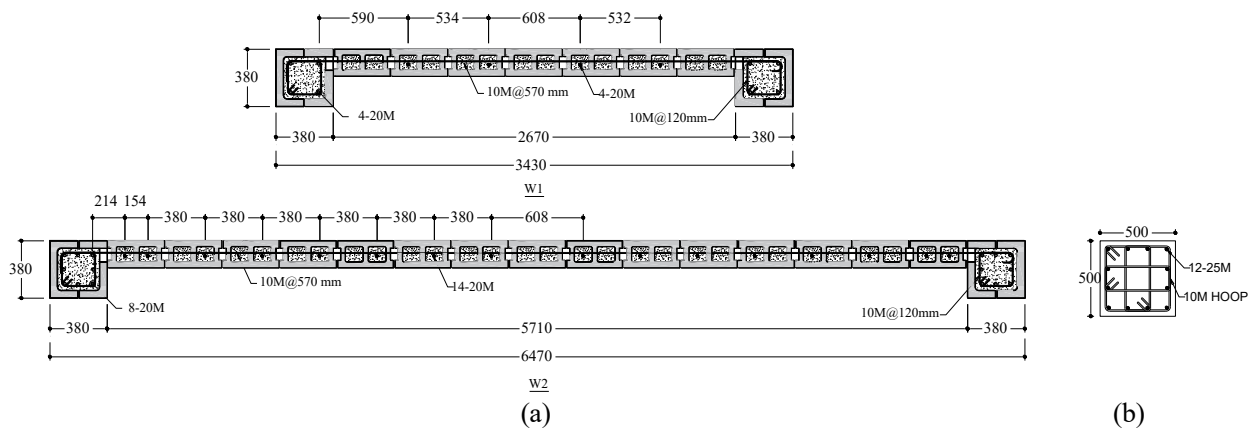
Figure 5.4. Dimensions and reinforcement details of: (a) RM shear walls with masonry boundary elements; (b) Gravity reinforced concrete column

5.5　Seismic Analysis and Performance Assessment

Incremental Dynamic Analysis (*IDA*) was conducted to identify the initiation of the collapse to assess the seismic performance of the buildings (Vamvatsikos, 2002). The numerical model was analyzed against two sets of far-field and near-field ground motion database to better assess the impact of the frequency content of available accelerograms (Atkinson 2009). The method of selection and scaling of the ground motion are elaborated in the subsequent section. The outcome of this part is used to assess the structural and non-structural losses of the RMSW building due to

98

a seismic event. The structural damages are more related to the displacement or inter-storey drift demand of structure, while the non-structural damages are comprised of the damages that occurred in the drift-sensitive and acceleration-sensitive components.

5.5.1   Ground Motion Selection and Scaling

The selection of the ground motion records is the initial and fundamental step towards performing Nonlinear Time History Analysis (NLTHA) due to the disruption of results that record-to-record variability and the frequency content of each record could cause. A simple, yet accurate, approach to overcome the uncertainties arising from record selection is to choose as many records as that are available for the specific seismic hazard zone. Nonetheless, there are not many strong motion data sets available in eastern Canada. On the other hand, ASCE/SEI 7 (ASCE 2016) requires a ground motion suite of at least 11 ground motions per each target design spectrum that have a close tectonic regime, consistent magnitude, and similar spectral profile to the design spectrum of the location of interest. Hence, two sets of 44 far-field and near-field spectrum-compatible ground motions (i.e., 88 ground motions in total) were selected from the simulated accelerograms originally developed by Atkinson (2009). It is worth noting that artificial records often do not take the effect of records' directivity into account (Michaud and Léger 2014), which may have some effect on the wave propagation, and hence, wave energy cannot be precisely considered. In other words, not only the distance to the fault is critical but also the direction of the propagation influences the amplitude of the artificial records. Therefore, it is recommended to use more records to reduce these unwanted record uncertainties. The differentiation of the records was defined based on ground motions magnitudes, M, between 6.75 and 7.25 with R_{fault} of 10 to 90 km for the far filed records and M, between 5.5 and 6.5 with the distance to fault, R_{fault} of 0 to 15 km for near field records, respectively. The details and characteristics of the selected ground motion records along with their Peak Ground Acceleration (PGA) and maximum velocity to acceleration ratio (v/a) are summarized in Table 5.3 and Table 5.4 and Figure 5.5 depicted their time history.
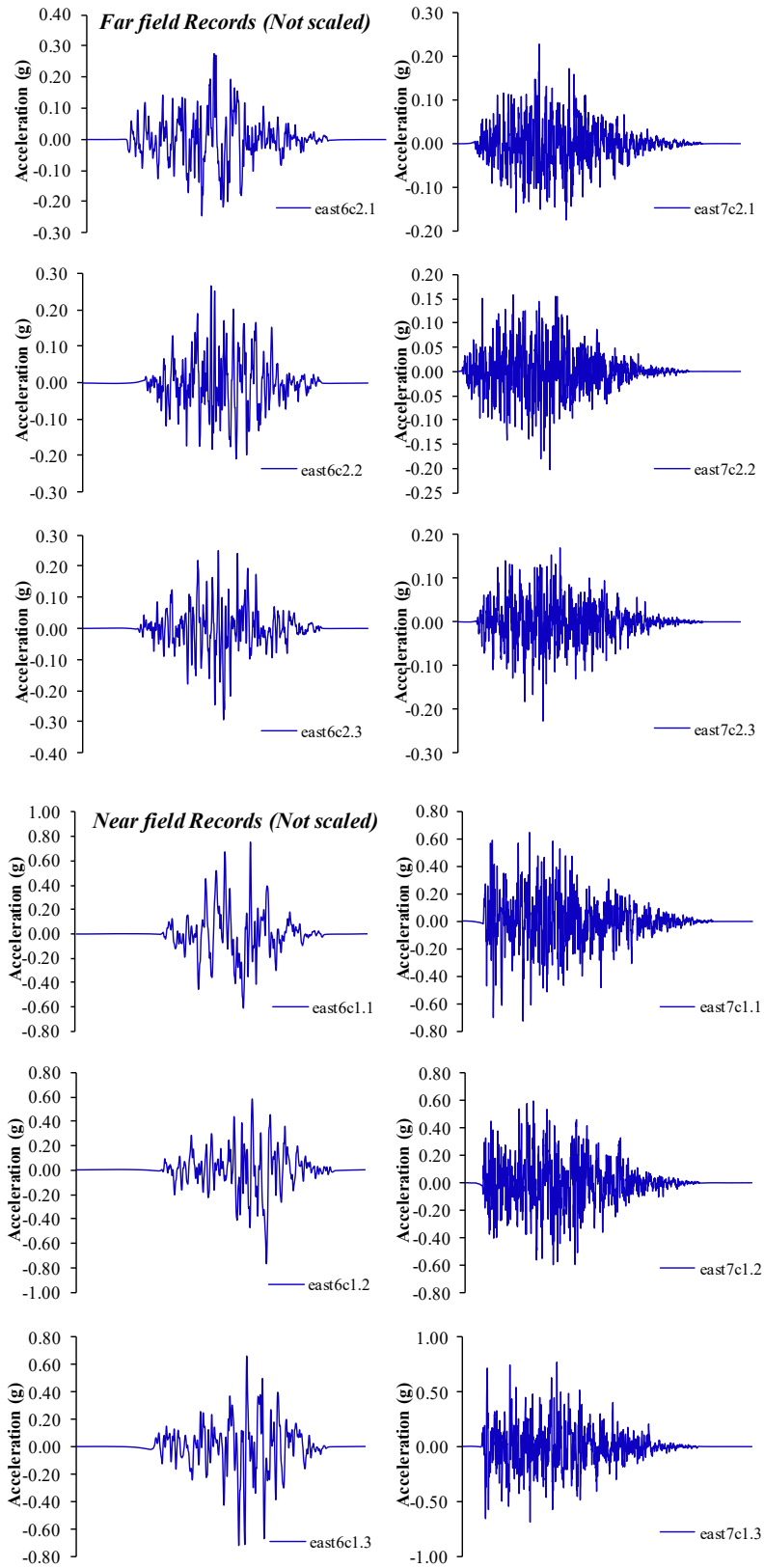
Figure 5.5. Time history of the far- and near-field records

Table 5.3. Characteristics of the unscaled simulated ground motions dataset

Far-field ground motions

Event	M	R_{fault} (km)	PGA (g)	v/a	Event	M	R_{fault} (km)	PGA (g)	v/a
east6c2.1	6	20.8	0.277	0.0458	east7c2.1	7	41.6	0.229	0.0647
east6c2.2	6	20.8	0.268	0.0266	east7c2.2	7	41.6	0.203	0.0567
east6c2.3	6	20.8	0.295	0.0397	east7c2.3	7	41.6	0.229	0.0602
east6c2.4	6	21.5	0.311	0.0298	east7c2.4	7	50.3	0.151	0.0504
east6c2.5	6	21.5	0.279	0.0295	east7c2.5	7	50.3	0.148	0.0759
east6c2.6	6	21.5	0.192	0.0555	east7c2.6	7	50.3	0.122	0.0789
east6c2.7	6	16.9	0.267	0.0387	east7c2.7	7	45.2	0.204	0.0522
east6c2.8	6	16.9	0.315	0.0404	east7c2.8	7	45.2	0.184	0.0539
east6c2.9	6	16.9	0.287	0.0480	east7c2.9	7	45.2	0.180	0.0730
east6c2.10	6	21.1	0.232	0.0430	east7c2.10	7	50.3	0.125	0.0949
east6c2.11	6	21.1	0.296	0.0361	east7c2.11	7	50.3	0.127	0.0610
east6c2.12	6	21.1	0.218	0.0336	east7c2.12	7	50.3	0.122	0.0643
east6c2.13	6	21.6	0.267	0.0412	east7c2.13	7	50.3	0.153	0.0515
east6c2.14	6	21.6	0.272	0.0292	east7c2.14	7	50.3	0.163	0.0859
east6c2.15	6	21.6	0.239	0.0570	east7c2.15	7	50.3	0.126	0.0940
east6c2.16	6	21.1	0.196	0.0400	east7c2.16	7	62.6	0.089	0.0810
east6c2.17	6	21.1	0.321	0.0272	east7c2.17	7	62.6	0.104	0.0675
east6c2.18	6	21.1	0.209	0.0292	east7c2.18	7	62.6	0.094	0.0635
east6c2.19	6	26.3	0.170	0.0387	east7c2.19	7	51.9	0.137	0.0566
east6c2.20	6	26.3	0.192	0.0308	east7c2.20	7	51.9	0.117	0.0705
east6c2.21	6	26.3	0.147	0.0333	east7c2.21	7	51.9	0.101	0.0776
east6c2.22	6	26.1	0.184	0.0320	east7c2.22	7	69.9	0.090	0.1087

Table 5.4. Characteristics of the unscaled simulated ground motions dataset

Near-field ground motions

Event	M	R_{fault} (km)	PGA (g)	v/a	Event	M	R_{fault} (km)	PGA (g)	v/a
east6c1.1	6	12.8	0.756	0.0467	east7c1.1	7	13.8	0.727	0.0525
east6c1.2	6	12.8	0.768	0.0406	east7c1.2	7	13.8	0.598	0.0856
east6c1.3	6	12.8	0.717	0.0253	east7c1.3	7	13.8	0.770	0.0437
east6c1.4	6	12.5	0.646	0.0455	east7c1.4	7	15.3	0.806	0.0570
east6c1.5	6	12.5	0.597	0.0398	east7c1.5	7	15.3	1.162	0.0562
east6c1.6	6	12.5	0.661	0.0337	east7c1.6	7	15.3	0.871	0.0384
east6c1.7	6	12.8	0.523	0.0573	east7c1.7	7	14.2	0.922	0.0738
east6c1.8	6	12.8	0.565	0.0355	east7c1.8	7	14.2	0.764	0.0534
east6c1.9	6	12.8	0.411	0.0359	east7c1.9	7	14.2	1.085	0.0642
east6c1.10	6	12.8	0.431	0.0363	east7c1.10	7	14.9	0.971	0.0551
east6c1.11	6	12.8	0.405	0.0447	east7c1.11	7	14.9	0.971	0.0385
east6c1.12	6	12.8	0.533	0.0314	east7c1.12	7	14.9	0.844	0.0828
east6c1.13	6	10.7	0.558	0.0346	east7c1.13	7	14.8	1.018	0.0533
east6c1.14	6	10.7	0.614	0.0303	east7c1.14	7	14.8	0.934	0.0548
east6c1.15	6	10.7	0.920	0.0281	east7c1.15	7	14.8	0.967	0.0583
east6c1.16	6	13.6	0.644	0.0470	east7c1.16	7	20.6	0.584	0.0635
east6c1.17	6	13.6	0.481	0.0333	east7c1.17	7	20.6	0.586	0.0391
east6c1.18	6	13.6	0.657	0.0460	east7c1.18	7	20.6	0.485	0.0685
east6c1.19	6	14.4	0.532	0.0382	east7c1.19	7	20.1	0.653	0.0634
east6c1.20	6	14.4	0.461	0.0642	east7c1.20	7	20.1	0.476	0.0480
east6c1.21	6	14.4	0.524	0.0361	east7c1.21	7	20.1	0.590	0.0616
east6c1.22	6	14.4	0.603	0.0314	east7c1.22	7	14.3	0.903	0.0551

NBCC 2015 does not clearly state the provisions related to the scaling of the ground motions. However, it is indicated that the records need to be scaled such that the response spectrum of the records matches the Uniform Hazard Spectrum (UHS) at the fundamental period of the structure. The excitation level considered for the scaling was the design level UHS of Montreal with the probability of exceedance of 2% per 50 years corresponding to the Maximum Credible Earthquake (MCE) level. Furthermore, ASCE/SEI 7 (ASCE 2016) recommends that ground motions can be scaled either by their amplitude or can be spectrally matched to the MCE level UHS with a period range limitation. ASCE/SEI 7 (ASCE 2016) states that the median response spectrum of the records should match the respective response spectra having an upper bound range of period equal or greater than two times the largest fundamental period in each horizontal direction of the building, T_1, not less than 1.5 times of the T_1; and lower bound range of period that includes at least 90% of mass participation in each principal horizontal direction of motion. As per as spectral matching method, each pair of ground motions need to be scaled in a way that the average of the maximum-direction spectra for the ground motion suite equals or exceeds 110% of the target spectrum over the above-mentioned period range. Respecting the ASCE/SEI 7-16 (ASCE 2016) standard method, all ground motion records were scaled to be equal or exceed the target design spectrum over the period interval of $0.2T_1$ to $2.0T_1$, where T_1 is the first-mode period of vibration calculated based on the modal analysis performed in *OpenSees* model. Figure 5.6 shows the response spectrum of the original far-and-near-field records before and after scaling together with the median of the original and scaled records and target design spectrum of Montreal proposed by NBCC 2015.
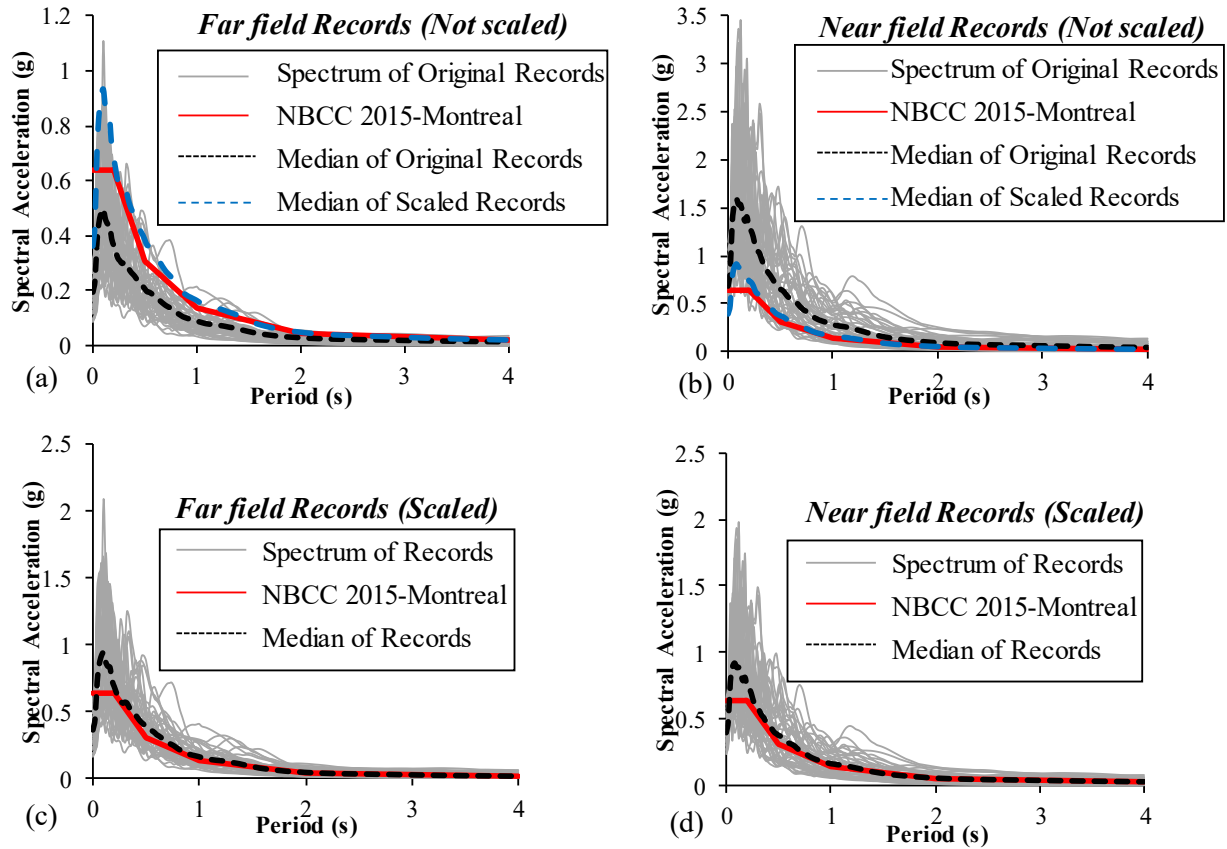
Figure 5.6. Response spectra of 44 far-field and near-field records for Montreal

5.5.2 Analytical Failure Benchmarks

Since some of the failure modes cannot be directly modelled in numerical approaches, they can be captured through the post-processing of the developed results. Generally, these failure modes are divided into material-based and performance-based failure criteria and are summarized as follows:

- Steel Reinforcement Buckling/Fracture: The *MinMax* material was incorporated in order to refrain the strain capacity of the steel reinforcement; however, failure of a single row of reinforcement found to be inadequate in the indication of collapse. Therefore, the fracture and/or buckling of steel rebars were monitored approximately from 25% offset of each side of the walls to indicate the collapse initiation. These criteria are common in literature and are recommended by various studies (e.g., NIST 2010, Gogus

and Wallace 2015, Thomson and Wallace 1995, Arabzadeh and Galal 2017). A failure strain of 0.06 was considered for the unconfined reinforcement for all RM shear wall specimens. For confined zones, a failure strain of 0.10 was considered as recommended by NIST (2010).

- Masonry Crushing: the failure criteria considered in crushing were similar to reinforcement failure, i.e., if a specified wall-length reaches the critical compressive strain, the collapse will occur. The specified length was considered to be 25% of the shear wall's length measured from their ends, whereas for the confined walls, the strain of confined area was observed to find the crushing point.

- Shear Failure: the potential of shear failure in slender walls does also exist. By crack initiation on the tension side of the wall, a higher value of sliding shear was observed as a result of flexural cracking, which leads to a more dowel action contribution (Paulay and Priestly 1992). Therefore, in order to precisely capture the shear behaviour of the wall; a bilinear Force-Deformation relationship was considered and applied to the horizontal shear spring to mimic the shear behaviour. Finally, a limit was defined to capture the failure due to exceeding the amount of shear demand than the wall's shear capacity.

- Axial failure: the concept of axial failure of the shear walls was interpolated with their lateral drift for lightly reinforced wall piers (Wallace et al. 2008). Hence, the drift value of 5% was considered as an index of axial failure in accordance with GCR 10-917-8 (NIST 2010) and Gogus and Wallace (2010).

5.6   Results and Discussion

5.6.1   Incremental Dynamic Analysis of RM Shear Walls

The seismic performance of the two modelled RM shear wall buildings were investigated before and after incorporating MBEs through performing nonlinear Incremental Dynamic Analysis (IDA) (Vamvatsikos, 2002). The IDA curves were extracted by post-processing the data of dynamic analysis. Figure 5.7shows the IDA response plot of the building without having MBEs. The horizontal axis shows the inter-storey drift ratio versus the intensity measure (*IM*) which is 5% spectral acceleration at the fundamental period of the structure, *T*. Two collapse indication can be obtained through *IDA* curves, exceedance of a specific inter-storey drift ratio and/or degrading the slope of the IDA curve to less than 20% of the initial elastic slope (Vamvatsikos, 2002). The IDA response curves of the RM shear walls with MBEs are shown in Figure 5.8. As shown, the introduction of MBEs helped the building to achieve additional reserved strength and the collapse of the structure was postponed subsequently. The comparison between the IDA response of the building with- and without- MBEs is shown in Figure 5.9.
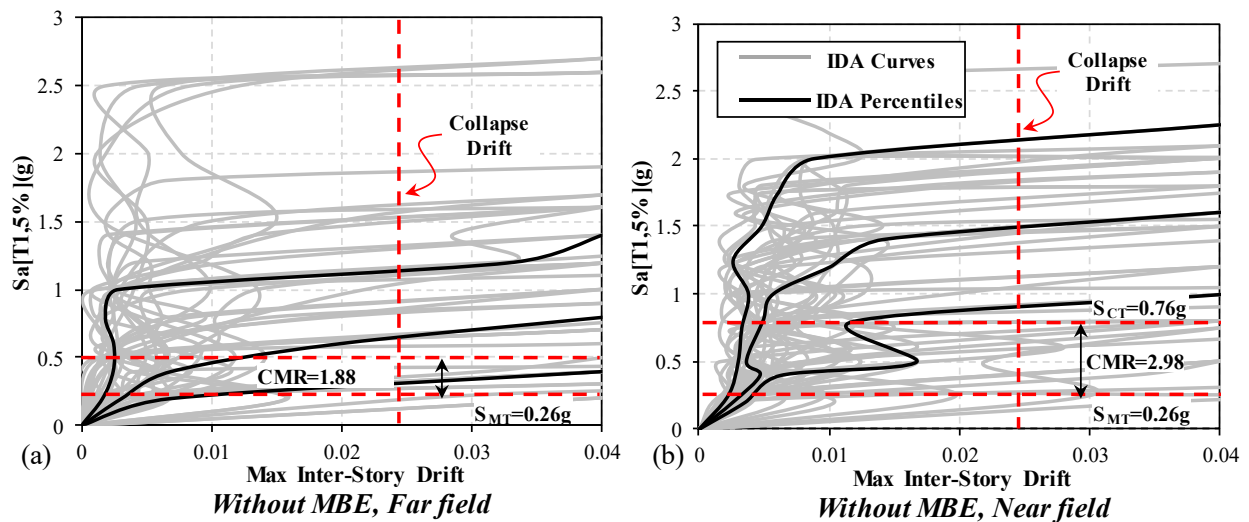
Figure 5.7. Individual IDA curves of the walls without MBEs along 16, 50, and 84 percentiles: (a) Far-field records; (b) Near field records
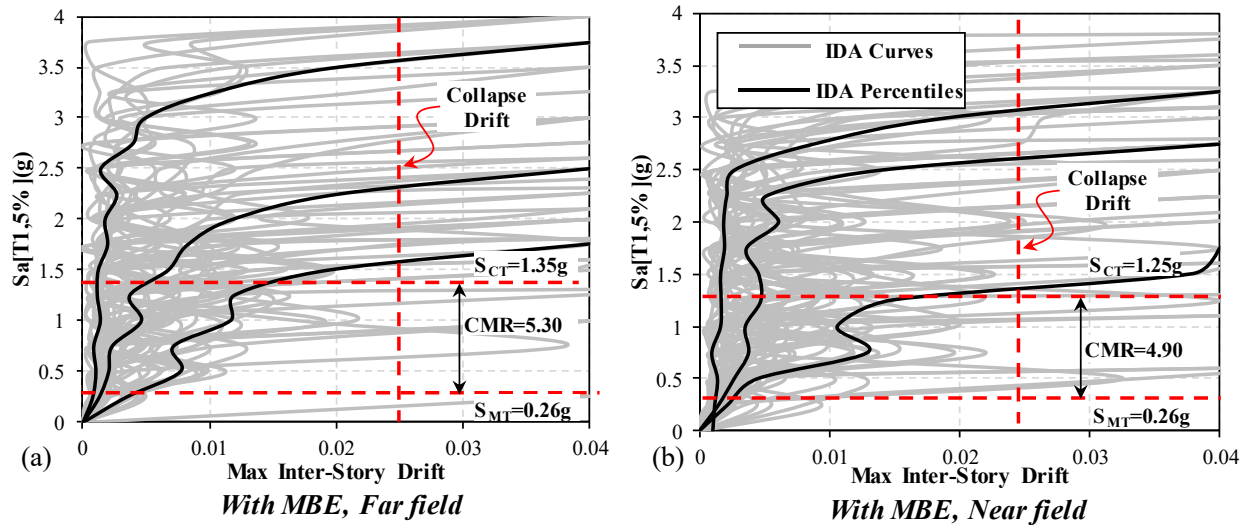
Figure 5.8. Individual IDA curves of the walls with MBEs along 16, 50, and 84 percentiles: (a) Far-field records; (b) Near field records
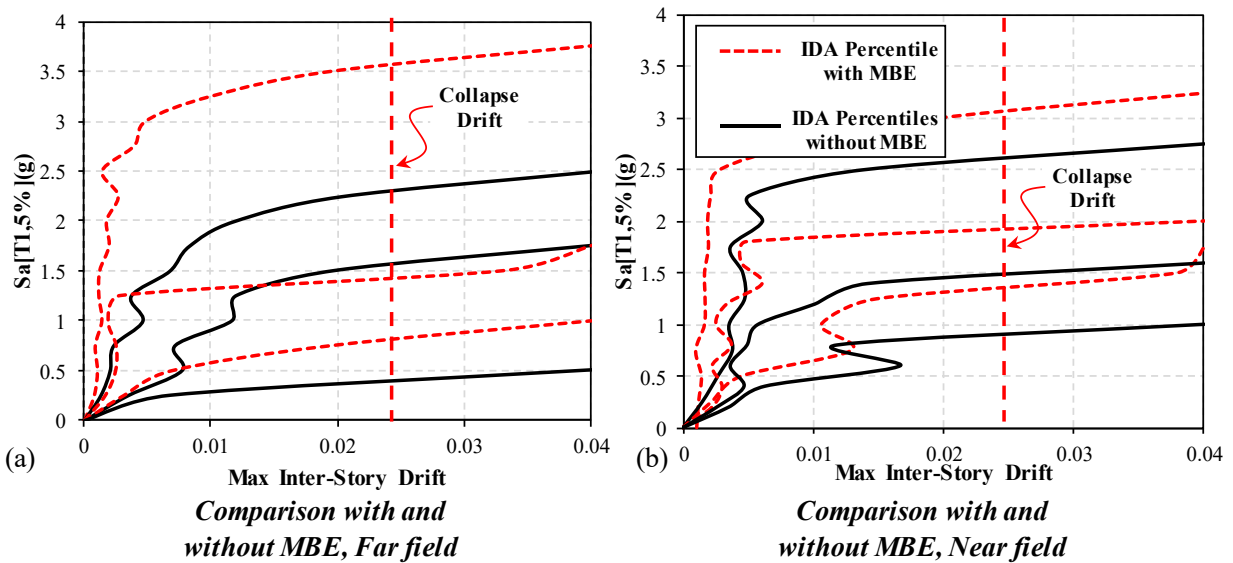
Figure 5.9. Comparison of IDA response curves for RMSW with and without MBEs: (a) Far-field records; (b) Near-field records

5.6.2 Fragility Curves Development, Performance, and Damage Criteria

Fragility Functions are the most important outcome derived directly from the IDA Curves, which basically represents the probability of exceeding of a certain damage state or performance level as a function of the Intensity Measure (*IM*) or an Engineering Demand Parameter (*EDP*) such as inter-storey drift, floor acceleration, and/or spectral displacement. As noted above, fragility curves can be extracted based on two analytical methods, namely *IM*-based and *EDP*-based

107

approaches. Since the structural damages are mostly correlated with the displacement and drift represented measures instead of ground motion intensities, the *IM*-based method is not a feasible method to be used. For this reason, the *EDP*-based formulation is frequently adopted to assess the damage probabilities. There are two assumptions taken while using the *EDP*-based fragility functions. The first assumption is that the Seismic demand, *D*, follows a lognormal distribution (Cornell et al, 2002) (Eq. 5.1).

$$P[D \geq d \mid IM = x] = 1 - \phi[\frac{\ln(d / m_{D|IM=x})}{\beta_{D|IM}}] = G_{D|IM}(d \mid x) \tag{5.1}$$

Where *x* is the given earthquake intensity level, ϕ is the standard normal cumulative distribution function of the probability of exceedance $P[D \geq d \mid IM = x]$. $G_{D|IM}(d \mid x)$ shows the probabilistic seismic demand model, and $\beta_{D|IM}$ and $m_{D|IM=x}$ shows the dispersion and median of the seismic demand, respectively. The second assumption implies that the capacity of the structure, *C*, also follows a lognormal distribution (Cornell and Jalayer, Hamburger 2002) (Eq. 5.2).

$$P[C \leq d] = \phi[\frac{\ln(d / m_C)}{\beta_C}] = F_C(d) \tag{5.2}$$

Where $F_C(d)$ is the probabilistic seismic capacity model, and β_C and m_C shows the dispersion and median value, respectively. Combining the above-mentioned analytical functions of demand and capacity, the displacement-based fragility format, $F_{R,Disp}(x)$, can be generated as follows (Wen et al, 2004) (Eq. 5.3):

$$F_{R,Disp}(x) = \phi\left[\frac{\ln m_{D|IM=x} - \ln m_C}{\sqrt{\beta_{D|IM=x}^2 + \beta_C^2 + \beta_M^2}}\right] \tag{5.3}$$

Where β_M is the uncertainty correlated to the modelling approach, which cannot be neglected in the analysis. An approximated value of 0.2 was considered for β_M as recommended by FEMA-P695 for simplification. The fragility function of non-structural components was extracted from *PACT* fragility database proposed by *ATC* Council (2011). A sample data set used for the generation of the fragility curve is summarized in Table 5.5 shows the ratio between the numbers

of records caused collapse at a certain *IM* to the total number of performed analyses. The median and dispersion of the data were used to model the collapse debris of each storey level as a structural analysis result input of the *PACT* Building modeller for further loss estimation. The collapse margin ratio (*CMR*) is a key parameter for characterizing the collapse of structures and was calculated for the building before and after MBE implementation. *CMRs* can be calculated as the ratio of the median collapse capacity, S_{CT}, to the Maximum Considered Earthquake (*MCE*) spectral acceleration, S_{MT}. The median collapse capacity can be found using the fragility curve of a structure originally extracted from IDA results (Figure 5.10). The *CMR* values are summarized in Table 5.6 for the walls with and without MBEs. It can be concluded that adding MBEs to the shear walls has increased the CMR value significantly relative to the walls without MBEs. The CMR value was increased up to 64% and 180% for near- and far-field records, respectively. The higher value of CMR implies the fact that the designated seismic force modification factors (i.e., ductility-related force modification factor, R_d, and overstrength-related force modification factor, R_o) associated to the RM shear walls can be modified for the walls with masonry boundary element since they proved to reveal more ductile behaviour. In this research study, the fragility curves were developed for different performance levels of ASCE41-17 (ASCE 2017). Three performance levels of Immediate Occupancy (IO), Life Safety (LS), and Collapse Prevention (CP) were considered for the collapse assessment of each building configuration. Figure 5.11 shows the probability of collapse corresponding to different damage levels of the walls before and after having MBEs. A comparison was made between the median spectral capacity of each model to highlight the effect of adding MBEs to RMSWs which is presented in Table 5.7 for different damage states. The naming convention was in the form of MTL-10S-<u>MBE</u>-<u>F</u>-<u>CP</u>, in which MTL represents the location of the building, which is Montreal, 10S shows the number of the stories. The last three underlined variables are as such: MBE is shown whenever the wall has masonry boundary elements at its extremes, the letter F or N shows the model analyzed versus far-field or near-field records, respectively, and IO, LS, CP shows the level of damage of the fitted fragility function. As can be seen, the median collapse capacity of both buildings with rectangular walls and those with MBEs remained identical for far-field and near-field records, which shows that the building can preserve its lateral strength against various levels of the frequency contents. However, rectangular walls possess a minimum 75% lower collapse capacity at IO level and a maximum of 90% lower collapse capacity than the walls with MBEs at LS performance level. This phenomenon can be

justified because walls with masonry boundary elements possess higher inherent ductile performance because of additional confined zones that postpone the initiation of collapse and reinforcement buckling in this type of shear walls.

Table 5.5. Sample Dataset used to develop Fragility Function

IM	Number of analyses	Number of collapses	Fraction causing collapse	Theoretical fragility function
0.10	44	0	0.00	0.00
0.25	44	1	0.02	0.02
0.50	44	7	0.16	0.13
0.75	44	12	0.27	0.26
1.00	44	17	0.39	0.39
1.25	44	21	0.48	0.50
1.50	44	25	0.57	0.59
1.75	44	29	0.66	0.66
2.00	44	31	0.70	0.72
2.25	44	33	0.75	0.76
2.50	44	34	0.77	0.80
2.75	44	36	0.82	0.83
3.00	44	37	0.84	0.86
3.25	44	38	0.86	0.88
3.50	44	40	0.91	0.90
3.75	44	42	0.95	0.91
4.00	44	42	0.95	0.92

Table 5.6. Summary of collapse margin ratio of the building

Building ID	Record Scheme	Configuration	$S_{MT}[T](g)$	$S_{CT}[T](g)$	CMR
MTL-10S-MBE-F	Far field	With MBE	0.255	1.35	5.30
MTL-10S-F	Far field	Without MBE	0.255	0.48	1.88
MTL-10S-MBE-N	Near field	With MBE	0.255	1.25	4.90
MTL-10S-N	Near field	Without MBE	0.255	0.76	2.98

Table 5.7. Median spectral capacity of the structures corresponding to ASCE41-17 damage states

Building ID	Limit state		
	IO	LS	CP
MTL-10S-MBE-F	0.73	1.0	1.25
MTL-10S- F	0.42	0.51	0.89
MTL-10S-MBE-N	0.72	1.0	1.24
MTL-10S-N	0.42	0.53	1.05
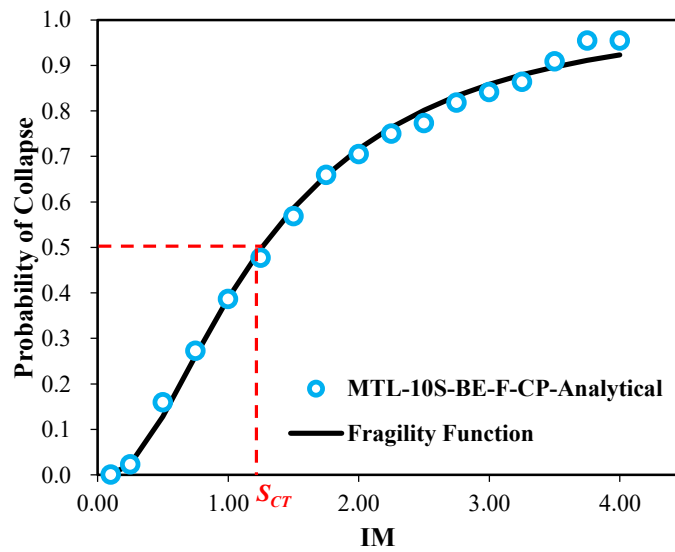
Figure 5.10. Sample Fragility curve fitting derived from IDA results
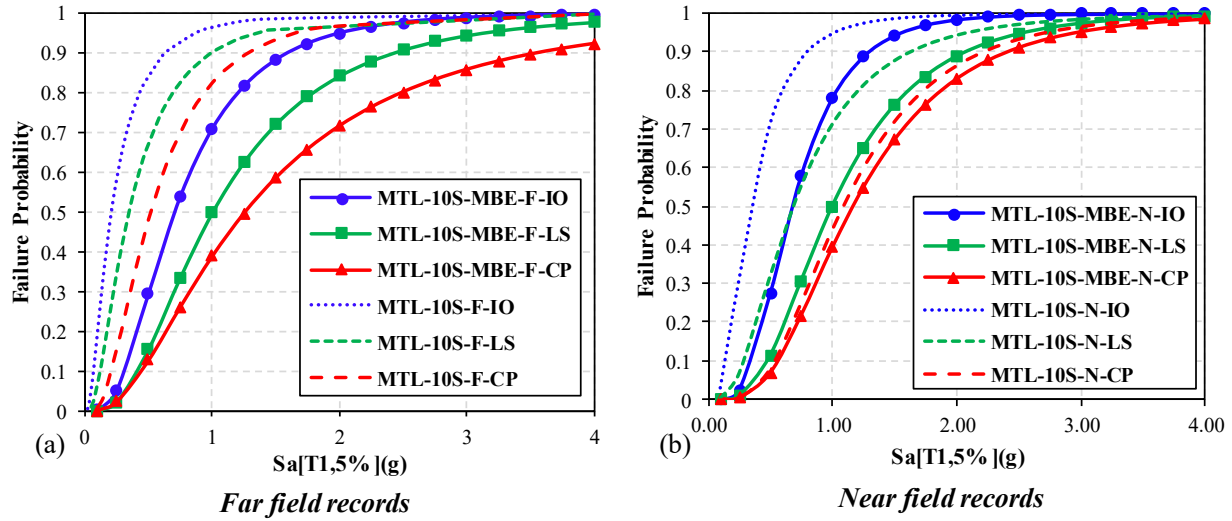
Figure 5.11. Fragility curves of RMSWs with and without BEs: (a) Far-field records; (b) Near-field

5.6.3   Inter-Storey Drift Fluctuation

The variation of inter-storey drift has a significant effect on structure performance since it alters the structural and non-structural damage portion if reduced without having a direct impact on the strength of the structure. The box-plot analogy was utilized to visualize the variation of the inter-storey drift. Figure 5.12 shows the variation of storey drift of the buildings before and after implementation of the MBEs prone to far-field and near-field records. The solid error lines demonstrate the maximum and minimum value of the inter-storey drift corresponding to each record, while the box itself determines the first and third quartile range of the data (Q3-Q1), respectively. The median of the data is also indicated as a solid line inside the boxplot. As shown, the minimum and maximum of inter-storey drift ratios of the walls without MBEs are 0.1% and 1.35% for near-field and 0.15% and 2.6% for far-field records, respectively. On the other hand, by using MBEs the maximum inter-storey drift was reduced to 1.1% for near-field and 1.8% for far-field records considering all storey levels. However, the reduction in the minimum value was minor in both cases, the overall inter-storey drift was reduced significantly in all buildings with MBEs. The median value fluctuates a bit after adding MBEs with a maximum decrease of 26% of inter-storey drift for near-field records and a maximum decrease of 48% for far-field records. The presence of MBEs helped to increase the ultimate displacement capacity and increased the axial strength of the compressive zone by providing enough confinement. The confined zones possessed

higher compression strength, which helped to decrease the yield curvature and to increase the ultimate curvature resulting in higher overall curvature ductility (Paulay and Priestly 1992). In this regard, MBEs were found to be significantly effective in reducing the inter-storey drift ratio of the building resulting in lower structural and non-structural losses and more ductile behaviour with higher dissipation of energy for the structure under a seismic event. It is worth noting that, due to the spectrum-based ground motion scaling, the near-field records triggered a lower value of inter-storey drift than far-field records (Michaud and Léger 2014).
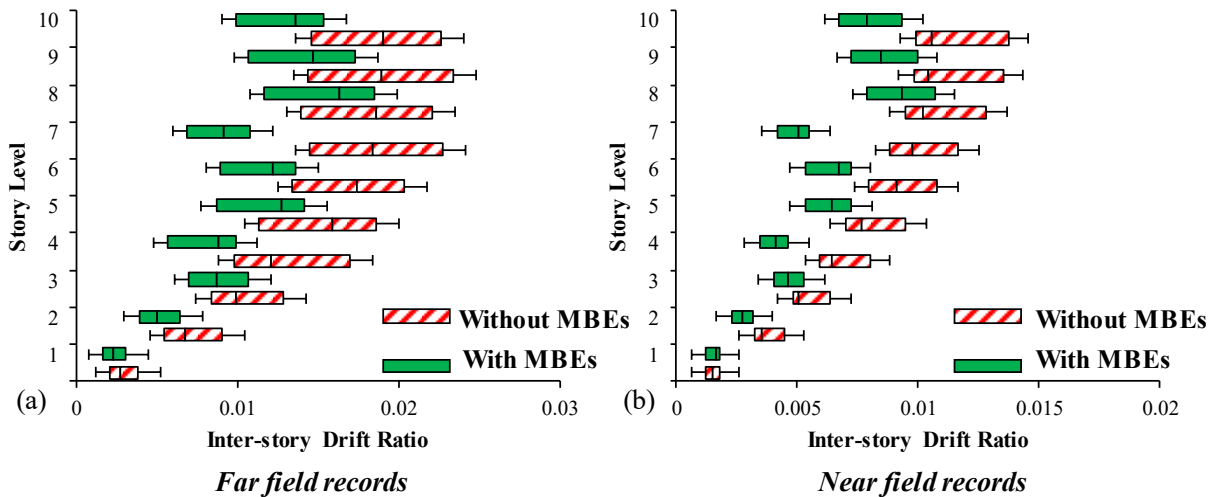
Figure 5.12. Inter-storey Drift variation at Design Level: (a) Far-field Records; (b) Near-field records

5.6.4 Storey Shear Response Plot

The effect of MBEs on the storey shear demand is shown in Figure 5.13 for each far-field and near-field individual ground motion dataset. As can be seen, by using MBEs the shear demands were increased in all cases due to the fact that shear walls with MBEs can alter the ultimate stiffness of the system, absorbing more lateral forces as a result of having higher compressive strength at the wall's extreme zone. Moreover, by providing more confinement the strength deterioration of the walls was postponed resulting in higher demands at the upper half floors of the building without a significant increase in the initial stiffness of the original building. A comparison was made among different percentiles for the building after adding MBEs (Figure 5.14). The results reveal that the storey shear forces were shifted to the right significantly over the height of the building on the far-field records; however, the impact was minor for near-field accelerogram. The median value of

maximum base shear was increased by 30% and 25% for near-field and far-field records, respectively. The spectrum-based scaling method was found to cause this result, which again highlights the fact that a target response spectrum needs to be developed for near-source dataset scaling.
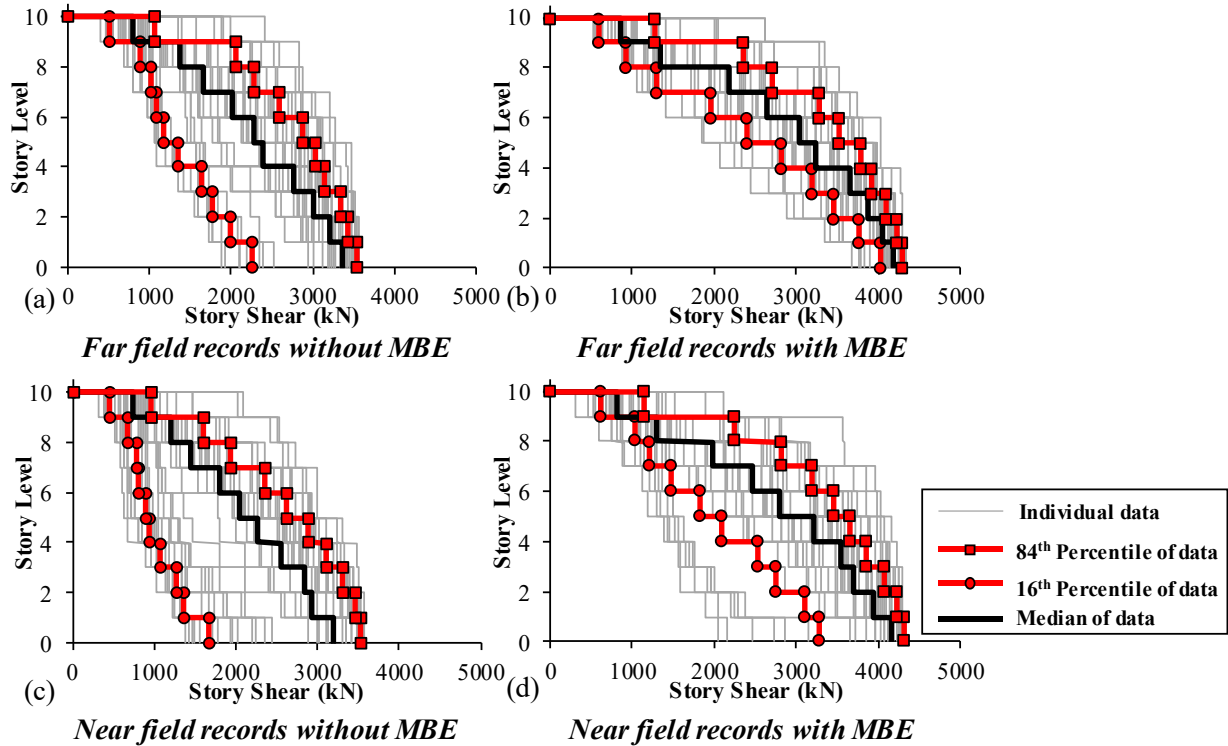
Figure 5.13. Storey shear profile of different dataset over the height of the building
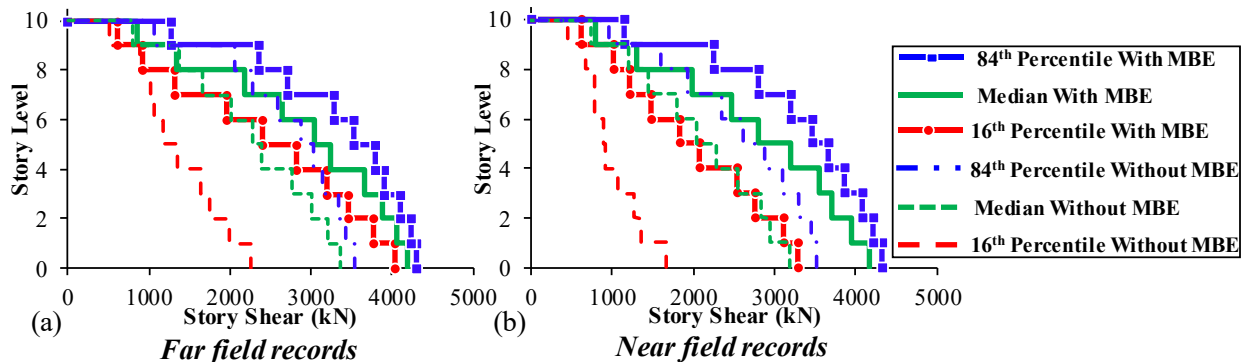
Figure 5.14. Comparison of Storey Shear Demands before and after adding masonry boundary elements: (a) Far-field records; (b) Near-field records

5.7   Seismic Resilience Methodology Framework

Seismic resilience can be interpreted as the loss and the recovery due to the loss required to maintain the functionality of the structure with minimum disruption. In accordance to the definition of MCEER, (2009) Resilience (R) is defined as a function indicating the capability of the structure to sustain a level of performance over the control time, T_{LC}, and analytically can be defined as Eq. 5.4

$$R(r) = \int_{t_{OE}}^{t_{OE}+T_{LC}} Q(t)/T_{LC}dt \tag{5.4}$$

where $Q(t)$ is the performance function, T_{LC} is the control time which is considered to be 50 years for residential buildings which shows the life span of the structure, and t_{0E} is the time that the event occurs (i.e., in this case, the time earthquake shock happens). The performance function, $Q(t)$, follows a non-stationary stochastic procedure, where it is measured as a percentage of the system's function over time. The performance function can be formulated as functions of loss, recovery scheme, and the earthquake intensity (Cimellaro et al. 2009).

The two key components on resilience assessment are the time and path of recovery that should be evaluated meticulously to avoid any overestimation in the structural performance. Losses due to earthquakes are not easy to predict because of the high level of uncertainty associated with the nature of earthquake losses. However, some common parameters triggering the losses can be determined and examined. The loss function can be formulated as a function of earthquake intensity, I, and recovery time, T_{RE} (Cimellaro 2009). The loss function can be divided into two main divisions of Direct, L_D, and Indirect losses, L_I. Direct losses are the ones that occur instantly during the disaster, while indirect losses can happen during and after the disaster. The breakdown can be extended to two subcategories of Economic losses, L_E, and Casualties losses, L_C. In this study, only the impact of Direct Economic losses, L_{DE}, was considered as they have the maximal effect on the structural and non-structural components of the buildings. Direct Economic losses can be determined as the ratio of the building replacement or repair cost. The total losses are the result of structural and non-structural losses and can be derived using Eq. 5.5.

$$L(I, T_{RE}) = L_S(I) + L_{NS}(I, T_{RE})$$ (5.5)

where $L_S(I)$ represents structural losses, and $L_{NS}(I, T_{RE})$ denotes non-structural losses at the given earthquake intensity, I, within specified recovery time, T_{RE}. It worth mentioning that the complete structural losses are associated with the replacement cost of structure; however, structural repair refers to the repair of structural components (e.g., lintel beams, shear walls). The physical structural losses can be determined using Eq. 5.6 as a function of building replacement costs and the probability of exceedance of a given damage state.

$$L_S = \sum_1^N CS_{DS} = BRC \times \sum_1^N POSTR_{DS} \times RCS_{DS}$$ (5.6)

where CS_{DS} is the cost of the structural damage corresponding to the given damage level; N is the number of damage states considered in the study, and BRC is the building replacement cost estimated based on the average cost per square feet using RS Means (2019) in the Canadian dollar. $POSTR_{DS}$ equals the probability of collapse at a given intensity of the damage state of interest, which can be derived using developed analytical fragility functions. RCS_{DS} shows the structural repair cost ratio of a certain damage state provided by HAZUS MH 2.1 (2016). A similar calculation can be performed for non-structural components. Howbeit, non-structural elements are divided into acceleration-sensitive, L_{NSA}, and drift-sensitive, L_{NSD}, components (Eq.5.7, 5.8, 5.9).

$$L_{NS} = L_{NSD} + L_{NSA}$$ (5.7)

$$L_{NSD} = \sum_1^N CNSD_{DS} = BRC \times \sum_1^N PONSD_{DS} \times RCD_{DS}$$ (5.8)

$$L_{NSA} = \sum_1^N CNSA_{DS} = BRC \times \sum_1^N PONSA_{DS} \times RCA_{DS}$$ (5.9)

where, $CNSD_{DS}$ and $CNSA_{DS}$ represent non-structural drift and acceleration sensitive damage costs, respectively, at the considered damage state; BRC is the building replacement cost; $PONSD_{DS}$ and $PONSA_{DS}$ is the probability of exceedance of a certain damage state for non-structural drift and acceleration sensitive elements; RCD_{DS} and RCA_{DS} represent the drift and acceleration sensitive repair and replacement ratio of the specified damage state DS; and N is the

number of damage states considered for the building. The repair cost ratios for each damage state are shown in Table 5.8, for structural and non-structural components. The probabilities of non-structural damage states are adopted from the fragility curve database of *PACT* (ATC Council 2011) for both drift- and acceleration-sensitive components. Subsequently, total losses due to structural damages along with drift- and acceleration-sensitive non-structural damages, and total replacement cost of the structure are summarized in Table 5.9. As tabulated in Table 5.9, the contribution of non-structural damages is almost ten times higher than the structural losses.

In order to estimate the recovery time, the method provided by *PACT* was adapted, which will estimate the recovery time as a summation of clean up and repair time and construction time and time necessary to obtain the financing and functionality of the building. The recovery path was selected to follow a trigonometric fashion based on the recommendation of Cimellaro et al. (2010).

Table 5.8. Structural and non-structural repair cost ratio (in % of Structure replacement cost)

Occupancy Class	Type of component	Structural Damage State		
		Moderate	Extensive	Complete
Residential	Structural	1.4	6.9	13.8
Residential	Non-Structural, Acceleration-Sensitive	4.3	13.1	43.7
Residential	Non-Structural-Drift Sensitive	4.3	21.3	42.5

Table 5.9. Estimated losses for the Buildings before and after adding MBEs

| Building ID | Replacement Cost (BRC) | Structural Losses | Non-structural Losses | | Percentage of Structural losses (%) | Percentage of Non-structural losses (%) | Total Loss |
			Drift-sensitive components	Acceleration-sensitive components			
MTL-10S-MBE-F	C$18,895,240	C$315,702	C$992,756	C$551,193	1.67	8.17	C$1,859,651
MTL-10S- F	C$18,451,160	C$381,219	C$969,424	C$979,554	2.07	10.56	C$2,330,197
MTL-10S-MBE-N	C$18,895,240	C$346,274	C$992,756	C$869,880	1.83	9.86	C$2,208,910
MTL-10S-N	C$18,451,160	C$376,348	C$1,032,250	C$1,083,286	2.04	11.47	C$2,491,885

5.7.1   Seismic Resilience Assessment of The Studied Buildings

The building resilience as a non-dimensional parameter shows the remaining functionality of the structure after an earthquake. For instance, the resilience of 100% means there is no damage to the structure, whereas total loss of the structure corresponds to 0% resilience. The control time T_{LC} was selected to be 50 years as a typical value for residential buildings and also is consistent with the selected hazard level of 2% probability of exceedance in 50 years. Figure 5.15 shows the seismic resilience of the RMSW buildings before and after the adoption of masonry boundary elements. As shown, the vertical axis represents the building functionality estimated based on losses associated with structural and non-structural elements, while the horizontal axis represents the time (days). Graphically, the resilience is defined as the area beneath the $Q(t)$ function. As can be seen, by adding MBEs, the resilience of building has increased by 10% for near-field and 15% for far-field records, respectively. This increase can be justified as a result of lowering the amount of structural and non-structural losses by reducing the inter-storey drift and providing a higher level of ductility in the structure after the adoption of MBEs.
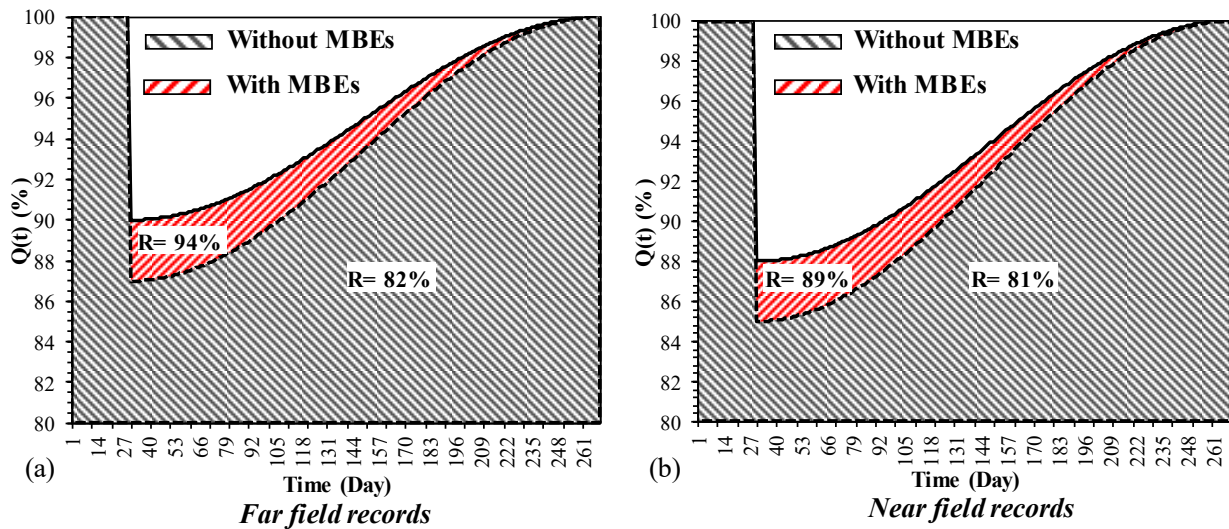
Figure 5.15. Functionality Curve: (a) Far-field records; (b) Near-field records

5.8   Conclusions

This study utilized a framework to assess the seismic response of the RMSW buildings prior and after adopting masonry boundary elements using the seismic design parameters of rectangular walls. A macro-modelling approach was utilized and enhanced to precisely considering the

characteristics of the RMSW buildings after careful validation against experimental results of tested RMSW building. Later, two 10-storey RMSW buildings were designed (i.e., with and without MBEs) in accordance with the NBCC 2015 and numerically simulated to investigate the inelastic seismic response of the structure as well as predicting the seismic loss and resilience. A large dataset of far- and near field ground motion records were selected and scaled to perform IDA analysis on the building model. Fragility analysis was performed, and fragility curves were derived from the IDA results for different analytical failure criteria, including *EDP*-based and material-based criteria available in the literature. Subsequently, the impact of masonry boundary elements on the seismic response and performance level of the building were studied to estimate the seismic structural and non-structural losses and seismic resilience of each building. The following remarks were concluded are:

- The developed modelling approach was able to capture both elastic and inelastic hysteretic behaviour of RMSW building with acceptable accuracy. The difference between an experimentally obtained results and the developed model did not exceed 7%, and 9% for the peak lateral force and the initial stiffness, respectively. Generally, the modelling technique was able to resemble the overall behaviour of the structure with great precision in terms of energy dissipation, cyclic and in cycle degradation, stiffness degradation, and pinching behaviour.

- The results of IDA analysis proved that by using MBEs, the median collapse intensity of the building has increased by 73% at IO performance level, 88% for LS performance level, and 40% for CP performance level. Also, the results indicate that a higher value of CMR can be associated with the walls with MBEs. A maximum increase of 64% and 180% was observed for RMSW buildings imposed on near-field and far-field records, respectively. The higher value of CMR highlights the fact that the designated seismic force modification factors of the RM shear walls can be increased for the walls with MBE as they perform with a more ductile behaviour.

- The inter-storey drift ratio of the buildings with MBE has decreased significantly since boundary elements have increased the compressive strength of the shear walls causing a lower probability of axial failure. The median value of the inter-storey drift ratio decreased with a maximum reduction of 26% for near-field records and 48% for far-field records, respectively. The reduction of the inter-storey drift ratio helped the structure to

experience lower structural and non-structural losses as well.

- By incorporation of MBEs, the shear demands were increased due to having more confinement resulting in lower strength deterioration of the walls at the ultimate loading stage. There was a maximum of 30% and 25% increase in the response storey shear of the building after adding MBEs for near-field and far-field records (i.e., storey shear diagram shifted rightwards in the upper stories after utilizing MBEs).

- Utilizing MBEs had a noticeable impact on the seismic resilience of the RMSW buildings. MBEs have reduced the structural and non-structural losses of the RMSW building by 24% and 30%, respectively. Also, the results indicate that the seismic resilience increases 10% for near-field and 15% for far-field records after adding MBEs to the ends of the RM shear walls.

Chapter 6

Probabilistic Seismic Resilience Quantification of Reinforced Masonry Shear Wall System with Boundary Elements Under Bidirectional Horizontal Excitations

6.1   Abstract

The concept of resilience is gaining increased attention in the field of disaster management due to the recent awareness of the need to reduce the detrimental post-event effects from natural disasters such as earthquakes. Resilience is a practical concept that includes pre-event activities (preparedness and mitigation) as well as post-event activities (response and recovery). Quantitative resilience assessment approaches are needed to compare the available mitigation strategies in order to be able to decide on the most suitable strategy and to provide better support for the decision-making procedure. In this study, a methodology for quantification of seismic resilience of Reinforced Masonry Shear Wall (RMSW) buildings having end-confined Masonry Boundary Elements (MBEs) is implemented. The uncertainties associated with the structural and non-structural losses, as well as estimated recovery time uncertainties, are considered in the quantification of the resilience index of RMSW buildings. The studied archetype buildings are 8-, 10-, and 12-story height and are located in Vancouver, representing a high seismic zone in Canada. In the first phase of this study, a numerical model was developed in OpenSees in order to derive the fragility surface for studied archetypes subjected to bidirectional horizontal excitation. In the second phase, the Monte Carlo simulation was performed to quantify the resilience index of each archetype, considering the abovementioned uncertainties. The results proved the robustness of ductile RMSW having end-confined MBEs in mitigating the losses associated to the disastrous event. The findings of this study provide comprehensive and useful information for earthquake mitigation measures and disaster risk reduction programs.

6.2   Introduction

The concept of resilience engineering is gaining increased attention during the past decade due to the efforts done to reduce the negative aftermath of disastrous events. The unpredictable nature of earthquake events increases the need for structural systems to be more resilient in order to act operationally before, during, and after the seismic event happens. Structural resilience-based design is believed to be able to improve efforts in emergency management to prepare, respond, recover, and mitigate risks. Determining the necessary steps in reducing the adverse effects of natural disasters is challenging for decision-makers when resources are limited. Having a resilient system needs preparation and mitigation plans and a tool to quantify and compare the effectiveness of preparation and mitigation strategies. There are not many approaches available in the literature to quantify the seismic resilience of RMSW buildings, although some available methodologies will be discussed subsequently.

Bruneau et al. (2003) and Bruneau and Reinhorn (2007) set up a framework for conceptualizing and identifying seismic resilience through engineering perspectives. They also suggested that there are four dimensions of resilience, namely, technical, organizational, social, and economical. They showed that all these dimensions cannot be represented only by the performance of a system. Thus, different measurements need to be utilized for distinctive systems. Cimellaro et al. (2009) also studied seismic resilience of health care facilities and developed a detailed conceptual framework for evaluating resilience capacity, including technical and organizational aspects. Corotis (2011) examined the conceptual and analytical gaps in outcomes and uncertainty between resilience and reliability of seismic risks and identified the differences between resilience and reliability. Another effort was done lately by Tirca et al. (2016) to quantify the enhancement in seismic resilience of office building with steel concentrically braced frames (CBF). In that research, three-story and six-story office buildings with CBFs were studied for both Eastern Canada (Montreal and Quebec City) and Western Canada (Vancouver). They concluded that all studied retrofitted buildings showed improved seismic resilience. Cimellaro et al. (2018) proposed a new framework according to the PEOPLES (Population and demographics, Environmental and ecosystem, organized governmental services, Physical infrastructure, Lifestyle and community competence, Economic development, and Social-cultural capital) approach that would be useful for emergency decision-makers. The above approach was used to understand the

123

interdependencies between road networks and earthquake-affected building units. O'Reilly et al. (2018) studied the seismic evaluation of three existing school buildings representing the building stock in Italy. They measured the expected annual loss (EAL) using and collapse safety of the school network using PEER-PBEE (the Pacific Earthquake Engineering Research Center - Performance-Based Earthquake Engineering) methodology.

While the foregoing studies provide a lot of useful information about the resilience of the critical facilities, there is still a vital need to assess the resilience index after an event such as an earthquake by considering probable damages. As a novel concept, resilience engineering has to track system risks and takes the required steps to reduce the system's chance of failure. However, resilience assessment possesses a high level of uncertainties due to its nature (Wen et al., 2004). As such, quantitative resilience assessment methods need to be developed to evaluate and determine the most suitable mitigation strategies and provide better support and decision-making. To reach this goal, a methodology is developed to quantify the seismic resilience of Reinforced Masonry Shear Wall (RMSW) buildings having Masonry Boundary Elements (MBEs). The presented methodology deals with several uncertain parameters such as structural and non-structural loss ratios and expected recovery times to evaluate the sensitivity of seismic resilience to those parameters. Damage levels were defined as a function of performance levels associated with earthquake intensity by introducing a fragility surface for the archetype buildings subjected to multi-directional seismic excitation. A set of 8-, 10-, and 12- story buildings were selected and designed conforming to the provision of NBCC 2015 and CSA S304-14 code located in the high seismic zone of Canada (i.e., Vancouver, BC). Later, a stochastic simulation approach is employed to analyze the resilience index of RMSW buildings having Masonry Boundary Elements (MBEs). This initiative is believed to be useful in comparing different preparation and mitigation measures to enhance the structural seismic resilience in case of an earthquake disaster. Quantification of the out-of-plane response of RMSW with MBEs was also presented in terms of story shear contribution ratios.

6.3   Characteristics of Selected Archetype Buildings

The archetype building of this study is selected to cover a range of mid- to high-rise RM shear wall buildings. The archetype is located in the high seismic zone of Vancouver, Canada, having ductile RM shear walls with Masonry Boundary Elements. The building layout and design

was originally done by Albutainy (2016, 2018) and has been used in this chapter as the case study. The number of stories is selected to be 8, 10, and 12 stories, respectively. The archetype buildings are selected in a way to conform with the height limits proposed by NBCC 2015. Additionally, considering different heights for the building help in quantifying the impact of the number of stories on the collapse capacity and performance of the structure. The typical considered story height of the building was selected to be 3.2 m for each story, leading to 25.6, 32, and 38.4 m total height of the studied buildings, respectively. The complete characteristic of the buildings is summarized in Table 6.1.

Table 6.1. Specification of the RM shear walls of archetype buildings with MBEs

Number of stories	Archetype Shear Wall ID	Proposed Location	Height (m)	Length (m)	Aspect Ratio	$f'_m (MPa)$	$f_{yv} (MPa)$	$f_{yh} (MPa)$
8-Story Building	W1	Vancouver, BC	25.6	3.5	7.31	30[a], 13.5[b]		
	W2	Vancouver, BC	25.6	6.5	3.94	30[a], 13.5[b]		
10-Story Building	W1	Vancouver, BC	32	3.5	9.14	30[a], 13.5[b]	400	400
	W2	Vancouver, BC	32	6.5	4.92	30[a], 13.5[b]		
12-Story Building	W1	Vancouver, BC	38.4	3.5	10.97	30[a], 13.5[b]		
	W2	Vancouver, BC	38.4	6.5	5.91	30[a], 13.5[b]		

[a]Confined Masonry zones, [b]Unconfined Masonry zones

The archetypes are selected to represent residential buildings having the plan layout and schematic three-dimensional perspective shown in Figure 6.1. The seismic force-resisting system of the building is comprised of 8 fully grouted ductile RM shear walls in the E-W and 8 fully grouted ductile RM shear walls in the N-S directions. The walls' length is selected to be either 3.5 m (W1) or 6.5m (W2), including the masonry boundary elements for the long and short walls, respectively. The primary ductile walls are designed to resist all the lateral forces and part of gravity loads with respect to its tributary area, while the Reinforced Concrete (RC) columns mainly transfer the vertical forces from gravity loads. Moreover, the RC columns are controlled to ensure their deformation capacity conforms to the ductile shear walls at the extreme stage of loading. The above-mentioned structural layout ensures that the level of axial forces is maintained within normal limits and will not negatively affect the displacement capacity as well as the lateral

resistance and ductility level of the RM shear walls with MBEs. Stiffness modifiers are introduced to the effective cross section properties to decrease the lateral stiffness of the RC columns and to eliminate their contribution to the lateral resistance of the RM shear walls. The gravity flooring system is comprised of a 200 mm concrete flat plate supported by the square RC columns and RM shear walls.

(a)   (b)
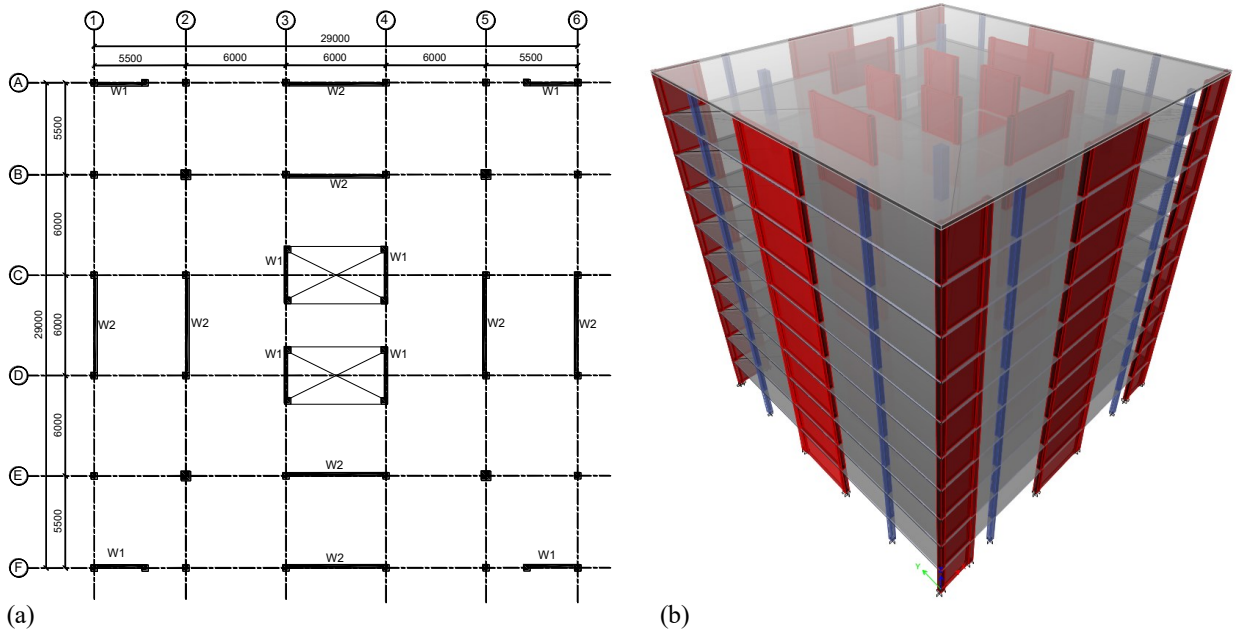
Figure 6.1. RMSW with MBE archetype building (a) Plan view layout of the building; and (b) 3D schematic view of the 10-storey building

6.3.1 Design of the archetype buildings

The archetype buildings were designed according to the design loads of NBCC 2015. A uniform surface load of 1.5 kPa was considered as finishing and partition load. The reference soil site class C proposed by NBCC 2015 was considered to estimate the lateral forces acting to the structures. This soil type represents an intermediate seismic hazard index as per NBCC. It is worth noting that selecting different soil classes would change the seismic hazard index of the studied location.

The calculation of seismic demand was conducted following the linear dynamic analysis procedure elaborated in clause 4.1.8.12 of NBCC 2015. This method follows a modal response spectrum analysis to capture the impact of higher modes and contribution of different mode shapes

126

in estimating the lateral forces. A sufficient number of modes need to be considered, such that the mass participation ratio exceeds the minimum value of 90% in all applicable degrees of freedom. A comparison was made between lateral forces arising from wind and earthquake to see which governs the design.

The design of ductile shear walls conforms to the special seismic design provision (i.e. clause 16) of CSA S304-14. The shear walls are designed to have fully grouted standard concrete masonry blocks in the web and fully grouted C-shaped blocks for the masonry boundary elements. Using C-shaped blocks will help with being more versatile in terms of the number of rebars, grout strength, and hoop spacing, resulting in greater flexibility in both design and fabrication of the shear walls. Hence, it can lead to an increase in the stress and strain capacities of the masonry boundary elements, which reflects in increasing the ductility of the overall RMSW with MBEs.

The compressive strength of 30 MPa was considered for RC columns. However, the lower value of 13.5 MPa was considered for the shear wall web in accordance with Table 4 of CSA S304-14. For the masonry boundary element of ductile walls, a higher value needed to be considered in order to meet the minimum inelastic rotational demand proposed by the design code. Based on a previous study by Drysdale and Hamid (1979), increasing the block and grout compressive strength would increase the masonry compressive prism strength when both components (i.e., block and grout) have similar stiffness properties. Therefore, a compressive strength (f'_m) of 30 MPa was considered for the ductile wall's masonry boundary elements. The summary of the design detail of ductile shear walls with masonry boundary elements (i.e., dimensions and reinforcement) is shown in Figure 6.2.
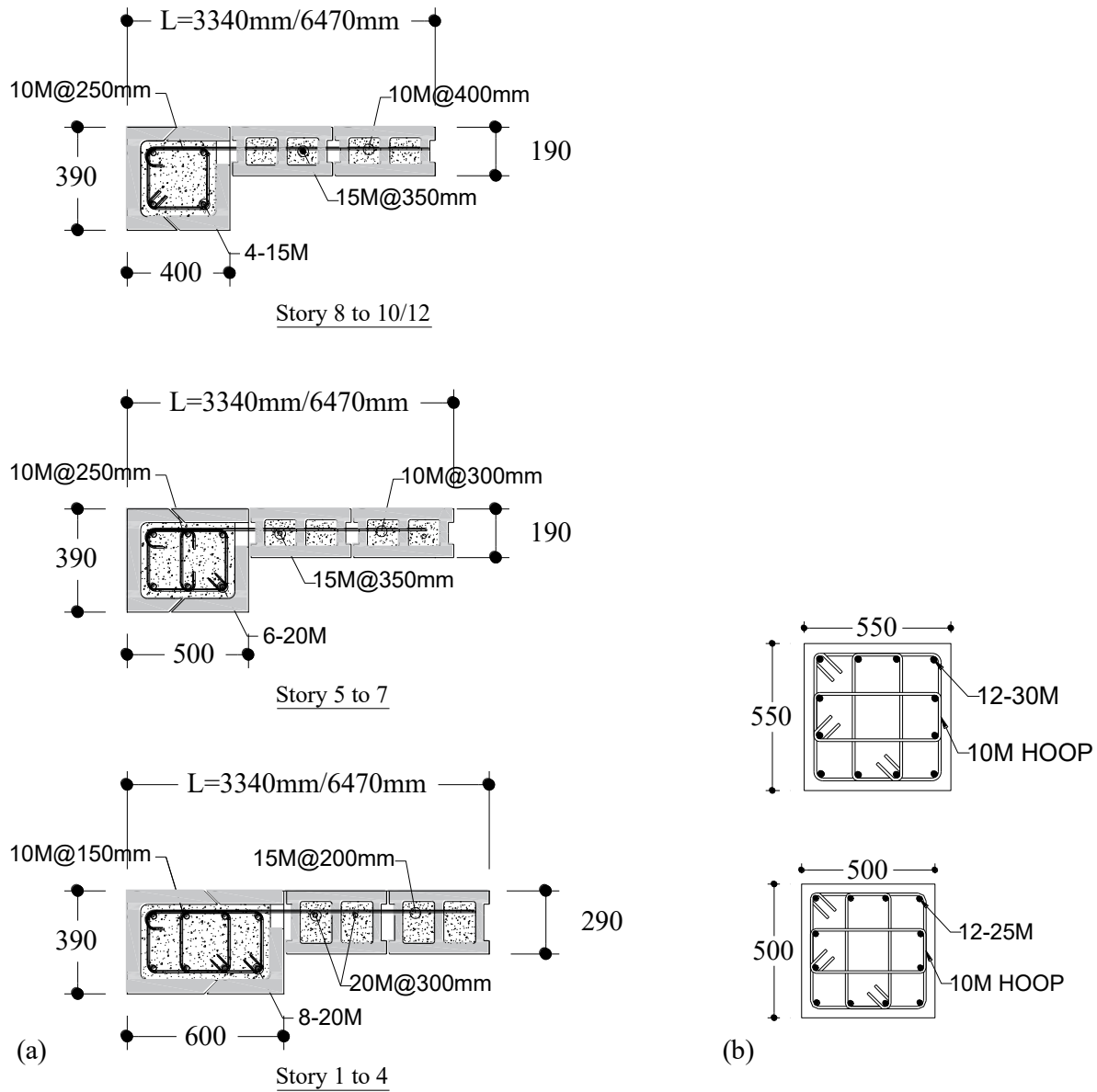
Figure 6.2. Reinforcement and dimension details of the designed Archetype building: (a) Detail of ductile RMSW with MBEs; (b) Gravity RC columns

6.4 Numerical Modelling Approach

In order to capture the overall behaviour of the structure, a macro modelling approach was developed in *OpenSees*. Fibre-based displacement-based beam-column elements were employed to model axial and flexural deformation of shear wall element. In addition, shear springs were considered to model the shear flexibility of the wall and to be able to capture failure due to shear

deformation of the walls. This distributed inelasticity element model was found to be capable of predicting the failure along the length of the RM shear walls' component as well as the fibre cross-section. It is noteworthy that macro modelling approach is the most appropriate technique when many nonlinear static and dynamic analyses are involved. The developed model evens out between the results precision as well as computational efforts. The elaborated details of the modelling approach can be found in Hosseinzadeh and Galal (2019) and skipped here to avoid repetition.

6.4.1 Material Characteristics and Behaviour

The material definition is crucial since the modelling technique mainly depends on the discretization of the fibres, which resembles the axial and flexural response of the structural elements. A uniaxial stress-strain relationship is assigned to each fibre of masonry and reinforcement bars. There is no constitutive material model developed solely to capture the response of fully grouted concrete masonry in most of the available numerical platforms, a concrete constitutive material model proposed by Mander et al. (1989) was selected to simulate fully grouted concrete masonry cyclic behaviour. Nonetheless, it has been proven by various studies (Banting and El-Dakhakhni, 2014; Shedid and El-Dakhakhni 2010) that the characteristics of a well-detailed fully grouted concrete masonry having transverse and longitudinal reinforcement are very close to the behaviour of concrete members having similar conditions. Hence, the modelling parameters of the material model were selected to be consistent with the recommended values as per the design code (i.e., CSA S304-14), especially the peak compressive strength (f_m') and corresponding strain (ε_m). Furthermore, the behavioural variation among concrete and fully grouted concrete masonry is substantially decreased by proper calibration of the material properties, which leads to sufficient accuracy in capturing the global response of the concrete masonry section. This statement can be proven by the comparison of experimental test results versus the global response of the grouted RMSWs. In order to mimic the effect of confinement of the confined zones, a constant confining pressure is assumed over the range of stress-strain. The stress-strain curve is multiplied by the confinement factor, which is defined as the ratio of the compressive strengths of confined and unconfined concrete (Chang and Mander, 1994).

The adapted material model to simulate the cyclic response of steel reinforcement is represented using the uniaxial stress-strain relationship derived by Menegotto and Pinto (Filippou

et al., 1983). The material model is capable of exhibiting the cyclic reinforcement response as well as isotropic strain hardening of the material when subjected to loading histories with extensive reversals in loading cycles. It can also take the pinching of hysteretic loops and Baushinger effect into account since they are the most important factor that drives the global response of the steel reinforcement. The model is also known for its simplicity while being reliable and numerically stable. The modelling parameters, including Young's modulus, yielding and ultimate strength, and fracture/buckling strain, are carefully calibrated to represent the precise cyclic response of the steel reinforcement. Notably, steel reinforcement yield strength (f_y) and Young's modulus (E_s) are considered to be 400 MPa and 200 GPa, respectively, as recommended by CSA S304 (2014).

6.4.2 Record selection and scaling method

The selection of ground motion records is consistent with the intensity-based method presented in FEMA P58-1 (2012). the ground motion selection should provide unbiased estimates of median spectral response when employed in nonlinear dynamic analysis. In that light, ground motion records are selected to match the target response spectrum on average over the minimum to the maximum period range. Based on the recommendation of FEMA P58-1 (2012), T_{min} is selected 0.2 times the lesser period of the first two orthogonal mode shape of vibration; as for T_{max} this value is the larger of 2 times the period of first two orthogonal mode shape of vibration. Moreover, it is recommended that in addition to frequency content, the chosen ground motion suites should have fault mechanisms, site-to-source distances, and local geology similar to those that govern the seismic hazard at the specific intensity level.

Due to paucity of strong ground motion data sets in western Canada, the chosen ground motions of this study are selected from a database of synthetic time histories developed for Canada by Assatourians and Atkinson (2010). A group of 44 horizontal artificial ground motion records were selected to reliably assess the failure probability of the given archetypes. The selected ground motions are developed for site class C soil subgrade having a magnitude of 6.5 and 7.5 with a various site to fault distance to include both near-field and far-field records. In addition, these records are representative of the types of seismic events that coordinate the similar hazard level of the west coast (i.e., crustal and megathrust subduction inter-plate earthquakes, also known as intra-slab subduction mechanism records). The selected records and their main characteristics are shown in Table 6.2.

Table 6.2. Characteristics of Selected Unscaled Ground Motions

Event	M	R_{fault} (km)	PGA (g)	v/a	Event	M	R_{fault} (km)	PGA (g)	v/a
west6c2.1	6.5	19.7	0.223	0.0959	west7c1.19	7.5	21.6	0.433	0.1032
west6c2.2	6.5	19.7	0.27	0.087	west7c1.20	7.5	21.6	0.309	0.0989
west6c2.4	6.5	21.6	0.222	0.0799	west7c1.22	7.5	20.3	0.341	0.1044
west6c2.5	6.5	21.6	0.244	0.0776	west7c1.23	7.5	20.3	0.325	0.1596
west6c2.10	6.5	21.6	0.174	0.0788	west7c1.25	7.5	18.1	0.58	0.0949
west6c2.11	6.5	21.6	0.184	0.0848	west7c1.26	7.5	18.1	0.516	0.11
west6c2.16	6.5	21.8	0.239	0.0753	west7c1.31	7.5	26.3	0.33	0.0811
west6c2.17	6.5	21.8	0.176	0.1013	west7c1.32	7.5	26.3	0.284	0.1289
west6c2.22	6.5	25.8	0.168	0.0676	west7c1.34	7.5	26.3	0.179	0.1224
west6c2.23	6.5	25.8	0.208	0.0968	west7c1.35	7.5	26.3	0.248	0.109
west6c2.37	6.5	27.8	0.183	0.076	west7c1.37	7.5	26.3	0.245	0.1182
west6c2.38	6.5	27.8	0.204	0.0854	west7c1.38	7.5	26.3	0.229	0.0928
west7c1.1	7.5	16.4	0.522	0.112	west7c1.40	7.5	26.3	0.262	0.0815
west7c1.2	7.5	16.4	0.588	0.0793	west7c1.41	7.5	26.3	0.22	0.1371
west7c1.4	7.5	17.1	0.327	0.0931	west7c1.43	7.5	26.3	0.185	0.1376
west7c1.5	7.5	17.1	0.284	0.108	west7c1.44	7.5	26.3	0.276	0.1103
west7c1.10	7.5	17.1	0.342	0.1067	west7c2.1	7.5	47.4	0.162	0.1321
west7c1.11	7.5	17.1	0.413	0.1106	west7c2.2	7.5	47.4	0.189	0.1293
west7c1.13	7.5	17.1	0.351	0.0704	west7c2.4	7.5	45.7	0.253	0.1108
west7c1.14	7.5	17.1	0.32	0.1297	west7c2.5	7.5	45.7	0.197	0.1319
west7c1.16	7.5	21.6	0.294	0.1208	west7c2.13	7.5	30.2	0.203	0.208
west7c1.17	7.5	21.6	0.392	0.1165	west7c2.14	7.5	30.2	0.256	0.0984

The adopted scaling method is based on the proposed methodology by ASCE/SEI 7 (2016). ASCE/SEI 7 requires that the records are scaled such that the mean spectrum of records is not less than 110% of the Maximum Considered Earthquake (MCE) level in the period range of 0.2T to

2.0T in which T is the fundamental period of the structure based on the result of modal analysis performed in OpenSees model. There is a difference between the definition of MCE level and the design spectrum in ASCE/SEI 7. The MCE level corresponds to a very severe earthquake event with 2 percent likelihood of being exceeded in 50 years, whereas the design level is considered to be two-third of the MCE level event. On the contrary, the NBCC 2015 design response spectrum corresponds to 2% probability of exceedance (i.e., MCE level) outlined by ASCE/SEI 7. Thus, scaling the ground motion records to match the NBCC 2015 design level is equal to matching the ASCE/SEI 7 MCE level.

6.4.3   Nonlinear dynamic analyses under bidirectional horizontal excitations

In this part, the numerical 3D model of the selected archetypes is subjected to bidirectional orthogonal ground motions. The seismic excitation was applied to the structure in different angles using incremental dynamic analysis approach considering all the applicable loading scenarios, including uni- and bi-directional schemes. This was done by subjecting the structure to a single component of horizontal time history in different angles. This method was utilized by other researchers to address the uncertainties associated to the angle of excitation application [ref]. The fragility surface was derived accordingly, presenting Intensity Measure (IM) in two horizontal orthogonal directions versus the probability of exceedance for different damage states. A total of 2112 nonlinear dynamic time history analysis is performed to examine the collapse capacity of the archetype buildings. In order to consider the accidental torsion for all building configuration, the center of mass and center of rigidity was shifted by a distance equal to 5% of the plan dimension of the building perpendicular to the direction of seismic loading. Incremental Dynamic Analysis (IDA) was first developed by Luco and Cornell (1998) and expanded subsequently in detail by Vamvatsikos and Cornell (2002). The analysis is performed by subjecting the structure to a suite of ground motions while increasing their intensity measure (i.e., 5% damped spectral acceleration at the fundamental period of the structure) until the collapse of the structure happens. However, successively increasing the ground motion intensity using a scale factor does not necessarily result in realistic ground motion; it can carry out the failure mechanism along with its trend from elastic range into inelastic nonlinear phase (e.g., global dynamic instability) of the structure. To model structural damping mass and stiffness proportional Rayleigh damping method is employed in *OpenSees*. It is important to note that the Rayleigh damping feature in *OpenSees* can estimate the

132

damping matrix using the initial, current, and/or last committed stiffness matrix; however, the committed stiffness matrix was used for all archetype buildings. The analysis was continued at least for 20 sequentially increasing IM increments until reaching the maximum allowable peak inter-story drift ratio, which designates the collapse of the structure. A maximum of 2.5% inter-story drift limit is selected as per article 4.1.8.13. 3) of NBCC2015 recommendation, as the collapse drift of the structures.

6.5 Results and Discussion

6.5.1 Development of fragility surfaces

This section presents the adopted framework to develop fragility surfaces for the buildings subjected to bi-directional seismic excitation. The fragility curve corresponding to each different angle of loading was derived using classical fragility function. Subsequently, a curve was fitted to the obtained individual fragility functions by interpolation in order to form the fragility surface for each studied building. This fragility surfaces express the likelihood that a structure meets or exceeds a specific Damage State (DS) at a given ground motion intensity, with respect to the initial state of the structure.

In order to extract fragility functions, IDA results are used to calibrate the probabilistic seismic demand model that relates the structure's median demand (i.e., peak inter-story drift ratio) to the IM. The relationship between the demand (also known as Engineering Demand Parameter, EDP) and IM can be outlined in the power form Eq. 1. (Cornell et al., 2002).

$$S_D = a(IM)^b \tag{6.1}$$

Where S_D is the median value of the EDP as a function of an IM, and parameters a and b can be calculated using linear regression of $\ln(S_D)$ on $\ln(IM)$. Using the result of linear regression analysis, a closed-form equation for fragility function can be formulated as such (Eq. 6.2.)

$$P[D > C \mid IM] = \Phi\left[\frac{\ln(S_D / S_C)}{\sqrt{\beta_{D|IM}^2 + \beta_C^2 + \beta_M^2}}\right] \tag{6.2}$$

where C and D are structural capacity and seismic demand, and; S_D and S_C are the median value

of demand and structural limit state, as $\beta_{D|IM}$ and β_C are the dispersion of the demand and structural limit state, respectively. β_M shows the modelling uncertainties which is taken 0.2 as per the recommendation of Celik and Ellingwood (2010), and Φ shows the normal cumulative distribution function. Lastly, the dispersion of all structural limit states (β_C) is assumed to be 0.3 per Wen et al. (2004). Figure 6.3 to Figure 6.5 show the final derived fragility surface for different DS and its corresponding contour plot for better representation exposed to multi-directional lateral excitation. The selected DS are consistent with HAZUS-MH (2015), namely moderate, extensive, and complete damage which corresponds to the onset of reaching various structural limit state (i.e., prescribed allowable EDP limit). Both the fitted fragility surface and the counter lines are shown to depict the differentiation of probability of failure against bidirectional excitation. The steeper curves indicate the occurrence of severe strength loss of the structure, which in turn leads to achieving higher drift levels. As shown, the results indicate a higher probability of failure for the taller buildings. This is associated with the higher mode effects that is more prone to occur in taller archetypes. The result of this section will be subsequently used as the probability of being in a specific DS in order to quantify the resilience index of each archetype model.
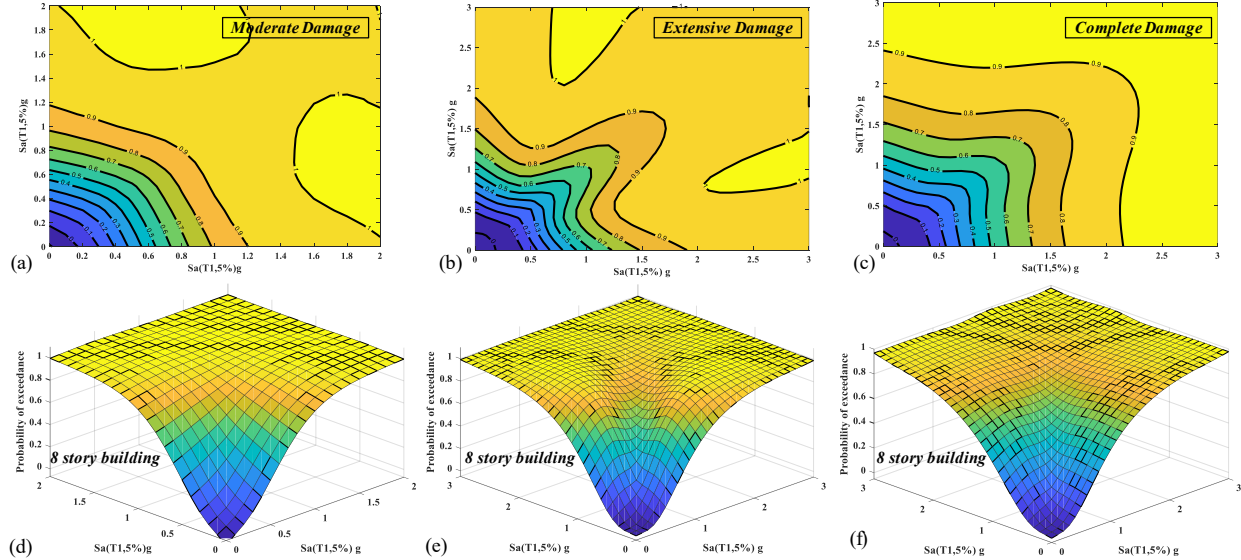
Figure 6.3. Fragility surfaces of 8 storey building for different damage states
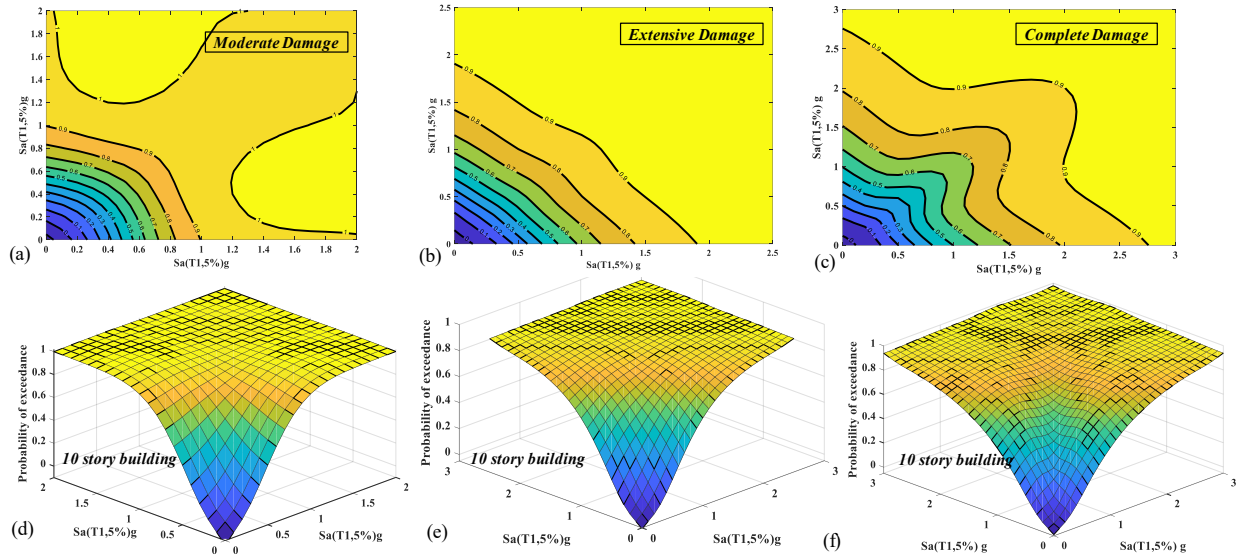
Figure 6.4. Fragility surfaces of 10 storey building for different damage states
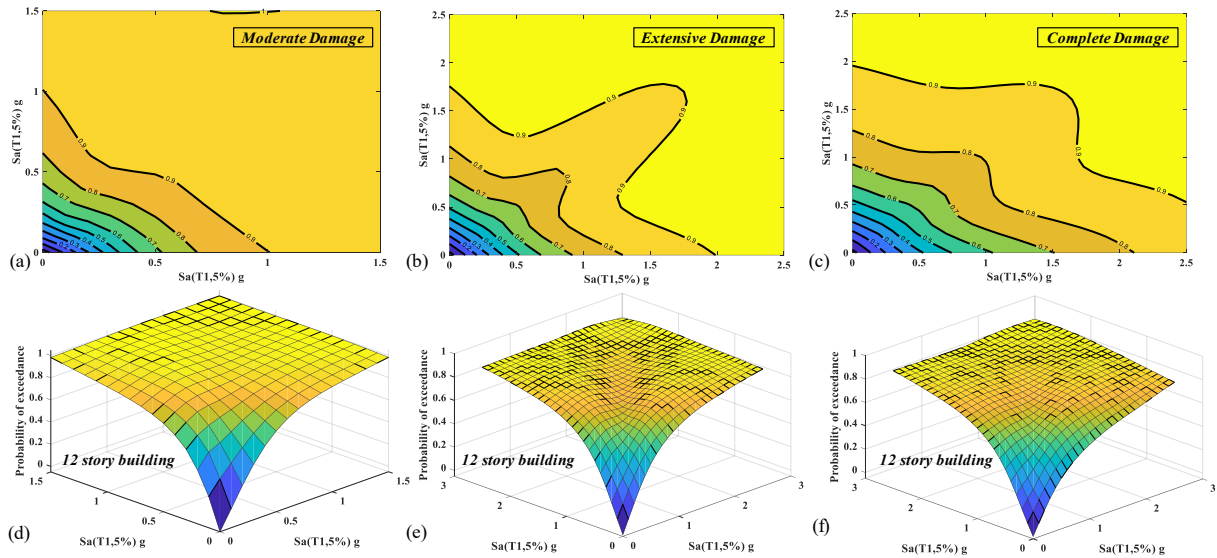
Figure 6.5. Fragility surfaces of 12 storey building for different damage states

6.5.2 Contribution of out-of-plane walls

One of the advantages of studying the behaviour of the structures at system-level (i.e., studying the overall behaviour of a building) is that some parameters can be assessed that normally are omitted when performing the component assessment. One of the most important parameters that can be quantified through system-level assessment is the out-of-plane response of shear wall buildings as well as the torsional forces effect due to the irregularities if the structure. It has been proven that introducing MBEs can enhance the RM shear walls in-plane behaviour as a result of

135

providing more confinement by providing horizontal steel ties that increase the compressive stress and strength capacity and in overall, improves the walls' displacement and curvature ductility (Aly and Galal). However, their performance has not been well assessed both numerically and experimentally when subjected to out-of-plane lateral forces. Hence, in this part, the contribution of the RM shear walls with MBEs to the wall out-of-plane behaviour is quantified in terms of their story shear contribution when subjected to lateral seismic loads. In this respect, the result of Nonlinear Time History Analysis (NTHA) is used to compare the story shear at different story levels of RMSW building archetype. A comparison was made between the story shear forces of the buildings, including lateral stiffness of in-plane and out-of-plane walls with the case where ideally, the stiffness of out-of-plane walls is taken out of the equations (i.e., not their mass participation) to quantify their impact on the forces.

The normalized storey shear profile of each studied archetype building is depicted in Figure 6.6 along with their distribution percentile. As shown, most of the out-of-plane shear wall's storey shear contribution is happening in the middle stories where higher mode effects are more dominant. This fact highlights the significance of out-of-plane walls in withstanding seismic forces, while it has been neglected in most of the design practice building code. The quantification of out-of-plane walls resistance is shown in Figure 6.7 for all archetype buildings. The outcome outlines a minimum of 16% and a maximum of 24% for 8 story building, 13.4% and 28% for 10 story building, and 11% and 34.75% for story shear contribution of 12 story building, respectively. It is vivid that the out-of-plane wall's contribution has increased by escalating the number of floors, which insinuate the larger contribution of out-of-plane walls when higher modes effects are overriding. It is noteworthy that the in-plane walls have a minimum of 76% and a maximum of 84% contribution for 8 story building; 72% and 87% for 10 story building; and 65% and 89% contribution for 12 story building, respectively.
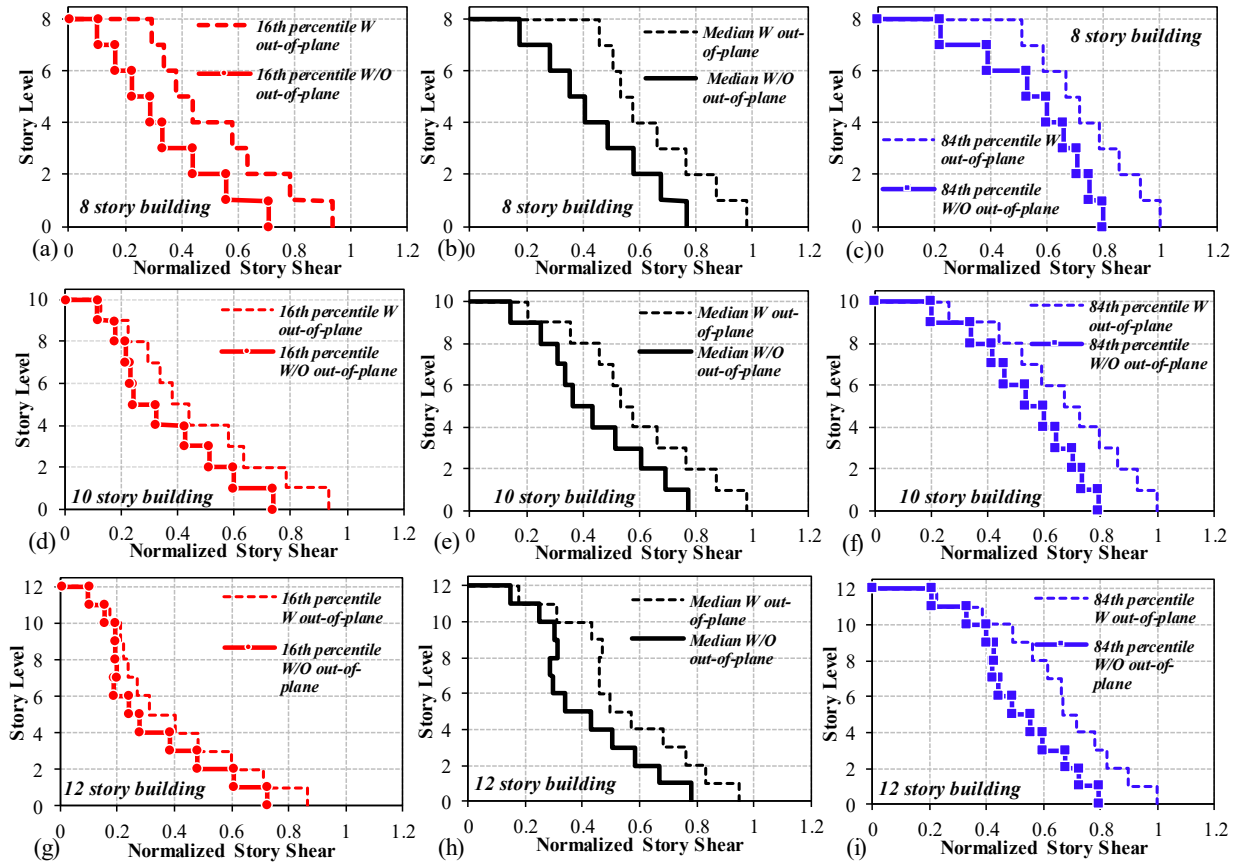
Figure 6.6. Distribution of normalized storey shear and its percentile of all archetype buildings
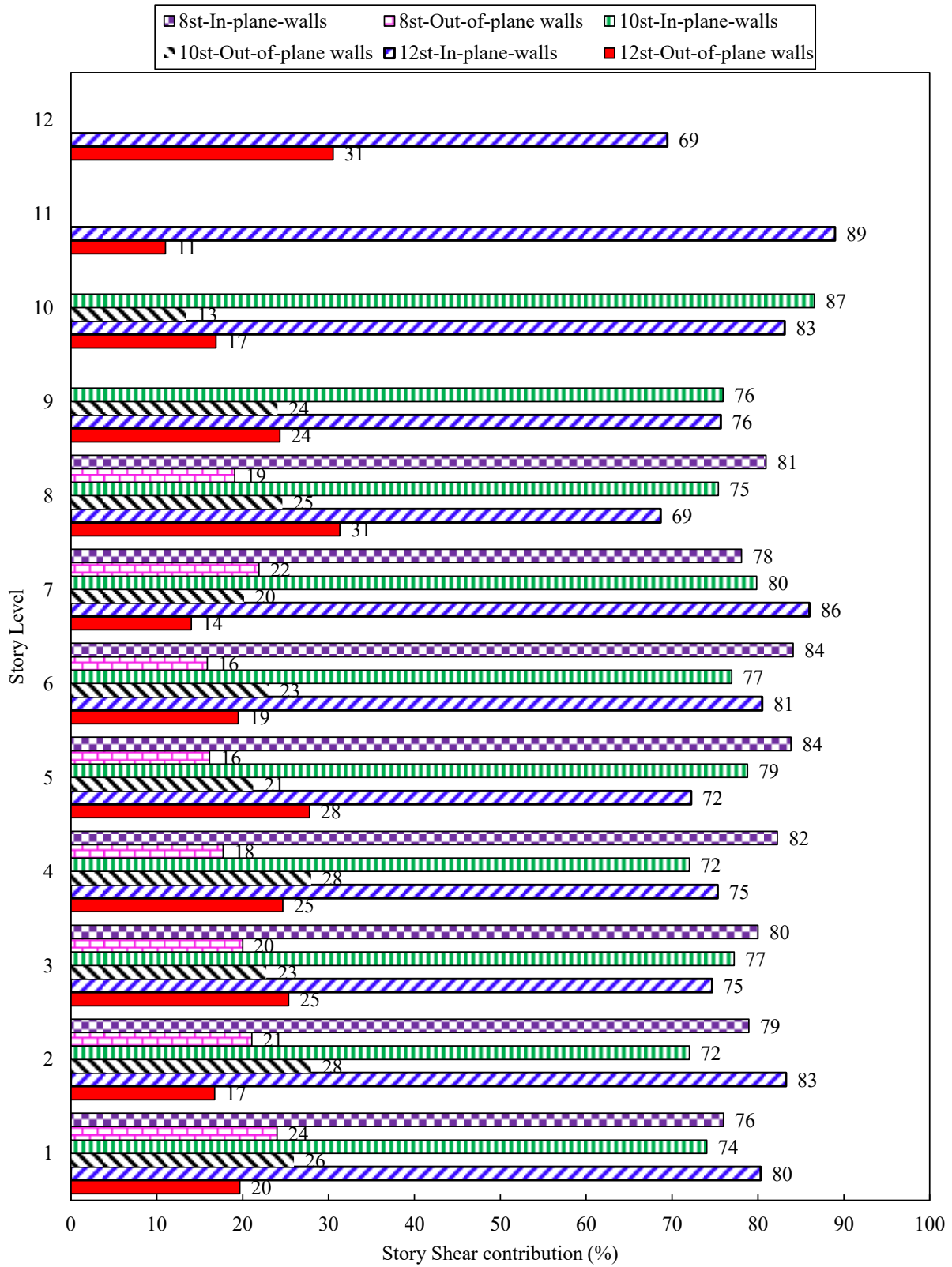
Figure 6.7. Contribution of out-of-plane RM shear walls to the storey shear

138

6.6   Probabilistic seismic resilience quantification

Quantification of resilience can be achieved using loss estimation models. Loss estimation models help in evaluating system resilience and provide a desired measure for it (Chang & Shinozuka, 2004); however, it suffers from possessing high level of uncertainties. There are various models and tools that attempted to estimate the losses arising from an unwanted event; however, few could provide a comprehensive definition of the correlation of losses and recovery actions needed. In this section, a method of quantifying seismic resilience of RMSW buildings is presented, considering the uncertainties arising from loss estimation and recovery time.

One of the initial efforts for quantification of resilience was conducted by a group of researchers from Multidisciplinary Center for Earthquake Engineering (MCEER) of the University of New York, Buffalo, which resulted in the definition of functionality curve (Q), which reflects the serviceability of a system versus time. If an interruption occurs at a time, t_{OE}, the system loses its functionality (Buneau et al., 2003). The system is assumed resilient when fully or partially recovered to reach a desired level of functionality. Subsequently, the resilience index (R) percentage is defined graphically as the normalized area beneath the functionality curve, as shown in Figure 6.8 and expressed as Eq. 6.3. (Bruneau & Reinhorn, 2007).

$$R = \int_{t_{OE}}^{t_{OE}+T_{LC}} Q(t)/T_{LC}\,dt \tag{6.3}$$

where T_{LC} shows the life span of the studied system, and the system's functionality (Q) is defined as per the developed model by Cimellaro et al. (2009). The definition of functionality curves relies on the loss function and recovery time, T_{RE}, for a specified event. These two variables exhibited a high level of uncertainty as a result of their nature. To overcome this high level of uncertainties, a simple yet representative approach is to implement stochastic approaches such as Monte Carlo simulation in order to alleviate the undesirable outcomes and reach a more reliable solution.
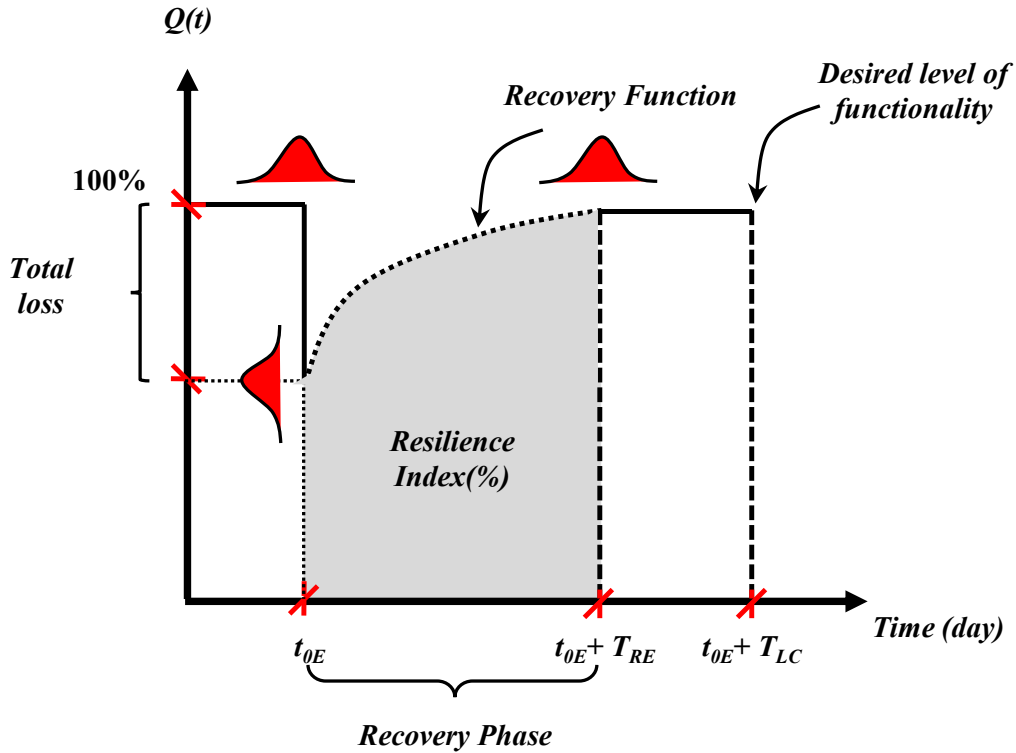
Figure 6.8. Schematic representation of seismic resilience and functionality curve during the recovery time

6.6.1 Loss and Recovery Functions

Most of the loss estimation approaches are probabilistic (Jain et al., 2005) and possess a high level of uncertainty. The adopted loss estimation approach for this study was implemented in HAZUS MH 2.1 (2015) for the earthquake model. In general, the loss function is comprised of two parts, including direct and indirect losses (Eq. 6.4.) (Cimerallo 2010).

$$L(I,T_{RE}) = L_D + \alpha L_I \tag{6.4}$$

where $L(I,T_{RE})$ is the loss function for the intensity of I, LD is the direct losses which happen instantly during the disaster including structural and non-structural losses as well as direct casualties; while the indirect losses (LI) are caused by the downtime associated to the direct losses. In Eq. 4, the weight factor (α) is multiplied by the indirect losses to take the importance of the facilities for the society and its influence on the other system into account. In this research, the indirect losses were not represented in order not to bias the outcome of the study, and to be able to focus on assessing the effect of direct losses on the resilience of the studied buildings. Direct

economic losses, including structural and non-structural losses, are characterized as the ratio of building repair costs to replacement costs and are the ones considered in current work. The total losses are the result of structural and non-structural losses and can be derived using Eq. 6.5.

$$L(I, T_{RE}) = L_S(I) + L_{NS}(I, T_{RE})$$ (6.5)

where $L_S(I)$ represents structural losses, and $L_{NS}(I, T_{RE})$ denotes non-structural losses at the given earthquake intensity, I. the physical structural losses can be formulated in accordance with the recommendation of HAZUS using Eq. 6.6.

$$L_S = \sum_1^N CS_{DS} = BRC \times \sum_1^N POSTR_{DS} \times RCS_{DS}$$ (6.6)

In which CS_{DS} is the cost of the structural damage corresponding to the given damage level, BRC is the building replacement cost estimated based on the average cost per square feet. $POSTR_{DS}$ equals the probability of collapse at a given intensity of the damage state of interest, which can be derived using developed analytical fragility surfaces. RCS_{DS} shows the structural repair cost ratio of a certain damage state provided by HAZUS MH 2.1 (2015). A similar calculation can be performed for non-structural components. However, non-structural elements are divided into acceleration-sensitive, L_{NSA}, and drift-sensitive, L_{NSD}, components (Eq. 6.7 to 6.9).

$$L_{NS} = L_{NSD} + L_{NSA}$$ (6.7)

$$L_{NSD} = \sum_1^N CNSD_{DS} = BRC \times \sum_1^N PONSD_{DS} \times RCD_{DS}$$ (6.8)

$$L_{NSA} = \sum_1^N CNSA_{DS} = BRC \times \sum_1^N PONSA_{DS} \times RCA_{DS}$$ (6.9)

In which $CNSD_{DS}$ and $CNSA_{DS}$ shows non-structural drift and acceleration sensitive damage costs, respectively, at the considered damage state; $PONSD_{DS}$ and $PONSA_{DS}$ are the probability of exceedance of a certain damage state for non-structural drift and acceleration sensitive elements; RCD_{DS} and RCA_{DS} represent the drift and acceleration sensitive repair and replacement ratio of the specified damage state DS, and N is the number of damage states considered for the building.

The process of recovery is a complex task, and it is affected by many factors, time dimensions, and spatial dimensions, showing differences in the same group or state between different geographic areas, suggesting different rates and recovery quality (Samadian et al., 2019). Different types of recovery functions can be selected based on the response of the system and society preparation. There are three common recovery functions, namely linear, exponential, and trigonometric (Kafali & Grigoriu 2005, Cimerallo et al. 2010). In this study, the exponential and trigonometric recovery functions are selected (Eq. 6.10 and 6.11), and the outcome of the resilience assessment of these two methods is compared successively (Cimerallo et al. 2010).

$$f_{REC}\left(t,t_{0E},T_{RE}\right)=\exp\left[-\left(t-t_{0E}\right)\left(ln200/T_{RE}\right)\right] \tag{6.10}$$

$$f_{REC}\left(t,t_{0E},T_{RE}\right)=0.5\times\left\{1+\cos[\pi(t-t_{0E})/T_{RE}]\right\} \tag{6.11}$$

6.6.2 Monte Carlo Simulation

In this section, the Monte Carlo simulation was employed by appointing justifiable distributions to the resilience parameters (i.e., Loss ratios, and recovery time) to evaluate the variation of the resilience index to these parameters. Despite the fact that these methods reduce uncertainty due to a lack of accurate and complete data sets, they need a large amount of time-series data that is very hard to collect. In this respect, random data generation is done following a uniform distribution of loss ratios and Rayleigh distribution for expected recovery time. Loss ratios (i.e., the ratio of repair costs to replacement costs), have a uniform distribution with means of 0.2, 0.45, and 0.8, for moderate, extensive, and complete damage, respectively. The estimated recovery time is generated to be consistent with HAZUS recommendation recovery time for each *DS* of moderate, extensive, and complete to have a mean value of 120-, 360-, and 720-days following Rayleigh destruction density, respectively. Estimating the recovery time correctly to measure resilience is crucial since the results are so sensitive to this parameter. HAZUS assumes that the system can regain its functionality after two years, which is not always realistic. The total expected recovery time can be formulated as per Eq. 6.12 as a function of earthquake intensity.

$$T_{\exp}=\sum_{i=1}^{N}T_{e}^{i}P_{i}(DS_{i}/I) \tag{6.12}$$

where the expected recovery time for each damage state, T_e^i, is weighed corresponding to the probability of being in a specific damage state $P_i(DS_i / I)$ and accumulated to form the total expected recovery time, T_{exp}. Monte Carlo simulation was used to evaluate the impact of variation and uncertainties in these parameters on the resilience index of RMSW buildings having MBEs. In this light, a set of 10,000 random data was generated for loss ratios and recovery times for different *DS* having the abovementioned distribution. Figure 6.9 and Figure 6.10 show the generated random data set for loss ratio and expected recovery time as well as their considered variation range and their respective probability distribution. The distribution of the generated numbers and their extreme is also presented in Table 6.3.

Table 6.3. Distribution of randomly generated numbers along their extremes

Uncertainty parameters	Minimum	Maximum	Mean	Probability distribution
DS1 (Moderate, %)	0.10	0.30	0.20	Uniform
DS2 (Extensive, %)	0.30	0.60	0.45	Uniform
DS3 (Complete, %)	0.60	1.00	0.80	Uniform
T1 (Days)	5	400	120	Rayleigh
T2 (Days)	20	1310	360	Rayleigh
T3 (Days)	30	2620	720	Rayleigh
T_{exp} (Days)	12	2098	700	None

T_1 = Moderate damage, T_2 = Extensive damage, T_3 = Complete damage

In order to distinguish between a resilient and non-resilient case, an underlay threshold is defined after calculation of the resilience index, R, for all the studied archetype buildings. These thresholds are defined as desirable, borderline, and undesirable spectrum. The limits between these thresholds are based on the percentage of loss ratio, L_S+L_{NS}, i.e., 10-30%, 31-60%, and 61-100% loss ratios, for desirable, borderline, and undesirable resilience indices, respectively. The estimated resilience index, R, and their acceptability zone are shown in Figure 6.11. As can be seen, the RMSW building having boundary element are capable of being resilient (i.e., having either desirable or borderline resilience index, R) against the imposed lateral loads of respective high seismic hazard zone. The summary of the Monte Carlo simulation is presented in Table 6.4

showing of the replicas indicate enough resiliency (i.e., falling in the desirable, and borderline zone) while only a tiny portion failed to have enough resilience index (i.e., falling in undesirable zone).

Table 6.4. Summary of the Monte Carlo simulation of the Resilience Index of different archetype building

Archetype Building ID	Recovery Function	Mean	Standard Deviation	Desirable (%)	Borderline (%)	Undesirable (%)
8-Storey Building	Exponential	93.38	2.56	84.95	15.01	0.04
	Trigonometric	90.61	2.52	49.41	50.51	0.08
10-Storey Building	Exponential	93.53	2.43	86.92	13.06	0.01
	Trigonometric	90.44	2.39	44.27	55.66	0.06
12-Storey Building	Exponential	93.07	2.81	82.97	16.91	0.11
	Trigonometric	89.44	2.75	23.26	76.58	0.15
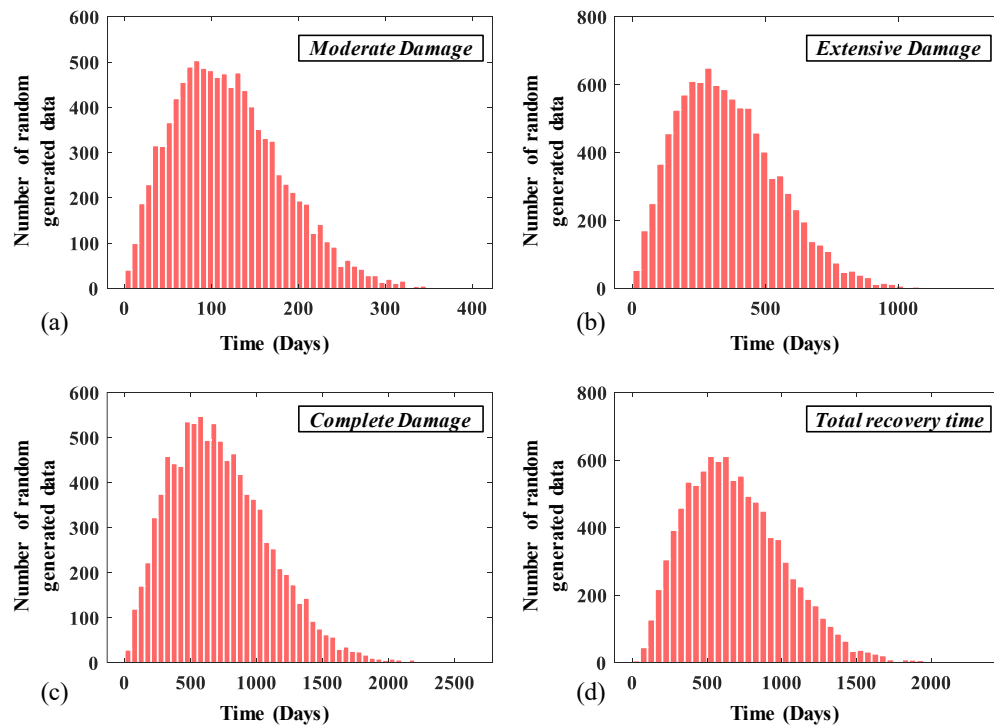
Figure 6.9. Histograms of random recovery times of the studied 10 story building for different damage states when subjected to a 45-degree earthquake ground motion
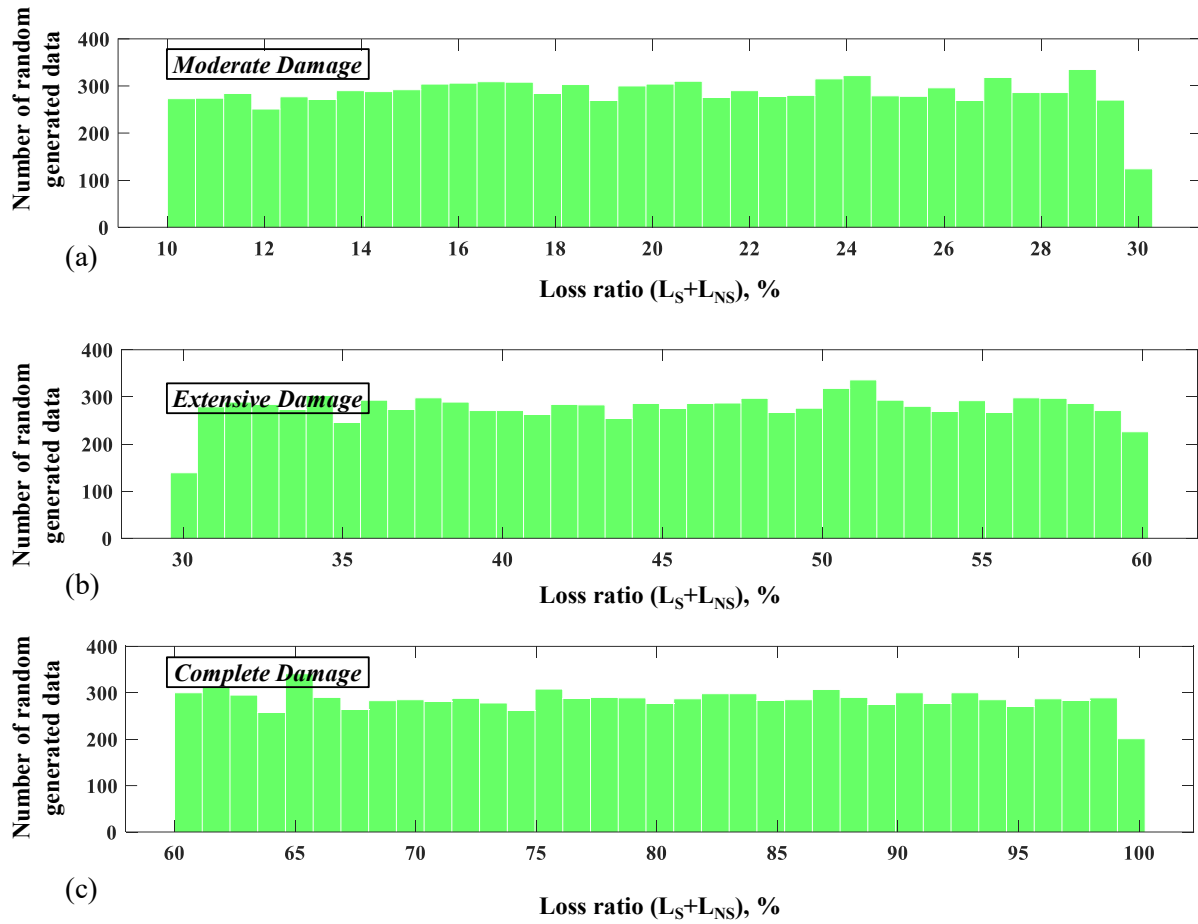
Figure 6.10. Histograms of random loss ratio (LS+LNS) of the studied 10 story building for different damage states when subjected to 45-degree earthquake ground motions
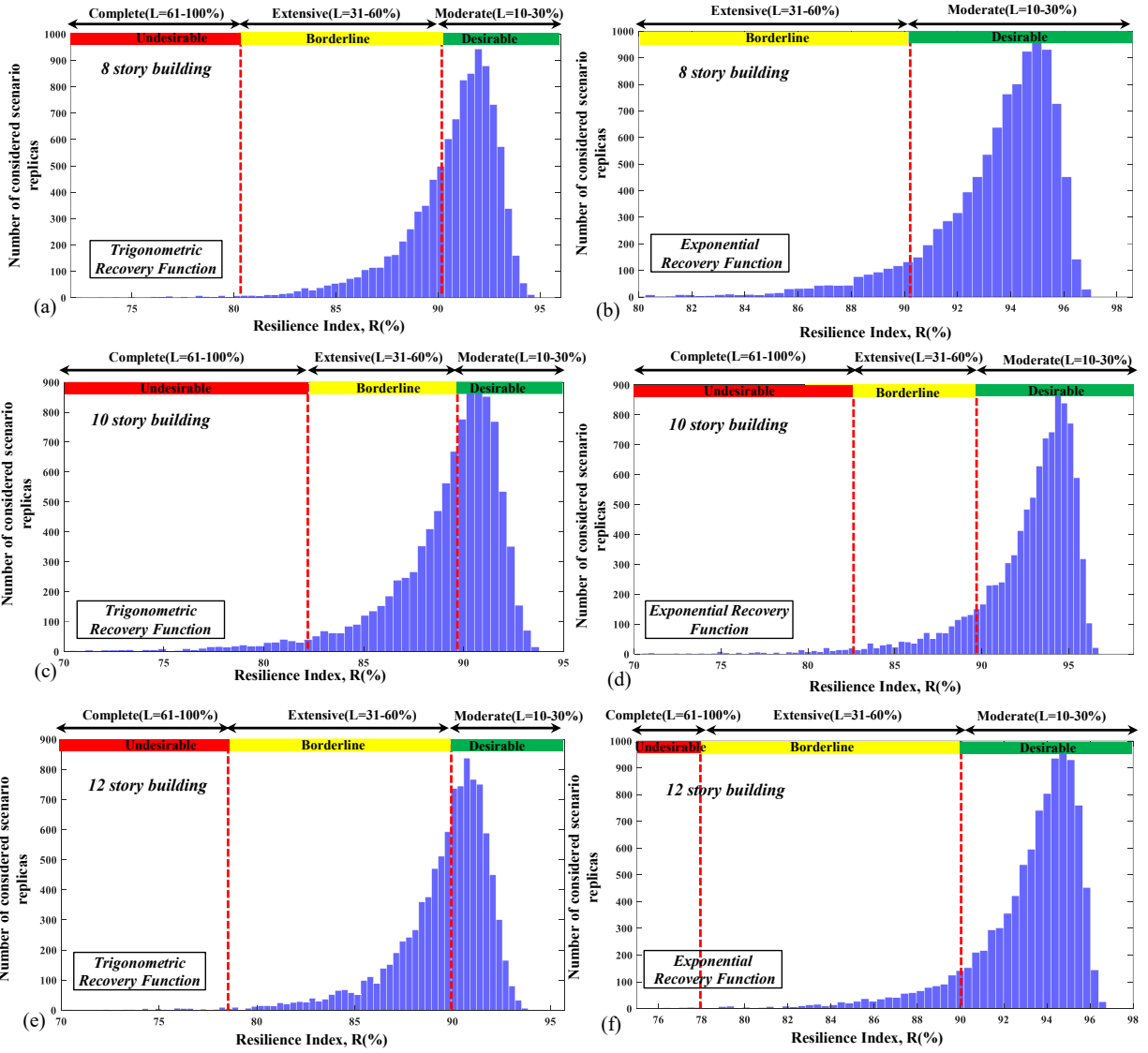
Figure 6.11. Histogram of estimated resilience index along with the underlay border of different recovery function

6.6.3 Sensitivity Analysis

In this section, a sensitivity assessment is conducted to visualize the sensitivity of the resilience index, R, to each of the studied parameters. In this section, random numbers are just generated for the parameter for which sensitivity of the resilience index was assessed, and the rest of the parameters remained constant all the time. This procedure was repeated for each variable and subsequently presented.

6.6.3.1 Sensitivity of R index to loss ratio

The result of the sensitivity assessment of to loss ratio of moderate, extensive, and complete damage state is presented in this part. For this purpose, random numbers were generated for each specific damage state using its respective probability distribution, while the other variables remained constant. The resulting resilience histograms of different damage states are depicted in Figure 6.12 for 10 story RMSW building. It can be seen that the resilience index is more sensitive when the trigonometric recovery function is used. It can also infer that the extensive and complete loss ratios have the most impact on the R index compared to the moderate loss ratio. Nonetheless, more dispersion of data was observed for the complete damage loss ratio. It is noteworthy that the R index remained in the desirable limit for all considered scenario, which indicates the fact that RMSW building having MBEs can be utilized as a resilient Seismic Force Resisting System (SFRS) in high seismicity zones.

6.6.3.2 Sensitivity of R index to expected recovery time

The sensitivity results of the expected recovery time of moderate, extensive, and complete damage state are summarized in this section. Similar to the loss ratio, random numbers were generated for each specified damage state having Rayleigh distribution function, whereas the rest of the parameters remained identical for all replicas. Figure 6.13 presents the R index histogram of the 10 story RMSW building for different *DS* and recovery functions. The calculated results indicate that the R index is more sensitive to the Complete Damage expected recovery time. This acknowledges the fact that reaching the complete functionality of a system after a disastrous event is almost unfeasible and/or needs lots of resources and possess a high level of uncertainty. However, having a desirable level of seismic resilience is more achievable within moderate to extensive loss scenarios. In addition to that, both recovery functions found to yield identical measures at the end of expected recovery time (i.e., their trend to reach full functionality is different while the ultimate goal is equal depending on the level of preparedness and resourcefulness).
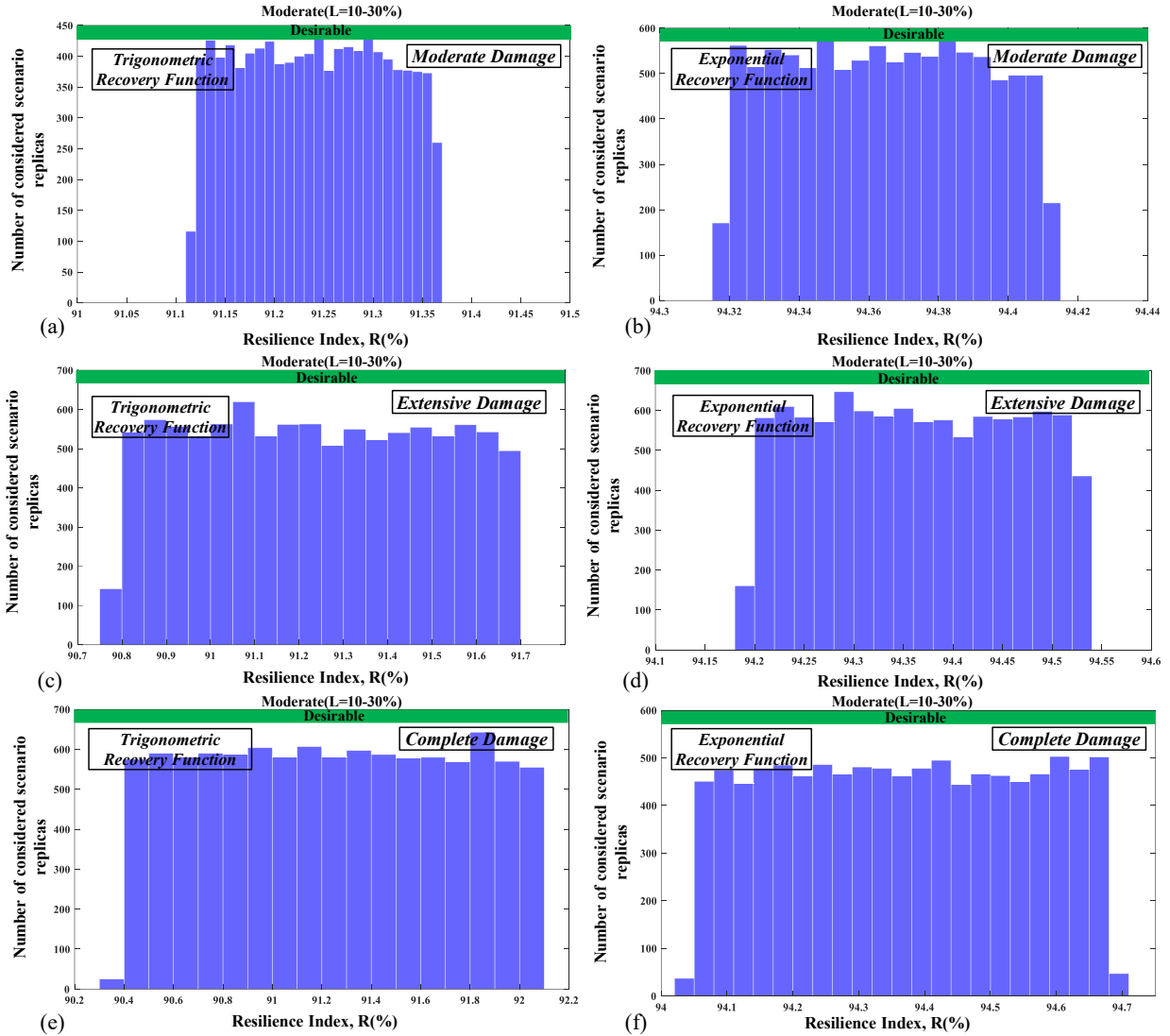
Figure 6.12. Histogram of resilience index for different recovery functions representing the sensitivity of loss ratio for different damage states
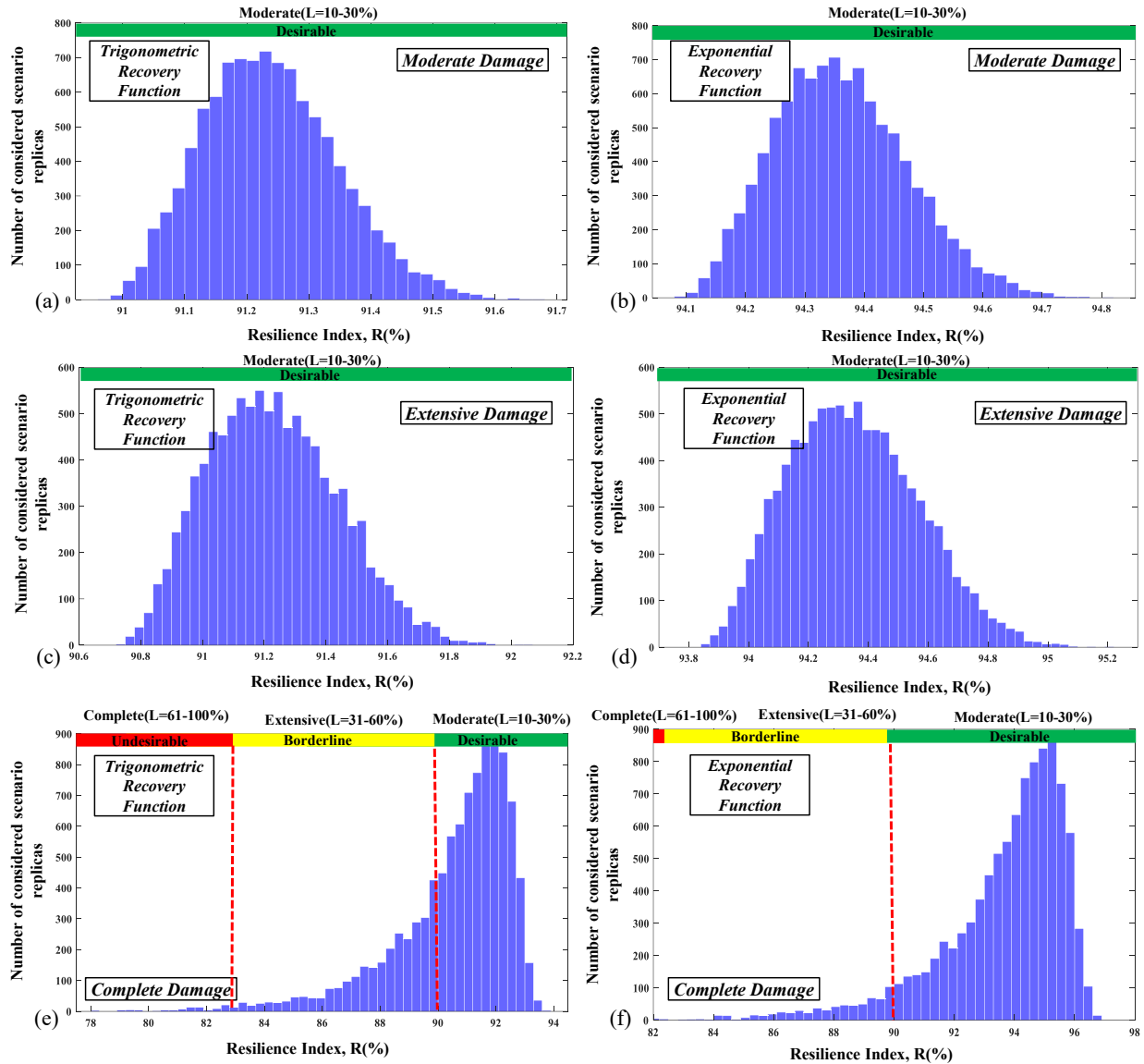
Figure 6.13. Histogram of resilience index for different recovery functions representing the sensitivity of expected recovery time for different damage states

6.6.4 Monte Carlo Simulation Convergence Criteria

It is mandatory to verify the Monte Carlo simulation convergence by providing a sufficient number of replicas. In the early stage of the study, a series of 10,000 randomly generated numbers have been used in analyses even though one replica might not be able to satisfy the desired level of accuracy. Therefore, an investigation of error was conducted to achieve anticipation of enough required case replicas of random numbers. The absolute cumulative error was calculated for the mean value of each replica for all the archetype buildings considering a 0.001% desired error. The

convergence result is shown in Figure 6.14 representing that 20 replicas are enough to reach the desired level of error and have been considered as an index for number of simulations conducted in this study.
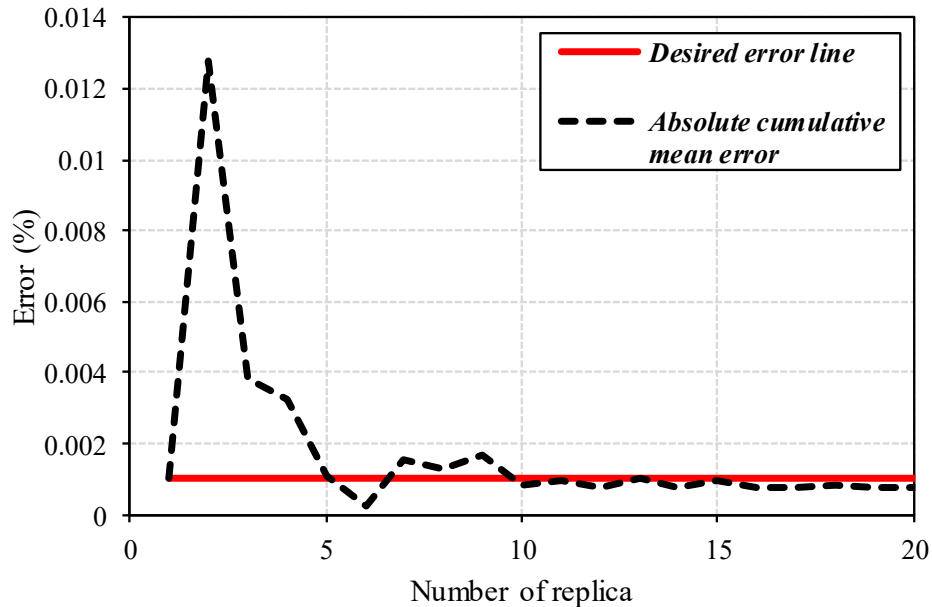
Figure 6.14. Absolute cumulative mean error and convergence of Monte Carlo Simulation

6.7   Conclusions

This study presents a framework to quantify the seismic resilience of RMSW buildings with MBEs using probabilistic methods. A macro-modelling numerical approach was employed to simulate the dynamic response of the selected archetype buildings. The archetype buildings are comprised of 3 different heights conforming with the height limits proposed by NBCC 2015 and were considered to be built on soil type C of high seismicity of Vancouver, Canada. These buildings have RM shear walls with MBEs as the SFRS, while the gravity loads were assumed to be transferred using RC columns. Fully grouted C-shaped blocks were considered in MBEs, which helps with better adaptability of higher compressive strength, a greater number of rebars, a lager grout core strength, and suitable hoop spacing. Utilizing incremental nonlinear dynamic analysis by bi-directional loading scheme helped in the development of fragility surfaces. The outcome of fragility surfaces helps in predicting the probability of being in a specific damage state while a disastrous event hits the structure. Quantification of story shear contribution of in-plane and out-

of-plane walls were conducted when the structure is subjected to bi-directional loading. Finally, a stochastic approach was implemented to understand the impact of various factors in the seismic resilience index of the system.

Based on this study, the following is concluded:

- The developed fragility surfaces provide additional perspectives for decision-makers and policymakers on the seismic vulnerability of the RMSW buildings having MBEs in the west coast of Canada to earthquakes that are plausible in the high seismic zone. These surfaces can predict the probability of failure independent of the angle of loading since the direction of the seismic excitations is always unknown.
- The influence of the out-of-plane walls in the seismic performance of the archetype buildings was considerable, especially when the seismic response if more affected by the higher modes. A minimum of 11% and a maximum of 34.75% story shear contribution was observed for out-of-plane walls. This means that the seismic demand of in-plane walls ranged from 65% to 89% of the overall demand. It can be concluded that accounting for the out-of-plane response of RMSW, which is typically neglected conservatively, increases the seismic capacity of buildings.
- The results of the 20 replicas of Monte Carlo simulation indicates that RMSW building with MBEs is resilient and reliable enough to be utilized in high seismicity zone. They showed that they would be able to remain functional in case of an unexpected disastrous earthquake hits the region.
- A comprehensive threshold was developed to differentiate a resilient and non-resilient structure. It is believed that this kind of resilience representation can lead to the goal of disaster mitigation and preparedness. For the first time, the resilience index is calculated for multi-directional loading by means of fragility surfaces.
- The sensitivity of resilience index to loss ratio and expected recovery time proves the fact that reaching full functionality of the structure after a shock is not necessarily feasible. However, achieving a desirable level of functionality is possible if a resilient SFRS is adopted. Extensive and complete damage states found to be the most effective parameters in resilience index estimation and need to be justified carefully to avoid unrealistic and vague predictions.

Chapter 7

Summary, Conclusions, and Recommendations for Future Work

7.1 Summary

This study investigated the seismic performance and resilience of Reinforced Masonry shear walls buildings having different end configurations including flanges and end-confined Masonry Boundary Elements. The study included the collapse assessment of the above-mentioned system at both the structural element and building level. To the best of the author's knowledge, there are very few studies that addressed the inelastic behaviour of full-scale RMSW buildings with various end-configuration (i.e., most of them studied rectangular walls without confinement). This study enriches the gap in the area by providing a numerical modelling approach capable of capturing the most effective characteristics of the shear wall buildings.

This dissertation consists of numerical macro-modelling approach to quantify the seismic response of the RM shear walls subjected to in-plane and out-of-plane lateral forces. To reach this goal, a simplified macro-model was developed and validated against the available experimental test data in the literature. A collapse risk assessment of RM shear walls subjected to an ensemble of ground motions was performed analytically. A comparison was made between the models with and without the masonry boundary elements to quantify the impact utilizing end-confinement and flanges on the dynamic response of the structure.

The seismic resilience of the RM shear wall system and its sustainability was assessed following the recently available guidelines to ensure its capability to resist and withstand against unwanted events arising from earthquake impact. In order to achieve the objective, fragility curves were derived by postprocessing the result of IDA analysis.

In the last part of the dissertation, a methodology was proposed to quantify the seismic resilience of residential buildings having different heights located in a high seismic zone of Canada (i.e., Vancouver, BC). The seismic resilience is calculated by using fragility surfaces developed for the multi-directional loading scheme. Fragility surfaces are used to evaluate the probability of being in a specific damage state based on the seismic intensity. An acceptance threshold was

considered to differentiate the non-resilient structures form the ones that have enough seismic resiliency. The losses were also estimated, including structural and non-structural losses due to drift sensitive and acceleration sensitive components. Subsequently, the sensitivity of the resilience index was studied against the variation of the expected recovery time and loss ratios uncertainties by means of Monte Carlo simulation. Different recovery functions (i.e., exponential and trigonometric) was also utilized to assess the level of preparedness against a disastrous event. The availability of different types of recovery functions provides great versatility in evaluating resilience and helps model a system or society's response more accurately

The summary of the numerical studies is included in the following:

- In the first part of the study, a macro-modelling approach was used to assess the collapse capacity of the RM core walls, which can be related to the flanged walls in CSA S304. The developed numerical model was verified against experimental test results at both component level (Wall segment) and system-level (entire building) using SeismoStruct software.

- Due to the limitation associated with the commercial software, the next of the study was conducted by developing a fibre-based modified wide column model using OpenSees. Displacement-Based Beam-Column elements were used along with the shear springs to capture the shear flexibility of the wall's segments. The proposed macro-model proved to be able to simulate the behaviour of reinforced masonry shear walls (with and without flanges, and end confinement of masonry boundary element) under cyclic loading with a great level of accuracy.

- Macro modelling using fibre section elements was found to be an efficient modelling approach for engineering practice. The impact of utilizing different end-configuration was studied through performing successive dynamic analysis for various building height and configuration. Fragility curves were derived from the results of IDA analysis and were used to assess the vulnerability of the RM shear walls before and after incorporating boundary elements and/or flanges. Subsequently, the variation of Engineering Demand Parameters (EDPs) like the inter-storey drift ratio and storey shear was monitored to understand the effect of using flanges and MBEs at the walls' extreme.

- Collapse risk assessment of RM flanged walls was performed under the MCE level earthquake using the same seismic performance factor adopted to the rectangular RM shear walls systems. The destabilizing impact due to gravity P-Δ effect was considered using leaning column analogy. Five archetype model was studied taken from NIST GCR 10-917-8 and were verified as a further benchmark.
- The selected archetypes were evaluated using the FEMA-P695 methodology to see if they meet the acceptance criteria proposed by the guideline after the adoption of flanges. The methodology consists of developing an analytical model, selecting and scaling the ground motion data, performing Nonlinear Pushover Analysis and Incremental Dynamic Analysis, generating IDA and fragility curves to explain the structural system's failure probability.
- Evaluation of seismic resilience of the RM Shear wall structures was performed before and after the use of the flanged elements in order to estimate total loss and recovery time due to seismic events.
- A system-level seismic response of a ten-storey full 3D building was done successively. The results were compared for the building prior and after adding masonry boundary elements.
- The previously discussed modelling approach was updated in order to capture the shear deformation of out-of-plane walls by having an out-of-plane shear spring. The modelling approach was verified versus the test result of one-third scale two-storey building to ensure its capability in predicting the system-level behaviour as well as component response. The building was subjected to multiple far-field and near-field ground motion records considering various frequency content on the response of the structure.
- The impact of utilizing MBEs on the earthquake losses was quantified through the seismic resilience framework for the studied building considering losses due to structural and non-structural acceleration- and drift-sensitive components.
- In the last stage of the study, a framework was developed in order to quantify the seismic resilience of RMSW buildings having MBEs made by C-shaped blocks located in the high seismicity zone of Vancouver, BC, Canada. The sensitivity of the resilience index against different parameters was assessed using the Monte Carlo simulation method.

- The uncertainties associated with the structural and non-structural losses, as well as estimated recovery time uncertainties, are considered in the quantification of the resilience index of RMSW buildings by generating enough random scenarios.
- A sensitivity analysis was followed for different damage states to study the importance of each parameter and their effect on the archetype's resilience index.
- Different height of 8- 10- and the 12-storey building was studied respecting the proposed height limits of NBCC, while the buildings were subjected to multi-directional seismic excitations. Subsequently, the fragility surfaces were derived for different damage states representing the probability of failure of a specific intensity measure (i.e., earthquake).
- The contribution of in-plane and out-of-plane RM shear walls was quantified by means of a storey shear step diagram.

7.2   Conclusions and main contributions

The followings remarks are concluded for different phases of the study:

- In the first phase of the study, it has been shown that utilizing C-shaped walls instead of the individual walls will increase the ultimate curvature due to the added contribution of the effective length of the flange. This finding was the initiative to assess the effect of different end-configuration on the seismic response of the RM shear wall system.
- The results indicate that the lateral capacity of the structure increased by 45% in N-S direction and by 55% in the E-W direction. Furthermore, the utilization of the C-shaped wall resulted in a 190% increase in the period-based ductility of the building.
- C-Shaped walls had a higher seismic collapse capacity due to the fact that they can increase the curvature and overall ductility of the structure by decreasing the compression depth zone.
- In the next phase, a modified version of wide column macro-model was able to capture both elastic and inelastic characteristics of the response of RMSW with an outstanding level of accuracy. A maximum difference of 7% and 13% was observed in capturing maximum peak strength and hysteresis energy dissipation, respectively. Moreover, the unloading stiffness of the simulated walls was predicted with the maximum divergence of 11%.

- The result of pushover analysis shows that the adoption of flanges led to more energy dissipation. The walls with the flanges are more ductile and possess a higher level of lateral load resistance against applied forces compared to the rectangular walls. The overstrength factor of the walls with flanges was increased substantially as a result of an increase in the ultimate curvature and displacement ductility. The results revealed an up to 70% increase in the displacement ductility.

- It has been shown that adding flanges to walls enhances the seismic performance of low-rise walls to fulfill the methodology's criteria by obtaining greater levels of ductility. More importantly, the results indicate that a possibly larger response modification factor can be considered for the walls with flanges relative to rectangular RM shear walls.

- A 28% reduction was observed after utilizing flanges into RM shear walls, which outlines lower structural and non-structural direct and indirect losses accordingly. Less fluctuation (more predictable behaviour) of drift ratios was observed relative to the corresponding values in the original structures.

- At the structural element level, it has been shown that using flanged walls had minimal impact on the seismic resilience and functionality of the models compared to the original archetypes. From the fragility analysis, it is concluded that RM flanged walls experience less damage and are more rapid to be functional after an earthquake event. In addition, losses calculated for the mid-rise archetypes are relatively larger than the low-rise models. The average seismic resilience of the flanged walls was 98.12%, which is around 2% higher than the non-flanged walls.

- In the second phase and studying the building level, it has been concluded that IDA curves show higher collapse capacity for the shear walls with Boundary elements, and lower dispersion of data was found after utilizing MBEs.

- The updated modelling approach in system-level was able to capture both elastic and inelastic hysteretic behaviour of RMSW building with acceptable accuracy. The difference between an experimentally obtained results and the developed model did not exceed 7%, and 9% for the peak lateral force and the initial stiffness, respectively. Overall, the modelling approach found precise enough to resemble the most effective characteristics of RMSW buildings with a minor error.

- The results of IDA analysis for the 10-storey building located in Montreal proved that by using MBEs, the median collapse intensity of the building has increased by 73% at IO performance level, 88% for LS performance level, and 40% for CP performance level. Also, the results indicate that a higher value of CMR can be associated with the walls with MBEs. A maximum increase of 64% and 180% was observed for RMSW buildings imposed on near-field and far-field records, respectively.

- The inter-storey drift ratio of the buildings with MBE has decreased significantly in both 5-storey and 10-storey archetype buildings located in Montreal since boundary elements have increased the compressive strength of the shear walls causing a lower probability of axial failure. The median value of the inter-story drift ratio decreased with a maximum reduction of 26% for near-field records and 48% for far-field records, respectively. The reduction of the inter-story drift ratio helped the structure to experience lower structural and non-structural losses as well.

- In the 10-storey building in Montreal, after incorporation of MBEs, the shear demands were increased due to having more confinement resulting in lower strength deterioration of the walls at the ultimate loading stage. There was a maximum of 30% and 25% increase in the response storey shear of the building after adding MBEs for near-field and far-field records.

- For the same archetype building, it has been shown that utilizing MBEs had a noticeable impact on the seismic resilience of the RMSW buildings. MBEs have reduced the structural and non-structural losses of the RMSW building by 24% and 30%, respectively. Also, the results indicate that the seismic resilience increases 10% for near-field and 15% for far-field records after adding MBEs to the ends of the RM shear walls.

- For the 5-storey building in Montreal, a 50% increase in the CMR value was observed after adding Boundary Elements to the RMSW Building. This can be justified since BEs will delay the buckling of the vertical reinforcement besides confining the extreme sides of the shear walls, which in turn leads to higher ductility and safeguards against collapse. The collapse fragility curves of the walls with BEs had up to 65% lower probability of failure for specified IM at for all performance levels because of higher ductility levels.

- In the 5-storey building model, there was a maximum of 20 % increase in the response storey shear after adding BEs, and storey shear diagram shifted rightwards in the upper

stories by having BEs. The Inter-Storey Drift ratio of the RMSW building with BEs had decreased dramatically for most of the records. Hence, a lower level of damages is expected for structural and non-structural components of the building with MBEs.

- In the last phase of the study, fragility surfaces were developed after subjecting the buildings to the bi-directional excitation. The probability of failure of the structure can be predicted using the developed fragility surfaces regardless of the direction of the loading.

- It has been shown that the out-of-plane walls have a greater contribution to transfer shear forces when there are greater chances of having higher mode effects. A minimum of 11% and a maximum of 34.75% storey shear contribution was observed for out-of-plane walls. This number was 65% and 89% for minimum and a maximum contribution of in-plane walls, respectively. This finding stresses the fact that the contribution of out-of-plane walls can be quite significant and need to be possibly considered in the design procedure.

- After performing a stochastic assessment, it has been shown that the RMSW building having MBEs are resilient and are able to withstand and mitigate the impact of MCE level earthquake without heavily losing their functionality. A comprehensive threshold was developed to differentiate a resilient and non-resilient structure. It is believed that this kind of resilience representation can lead to the goal of disaster mitigation and preparedness. For the first time, the resilience index is calculated for multi-directional loading by means of fragility surfaces.

- The result of sensitivity analysis shows that full recovery of the system can only be ideally achieved, nonetheless, reaching that functionality level needs lots of resources which might not be economical. Nevertheless, reaching a desirable level of functionality is possible if a resilient SFRS is adopted. Extensive and complete damage states found to be the most effective parameters in resilience index estimation, and a comprehensive justification is needed when estimating these parameters in order to evade unrealistic and fake goals.

7.3 Limitations of the study

The presented methodology has some limitations due to its nature, which needs to be considered in future studies. The most significant parameters that deals with these uncertainties are outlined in the following:

- The loss estimation procedure has a certain level of uncertainty based on the adopted methodology. The region-specific estimation of repair cost ratio can be known as the most significant one.
- The main objective of this study was to evaluate the seismic resilience of RMSW system having different end configurations. At the same time, these outcomes depend on post-earthquake data as well as loss estimation studies. However, it is not easy to find post-earthquake data for this type of building, which makes it hard to verify/calibrate the generated data in this study.
- There are still limited recovery functions available in the literature that needs further studies to form a more comprehensive and inclusive understanding of the economic and social impact of resilience-based engineering.

7.4   Recommendations for Future Research

The findings of this study are limited to the parameters that were considered here. Hence, to further expand the knowledge in this field, other parameters need to be studied. Some recommendations for future research work are outlined as followings:

- As mentioned earlier in the limitation part, there is still a great need to validate and solidify the outcome of research by performing more experimental and numerical studies. These studies are important in a way to provide more post-earthquake data for verification and mitigation procedure.
- The proposed methodology of seismic resilience quantification has a great potential of expansion for other types of disastrous events (i.e., flood, hurricane, fire) as well as other types of buildings.
- In this study, only residential structures are considered for study since they dominate most structures built-in community. Other types of buildings, such as post-disaster and commercial buildings need to be assessed for future reference. Such a study is useful in predicting the entire community resilience.
- More numerical and experimental tests are needed to quantify the out-of-plane behaviour of the RMSW buildings.

- Expanding the developed numerical modelling of this study to investigate the effects of design parameters such as compressive strength of the concrete masonry, yield strength of the reinforcement, detailing of the reinforcement, and geometry of the C-shaped blocks.

References

Ahmadi Koutalan, F. (2012). "Displacement-based Seismic Design and Tools for Reinforced Masonry Shear-Wall Structures." Ph. D. Thesis, The University of Texas at Austin, U.S.A.

Ahmadi, F., M. Mavros, R. E. Klingner, B. Shing, and D. McLean. (2015). "Displacement-based seismic design for reinforced masonry shear-wall structures. 2: Validation with shake-table tests." Earthquake Spectra 31 (2): 999–1019. https://doi.org/10.1193/120212EQS345M.

Albutainy, M., (2016). "Quantification of the Seismic Performance Parameters of Reinforced Concrete Block Shear Walls with Boundary Elements/Walls design, test matrix and test setup", Internal Report, Department of Building, Civil and Environmental Engineering, Concordia University, Montreal, Quebec, Canada.

Albutainy, M., (2018). Personal Communication, "Layout and reinforcement design detail of RM Building in Montreal", Concordia University, Montreal, Quebec, Canada.

Aly, N., and Galal K. (2020). "In-Plane Cyclic Response of High-Rise Reinforced Concrete Masonry Structural Walls with Boundary Elements," Engineering Structures Journal, Elsevier, 219, 110771.

Arabzadeh, Hamid, and Khaled Galal. (2017). "Seismic Collapse Risk Assessment and FRP Retrofitting of RC Coupled C-Shaped Core Walls Using the FEMA-P695 Methodology." Journal of Structural Engineering 143 (9): 4017096. https://doi.org/10.1061/(ASCE)ST.1943-541X.0001820.

ASCE, (2016). "Minimum Design Loads and Associated Criteria for Buildings and Other Structures", ASCE Standard ASCE/SEI 7-16, American Society of Civil Engineers, Reston, VA.

ASCE. (2013). "Seismic evaluation and retrofit of existing buildings." ASCE 41-13, Reston, VA.

ASCE. (2016). "Minimum Design Loads and Associated Criteria for Buildings and Other Structures" ASCE/SEI 7-16, Reston, VA.

ASCE/SEI 41 (2017). "Seismic evaluation and retrofit of existing buildings." American Society of Civil Engineers, ASCE/SEI 41–17, Reston, VA.

Ashour A. (2016). "Wall-diaphragm out-of-plane coupling influence on the seismic response of reinforced masonry buildings." Ph.D. thesis, McMaster University, Hamilton, Canada.

Assatourians, K., and Atkinson, G. (2010). "Database of processed time series and response spectra for Canada: An example application to study of the 2005 MN 5.4 Riviere du Loup, Quebec. Earthquake." Seismological Research Letters, 81, 1013–1031.

ATC (Applied Technology Council), (2009a). "Background document: Damage states and fragility curves for reinforced masonry shear walls." FEMA 58-1/BD 3.8.10, FEMA, Washington, DC.

ATC (Applied Technology Council). (1985). "Earthquake damage evaluation data for California." ATC-13. Redwood City, CA: ATC.

ATC (Applied Technology Council). (2006). "Next-generation performance based seismic design guidelines program plan for new and existing buildings". FEMA 445. Washington, DC: FEMA.

ATC (Applied Technology Council). (2009b). "Quantification of building seismic performance factors." FEMA-P695. Washington, DC: FEMA.

Atkinson, G. (2009). "Earthquake time histories compatible with the 2005 National Building Code of Canada uniform hazard spectrum." Can. J. Civil Eng., 36(6), 991–1000. https://doi.org/10.1139/L09-044.

Baker, J. W. (2015). "Efficient analytical fragility function fitting using dynamic structural analysis." Earthquake Spectra, 31(1), 579–599.

Bankoff, G., Frerks, G., and Hilhorst, D., eds. (2004). "Mapping vulnerability: disasters, development and people." Earthscan, London, UK.

Banting, B., and El-Dakhakhni, W. (2012). "Force- and Displacement-Based Seismic Performance Parameters for Reinforced Masonry Structural Walls with Boundary Elements." Journal of Structural Engineering, 138(12), 1477-1491.

Banting, B., and El-Dakhakhni, W. (2014). "Seismic Performance Quantification of Reinforced Masonry Structural Walls with Boundary Elements." Journal of Structural Engineering, 140(5), 04014001

Berry, M., P., and Eberhard, M., O. (2005). "Practical performance model for bar buckling." J. Struct. Eng., 131(7), 1060-1070.

Beyer, K., Dazio, A., and Priestley, M. J. N. (2011). "Shear deformations of slender reinforced concrete walls under seismic loading." ACI Struct. J., 108(2), 167–177.

Beyer, K., Dazio, A., and Priestley, M.J.N. (2008) "Inelastic Wide-Column Models for U-Shaped Reinforced Concrete Walls," Journal of Earthquake Engineering 12: Sp1, 1-33.

Bohl, A., and Adebar, P. (2011). "Plastic hinge lengths in high-rise concrete shear walls." ACI Structural Journal. 108(2), 148-157.

Bresler, B., and Gilbert, P. H. (1961). "Tie requirements for reinforced concrete columns." ACI Structural Journal, 58(5), 555-570.

Bruneau, M. & Reinhorn, A., (2007). "Exploring the concept of seismic resilience for acute care facilities." EERI Spectra Journal, 23(1), 41-62.

Bruneau, M., and Reinhorn, A. M. (2004). "Seismic resilience of communities conceptualization and operationalization." Proc., Int. Workshop on Performance-Based Seismic Design Concepts and Implementation, P. Fajfar and H. Krawinkler, eds., Bled, Slovenia, 161–172.

Bruneau, M., Chang, S., Eguchi, R., Lee, G., O'Rourke, T., Reinhorn, A., Shinozuka, M., Tierney, K., Wallace, W., & von Winterfelt, D. (2003). "A framework to quantitatively assess and enhance the seismic resilience of communities." EERI Spectra Journal, 19(4), 733-752.

Calabrese, A., Almeida, J., and Pinho, R. (2010). "Numerical Issues in Distributed Inelasticity Modelling of RC Frame Elements for Seismic Analysis." Journal of Earthquake Engineering, 14(sup1), 38-68.

Calugaru, V., & Panagiotou, M. (2012). "Response of tall cantilever wall buildings to strong pulse type seismic excitation." Earthquake Engineering & Structural Dynamics, 41(9), 1301-1318.

Canadian Standards Association (CSA). 2014 "Design of masonry structures." S304-14, Mississauga, Ontario, Canada.

Cancelliere, I., Imbimbo, M., and Sacco, E. (2010). "Experimental tests and numerical modelling of reinforced masonry arches." Engineering Structures, doi:10.1016/j.engstruct.2009.12.005

Celik OC, Ellingwood B. (2010). "Seismic fragilities for non-ductile reinforced concrete frames – Role of aleatoric and epistemic uncertainties" Structural Safety, doi: 10.1016/j.strusafe.2009.04.003.

Chang, G A, and John B Mander. (1994). "Seismic Energy Based Fatigue Damage Analysis of Bridge Columns: Part 1 - Evaluation of Seismic Capacity." NCEER Technical Report No. NCEER-94-0006, 230. https://doi.org/Technical Report NCEER-94-0006.

Chang, S. E. & Shinozuka, M. (2004). "Measuring improvements in the disaster resilience of communities." Earthquake Spectra, 20 (3), 739-755.

Cimellaro GP, Arcidiacono V, Reinhorn AM. (2018). "Disaster resilience assessment of building and transportation system." Journal of Earthquake Engineering https://doi.org/10.1080/13632469.2018.1531090.

Cimellaro GP, Fumo C, Reinhorn AM, Bruneau M. (2009). "Quantification of seismic resilience of health care facilities." MCEER technical report-MCEER-09-0009. Buffalo (NY): Multidisciplinary center for earthquake engineering research.

Cimellaro, G. P., Reinhorn, A. M., and Bruneau, M. (2006). "Quantification of seismic resilience." Proc., 8th Nat. Conf. of Earthquake Eng., paper No. 1094, San Francisco, CA.

Cimellaro, Gian Paolo, Andrei M. Reinhorn, and Michel Bruneau. (2010). "Framework for Analytical Quantification of Disaster Resilience." Engineering Structures 32 (11). Elsevier Ltd: 3639–49. https://doi.org/10.1016/j.engstruct.2010.08.008.

Cornell, C.A., Jalayer, F., Hamburger, R.O., et al. (2002). "The probabilistic basis for the 2000 SAC/FEMA steel moment frame guidelines." ASCE Journal of structural engineering, 128(4), 526-533.

Corotis RB. (2011) "Conceptual and Analytical Differences between Resiliency and Reliability for Seismic Hazards." Structural Congress, Reston, VA: American Society of Civil Engineers; 2011, p. 2010–20. doi: 10.1061/41171(401)175.

CSA (Canadian Standards Association). (2009). "Carbon Steel Bars for Concrete Reinforcement." CSA-G30.18-09, Canada.

CSA (Canadian Standards Association). (2014). "Design of masonry structures." CSA S304.14, Canada.

Cyrier, W. B. (2012). "Performance of Concrete Masonry Shear Walls with Integral Confined Concrete Boundary Elements", Master Thesis, Washington State University, Washington, USA

Deierlein, G., Reinhorn, M., and Willford, M. (2010). "Nonlinear structural analysis for seismic design." NIST GCR 10-917-5, National Institute of Standards and Technology, Gaithersburg, MD.

Dhanasekar, M. and Shrive, N. G. (2002). "Strength and Deformation of Confined and Unconfined Grouted Concrete Masonry." ACI Structural Journal, 99(6), p.819-826.

Drysdale RG, Hamid AA. (1979) "Behaviour of concrete block masonry under axial compression." ACI J 1979; 76:707–21.

El-Dakhakhni, W., and A. Ashour. (2017). "Seismic response of reinforced concrete masonry shear-wall components and systems: State of the art." Journal of Structural. Engineering, 143 (9): 03117001. https://doi.org/10.1061/(ASCE)ST .1943-541X.0001840.

Ezzeldin, M., El-Dakhakhni, W., and Weibe, L. (2017). "Experimental assessment of the system level seismic performance of an asymmetrical reinforced concrete block – wall building with boundary elements." Journal of Structural Engineering, 143(8), 1-13.

Ezzeldin, M., Wiebe, L., and El-Dakhakhni, W. (2016). "Seismic Collapse Risk Assessment of Reinforced Masonry Walls with Boundary Elements Using the FEMA P695 Methodology." Journal of Structural Engineering, 142(11), 04016108.

Ezzeldin, M., Wiebe, L., and El-Dakhakhni, W. (2017). "System-Level Seismic Risk Assessment Methodology: Application to Reinforced Masonry Buildings with Boundary Elements." Journal of Structural Engineering, 143(9), 04017084.

Federal Emergency Management Agency (FEMA) (2006). "NEHRP Recommended Provisions: Design Examples", FEMA 451, 2003 Edition, Washington, D.C.

Federal Emergency Management Agency. (2015). "Hazus–MH 2.1: Technical Manual." National Institute of Building Sciences and Federal Emergency Management Agency (NIBS and FEMA), 718. www.fema.gov/plan/prevent/hazus.

FEMA P695. (2009). "Quantification of Building Seismic Performance Factors.", Federal Emergency Management Agency, Washington, District of Columbia, USA

FEMA. (2012). "Seismic performance assessment of buildings, volume 1- Methodology." Rep. No. FEMA P-58-1, Washington, DC.

Filippou F.C., Popov E.P., and Bertero VV. (1983). "Modelling of R/C Joints under Cyclic Excitations." Journal of Structural Engineering, 109: 2666–2684.

Filippou, F. C., E. P. Popov, and V. V. Bertero. (1983). "Effects of bond deterioration on hysteretic behaviour of reinforced concrete joints. Rep. EERC 83-19." Berkeley, CA: Earthquake Engineering Research Center, Univ. of California.

Gogus, A. (2010). "Structural wall systems–Nonlinear modelling and collapse assessment of shear walls and slab-column frames." Ph.D. thesis, Univ. of California, Los Angeles.

Gogus, A., and Wallace, J. W. (2015). "Seismic safety evaluation of reinforced concrete walls through FEMA P695 methodology." Journal of Structural Engineering, 10.1061/(ASCE)ST.1943-541X.0001221, 04015002.

Hart, G., Noland, J., Kingsley, G., Engle, R., and Sajjad, N. A. (1988). "The Use of Confinement Steel to Increase the Ductility in Reinforced Concrete Masonry Shear Walls." Masonry Society Journal, 7(2), T19-42.

Heerema, P., Ashour, A., Shedid, M., and El-Dakhakhni, W. (2015). "System-level displacement and performance-based seismic design parameter quantifications for an asymmetrical reinforced concrete masonry building." Journal of Structural Engineering, https://doi.org/10.1061/(ASCE)ST.1943-541X.0001258

Heerema, P., Shedid, M., Konstantinidis, D., and Dakhakhni, W., (2015). "System-Level Seismic Performance Assessment of an Asymmetrical Reinforced Concrete Blocks hear Wall Building." Journal of Structural Engineering, 10.1061/(ASCE)ST.1943-541X.0001298.

Hervillard, T., McLean, D., Pollock, D., and McDaniel, C. (2005). "Effectiveness of Polymer Fibers for Improving Ductility in Masonry." 10th Canadian Masonry Symposium. Banff, Alberta, June 2005.

Hosseinzadeh, S, and Galal, K. (2019). "Seismic Fragility Assessment and Resilience of Reinforced Masonry Flanged Wall Systems." ASCE Journal of Performance of Constructed Facilities https://doi.org/10.1061/(ASCE)CF.1943-5509.0001383.

Hwang, H. H. M., and J. W. Jaw. (1990). "Probabilistic damage analysis of structures." Journal of Structural Engineering. 116 (7): 1992–2007. https://doi.org/10.1061 /(ASCE)0733-9445(1990)116:7(1992).

Jain, V. K., Davidson, R. & Rosowsky, D. (2005). "Modelling changes in hurricane risk over time." Natural Hazards Review, 6(2), 88-96.

Kafali C. & Grigoriu M. (2005). "Rehabilitation decision analysis." ICOSSAR'OS: Proceedings of the Ninth International Conference on Structural Safety and Reliability. Rome, Italy.

Kolozvari K. (2013). "Analytical Modelling of Cyclic Shear-Flexure Interaction in Reinforced Concrete Structural Walls", PhD Dissertation, University of California, Los Angeles.

Kolozvari, K., Wallace, J. W., (2016). "Practical Nonlinear Modelling of Reinforced Concrete Structural Walls" Journal of Structural Engineering, DOI: 10.1061/(ASCE)ST.1943-541X.0001492.

Li, J. and Weigel, T. A. (2006). "Damage states for reinforced CMU masonry shear walls." Advances in Engineering Structures, Mechanics and Construction, 140(2), 111-120.

Lignos, D. G., Krawinkler, H., and Whittaker, A. S. (2011). "Prediction and validation of sideway collapse of two scale models of a 4-storey steel moment frame." Earthquake Engineering and Structural Dynamics, 40(7), 807–825.

Lu, Y. & Panagiotou, M. (2014). "Three-Dimensional Nonlinear Cyclic Beam-Truss Model for Reinforced Concrete Non-Planar Walls." Journal of Structural Engineering, 140 (3).

Luco N, Cornell CA. (1998) "Effects of random connection fractures on the demands and reliability for a 3-storey pre-Northridge SMRF structure." In Proceedings of the sixth US national conference on earthquake engineering, Seattle, Washington; June 1998.

Luu, H., P. Léger, and R. Tremblay. (2013) "Seismic demand of moderately ductile reinforced concrete shear walls subjected to high-frequency ground motions." Can. J. Civ. Eng. 41 (2): 125–135. https://doi.org/10 .1139/cjce-2013-0073.

Magenes, G., and Calvi, M. (1997). "In-plane seismic response of brick masonry walls." Earthquake and Engineering and structural dynamics, Vol. 26, 1091-1112

Mander,J. B., Priestley, M.J.N., and Park, R. (1989). "Theoretical stress-strain model for confined concrete." Journal of Structural Engineering, 114:8(1804), 1804-1826.

Massone, L. M., Orakcal, K., and Wallace, J. W. (2006). "Modelling flexural/shear interaction in RC walls, deformation capacity and shear strength of reinforced concrete members under cyclic loadings." ACI SP- 236, American Concrete Institute, Farmington Hills, MI, 127–150

Mattock A. H. (1967). Discussion of "Rotational capacity of reinforced concrete beams" by W.G. Corley. J. Struct. Eng., 93(2), 399-412.

Mayes, R. L., Omote, Y. and Clough, R. W. (1976). "Cyclic shear tests of masonry piers Volume 1: Test Results." Report No. UCB/EERC-76-8, Earthquake Engineering Research Center, University of California Berkeley, USA.

McKenna, F., Fenves, G., and Scott, M. (2013). "Computer program OpenSees: Open system for earthquake engineering simulation." Pacific Earthquake Engineering Center, Univ. of California, Berkeley, CA.

Menegotto, M., and Pinto, P.E. (1973). "Method of analysis for cyclically loaded R.C. plane frames including changes in geometry and non-elastic behaviour of elements under combined normal force and bending." In Symposium on the Resistance and Ultimate Deformability of Structures Acted on by Well Defined Repeated Loads, Zurich, Switzerland. International Association for Bridge and Structural Engineering. pp. 15–22.

Michaud, D., and Léger, P. (2014). "Ground motions selection and scaling for nonlinear dynamic analysis of structures located in Eastern North America." Can. J. Civ. Eng., 41(3), 232–244. https://doi.org/10.1139/cjce-2012-0339.

Millard A. (1993). CEA-LAMBS Report No. 93/007 (Saclay, France, 1993) p. 186.

MJSC (Masonry Standards Joint Committee). (2013). "Building code requirements for masonry structures." ACI 530/ASCE 5, TMS 402, ASCE, Reston, VA.

Murcia-Delso, J., and Shing, B. (2011). "Fragility curves for in-plane seismic performance of reinforced masonry walls." Proc., 11th North American Masonry Conference, Minneapolis, Minnesota, Paper #2.04-3.

Nasiri, E., and Liu, Y. (2017). "Development of a detailed 3D FE model for analysis of the in-plane behaviour of masonry infilled concrete frames." Engineering Structures, http://dx.doi.org/10.1016/j.engstruct.2017.04.049

Nassar, A. A., and Krawinkler, H. (1991). "Seismic Demands for SDOF and MDOF Systems." Report No. 95, The John A. Blume Earthquake Engineering Centre, Stanford University, California, U.S.A.

NBCC (National Building Code of Canada). (2015) "National building code of Canada", National research council of Canada. Ottawa: NBCC.

NIST. (2010). "Evaluation of the FEMA P695 methodology for quantification of building seismic performance factors." NIST GCR 10-917-8, Gaithersburg, MD.

O'Reilly GJ, Perrone D, Fox M, Monteiro R, Filiatrault A. (2018) "Seismic assessment and loss estimation of existing school buildings in Italy." Engineering Structures 2018; 168:142–62.

Panagiotou, M. & Restrepo, J. I. (2011). "Nonlinear Cyclic Truss Model for Strength Degrading Reinforced Concrete Plane Stress Elements, Report No. UCB/SEMM-2011/01" Structural Engineering, Mechanics and Materials, Department of Civil and Environmental Engineering University of California, Berkeley, 37 pp., February 2011.

Panagiotou, M., and J. I. Restrepo. (2009). "Dual-plastic hinge design concept for reducing higher-mode effects on high-rise cantilever wall buildings." Earthquake Engineering Structural Dynamics 38 (12): 1359–1380. https://doi.org /10.1002/eqe.905.

Panneton, M., P. Léger, and R. Tremblay. (2006). "Inelastic analysis of a reinforced concrete shear wall building according to the National Building Code of Canada 2005." Canadian Journal of Civil Engineering 33 (7): 854–871. https://doi.org/10.1139/l06-026.

Pantazopoulou, S., J. (1998). "Detailing for reinforcement stability in RC members." Journal of Structural Engineering, 124(6), 623-632.

Park, R., and Paulay, T. (1975). "Reinforced concrete structures." John Wiley and Sons, New York, N.Y.

Park, Y. J. and Ang, A. H. S. (1985). "Mechanistic seismic damage model for reinforced concrete." Journal of Structural Engineering, 111(4), 722-739.

Paulay T., and Priestley M. J. N. (1992). "Seismic Design of Reinforced Concrete and Masonry Buildings." John Wiley and Sons, Inc.

Paulay, T. (1988). "Seismic Design in Reinforced Concrete – the State of the Art in New Zealand." Bulletin of the New Zealand National Society for Earthquake Engineering, 21(3), 208-232.

Paulay, T., and Uzumeri, S. M., (1975). "A Critical Review of the Seismic Design Provisions for Ductile Shear Walls of the Canadian Code and Commentary." Canadian Journal of Civil Engineering, 2(4), 592-600.

Priestley, M. J. N. (1976). "Cyclic testing of heavily reinforced concrete masonry shear walls." Research Report 76-12, Department of Civil Engineering, University of Canterbury, Christchurch, New Zealand.

Priestley, M. J. N. (2000). "Performance-based seismic design" Keynote Address, Proceedings of the Twelfth World Conference on Earthquake Engineering. Earthquake Engineering Research Institute, Auckland, New Zealand, Paper #2831.

Priestley, M. J. N. and Elder, D. M. (1983). "Stress-strain curves for unconfined and confined concrete masonry." ACI Journal, 80(3), 192-201.

Priestley, M. J. N., and Elder, D. M. (1982). "Cyclic loading tests of slender concrete masonry shear walls." Bulletin of the New Zealand National Society for Earthquake Engineering, 15(1), 3–21.

Priestley, M. J. N., and Kowalsky, M. J. (1998). "Aspects of drift and ductility capacity of rectangular cantilever structural walls." Bulletin of the New Zealand National Society for Earthquake Engineering, 31(2), 73-75.

Priestley, M. J. N., G. M. Calvi, and M. J. Kowalsky. (2007). "Displacement based seismic design of structures." Pavia, Italy: IUSS.

Priestley, M., J., N. and Bridgeman, D., O. (1974). "Seismic resistance of brick masonry walls." Bulletin of the New Zealand National Society for Earthquake Engineering, 7(4), 167-187.

169

Priestley, M.J.N., and Elder, D.M. (1982). "Stress-Strain Curves for Unconfined and Confined Concrete Masonry." ACI Journal, 80(3), 192-201.

Priestly, M. J. N., Calvi, G. M. & Kowalsky, M. J. (2007). "Displacement-Based Seismic Design of Structures." Pavia, IUSS Press.

Purba, R., and Bruneau, M. (2015). "Seismic Performance of Steel Plate Shear Walls Considering Two Different Design Philosophies of Infill Plates. I: Deterioration Model Development." Journal of Structural Engineering, 141(6), 4014160.

RS Means. (2019). "Yardsticks for costing 2019: Canadian construction cost data", Robert S Means, Norwell, 158–163.

Samadian, D., Ghafory-Ashtiany, M., Naderpour, H., Eghbali, M. (2019) "Seismic resilience evaluation based on vulnerability curves for existing and retrofitted typical RC school buildings", Soil Dynamics and Earthquake Engineering, https://doi.org/10.1016/j.soildyn.2019.105844

Scott, B. D., R. Park, and M. J. N. Priestley. (1982). "Stress-strain behaviour of concrete confined by overlapping hoops at low and high strain rates." J. Am. Concr. Inst. 79 (1): 13–27.

SeismoSoft, (2016). "SeismoStruct - A computer program for static and dynamic nonlinear analysis of framed structures", V 2016, available from URL: www.seismosoft.com.

Shedid, M. T. (2009). "Ductility of concrete block shear wall structures." Ph.D. Thesis, McMaster University, Hamilton, Canada.

Shedid, M. T., Drysdale, R. G. and El-Dakhakhni, W. W. (2008). "Behaviour of fully grouted reinforced concrete masonry shear walls failing in flexure: experimental results." Journal of Structural Engineering, 134(11), 1754-1767.

Shedid, M., El-Dakhakhni, W., and Drysdale, R. (2010a). "Alternative strategies to enhance the seismic performance of reinforced concrete-block shear wall systems." Journal of Structural Engineering, 136(6), 676–689.

Shedid, M., El-Dakhakhni, W., and Drysdale, R. (2010b). "Characteristics of rectangular, flanged, and end-confined reinforced concrete masonry shear walls for seismic design." Journal of Structural Engineering, 136(12), 1471–1482.

Shibata, A. and Sozen M. A. (1974). "The Substitute Structure Method for Earthquake-resistant Design of Reinforced Concrete Frames." University of Illinois at Urbana-Champaign, U.S.A.

Shing, P. B., Noland, J. L., Klamerus, E., & Spaeh, H. (1989). "Inelastic Behaviour of Concrete Masonry Shear Walls". ASCE Journal of Structural Engineering, 2204-2224.

Siyam, M. A., D. Konstantinidis, and W. El-Dakhakhni. (2016). "Collapse fragility evaluation of ductile reinforced concrete block wall systems for seismic risk assessment." Journal of Performance of Constructed Facilities. 30 (6): 04016047. https://doi.org/10.1061/(ASCE)CF.1943-5509.0000895.

Snook, M. (2005). "Effects of Confinement Reinforcement on the Performance of Masonry Shear Walls." M.S. Thesis, Department of Civil and Environmental Engineering, Washington State University, Pullman, WA.

Stavridis, A., and Shing, P. B. (2010). "Finite-element modelling of nonlinear behaviour of masonry-infilled RC frames" Journal of Structural. Engineering, 10.1061/(ASCE)ST.1943-541X.116, 285–296.

Structural Engineers Association of California (SEAOC). (1995). "Vision 2000: Performance-Based Seismic Engineering of Buildings." Structural Engineers Association of California, Sacramento, US, 1995.

Thomsen, J. H., and Wallace, J. W. (1995). "Displacement-based design of reinforced concrete structural walls: An experimental investigation of walls with rectangular and T-shaped cross sections." Rep. No. CU/CEE-95/06, Dept. of Civil Engineering, Clarkson Univ., Potsdam, NY.

Tirca, L., O. Serban, L. Lin, M. Wang, and N. Lin. (2016). "Improving the seismic resilience of existing braced-frame office buildings." Journal of Structural Engineering 142 (8): C4015003. https://doi.org/10.1061/(ASCE)ST.1943-541X.0001302.

Vamvatsikos, D., and Cornell, A. (2002). "Incremental dynamic analysis." Earthquake Engineering Structural Dynamics, 31(3), 491–514.

Vulcano, A., Bertero, V. V., & Colotti, V. (1988). "Analytical modelling of RC structural walls." In Proceedings of the 9th World Conference on Earthquake Engineering (Vol. 6, pp. 41-46).

Wallace, J. W., Elwood, K. J., and Massone, L. M. (2008). "Investigation of the Axial Load Capacity for Lightly Reinforced Wall Piers." Journal of Structural Engineering, 10.1061/(ASCE)0733-9445(2008)134:9(1548), 1548–1557.

Wang, F.L., Zhang, X.C., Zhu, F. (2016). "Research progress and low-carbon property of reinforced concrete block masonry structures in China." 16th International Brick and Block Masonry Conference. Padova, Italy. Taylor & Francis Group, London.

Wen, Y.K., Ellingwood, B. R., Bracci, J. (2004). "Vulnerability function framework for consequence-based engineering." MAE Center Project DS-4 Report.

Wiebe, L., and C. Christopoulos. (2009). "Mitigation of higher mode effects in base-rocking systems by using multiple rocking sections." Supplement, J. Earthquake Eng. 13 (S1): 83–108. https://doi.org/10 .1080/13632460902813315.

Wyllie, L.A., Abrahamson, N., Bolt, B., Castro, G., and Durkin, M. E. (1986). "The Chile Earthquake of March 3, 1985- Performance of Structures." Earthquake Spectra, 2(2), 93-371.

Yassin, M. H. M. (1994). "Nonlinear analysis of prestressed concrete structures under monotonic and cyclic loads." Ph.D. dissertation, Univ. of California, Berkeley, CA.

Zhao, J, and S Sritharan. (2007). "Modelling of Strain Penetration Effects in Fibre-Based Analysis of Reinforced Concrete Structures." ACI Structural Journal 104 (2): 133–141. https://doi.org/10.14359/18525.

Zong, Z., and Kunnath, S. (2008). "Buckling of reinforcing bars in concrete structures under seismic loads." 14th World Conf. on Earthquake Engineering, International Association for Earthquake Engineering, Tokyo.

Appendix A

Supplemental Information to Chapter 3

This appendix provides additional information with regards to the numerical study presented in chapter 3 of the thesis.

A.1 Building Description

The following plan outlines the adopted five-story residential building located in high seismic zone of Los Angeles (see Figures A.1 and A.2). The structural walls are made of 8-in.-thick concrete block masonry. It has an 8-in-thick hollow core precast, prestressed concrete planks as the rigid diaphragm. Site class D type of soil and seismic design category D is considered in design of the archetype building.
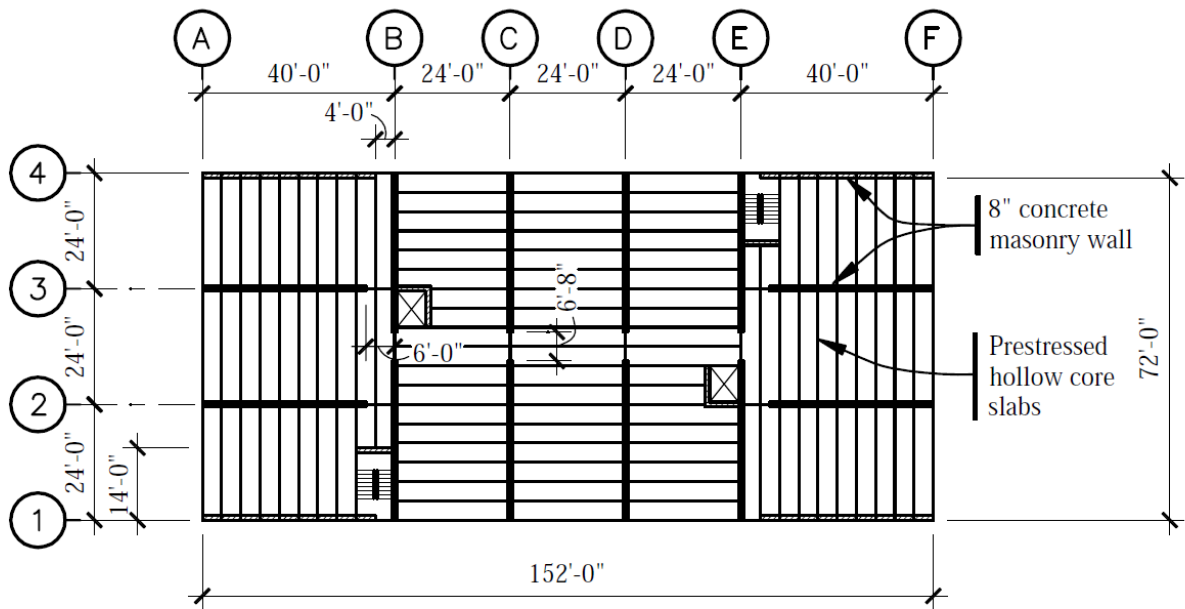

Figure A.1 Typical Floor plan of the studied archetype building (FEMA-451, 2006)
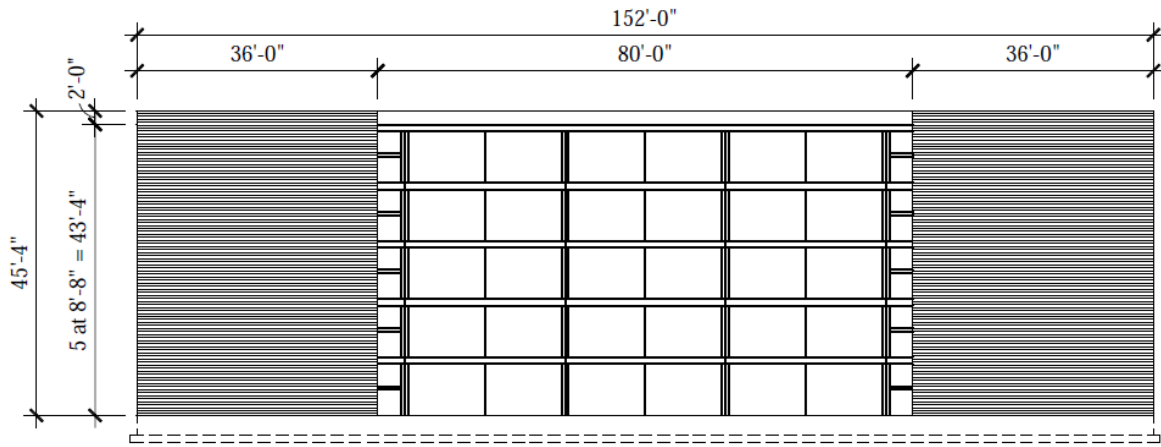
Figure A.2 Elevation view of the studied archetype building (FEMA-451, 2006)

The structure has no irregularities both in plan and elevation, and foundation is assumed to be able to carry the superstructure loads as well as overturning moments. The building is designed in a way to yield almost equal lateral resistance for both loading direction. The layout and wall naming are presented in Figure A.3.

| Wall length	
A	36'-0"
B	34'-0'
C	32'-8"
D	32'-8"
E	8'-0"
F	8'-0"
G	8'-0"
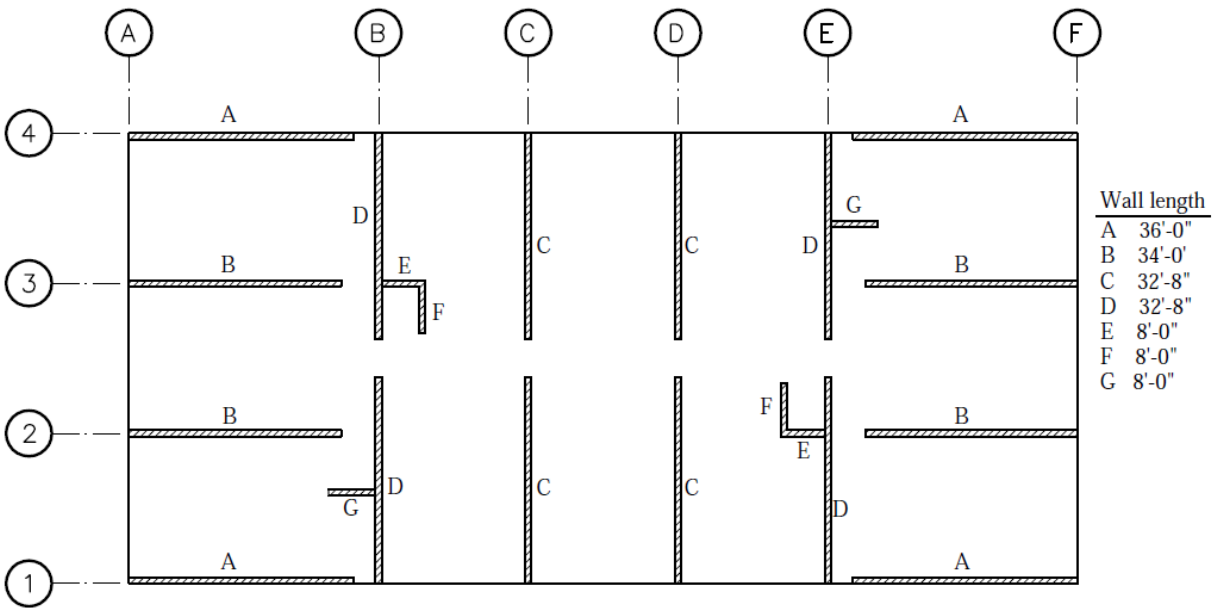
Figure A.3 Reinforced masonry shear walls layout (FEMA-451, 2006)

The compressive strength of masonry, f'_m, is taken as 2,000 psi and the steel reinforcement has a yield limit of 60 ksi.

A.2 Ground motion records

This part describes the selected ground motions as outlined by FEMA-P695 and used for collapse evaluation of the studied archetype building using incremental dynamic analysis. The main characteristics of Far-Field records (i.e., sites located greater than or equal to 10 km from fault rupture) is presented accordingly. There are few objectives that needs to be fulfilled when selecting ground motions. The ground motion records need to be code consistent and should be strong enough to trigger MCE motion level. In the meantime, they have to be site hazard and structure type independent, meaning that the record should be applicable in collapse evaluation of different structural systems. No single record exists to fulfill all above goals due to lack of limitation in available data. Therefore, selecting large number of time histories seems to be a viable choice to lower the uncertainties arising from record selection.

The Far-Field records include twenty-two pairs (i.e., 44 individual ground motion component) selected from the PEER NGA database. The summary of the characteristics of each record is presented in the Table A.1.

The scaling method proposed by FEMA-P695 comprised of two steps. the records need to be normalized at first and then scaled to MCE spectral acceleration level. First the records are normalized by their respective peak ground velocities. Normalization is done to remove unwarranted variability between records due to inherent differences that multiple records have. Later, the records are scaled upwards or downwards such that the median value of the scaled record set match the MCE demand at the fundamental period of the structure rather than a period range required by ASCE/SEI 7.

Table A.1 Characteristics of the unscaled ground motion data set
Far-field ground motions

Event	M	R_{fault} (km)	PGA (g)	PGV (cm/s)
Northridge	6.7	17.2	0.52	63
Northridge	6.7	12.4	0.48	45
Duzce	7.1	12	0.82	62
Hector Mine	7.1	11.7	0.34	42
Imperial Valley	6.5	22	0.35	33
Imperial Valley	6.5	12.5	0.38	42
Kobe	6.9	7.1	0.51	37
Kobe	6.9	19.2	0.24	38
Kocaeli	7.5	15.4	0.36	59
Kocaeli	7.5	13.5	0.22	40
Landers	7.3	23.6	0.24	52
Landers	7.3	19.7	0.42	42
Loma Prieta	6.9	15.2	0.53	35
Loma Prieta	6.9	12.8	0.56	45
Manjil	7.4	12.6	0.51	54
Superstition Hills	6.5	18.2	0.36	46
Superstition Hills	6.5	11.2	0.45	36
Cape Mendocino	7.0	14.3	0.55	44
Chi-Chi	7.6	10	0.44	115
Chi-Chi	7.6	26	0.51	39
San Fernando	6.6	22.8	0.21	19
Friuli	6.5	15.8	0.35	31

Appendix B

Supplemental Information to chapter 6

This appendix provides additional information with regards to determination of number of replicas and associated error calculation of the Monte Carlo simulation method.

B.1 Determination of number of replicas

A Monte Carlo simulation was conducted on chapter 6 using 10000 randomly generated number. However, one replica may not the representative and more scenario should be studied. To determine the sufficient number of replicas, absolute cumulative mean error needs to be defined. Considering $\mu_R(n)$ as the mean of the resilience pertaining to replica n and $\mu_R^c(N)$ is the cumulative mean of the resilience of N replicas, the absolute cumulative mean error can be formulated as Equation B.1, which is the difference between cumulative means of Nr and Nr-1 replicas.

$$\Delta_\mu(N) = |\mu_R^c(N) - \mu_R^c(N-1)| \tag{B.1}$$

The absolute error was calculated for all replicas and was compared against 0.001% as desired error. As shown in chapter 6, using 20 replicas found to be enough to reduce the absolute cumulative mean error under 0.001%. Therefore, 20 replicas were generated for Monte Carlo analysis as well as sensitivity analysis relative to the studied buildings.